COMPARISON OF GROUND MOTION SCALING METHODS BY CONSIDERING VERTICAL GROUND MOTIONS

A THESIS SUBMITTED TO
THE GRADUATE SCHOOL OF NATURAL AND APPLIED SCIENCES
OF
MIDDLE EAST TECHNICAL UNIVERSITY

BY

UMUT OĞUZ

IN PARTIAL FULFILLMENT OF THE REQUIREMENTS
FOR
THE DEGREE OF MASTER OF SCIENCE
IN
CIVIL ENGINEERING

MAY 2022

Approval of the thesis:

COMPARISON OF GROUND MOTION SCALING METHODS BY CONSIDERING VERTICAL GROUND MOTIONS

submitted by **UMUT OĞUZ** in partial fulfillment of the requirements for the degree of **Master of Science** i**n Civil Engineering, Middle East Technical University** by,

Prof. Dr. Halil Kalıpçılar
Dean, Graduate School of **Natural and Applied Sciences** _____

Prof. Dr. Erdem Canbay
Head of the Department, **Civil Engineering** _____

Prof. Dr. Ayşegül Askan Gündoğan
Supervisor, **Civil Engineering, METU** _____

Prof. Dr. Ahmet Yakut
Co-Supervisor, **Civil Engineering, METU** _____

Examining Committee Members:

Prof. Dr. Murat Altuğ Erberik
Civil Eng, METU _____

Prof. Dr. Alp Caner
Civil Eng, METU _____

Prof. Dr. Ahmet Yakut
Civil Eng, METU _____

Prof. Dr. Ayşegül Askan Gündoğan
Civil Eng, METU _____

Assoc. Prof. Dr. Alper Aldemir
Civil Eng, Hacettepe University _____

Date: 20.05.2022

I hereby declare that all information in this document has been obtained and presented in accordance with academic rules and ethical conduct. I also declare that, as required by these rules and conduct, I have fully cited and referenced all material and results that are not original to this work.

Name Last name : Umut Oğuz

Signature : 

ABSTRACT

COMPARISON OF GROUND MOTION SCALING METHODS BY CONSIDERING VERTICAL GROUND MOTIONS

Oğuz, Umut
Master of Science, Civil Engineering
Supervisor: Prof. Dr. Ayşegül Askan Gündoğan
Co-Supervisor: Prof. Dr. Ahmet Yakut

May 2022, 264 pages

The increasing popularity of nonlinear time history analysis has created a demand for ground motion data that is consistent with the seismicity of the region. To meet this need as well as the target design criteria, engineers have started to scale ground motion records. Recent studies have shown that the vertical component of a ground motion can significantly change the results of an analysis. This situation has created a debate about how to scale the vertical component of the ground motions. There exists two alternatives that are commonly applied. In the first alternative, a scaling factor determined only by considering horizontal components of ground motion records is applied to both horizontal and vertical components of a ground motion. In the second alternative, different scaling factors are applied to horizontal and vertical components of ground motions. In this study, the methods of ground motion scaling have been compared by conducting nonlinear time history analyses with ground motions scaled by the mentioned methods.For this purpose, nonlinear time history analyses are conducted for selected building typologies.

Keywords: Ground Motion Scaling, Nonlinear Time History Analysis, Vertical Ground Motion.

ÖZ

DÜŞEY DEPREM YER HAREKETİNİ DİKKATE ALAN DEPREM ÖLÇEKLENDİRME YÖNTEMLERİNİN KARŞILAŞTIRILMASI

Oğuz, Umut
Yüksek Lisans, İnşaat Mühendisliği
Tez Yöneticisi: Prof. Dr. Ayşegül Askan Gündoğan
Ortak Tez Yöneticisi: Prof. Dr. Ahmet Yakut

Mayıs 2022, 264 sayfa

Zaman tanım alanında linear olmayan analizin artan popularitesi, bölgelerin depremselliği ile uyumlu yer hareketi verilerine olan talebi arttırmıştır. Bu ihtiyacı karşılamak ve hedep tasarım kriterini sağlamak adına mühendisler yer hareket kayıtlarını ölçeklendirmeye başlamıştır. Son yıllarda yapılan çalışmalar yer hareketinin genellikle ihmal edilen düşey bileşenin analiz sonuçlarını önemli ölçüde değiştirebileceğini göstermiştir. Bu durum bir yer hareketinin düşey bileşenin nasıl ölçeklendirileceği konusunda bir tartışma yaratmıştır. Bu konuda yaygın olarak kullanılan iki alternatif yöntem bulunmaktadır. Bunlardan ilkinde sadece yatay bileşenler dikkate alınarak belirlenen ölçek katsayısı hem yatay hem de düşey bileşenlere uygulanmıştır. İkinci alternatifte ise düşey ve yatay bileşenler için ölçek katsayısı ayrı ayrı belirlenmiştir. Bu çalışmada zaman tanım alanında, bu iki yöntem kullanılarak ölçeklendirilmiş kayıtlar kullanılarak analiz yapılmış ve sonuçları kıyaslanmıştır. Bu amaçla, belirlenen bina tiplerinde zaman tanım alanında analizi uygulanmıştır.

Anahtar Kelimeler: Deprem Ölçeklendirme, Zaman Tanım Alanında Doğrusal Olmayan Analiz, Düşey Deprem Hareketi

To my family

ACKNOWLEDGMENTS

I would like to express my sincere gratitude to my advisor Prof.Dr. Ayşegül Askan Gündoğan and my co-advisor Prof.Dr.Ahmet Yakut for their guidance and understanding. They made the process much easier and less stressful for me.

I want to thank my friends Eren Küpçü, Engin Keskin and Korhan Kocamaz for their contributions. They helped me anytime I needed.

I would also like to thank Samet Can, Kerem Değirmenci and Doğuhan Yılmaz for the motivation they provide me.

Lastly, I want to thank my family for their encouragement and support.

TABLE OF CONTENTS

LIST OF TABLES

TABLES

LIST OF FIGURES

FIGURES

LIST OF ABBREVIATIONS

AFAD = Disaster and Emergency Management Presidency

ASCE = American Society of Civil Engineers

BKS = Building Occupancy Class

BYS = Building Height Class

EDC = Earthquake Design Class

NEHRP = National Earthquake Hazards Reduction Program

NIST = National Institute of Standards and Technology

PEER = Pacific Earthquake Engineering Research

PGA = Peak Ground Acceleration

PGV = Peak Ground Velocity

TBSC = Turkish Seismic Code

TS 500 = Requirements for Design and Construction of Reinforced Concrete Structures

LIST OF SYMBOLS

A_c = Area of a column

a_i = Distance between longitudinal reinforcement

$A_{k,o}$ = Spectral acceleration of a ground motion

b_o = Spectral acceleration of a ground motion

D = Overstrength Factor

E_c = Elasticity of concrete

E_{sec} = Secant elasticity of concrete

f_{cc} = Confined concrete strength

f_{cd} = Design compression strength of concrete

f_{ck} = Characteristic compression strength of concrete

f_{co} = Unconfined concrete strength

f_{ctd} = Design tension strength of concrete

f_{ctk} = Characteristic tension strength of concrete

f_e = Effective confinement pressure

f_y = Yield strength of reinforcement steel

f_{yw} = Yield strength of stirrups

h_o = Height of confined concrete

I = Building Importance Factor

l_{sn} = Span length of a slab

m = Ratio of slab dimensions

N_d = Axial load on a column

R = Response Modification Factor

S_{ae} = Elastic spectral acceleration

S_{D1} = 1.0 second design spectral acceleration

S_{DS} = Short period design spectral acceleration

S_{Fk} = Scale factor

T = Period

α_s = Ratio of continuous edges to total edges in a slab

ε_c = Concrete strain

ε_s = Strain of reinforcement steel

ε_{su} = Ultimate strain of reinforcement steel

ε_{sy} = Yield strain of reinforcement steel

λ_c = Confinement effect parameter

Υ_c = Material factor for concrete

Υ_s = Material factor for reinforcement steel

CHAPTER 1

INTRODUCTION

Earthquakes have always been a challenging event for structural engineers throughout history. They are very rare events however, it is essential to design a structure to ground motions to which it could be exposed to during its life cycle. Thus, most of the structures constructed in the modern era are designed such that they will deform inelastically and dissipate some portion of the energy created by earthquakes.

Due to modeling and computational complexities involved in the past engineers have designed structures elastically and inserted some factors to take into account inelastic deformations.However,in this millennium, the growing power of computers has started to change the way how engineers tackle seismic design as in every other aspect of life. Computational power obtained gave engineers a chance to make iterations with thousands of steps in less than a second. This enhancement led engineers to think about more accurate methods to design structures and engineers have started to design structures inelastically by using nonlinear analysis methods. Engineers had the opportunity to examine the effects of real earthquakes on structures by using nonlinear methods such as nonlinear time history analysis.

The above-mentioned developments have created a demand for earthquake data that are consistent with the seismic hazard of a region. To fulfill the created demand engineers have developed methods such as simulation of ground motions or scaling the real ground motions to make them consistent with the seismicity of a region.

Until recently engineers have focused only on the horizontal components of ground motions. However, recent studies have shown that vertical components of ground motions might have a considerable amount of effects on structures with specific features. Thus, engineers have started to take into account the effects caused by the

vertical components of ground motions. This situation has raised the question of how to scale ground motions by considering vertical components of ground motions.
Some engineers and institutions such as PEER Tall Building Initiative (PEER/TBI, 2010) have used the same scale factor that is calculated for horizontal ground motions. However, some codes such as ASCE 7-16 (2016) have employed a scaling factor that is calculated by using vertical design spectrum and it is different from the horizontal scaling factor.
The objective of this thesis is to study these two alternative scaling approaches on selected reinforced concrete frame structures and assess the differences.

1.1 Scope of the Study

In this study, it is aimed to increase in-depth knowledge about ground motion scaling by considering the vertical components of ground motions to contribute the literature about how to scale vertical ground motions. As Papazoglou and Elnashai (1996) show in their studies the vertical component of ground motions can cause compressive overstressing, failure due to tension and decrease in the shear resistance, scaling of it needs to be done carefully. Thus, Two commonly used vertical ground motions scaling is investigated by comparing the mentioned methods. The following steps are applied in order to achieve this goal.

- Two case study buildings located on two different soil conditions (NEHRP-soil class C and D) are designed. The buildings are selected to have a different range of fundamental periods.
- For each earthquake design level and two different soil classes, ground motion sets are selected.
- Ground motions are scaled by using the alternative methods mentioned.
- Nonlinear models of buildings are formed and nonlinear time history analysis are conducted.
- The analysis results are compared and interpreted.

1.2 Organization of the Study

This study includes seven chapters.

In the second chapter ground motion scaling studies in literature and different methods adopted by existing seismic codes are explained.

In the third chapter, information about the case study buildings is presented.

In the fourth chapter, ground motion selection procedure and selected ground motions are described.

In the fifth chapter, nonlinear modeling techniques used herein are explained.

In the sixth chapter, time history analysis results and their comparison are given.

In the final chapter, a summary and main findings of the study are presented.

CHAPTER 2

REVIEW OF EXISTING GROUND MOTION SCALING METHODS

2.1 Introduction

Structural engineers have started to use performance-based design methodology to simulate the seismic behavior of structures more realistically during the design phase. This situation led to an increase in the popularity of nonlinear time history analysis. However, there are many uncertainties related to response history analysis such as material properties, modeling technique and ground motion selection. Padgett and DesRoches (2007) performed a sensitivity analysis of these uncertainties and concluded that ground motion selection has a more pronounced effect on the results.

Due to the above-mentioned importance of ground motion selection on the nonlinear response of structures, it needs to be handled very carefully such that the selected ground motions should represent the seismic features of the construction site. Past ground motions that are consistent with the seismic characteristics of the regions are used in the representation of seismicity. However, there are not enough past ground motions to be used for this purpose. To solve this problem, two solutions are commonly applied. The first solution is the intensity-based scaling in which the response spectrum of ground motions is scaled to the desired level without changing the spectral shapes of ground motions. The second solution is spectral matching. Spectral matching has been done either by scaling ground motions in the frequency domain or by adding wavelets in the time domain to make the response spectrum of ground motions similar to the target spectrum. (e.g.: NIST 2011; Heo et al. 2011; PEER 2009; Hancock et al. 2008). Najafi and Tehranizadeh (2015) states that

intensity-based scaling methodologies are used more commonly instead of spectral matching since in latter approach, content of ground motions are modified and variability of ground motions are changed. Since the spectral matching is out of scope of this study, the detailed information on that method will not be included herein.

Different engineers utilized different intensity measures to represent ground motion characteristics. In the following sections, ground motion scaling methods with respect to several intensity measures are discussed.

2.2 Peak Ground Acceleration (PGA) Scaling

Peak Ground Acceleration scaling is the earliest version of intensity-based scaling of time histories. In this method, ground motions are scaled such that the PGA of the ground motion is the same with the target spectrum. An example of PGA scaled ground motion is given in Figure 2.1.

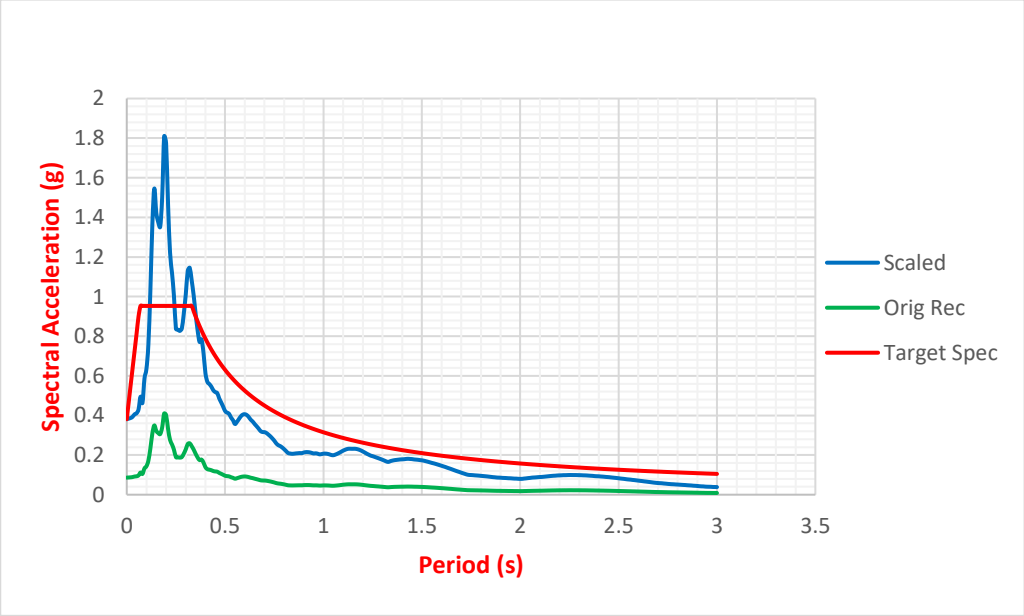

Figure 2.1. Illustration of PGA Scaling Method

Nau and Hall (1984) states that PGA is not reflecting ground motion characteristics since it does not represent the strength and frequency content of ground motions. Thus, it is not appropriate to use them in the determination of scale factors. Similarly, Shome et al. (1998) used PGA scaling in their studies and showed that the results obtained are too scattered. Thus, the results are not reliable.

2.3 $S_a(T_1)$ Scaling

The second commonly used method to scale ground motions is proposed by Shome (1998) and named as $S_a(T_1)$ scaling or spectral response acceleration at the structural fundamental period scaling. In this method, ground motions are scaled such that at the first natural vibration period of a structure, the spectral acceleration of scaled ground motions and the target spectrum have the same value. The illustration of $Sa(T_1)$ scaling for a structure with a natural vibration period of 1.0 s is shown in Figure 2.2.

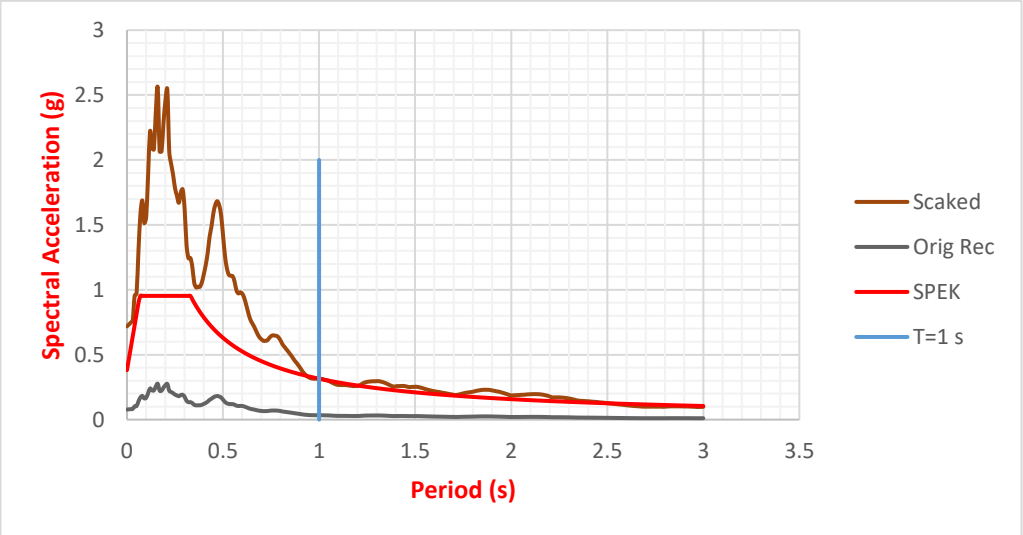

Figure 2.2. Illustration of $S_a(T_1)$ Scaling Method

Naumoski (2004) stated that the method has a good feature as it takes into account the structure under consideration during scaling and gives reliable results for first mode dominant structures. However, Kurama and Farrow (2003) criticized this method because it does not take into account nonlinear behavior such as yielding and higher mode effects. Thus, it is stated that the results may be dispersed.

Bazzurro (1998) proposed a modification for the method to take into account the higher modes. In this method, a vector intensity measure which considers the $S_a(T_1)$ and the ratio of $S_a(T_1)$ and $S_a(T_2)$ is used in the scaling of ground motions. Baker and Cornell (2006) state that the accuracy of the method is increased but the method still gives inaccurate results for the near-fault ground motions.

2.4 Acceleration Spectrum Intensity (SI_a) Scaling

The third commonly used method in linear scaling of ground motions is the acceleration spectrum intensity scaling. Acceleration spectrum intensity is an indicator for damage potential of an earthquake. It is calculated as the area under the response spectrum of an earthquake in the specified period range. Travasarou and Abrahamson (2003) showed that there is a strong correlation between acceleration spectrum intensity and displacement demand caused by an earthquake.

In this scaling method, a scale factor is applied such that acceleration spectrum intensity of the scaled ground motion and target spectrum are equal. In Figure 2.3, acceleration spectrum intensity scaling is illustrated, the scale factor is selected such that the shaded areas under the red and blue curves are equal.

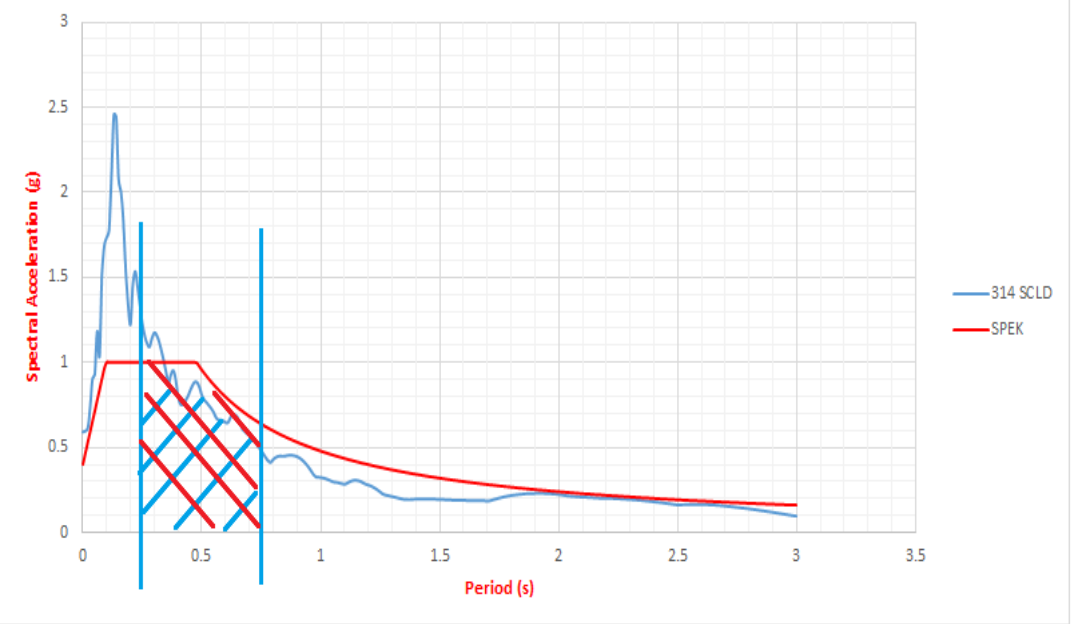

Figure 2.3. Illustration of Acceleration Spectrum Intensity Scaling

2.5 ATC Scaling

Applied Technology Council (2009) proposed a new scaling method. The method is applied in two steps. In the first step, to minimize the variation stemming from earthquake characteristics in the ground motion set, each ground motion is scaled such that the PGV of the ground motion equals the average PGV of the ground motion set.

In the second step, a new scale factor is applied to the ground motion set to make them consistent with the target spectrum. The scale factor is calculated by using the formula given in Equation 2.1.

$$SCF = \frac{Sa_{target}(T_1)}{Median\ (Sa_{response}(T_1))} \qquad (2.1)$$

2.6 Ground Motion Selection and Scaling Rules in Turkish Seismic Code (2018)

Turkish Seismic Code (2018) states that it is preferable to use historical records which are compatible with the seismological properties of the construction site. It is also stated that, if there are not enough records available, it is allowed to use scaled ground motions. The minimum number of records to perform response history analysis is specified as eleven.

For one and two dimensional analysis, ground motion scaling is done such that any spectral acceleration value on the average response spectrum of the scaled ground motion set will be larger than the target spectrum in between [0.2 T_p and 1.5 T_p].

For three-dimensional analysis, the method is similar but in three-dimensional analysis, scaling is done according to the SRSS combination of horizontal components and average response spectrum values needs to be greater than 1.3 times spectral acceleration values of target spectrum. An illustration of three-dimensional scaling according to Turkish Seismic Code (2018) is given in Figure 2.4. In the code, it is not stated how to scale the vertical components of records.

It is important to note that for some cases, it is allowed to use the conditional mean spectrum as a target spectrum and to decrease the scattering of results.

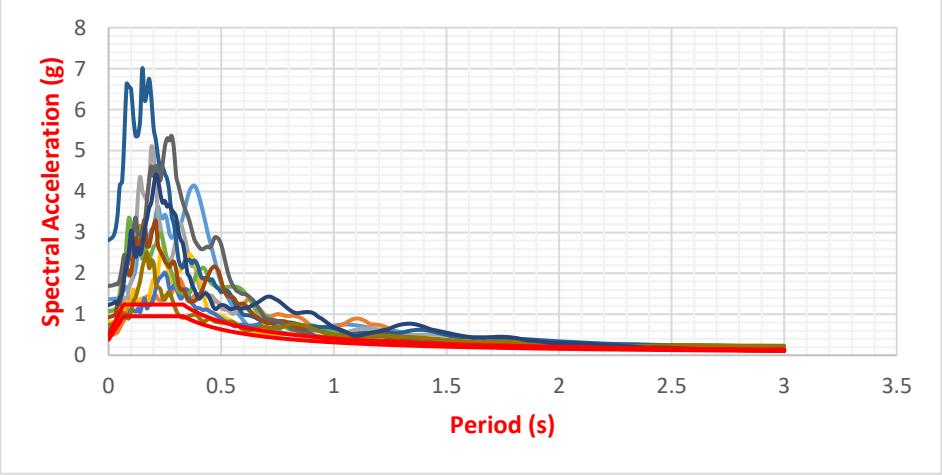

Figure 2.4. Illustration of three-dimensional scaling by Turkish Seismic Code

2.7 Ground Motion Selection and Scaling Rules Specified in Eurocode 8

Eurocode 8 allows the use of simulated or scaled accelerograms in response history analysis. It is stated that at least three ground motions are required in time history analysis. The selected ground motions should have at least 10 s of stationary duration.

In ground motion scaling, there are two basic rules applied. The first rule states that the mean peak ground acceleration of the ground motion set should be greater than the peak ground acceleration of the target spectrum. The second rule specifies that any value of the mean elastic response spectrum of ground motion needs to be larger than 90 % of the corresponding value of the target spectrum between [$0.2T_1$ and 2.0 T_1].

2.8 Ground Motion Selection and Scaling Rules Specified in ASCE 7-16

ASCE 7-16 specifies the minimum number of ground motions required for time history analysis as eleven and it is allowed to select these from amplitude scaled ground motions and spectrally matched ground motions.

The upper bound of period range is specified as twice of the largest first mode period in horizontal direction. However, if it is justified by dynamic analysis under the maximum considered earthquake, it is allowed to decrease the upper bound till 1.5 times of the first mode of the structure under consideration.

The lower bound is specified as the period in which 90 % mass participation rule is satisfied for each horizontal direction. However, the lower bound cannot be less than 20 % of the smallest first mode of each horizontal direction.

The lower bound of the period range for the vertical component is specified as the larger of the 0.1 seconds and the lowest period that is significantly contributing in the vertical direction.

Ground motions are scaled such that the maximum direction spectrum constructed from horizontal components matches with target spectrum over the specified period range. Also, average maximum direction spectra should be greater than the target spectrum within the period range.

Vertical ground motions are scaled such that the average spectral acceleration values specified in the period range will be greater than the vertical target spectrum.

2.9 Modal Pushover Based Scaling

Kalkan and Chopra (2011) proposed the modal pushover-based scaling method. In this method, ground motions are scaled by using an inelastic single degree of freedom system. Firstly, force deformation relationship is obtained for the system by using the first mode pushover analysis. After that scale factors are determined such that peak deformation obtained from nonlinear time history analysis and pushover analysis are almost the same.

Kalkan and Chopra (2011) in their study compared the ASCE 7-05 ground motion scaling method and modal pushover-based scaling method on six buildings and two bridges and made the following conclusions.

- The scatter of the engineering demand parameters is much smaller in the modal pushover-based scaling method.
- The median results of ground motions scaled with modal pushover analysis is much closer to the results.

2.10 An Alternative Target Spectrum: Conditional Mean Spectrum

The uniform hazard spectrum which is used by most of the design code is constructed for a determined possibility of exceedance by using the maximum spectral acceleration values at all periods. The uniform hazard spectrum is constructed by using the probabilistic seismic hazard analysis. Bommer and Sarma (2000) states that it is impossible for these spectral accelerations to occur at a single event.

Baker (2011) proposed an alternative method for uniform hazard spectrum. In this method spectral accelerations are conditioned at a user defined period rather than all periods. By doing so ground motions selected with this target spectrum, it is ensured that the selected ground motion will represent the properties of the site under consideration. An example of conditional mean spectrum for period value of 2.6 is given in Figure 2.5.

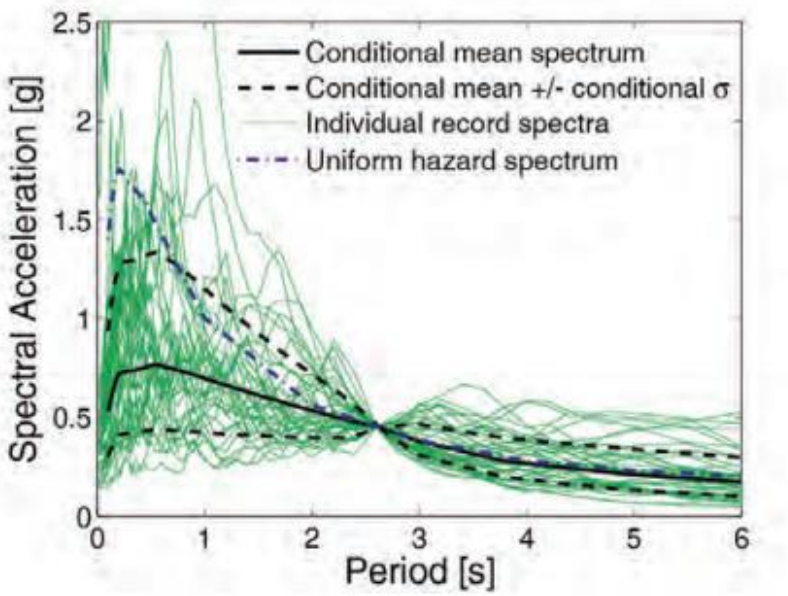

Figure 2.5. Example of Conditional Mean Spectrum (NIST, 2011)

CHAPTER 3

DESCRIPTION OF SELECTED BUILDINGS

In this chapter, two buildings that are designed within the context of this study will be introduced. The information on the geometry of buildings, materials used, loads and design criteria of the buildings will be mentioned.

3.1 Geometry of Buildings

The buildings both studied have a symmetrical orthogonal load bearing system and are concrete moment resisting frame type structures with four and nine storeys height. These buildings are planned to be used as residential units.

3.1.1 Geometry of the Nine Story Building

The nine storey building has a typical storey height of 3.5 meters and a total height 31.5 meters. The building has two spans with a length of 6 meters, two spans with a length of 7 meters and one span with a length of 8 meters in X direction. The total length of the building in X direction is 34 meters. In Y direction the building has four spans each with a length of 5 meters and with a total length 20 meters. The building have two consoles. The one located on X direction has a 2 meters length and the one in Y direction has a 2.5 meters length. Sizes of the columns used in stories above the fourth floor are decreased due to changes in the axial loads. The typical floor plan of the building is given in Figure 3.1.

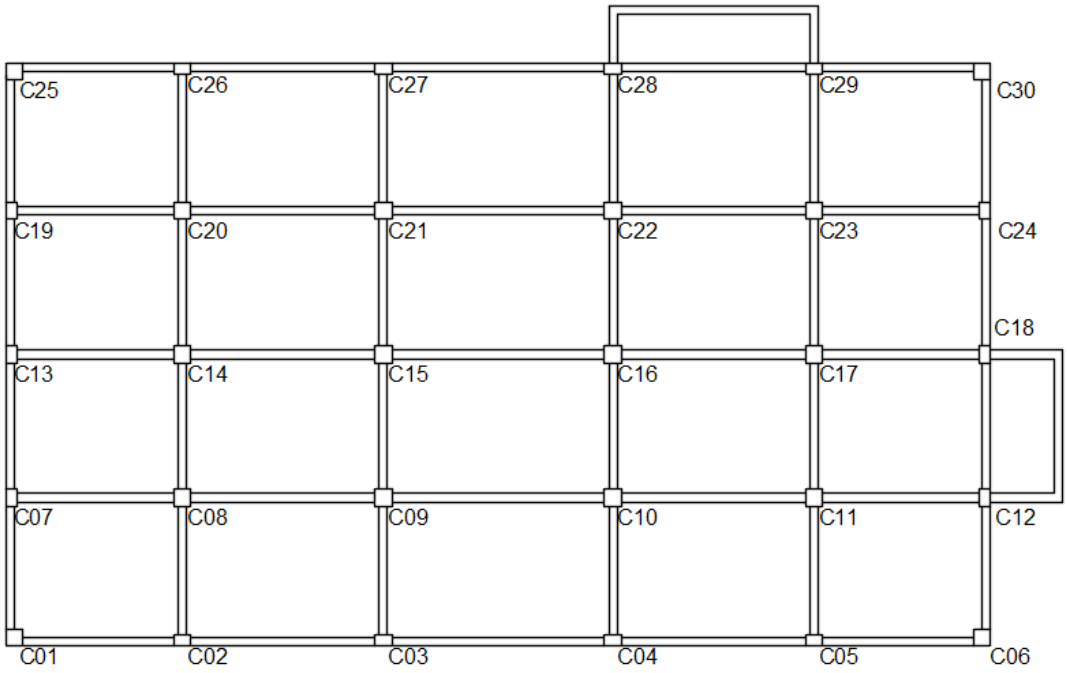

Figure 3.1. Typical Floor Plan Building with Nine Stories

3.1.2 Geometry of the Four-Story Building

The four storey building has a typical storey height of 3 meters. Total height of the building is 12 meters. The building has ten spans each with a length of 3.6 meters yielding a total length of 36 meters in X direction. In Y direction, the building is composed of two exterior spans with 6.7 meters length and one interior span with a 3.6 meters length. The total length in this direction is 17 meters. The building has two consoles. The one located on X direction has a 2.5 meters length and the one in Y direction has a 2 meters length. Since the building is a low rise building and tributary areas of the columns used in the building are similar, a uniform size of column is used along the building. Typical floor plan is given in Figure 3.2.

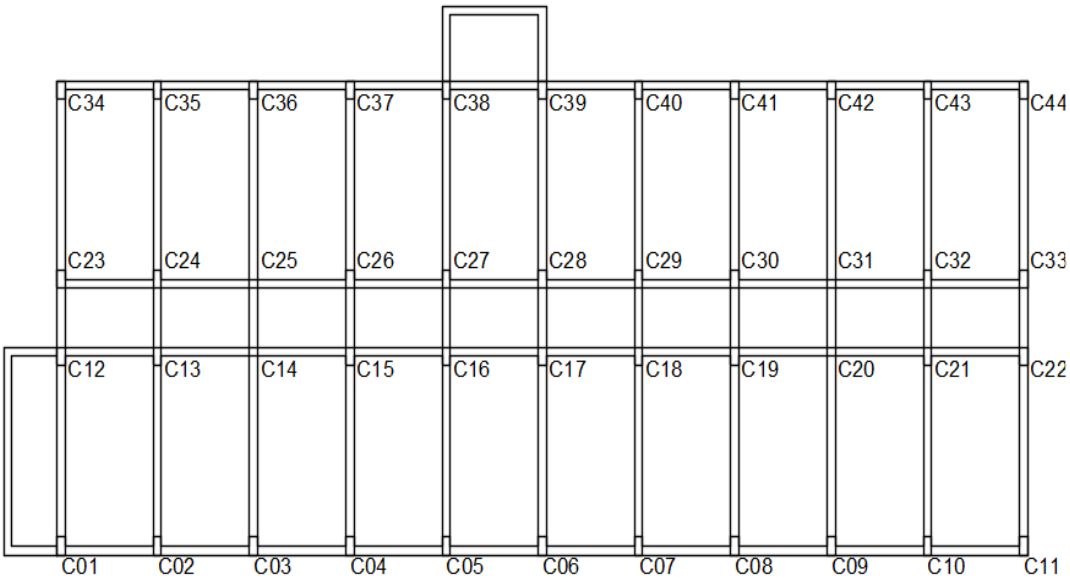

Figure 3.2. Typical Floor Plan Building with Four Stories

3.2 Structural Materials of the Selected Buildings

In this part properties of structural materials used in the buildings will be explained. In both of the buildings, C30 concrete grade is used. Properties of C30 concrete are given in Table 3.1.

Table 3.1. Properties of C30 Concrete

Property Definition	Formula	Value
Compressive Strength, f_{ck}	-	30 MPa
Tension Strength, f_{ctk}	$0.35\sqrt{f_{ck}}$	1.92 MPa
Design Compressive Strength, f_{cd}	$\frac{f_{ck}}{\Upsilon_c}$	20 MPa
Design Tension Strength, f_{ctd}	$\frac{f_{ctk}}{\Upsilon_c}$	1.28 MPa
Elasticity Modulus	$3250\sqrt{f_{ck}} + 14000$	31800 MPa

S420 grade reinforcement steel is used in the buildings. Mechanical properties of S420 reinforcement type are given in Table 3.2.

Table 3.2. Properties of S420 Reinforcement

Property Definition	Formula	Value
Yield Strength, f_y	-	420 MPa
Design Yield Strength, f_{yd}	$\frac{f_y}{\Upsilon_s}$	365 MPa
Ultimate Strength, f_u	(1.15 – 1.35)f_y	~ 520 MPa
Ultimate Strain	-	0.08
Elasticity Modulus	-	200 000 MPa

3.3 Horizontal Seismic Load

The buildings are designed according to the most recent Turkish Seismic Code (2018). The earthquake design level is selected as DD-2 which has a return period of 475 years. The building is assumed to be located on a hypothetical site at Marmara region of the Turkey. These hypothetical locations are selected near the Gölcük, Kocaeli. Seismicity parameters used in the design spectra is determined from seismic hazard maps published in the website of AFAD (https://tdth.afad.gov.tr/TDTH/main.xhtml).

3.3.1 Horizontal Elastic Design Spectrum

Horizontal elastic design spectra of the buildings are calculated as described in provision 2.3.4 of Turkish Seismic Code (2018). The formulation of horizontal elastic spectrum is given in Equation 3.1:

$S_{AE}(T) = (0.4 + 0.6\ T / T_A)\ S_{DS}$ $0 \leq T \leq T_A$

$S_{AE}(T) = S_{DS}$ $T_A \leq T \leq T_B$

$S_{AE}(T) = S_{D1} / T$ $T_B \leq T \leq T_L$

$S_{AE}(T) = S_{D1}\ T_L / T^2$ $T_B \leq T \leq T_L$

$T_A = 0.2\ (S_{D1} / S_{DS})$

$T_B = S_{D1} / S_{DS}$ $T_L = 6$ s (3.1)

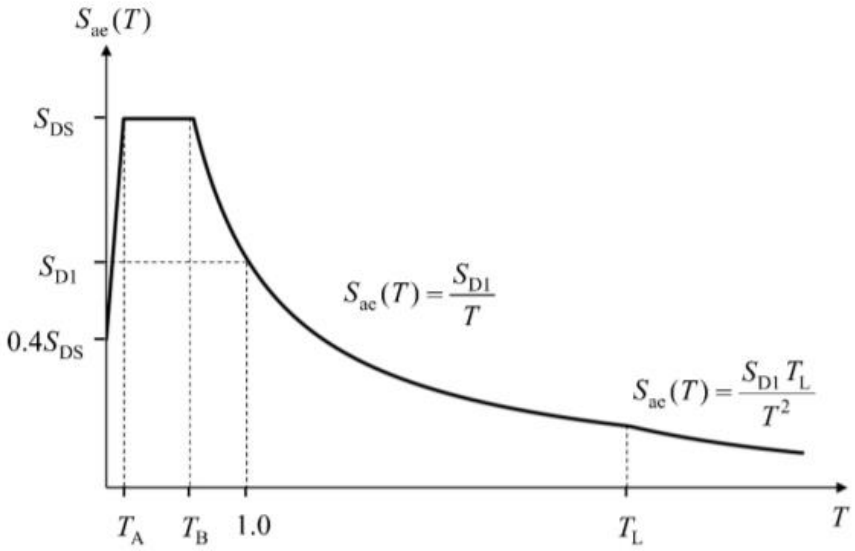

Figure 3.3. Horizontal Elastic Design Spectrum (Figure 2.1 of TBSC (2018))

The building with nine stories is planned to be constructed on soil type C. The horizontal elastic design spectrum of the building is given in Figure 3.4

$S_{DS} = 0.953g$ and $S_{D1} = 0.315g$

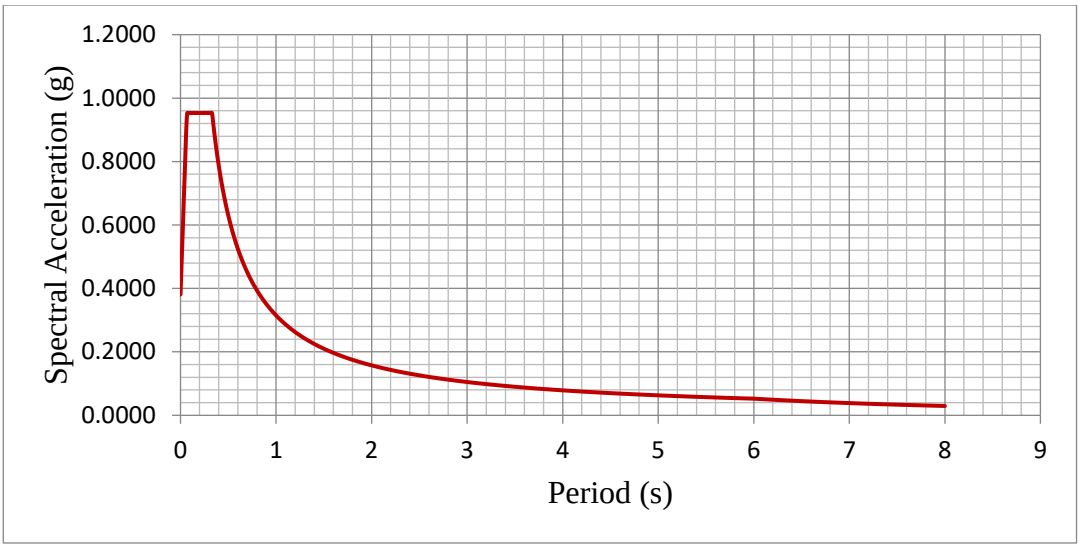

Figure 3.4. Horizontal Elastic Design Spectrum of Nine Story Building

The building with four stories is planned to be constructed on soil type D. Horizontal elastic design spectrum of the building is given in Figure 3.5. The design spectral accelerations are computed as follow; S_{DS} = 0.635g and S_{D1}= 0.349g

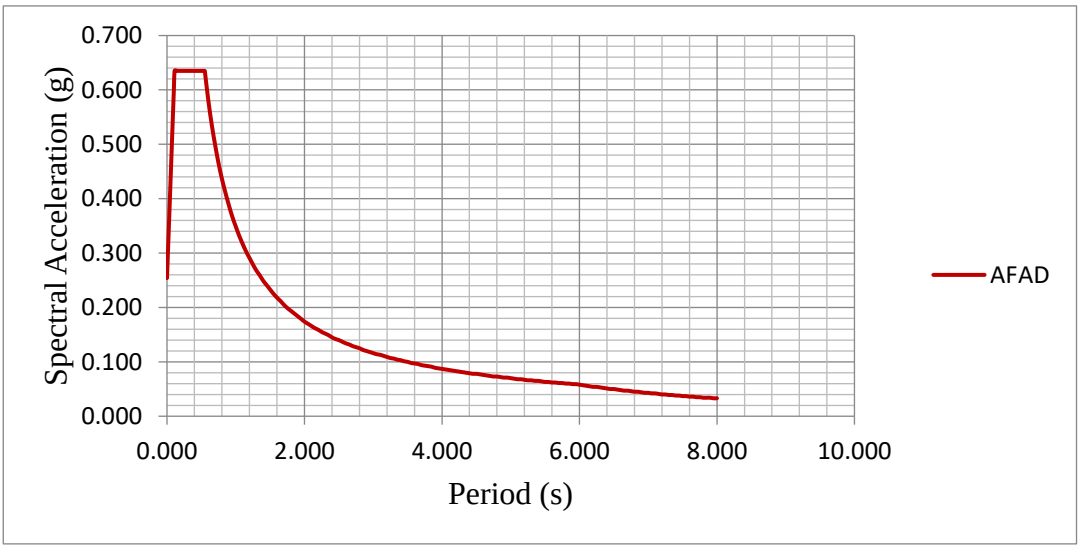

Figure 3.5. Horizontal Elastic Spectrum of Four-Story Building

3.3.2 Building Occupancy Category

Building occupancy category is determined from Table 3.1 of Turkish Seismic Code (2018) and both of the studied buildings are assumed to be BKS = 3. Explanation of building occupancy categories are given in Table 3.3.

Table 3.3. Building Occupancy Category Table (Table 3.3 of TBSC 2018)

Building Occupancy Category	Usage of Building	Building Importance Factor (I)
BKS = 1	Buildings that need to be used after an earthquake, Buildings which are densely populated for a long time Buildings which are used as safe deposit a) Buildings that need to be used after an earthquake (Hospitals, Fire Stations, PTT and other telecommunication facilities, Terminals, Power stations, Municipality buildings and so on. b) Schools and other educational buildings, dormitories, military posts and prisons c) Museums d) Building used to store toxic and explosive things	1.5
BKS = 2	Buildings which are densely populated for a short time Shopping Centers, Sport facilities, Cinema and theatre halls and so on	1.2
BKS = 3	Other Buildings	1.0

3.3.3 Earthquake Design Class

Earthquake design class is determined by using short period spectral acceleration values for DD-2 Earthquake Ground Motion Level and building occupancy category from Table 3.2 of Turkish Seismic Code (2018). The earthquake design class is used for determination of design methods. Earthquake design classes are explained in Table 3.4.

Table 3.4. Earthquake Design Classes (Table 3.2 of TBSC 2018)

Short Period Design Spectral Acceleration Value (S_{DS})	Building Occupancy Category	
	BKS = 1	BKS = 2, 3
$S_{DS} \leq 0.33$	EDC = 4a	EDC = 4
$0.33 < S_{DS} \leq 0.50$	EDC = 3a	EDC = 3
$0.50 < S_{DS} \leq 0.75$	EDC = 2a	EDC = 2
$0.75 < S_{DS}$	EDC = 1a	EDC = 1

By using Table 3.4, earthquake design class of nine story building is determined as EDC = 1 and building with four story as EDC = 2. The earthquake design classes will be used in determination of design methodology and building height class.

3.3.4 Building Height Class

Building height classes are determined from Table 3.3 of Turkish Seismic Code (2018) by using building heights and earthquake design class of the studied buildings. As mentioned in the beginning of this chapter, the height of the building with nine stories is 31.5 m and height of the building with four stories is 12 m. By using these height and earthquake design classes of the buildings, the height class of the building with nine stories is determined as BYS = 4 and building with four stories as BYS = 6. The details of building height classes are given in Table 3.5.

Table 3.5. Building Height Class Table (Table 3.3 of TBSC 2018)

Building Height Class	Building Height Range for Building Height Classes		
	EDC= 1, 1a, 2, 2a	EDC= 3, 3a	EDC= 4, 4a
BYS = 1	$H_N > 70$	$H_N > 91$	$H_N > 105$
BYS = 2	$56< H_N <70$	$70<H_N<91$	$91<H_N<105$
BYS = 3	$42< H_N <56$	$56<HN<70$	$56<H_N<91$
BYS = 4	$28< H_N <42$	$42< H_N <56$	
BYS = 5	$17.5< H_N <27$	$28< H_N <42$	
BYS = 6	$10.5< H_N <17.5$	$17.5< H_N <28$	
BYS = 7	$7< H_N <10.5$	$10.5< H_N <17.5$	
BYS = 8	$H_N<7$	$H_N <10.5$	

3.3.5 Response Modification Factor and Overstrength Factor

In linear elastic design of the buildings response modification factor is used to take into account nonlinear behavior of structural elements and energy dissipated by these deformations. Response modification factor and overstrength factors are determined by the using load carrying system of a building and building height class from Table 4.1 of Turkish Seismic Code (2018). The response modification factor for the studied buildings is selected to be 8 and the overstrength factor for the studied buildings are selected as 3. The details of response modification factor and overstrength factor are given in Table 3.6.

Table 3.6. Response Modification and Overstrength Factors (Table 4.1 of TBSC 2018)

Load Bearing System	Response Modification Factor (R)	Over Strength Factor (D)	Building Height Class
A. Cast in Place Concrete Structures			
A1. High Ductile Systems			
A11. Buildings that resist earthquake loads by concrete moment resisting frames	8	3	BYS ≥ 3
A12. Buildings that resist earthquake loads by coupled shear walls	7	2.5	BYS ≥ 2
A13. Buildings that resist earthquake loads by solid shear walls	6	2.5	BYS ≥ 2
A14. Building that resist earthquake loads by combined system of coupled shear walls and moment resisting frames	8	2.5	BYS ≥ 2
A15. Building that resist earthquake loads by combined system of solid shear walls and moment resisting frames	7	2.5	BYS ≥ 2

3.3.6 Seismic Load Reduction Factor

Seismic load reduction factor for the studied building is calculated by using Equation 3.2. Via this factor and horizontal elastic design spectrum, inelastic response spectrum is calculated. The inelastic response spectra are given in Figure 3.6 and 3.7 respectively for building with 9 and 4 stories.

$$R_a(T) = R / I \qquad T > T_B$$

$$R_a(T) = D + (R / I - D)\, T / T_B \qquad T \leq T_B \qquad (3.2)$$

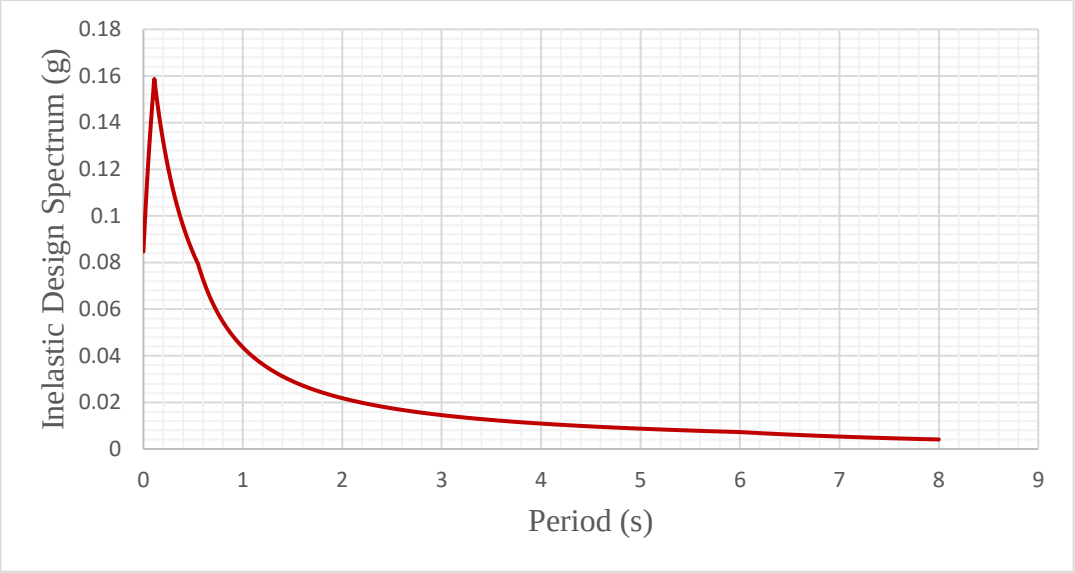

Figure 3.6. Inelastic Design Spectrum of Four-Story Building

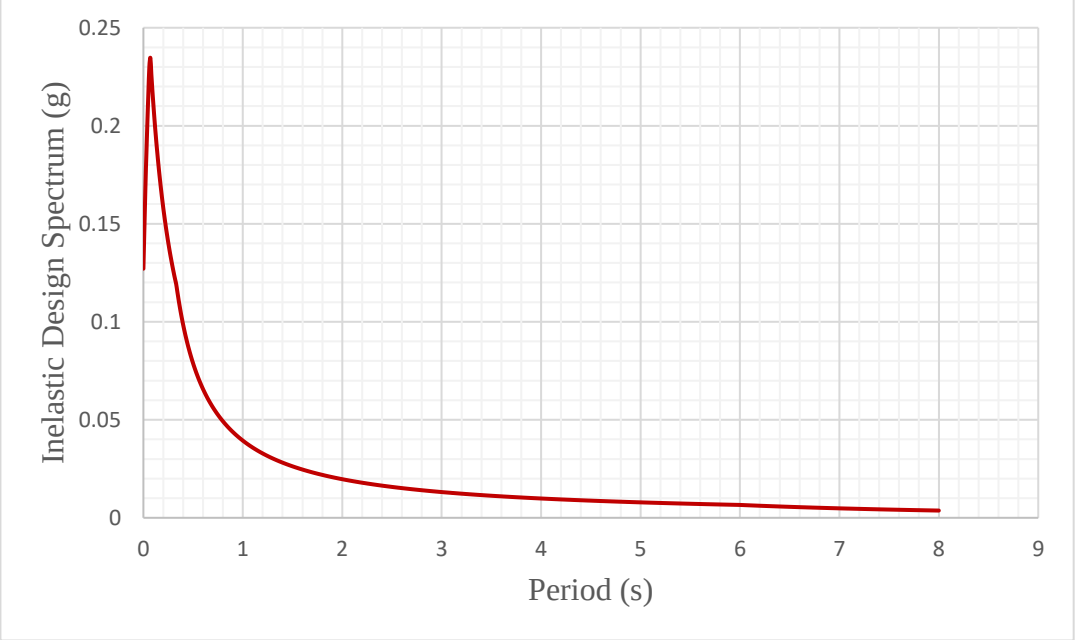

Figure 3.7. Inelastic Design Spectrum of Nine Story Building

3.3.7 Effective Section Rigidity Factor

Elastic design of the buildings is performed with the help of a models created on ETABS (COMPUTERS AND STRUCTURES, INC version 19.1.0). Models of the buildings are created by using cracked section properties. Cracked section properties are obtained by effective rigidity factors given in Table 4.2 of Turkish Seismic Code (2018). The effective rigidity factors are given in Table 3.7.

Table 3.7. Effective Rigidity Factors (Table 4.2 of TBSC 2018)

Load Bearing Member	**Effective Rigidty Factor**	
Wall – Slab (In Plane)	**Axial**	**Shear**
Shear Wall	0.50	0.50
Basement Wall	0.80	0.50
Slab	0.25	0.25
Wall – Slab (Out of Plane)	**Bending**	**Shear**
Shear Wall	0.25	1.00
Basement Wall	0.50	1.00
Slab	0.25	1.00
Frame Member	**Bending**	**Shear**
Coupling Beam	0.15	1.00
Beam Frame	0.35	1.00
Column Frame	0.70	1.00
Equivalent Frame for Shear Wall	0.50	0.50

3.4 Vertical Seismic Load Calculation

Vertical seismic loads are calculated according to provision 4.4.3 of Turkish Seismic Code (2018).

Vertical seismic loads are calculated with Equation 3.3 since none of the special cases expressed in the code exists;

- Beams spanning 20 m or more
- Console beams spanning 5 m or more
- Columns supported by beams
- Inclined columns

$$E_{d\,(Z)} = (2/3)\, S_{DS}\, G \qquad (3.3)$$

3.5 Slab Thickness

Slab thickness of the studied building determined with Equation 11.1 of TS 500 (2000).

$$h > \frac{l_{sn}}{15+\frac{20}{m}}\left[1-\frac{\alpha_s}{4}\right] \qquad (3.4)$$

where l_{sn}, m, α_s respectively refers to span length of slab, ratio of slab dimensions and ratio of continuous edge of slabs to total edges.

Slab thickness is determined as 150 mm for building with four stories and 200 mm for building with nine stories.

3.6 Beam Dimensions

Beam dimensions are selected according to provision 7.4.1 of Turkish Seismic Code (2018) in which it is stated that height of a beam should be at least three times slab height and width of a beam should be at least 250 mm.

Beam dimensions in the building with nine stories are selected such that beam width is 300 mm and beam height 600 mm. Beam width in the building with four stories is 300 mm and beam height is 500 mm. Detailing of beams has been done such that confinement zones with a length of two times beam height are created at each end of the beams.

3.7 Column Dimensions

Column dimensions in the studied buildings are selected depending on the axial load level of columns. Also, column dimensions are controlled to satisfy deflection limits set in Turkish Seismic Code (2018).

Axial load level on columns is checked with Equation 3.5 (Equation 7.7 TS 500 – 2000) and Equation 3.6.

$$A_c \geq N_{dm} / (0.9\, f_{cd}) \quad (3.5)$$

$$A_c \geq N_d / (0.4\, f_{cd}) \quad (3.6)$$

where N_{dm} is design axial load obtained from combinations excluding earthquake loads and N_d is design axial load obtained from combinations with earthquake load.

As explained in the first part of this chapter, in buildings with four stories, tributary areas of columns are similar to each other; in other words, axial load level is similar in columns. Thus, one type of column is used and dimensions of it are 500 mm x 500 mm.

In the building with nine stories, by considering axial load levels and deflection limits four types of columns used and column dimensions are decreased after the

fourth floor. As a result, eight type of column dimensions are used. Location of types on plan shown in Figure 3.8 and dimension of types are given in Table 3.8.

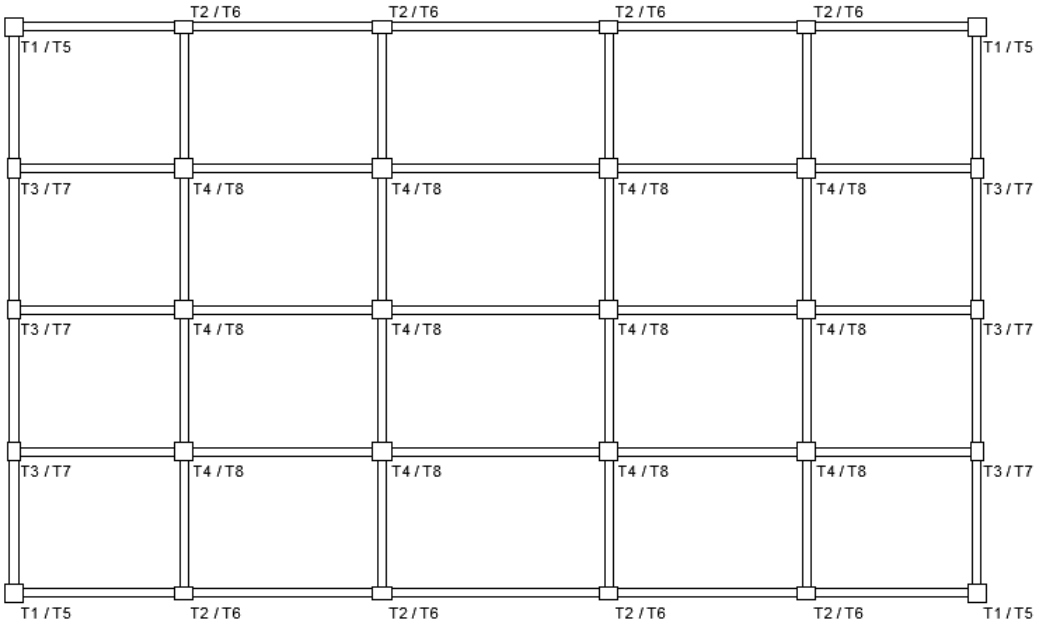

Figure 3.8. Location of Column Types

Table 3.8. Column Dimensions

Column Type	Width (mm)	Height (mm)
T1	650	650
T2	450	650
T3	650	450
T4	650	650
T5	550	550
T6	400	550
T7	550	400
T8	550	550

CHAPTER 4

GROUND MOTION SELECTION

Enhancements in computer technology and numerical methods have given engineers a chance to simulate effects of earthquakes on structures by using nonlinear time history analysis. However, nonlinear time history analysis involves several uncertainties such as nonlinear modeling technique, selection of material models, ground motion selection and so on. These uncertainties must be taken care of in detail to properly imitate the seismic hazard and behavior of structures. Kwon and Elnashi (2006) have shown in their study among aforementioned uncertainties, ground motion selection is the one that needs to be done very carefully to correctly simulate the seismic behavior.

The effect of vertical ground motion on structures has been disregarded in general. Nevertheless, recent studies have shown that the vertical component of a ground motion has a valuable effect on structures, especially long span structures. Keskin, E. (2020) in his study conducted a series of nonlinear time history analysis both by considering vertical ground motion and by disregarding. That study has indicated that inclusion of vertical ground motion significantly changes axial load on columns and it changes interstory drift ratio and story shear forces in a considerable amount. In light of these, the vertical component of ground motion is included in the ground motion selection procedure.

In literature there are many methods to select ground motions. In this study, the method proposed by Kwong and Chopra (2020) is used which includes the vertical ground motion in selection procedure. In the following parts, application of the method will be explained.

4.1 Construction of the Ground Motion Database

As a first step in the ground motion selection procedure, two ground motion databases are constructed for soil classes C and D. PEER NGAWest2 (https://ngawest2.berkeley.edu/) ground motion database is used for this purpose.

In ground motion selection there are several alternatives for fault mechanisms such as normal fault, strike slip fault and so on. In construction of ground motion databases, fault mechanism is specified as strike slip since it is the most common fault type in Turkey leading to multiple devastating earthquakes. In the strike slip fault mechanism, movement occurs in the vertical plane. In other words, this type of fault is the result of horizontal movement.

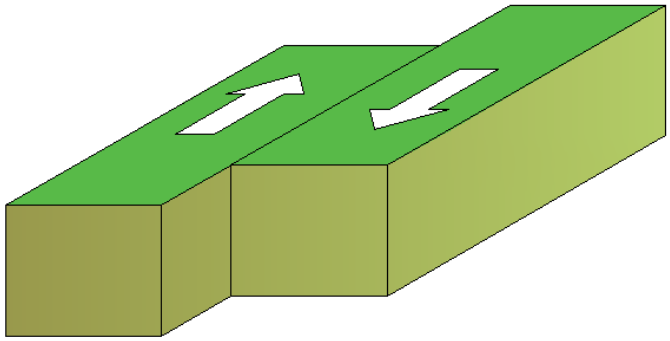

Figure 4.1. Illustration of Strike Slip Fault Mechanism

The second filter applied to construct the ground motion database is the moment magnitude of an earthquake. Moment magnitude scale is an objective scale related to the seismic energy release during an earthquake. In this study, ground motions are selected so that they have the minimum magnitude of 5.

The final filter applied is Joyner-Boore distance (R_{JB}) which is the shortest horizontal distance measured from surface projection to the site. Earthquakes are selected such that Joyner-Boore distance of them is between 10 km and 30 km. The R_{JB} values less than 10 km are not selected herein in order to eliminate near fault effects of earthquakes.

4.2 Scaling of Ground Motions

Ground motions are scaled as explained according to provisions specified in Turkish Seismic Code (2018) as explained in the Chapter 2. Initially, horizontal and vertical target spectra at a selected hypothetical site in Marmara region are obtained from the website of AFAD (Disaster and Emergency Management Presidency) which publishes seismic hazard maps of Turkey.

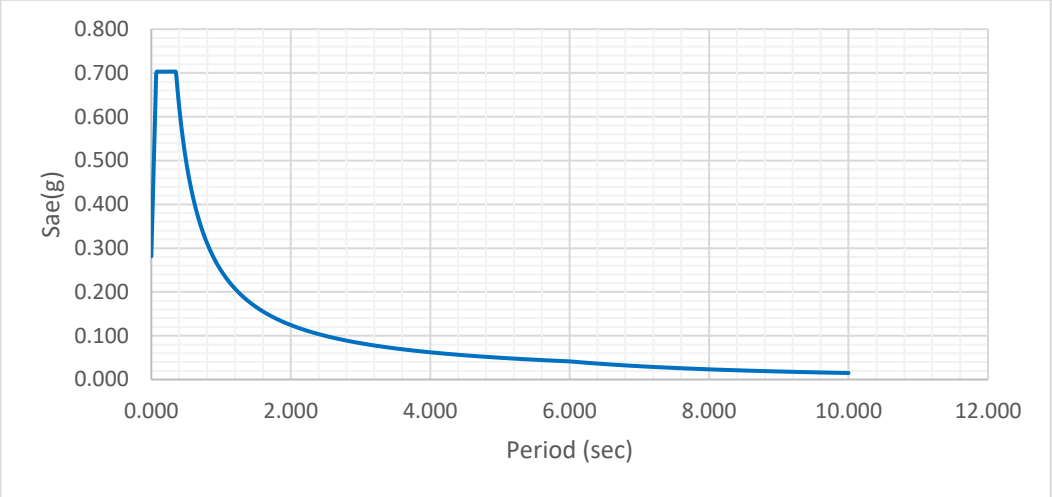

Figure 4.2. Horizontal Elastic Design Spectrum

After obtaining horizontal and vertical elastic spectra for each soil type and earthquake design classes, response spectra of each ground motion in the databases is obtained.

The next step applied in scaling of ground motion is to determine scaling factors. Scaling factors are determined according to Turkish Seismic Code (2018) division 2.5.2. Ground motion scaling factors are selected such that the SRSS combination of the response spectra of a ground motion in the databases is at least thirty percent higher than the elastic spectrum given in Turkish Seismic Code (2018).

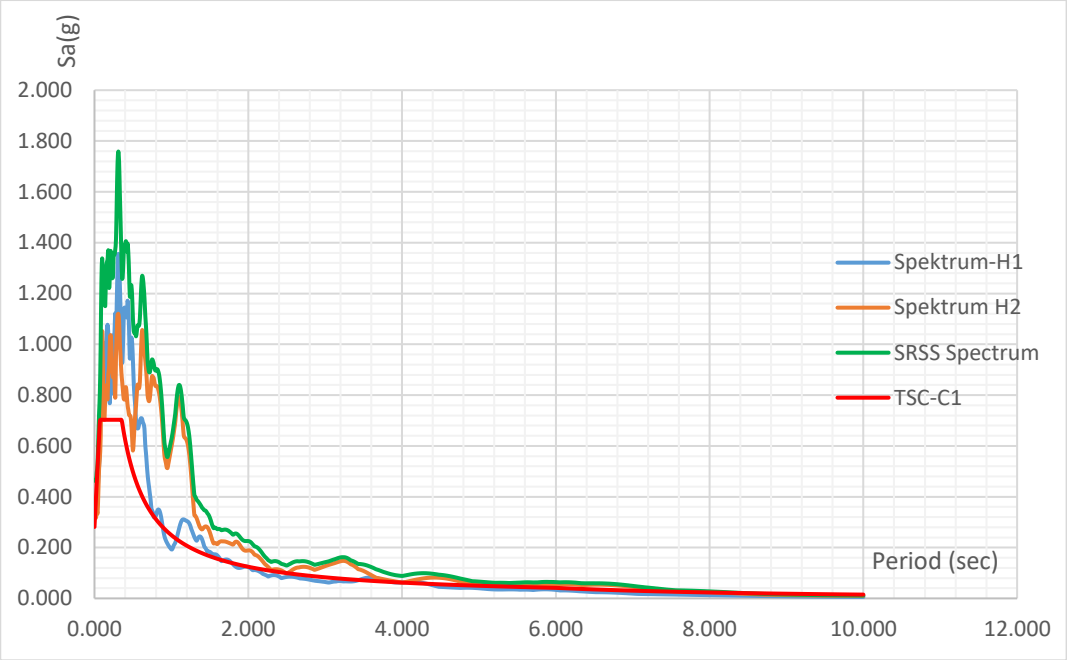

Figure 4.3. Example of a Scaled Ground Motion for Soil Type C and EDC 1

By conducting the procedure explained above, horizontal and vertical ground motion scaling factors for each ground motion in the databases are obtained for each soil type and earthquake design classes.

4.3 Identification of Error Index

In this part of the ground motion selection procedure, the standardized error between scaled spectrum of candidate ground motions and target spectrum is computed. The representation of this computation is given in the following figure.

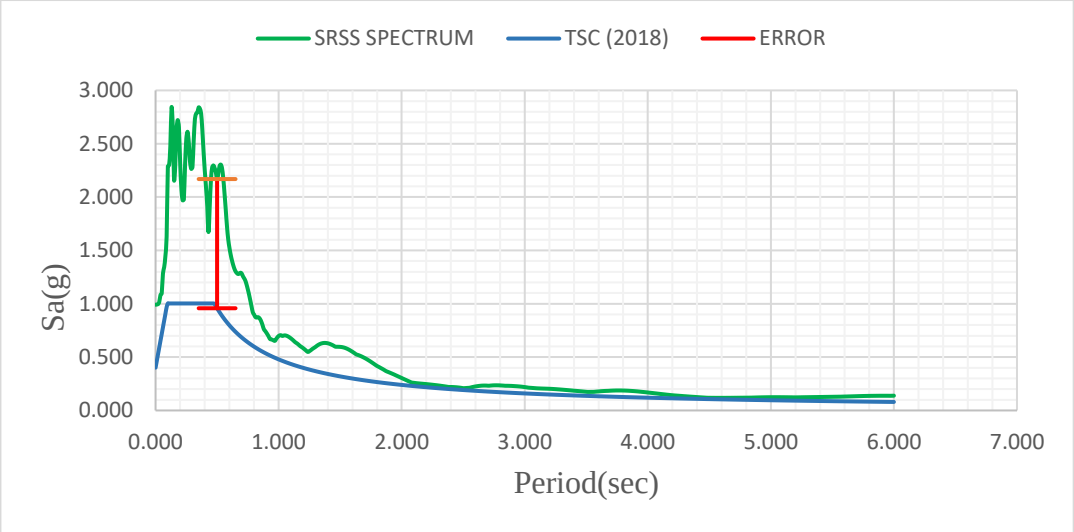

Figure 4.4. Illustration of Error

In literature there are many alternatives to use as an error index. Sum of the squared errors is the most common error index used in literature. Another common error index is calculated by logarithmic summation of the differences and it has been adopted in this study. Formulation of this type of index is as given in Equation 4.1.

$$SSD_K = \sum_{J=1}^{N_k} (\ln [SF_k x\, A_{k,0}(T_j)] - In[A_{k,TS}(T_j)])^2 \qquad (2.1)$$

In Equation 2.1 SF_k stands for scaling factor, $A_{k,0}$ is the spectral acceleration of corresponding period for ground motion and $A_{k,TS}$ is the spectral acceleration value of target spectrum.

The error index is calculated for each ground motion in the databases for both horizontal and vertical direction.

4.4 Error Index Combination

The error index is calculated for horizontal and vertical components seperately. To combine these indices and to obtain a single error index, weight function given in Equation 2.2 is used.

$$SSD_{combined} = w_H SSD_H + (1 - w_H) SSD_V \qquad (2.2)$$

It is accepted that internal forces caused by the horizontal components of ground motions are more pronounced than internal forces caused by the vertical components of ground motions. Thus, w_H is selected as 0.6, 0.7, 0.8 and 0.9. Finally, ground motions with minimum error index for each weight is determined and ground motions that are commonly existing in each weight scenarios are selected.

In the following tables, detailed information on ground motions selected for each soil type and earthquake design class are given.

Table 4.1. Ground Motions Selected for Soil Type C and EDC 1

Peer Id	Event	Year	Station	M_w	R_{JB}	$V_{s(30)}$	PGA
33	Parkfield	1966	Temblor pre-1969	6,2	16,0	528	0.45
164	Imperial Valley-06	1979	Cerro Prieto	6,5	15,2	472	0.23
210	Livermore-01	1980	APEEL 3E Hayward CSUH	5,8	29,2	517	0.09
237	Mammoth Lakes-03	1980	Long Valley Dam (Downst)	5,9	10,3	537	0.13
238	Mammoth Lakes-03	1980	Long Valley Dam (L Abut)	5,9	10,3	537	0.12
318	Westmorland	1981	Superstition Mtn Camera	5,9	19,3	362	0.13
454	Morgan Hill	1984	Gilroy - Gavilan Coll.	6,2	14,8	730	0.15
543	Chalfant Valley-01	1986	Benton	5,8	24,3	371	0.08
552	Chalfant Valley-02	1986	Lake Crowley - Shehorn Res.	6,2	22,1	457	0.19
1148	Kocaeli, Turkey	1999	Arcelik	7,5	10,6	523	0.25
6057	Big Bear-01	1992	Highland Fire Station	6,5	26,2	362	0.20

Table 4.2. Ground Motions Selected for Soil Type C and EDC 2

Peer Id	Event	Year	Station	M_w	R_{JB}	$V_{s(30)}$	PGA
33	Parkfield	1966	Temblor pre-1969	6,2	16,0	528	0.45
164	Imperial Valley-06	1979	Cerro Prieto	6,5	15,2	472	0.23
237	Mammoth Lakes-03	1980	Long Valley Dam (Downst)	5,9	10,3	537	0.13
238	Mammoth Lakes-03	1980	Long Valley Dam (L Abut)	5,9	10,3	537	0.12
318	Westmorland	1981	Superstition Mtn Camera	5,9	19,3	362	0.13
454	Morgan Hill	1984	Gilroy - Gavilan Coll.	6,19	14,8	730	0.15
543	Chalfant Valley-01	1986	Benton	5,77	24,3	371	0.08
552	Chalfant Valley-02	1986	Lake Crowley - Shehorn Res.	6,19	22,1	457	0.19
1148	Kocaeli, Turkey	1999	Arcelik	7,5	10,6	523	0.25
1614	Duzce, Turkey	1999	Lamont 1061	7,1	11,5	481	0.17
6057	Big Bear-01	1992	Highland Fire Station	6,5	26,2	362	0.20

Table 4.3. Ground Motions Selected for Soil Type C and EDC 3

Peer Id	Event	Year	Station	M_w	R_{JB}	$V_{s(30)}$	PGA
33	Parkfield	1966	Temblor pre-1969	6,2	16,0	528	0.45
164	Imperial Valley-06	1979	Cerro Prieto	6,5	15,2	472	0.23
210	Livermore-01	1980	APEEL 3E Hayward CSUH	5,8	29,2	517	0.09
237	Mammoth Lakes-03	1980	Long Valley Dam (Downst)	5,9	10,3	537	0.13
238	Mammoth Lakes-03	1980	Long Valley Dam (L Abut)	5,9	10,3	537	0.12
318	Westmorland	1981	Superstition Mtn Camera	5,9	19,3	362	0.13
552	Chalfant Valley-02	1986	Lake Crowley - Shehorn Res.	6,2	22,1	457	0.19
1148	Kocaeli, Turkey	1999	Arcelik	7,5	10,6	523	0.25
1633	Manjil, Iran	1990	Abbar	7,4	12,6	724	0.72
6057	Big Bear-01	1992	Highland Fire Station	6,5	26,2	362	0.20
6059	Big Bear-01	1992	Morongo Valley Fire Station	6,5	28,0	396	0.19

Table 4.4. Ground Motions Selected for Soil Type C and EDC 4

Peer Id	Event	Year	Station	M_w	R_{JB}	$V_{s(30)}$	PGA
33	Parkfield	1966	Temblor pre-1969	6,2	16,0	528	0.45
164	Imperial Valley-06	1979	Cerro Prieto	6,5	15,2	472	0.23
237	Mammoth Lakes-03	1980	Long Valley Dam (Downst)	5,9	10,3	537	0.13
238	Mammoth Lakes-03	1980	Long Valley Dam (L Abut)	5,9	10,3	537	0.12
318	Westmorland	1981	Superstition Mtn Camera	5,9	19,3	362	0.13
543	Chalfant Valley-01	1986	Benton	5,8	24,3	371	0.08
552	Chalfant Valley-02	1986	Lake Crowley - Shehorn Res.	6,2	22,1	457	0.19
1148	Kocaeli, Turkey	1999	Arcelik	7,5	10,6	523	0.25
1633	Manjil, Iran	1990	Abbar	7,4	12,6	724	0.72
4137	Parkfield-02, CA	2004	Parkfield - Vineyard Cany 6W	6,0	13,3	392	0.15
6057	Big Bear-01	1992	Highland Fire Station	6,5	26,2	362	0.20

Table 4.5. Ground Motions Selected for Soil Type D and EDC 1

Peer Id	Event	Year	Station	M_w	R_{JB}	$V_{s(30)}$	PGA
10	Imperial Valley-03	1951	El Centro Array #9	5,6	24,6	213	0.04
31	Parkfield	1966	Cholame - Shandon Array #8	6,2	12,9	257	0.37
167	Imperial Valley-06	1979	Compuertas	6,5	13,5	260	0.24
266	Victoria, Mexico	1980	Chihuahua	6,3	18,5	242	0.18
314	Westmorland	1981	Brawley Airport	5,9	15,3	209	0.23
848	Landers	1992	Coolwater	7,3	19,7	353	0.51
850	Landers	1992	Desert Hot Springs	7,3	21,8	359	0.23
1158	Kocaeli, Turkey	1999	Duzce	7,5	13,6	282	0.48
1602	Duzce, Turkey	1999	Bolu	7,1	12,0	294	1.09
1748	Northwest China-01	1997	Jiashi	5,9	24,1	240	0.36
4125	Parkfield-02, CA	2004	Parkfield - Gold Hill 6W	6,0	15,5	232	0.14

Table 4.6. Ground Motions Selected for Soil Type D and EDC 2

Peer Id	Event	Year	Station	M_w	R_{JB}	$V_{s(30)}$	PGA
31	Parkfield	1966	Cholame - Shandon Array #8	6,2	12,9	257	0.37
167	Imperial Valley-06	1979	Compuertas	6,5	13,5	260	0.24
266	Victoria, Mexico	1980	Chihuahua	6,3	18,5	242	0.18
458	Morgan Hill	1984	Gilroy Array #4	6,2	11,5	222	0.42
848	Landers	1992	Coolwater	7,3	19,7	353	0.51
850	Landers	1992	Desert Hot Springs	7,3	21,8	359	0.23
900	Landers	1992	Yermo Fire Station	7,3	23,6	354	0.29
1158	Kocaeli, Turkey	1999	Duzce	7,5	13,6	282	0.48
1602	Duzce, Turkey	1999	Bolu	7,1	12,0	294	1.09
1748	Northwest China-01	1997	Jiashi	5,9	24,1	240	0.36
4125	Parkfield-02, CA	2004	Parkfield - Gold Hill 6W	6,0	15,5	232	0.14

Table 4.7. Ground Motions Selected for Soil Type D and EDC 3

Peer Id	Event	Year	Station	M_w	R_{JB}	$V_{s(30)}$	PGA
31	Parkfield	1966	Cholame - Shandon Array #8	6,2	12,9	257	0.37
167	Imperial Valley-06	1979	Compuertas	6,5	13,5	260	0.24
266	Victoria, Mexico	1980	Chihuahua	6,3	18,5	242	0.18
458	Morgan Hill	1984	Gilroy Array #4	6,2	11,5	222	0.42
848	Landers	1992	Coolwater	7,3	19,7	353	0.51
850	Landers	1992	Desert Hot Springs	7,3	21,8	359	0.23
900	Landers	1992	Yermo Fire Station	7,3	23,6	354	0.29
1158	Kocaeli, Turkey	1999	Duzce	7,5	13,6	282	0.48
1602	Duzce, Turkey	1999	Bolu	7,1	12,0	294	1.09
1748	Northwest China-01	1997	Jiashi	5,9	24,1	240	0.36
4125	Parkfield-02, CA	2004	Parkfield - Gold Hill 6W	6,0	15,5	232	0.14

Table 4.8. Ground Motions Selected for Soil Type D and EDC 4

Peer Id	Event	Year	Station	M_w	R_{JB}	$V_{s(30)}$	PGA
31	Parkfield	1966	Cholame - Shandon Array #8	6,2	12,9	257	0.37
167	Imperial Valley-06	1979	Compuertas	6,5	13,5	260	0.24
266	Victoria, Mexico	1980	Chihuahua	6,3	18,5	242	0.18
458	Morgan Hill	1984	Gilroy Array #4	6,2	11,5	222	0.23
848	Landers	1992	Coolwater	7,3	19,7	353	0.51
850	Landers	1992	Desert Hot Springs	7,3	21,8	359	0.23
900	Landers	1992	Yermo Fire Station	7,3	23,6	354	0.29
1158	Kocaeli, Turkey	1999	Duzce	7,5	13,6	282	0.48
1602	Duzce, Turkey	1999	Bolu	7,1	12,0	294	1.09
1748	Northwest China-01	1997	Jiashi	5,9	24,1	240	0.36
4125	Parkfield-02, CA	2004	Parkfield - Gold Hill 6W	6,0	15,5	232	0.14

4.5 Scaling of the Selected Ground Motions

The selected ground motions are scaled by using the ground motion scaling procedure specified in Turkish Seismic Code (2018). The horizontal and natural vibration period of the buildings are given in Table 4.9.

Table 4.9. Natural Vibration Period of Case Study Buildings

Building with	$T_{Horizontal}$ (s)	$T_{Vertical}$ (s)
Four Stories	0.67	0.112
Nine Stories	1.95	0.166

Horizontal and vertical target spectra for Soil Class C are as given in Figure 4.5, 4.6 and for soil class D in Figure 4.7 and 4.8.

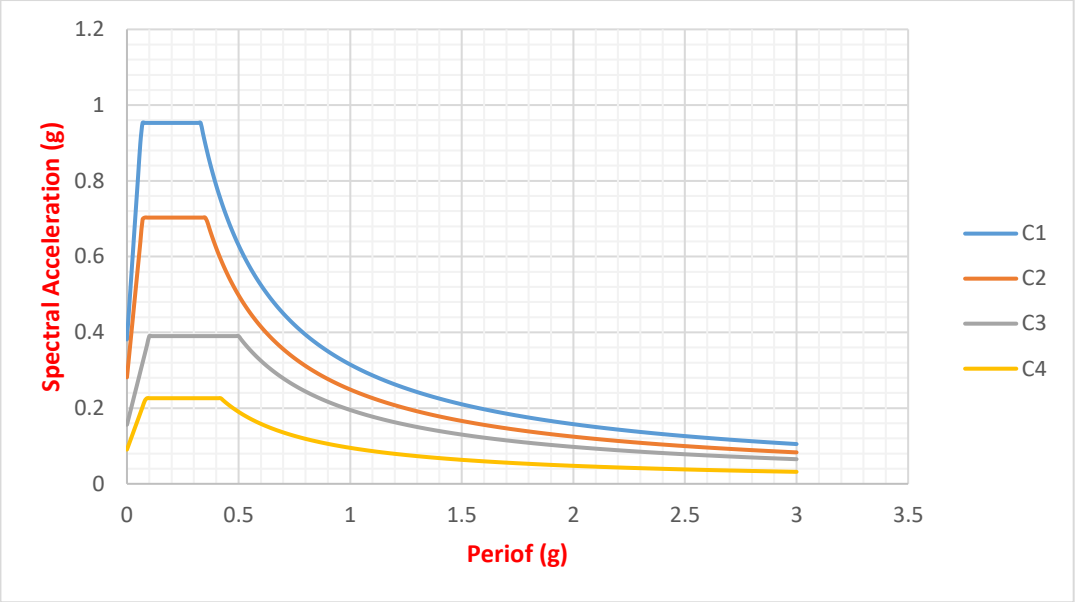

Figure 4.5. Horizontal Target Spectra for Soil Class C

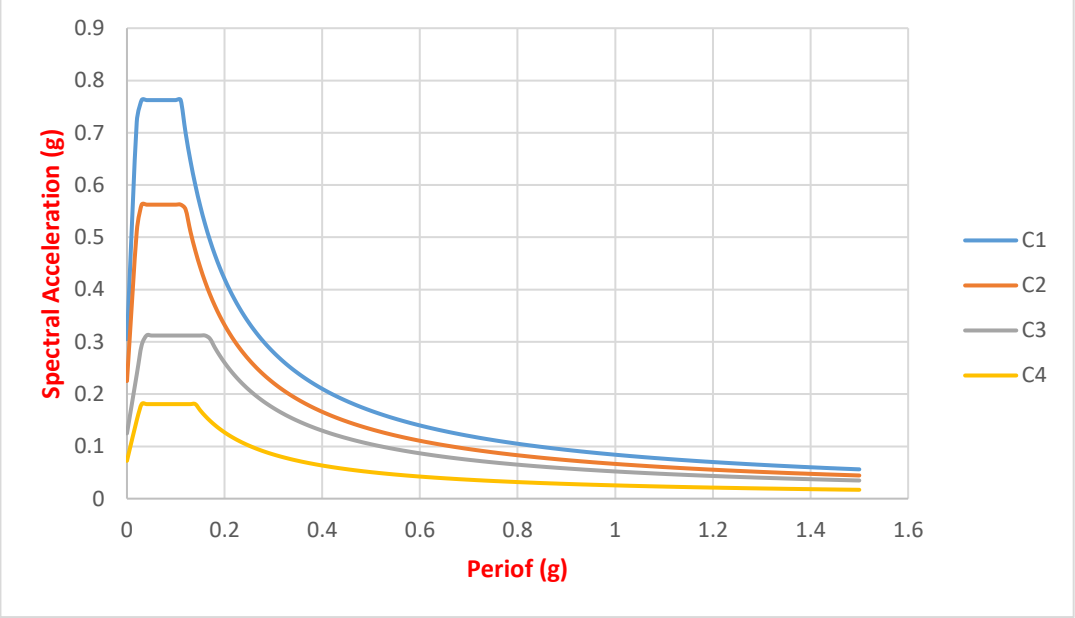

Figure 4.6. Vertical Target Spectra for Soil Class C

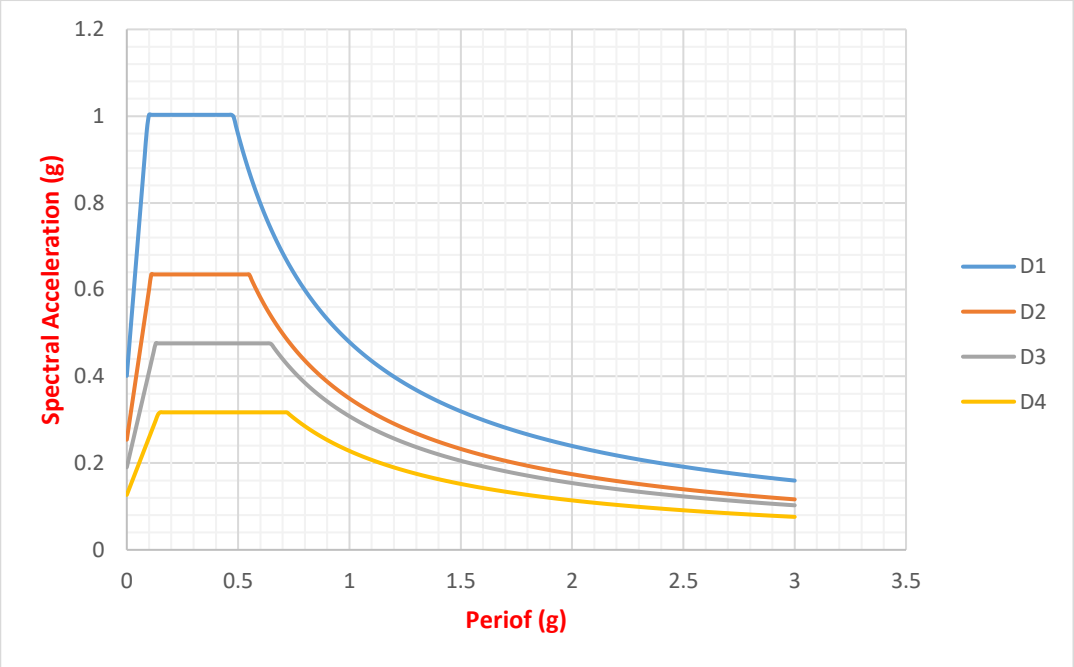

Figure 4.7. Horizontal Target Spectra for Soil Class D

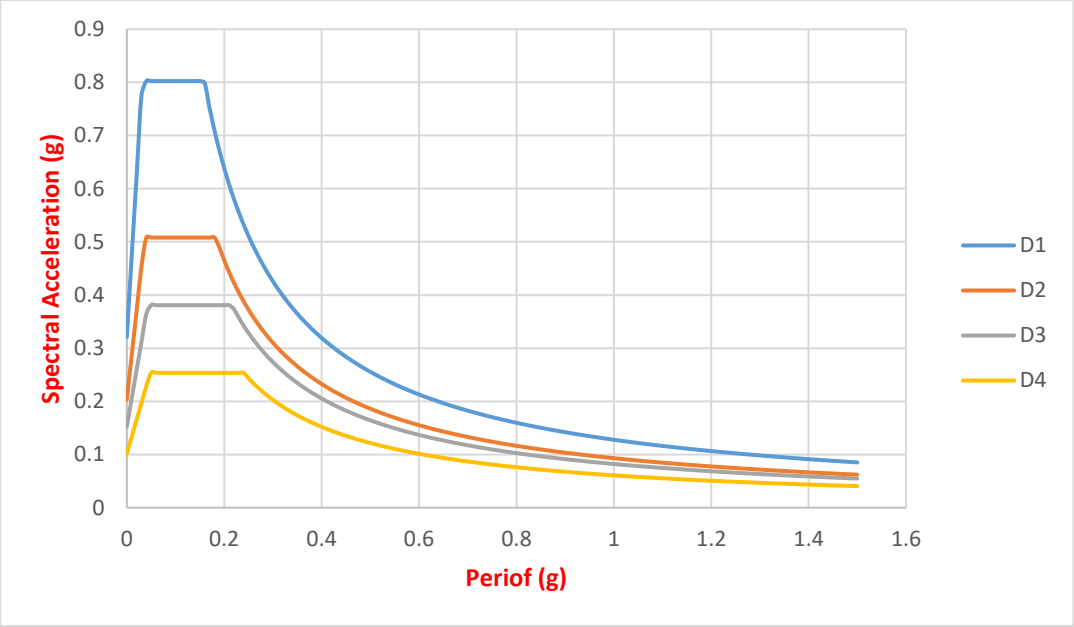

Figure 4.8. Vertical Target Spectra for Soil Class D

The horizontal and vertical scale factors for the selected ground motions are given in the following tables.

Table 4.10. Ground Motions Scale Factor for Soil Type C and EDC 1

Peer Id	Event	Year	Station	SCF_{hor}	SCF_{ver}
33	Parkfield	1966	Temblor pre-1969	3.049	5.247
164	Imperial Valley-06	1979	Cerro Prieto	2.149	2.901
210	Livermore-01	1980	APEEL 3E Hayward CSUH	12.448	37.557
237	Mammoth Lakes-03	1980	Long Valley Dam (Downst)	6.288	7.467
238	Mammoth Lakes-03	1980	Long Valley Dam (L Abut)	5.474	7.563
318	Westmorland	1981	Superstition Mtn Camera	8.156	12.198
454	Morgan Hill	1984	Gilroy - Gavilan Coll.	18.806	5.677
543	Chalfant Valley-01	1986	Benton	11.925	17.607
552	Chalfant Valley-02	1986	Lake Crowley - Shehorn Res.	9.001	7.836
1148	Kocaeli, Turkey	1999	Arcelik	2.979	4.663
6057	Big Bear-01	1992	Highland Fire Station	6.222	6.901

Table 4.11. Ground Motions Scale Factor for Soil Type C and EDC 2

Peer Id	Event	Year	Station	SCF_{hor}	SCF_{ver}
33	Parkfield	1966	Temblor pre-1969	2.410	3.871
164	Imperial Valley-06	1979	Cerro Prieto	1.699	2.14
237	Mammoth Lakes-03	1980	Long Valley Dam (Downst)	4.971	5.508
238	Mammoth Lakes-03	1980	Long Valley Dam (L Abut)	4.327	5.579
318	Westmorland	1981	Superstition Mtn Camera	6.447	8.998
454	Morgan Hill	1984	Gilroy - Gavilan Coll.	14.865	4.188
543	Chalfant Valley-01	1986	Benton	9.427	12.989
552	Chalfant Valley-02	1986	Lake Crowley - Shehorn Res.	7.115	5.78
1148	Kocaeli, Turkey	1999	Arcelik	2.355	3.44
1614	Duzce, Turkey	1999	Lamont 1061	3.609	9.145
6057	Big Bear-01	1992	Highland Fire Station	4.919	5.094

Table 4.12. Ground Motions Scale Factor for Soil Type C and EDC 3

Peer Id	Event	Year	Station	SCF_{hor}	SCF_{ver}
33	Parkfield	1966	Temblor pre-1969	1.772	2.029
164	Imperial Valley-06	1979	Cerro Prieto	1.248	1.116
210	Livermore-01	1980	APEEL 3E Hayward CSUH	7.235	15.369
237	Mammoth Lakes-03	1980	Long Valley Dam (Downst)	3.655	2.889
238	Mammoth Lakes-03	1980	Long Valley Dam (L Abut)	3.182	2.91
318	Westmorland	1981	Superstition Mtn Camera	4.740	4.692
552	Chalfant Valley-02	1986	Lake Crowley - Shehorn Res.	5.232	3.155
1148	Kocaeli, Turkey	1999	Arcelik	1.636	1.908
1633	Manjil, Iran	1990	Abbar	0.459	0.528
6057	Big Bear-01	1992	Highland Fire Station	3.616	2.657
6059	Big Bear-01	1992	Morongo Valley Fire Station	1.168	1.229

Table 4.13. Ground Motions Scale Factor for Soil Type C and EDC 4

Peer Id	Event	Year	Station	SCF_{hor}	SCF_{ver}
33	Parkfield	1966	Temblor pre-1969	0.851	1.244
164	Imperial Valley-06	1979	Cerro Prieto	0.600	0.688
237	Mammoth Lakes-03	1980	Long Valley Dam (Downst)	1.757	1.771
238	Mammoth Lakes-03	1980	Long Valley Dam (L Abut)	1.530	1.794
318	Westmorland	1981	Superstition Mtn Camera	2.279	2.893
543	Chalfant Valley-01	1986	Benton	3.332	4.176
552	Chalfant Valley-02	1986	Lake Crowley - Shehorn Res.	2.515	1.858
1148	Kocaeli, Turkey	1999	Arcelik	0.832	1.106
1633	Manjil, Iran	1990	Abbar	0.221	0.306
4137	Parkfield-02, CA	2004	Parkfield - Vineyard Cany 6W	1.687	1.245
6057	Big Bear-01	1992	Highland Fire Station	1.738	1.638

Table 4.14. Ground Motions Scale Factor for Soil Type D and EDC 1

Peer Id	Event	Year	Station	SCF_{hor}	SCF_{ver}
10	Imperial Valley-03	1951	El Centro Array #9	11.516	48.713
31	Parkfield	1966	Cholame - Shandon Array #8	2.767	4.481
167	Imperial Valley-06	1979	Compuertas	3.686	7.234
266	Victoria, Mexico	1980	Chihuahua	2.602	6.782
314	Westmorland	1981	Brawley Airport	3.418	6.522
848	Landers	1992	Coolwater	1.126	3.306
850	Landers	1992	Desert Hot Springs	2.420	3.974
1158	Kocaeli, Turkey	1999	Duzce	1.136	2.937
1602	Duzce, Turkey	1999	Bolu	0.617	2.812
1748	Northwest China-01	1997	Jiashi	3.123	3.109
4125	Parkfield-02, CA	2004	Parkfield - Gold Hill 6W	11.667	6.350

Table 4.15. Ground Motions Scale Factor for Soil Type D and EDC 2

Peer Id	Event	Year	Station	SCF_{hor}	SCF_{ver}
31	Parkfield	1966	Cholame - Shandon Array #8	2.212	3.003
167	Imperial Valley-06	1979	Compuertas	2.947	4.689
266	Victoria, Mexico	1980	Chihuahua	1.808	3.711
458	Morgan Hill	1984	Gilroy Array #4	1.199	0.734
848	Landers	1992	Coolwater	0.810	1.809
850	Landers	1992	Desert Hot Springs	1.682	2.357
900	Landers	1992	Yermo Fire Station	1.204	2.824
1158	Kocaeli, Turkey	1999	Duzce	0.790	1.607
1602	Duzce, Turkey	1999	Bolu	0.429	1.550
1748	Northwest China-01	1997	Jiashi	2.497	2.082
4125	Parkfield-02, CA	2004	Parkfield - Gold Hill 6W	9.328	4.096

Table 4.16. Ground Motions Scale Factor for Soil Type D and EDC 3

Peer Id	Event	Year	Station	SCF_{hor}	SCF_{ver}
31	Parkfield	1966	Cholame - Shandon Array #8	2.063	2.174
167	Imperial Valley-06	1979	Compuertas	2.801	3.394
266	Victoria, Mexico	1980	Chihuahua	1.459	2.463
458	Morgan Hill	1984	Gilroy Array #4	1.140	0.532
848	Landers	1992	Coolwater	0.769	1.220
850	Landers	1992	Desert Hot Springs	1.363	1.630
900	Landers	1992	Yermo Fire Station	0.972	1.955
1158	Kocaeli, Turkey	1999	Duzce	0.637	1.067
1602	Duzce, Turkey	1999	Bolu	0.347	1.046
1748	Northwest China-01	1997	Jiashi	2.373	1.508
4125	Parkfield-02, CA	2004	Parkfield - Gold Hill 6W	8.865	2.966

Table 4.17. Ground Motions Scale Factor for Soil Type D and EDC 4

Peer Id	Event	Year	Station	SCF_{hor}	SCF_{ver}
31	Parkfield	1966	Cholame - Shandon Array #8	1.549	1.437
167	Imperial Valley-06	1979	Compuertas	2.180	2.421
266	Victoria, Mexico	1980	Chihuahua	1.032	1.546
458	Morgan Hill	1984	Gilroy Array #4	2.021	1.486
848	Landers	1992	Coolwater	0.599	0.759
850	Landers	1992	Desert Hot Springs	1.007	1.015
900	Landers	1992	Yermo Fire Station	0.677	1.217
1158	Kocaeli, Turkey	1999	Duzce	0.443	0.669
1602	Duzce, Turkey	1999	Bolu	0.243	0.663
1748	Northwest China-01	1997	Jiashi	0.753	0.997
4125	Parkfield-02, CA	2004	Parkfield - Gold Hill 6W	6.468	1.960

CHAPTER 5

NONLINEAR TIME HISTORY ANALYSES OF THE SELECTED BUILDINGS

In this chapter, modelling techniques and assumptions used to represent inelastic behavior of the building models are introduced. The buildings studied are modelled in Perform 3D (COMPUTERS AND STRUCTURES, INC version 8.0.0, 2021). While modelling the beams and columns, frame elements are used. Slabs of the buildings have not been included to speed up the analyses. The loads that will be transferred by slab to beams have been calculated by hand calculations and applied to the beams in the models. Since slabs do not exist in the models, rigid diaphragm constraints are applied in the model to represent slab behavior.

Among many other nonlinear modelling approaches lumped plasticity and distributed plasticity are the most commonly used modelling approaches. In the lumped plasticity approach, it is assumed that when an internal force reaches its plastic capacity, inelastic deformations occur uniformly over a finite length called plastic hinge zone. Length of the plastic hinge zone is accepted as half of the minimum dimension of an element. However, in the distributed plasticity approach it is assumed that the inelastic deformations occur distributedly. In other words, inelastic deformations vary in a section. Thus, it is necessary to divide a section into small parts called fibers and to assign a nonlinear material model to these small fibers.

In this study,the lumped plasticity approach is adopted since it is faster and easy to apply. Also, it is stated in provision 5.3.1 of Turkish Seismic Code (2018) lumped plasticity works well for elements that can be modeled as frames.

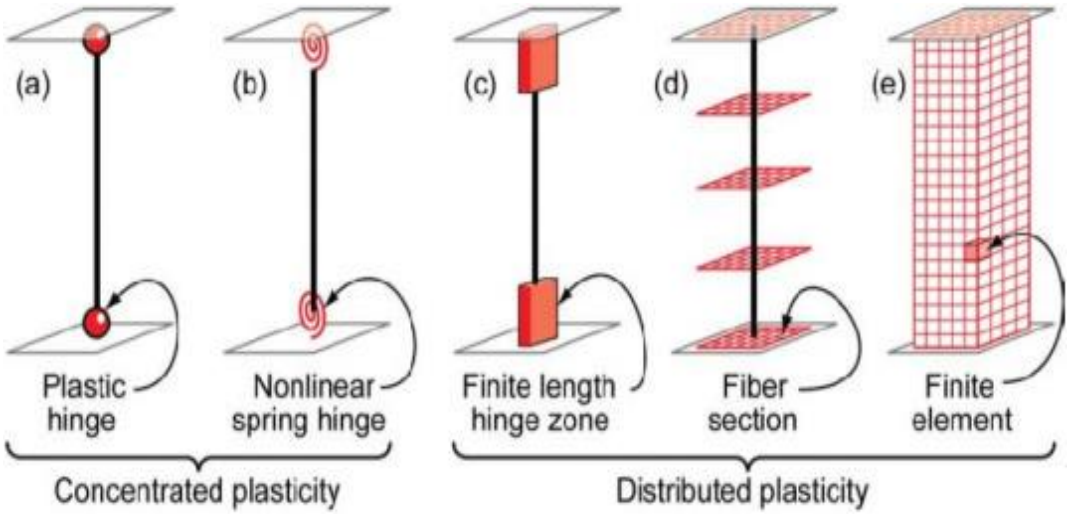

Figure 5.1.Illustartion of Plasticity Modelling Approaches (Tran and Nguyen,2020)

5.1 Material Models

In this part material models used for concrete and reinforcement are introduced.

5.1.1 Material Model for Concrete

In literature, there exists many concrete material models proposed by different academicians. Among many other alternatives, concrete model proposed by Mander (Mander and Park (1988)) is the most commonly used one and Turkish Seismic Code (2018) adopts the slightly modified version of this concrete model. In this study, the material model provided by Turkish Seismic Code (2018) is adopted. The formulation used in this model is given in Equation 5.1(Equation 5A.1 of TBSC (2018)). Sample material model is given in Figure 5.1.

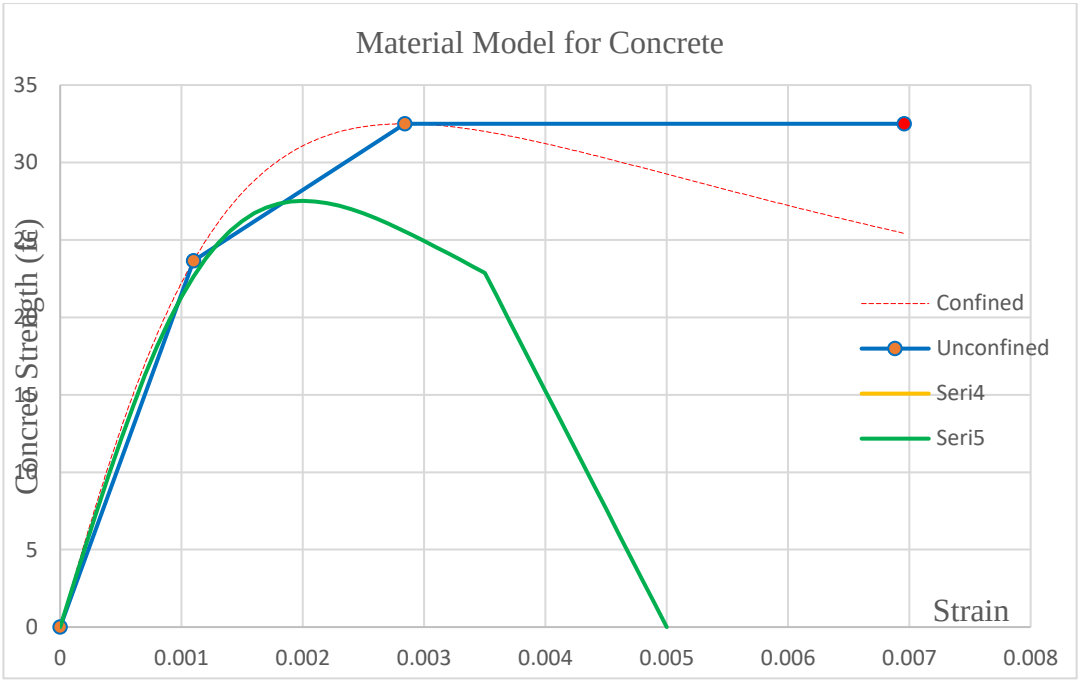

Figure 5.2. Material Model for Concrete

$$f_c = \frac{f_{cc}\, x\, r}{r - 1 + x} \qquad (5.1)$$

Where f_{cc} is the confined concrete strength which is calculated by Equation 5.2 (Equation 5A.2 of TBSC 2018) depending on unconfined concrete strength.

$$\mathbf{f_{cc} = \lambda_c\, f_{co}} \qquad (5.2)$$

In this equation λ_c is a parameter to take into account the confinement effect and calculated by Equation 5.3 (Equation 5A.2 of TBSC (2018)).

$$\lambda_c = 2.254 + \sqrt{1 + 7.94\frac{f_e}{f_{co}}} - \frac{2f_e}{f_{co}} - 1.254 \qquad (5.3)$$

In Equation 5.3, f_e represents the effective confinement pressure and it is calculated as the mean of X and Y direction. Effective confinement pressure for X and Y axis calculated according to Equation 5.4. (Equation 5A.3 of TBSC (2018))

$$f_{ex} = k_e \rho_x f_{yw} \qquad f_{ey} = k_e \rho_y f_{yw} \tag{5.4}$$

where f_{yw} is yield strength of stirrups and ρ is the volumetric ratio of stirrups and k_e is the factor for effective confinement and calculated according to Equation 5.5 (Equation 5A.4 of TBSC (2018))

$$k_e = \left(1 - \frac{\sum a_i^2}{6 b_o h_o}\right)\left(1 - \frac{s}{2 b_o h_o}\right)\left(1 - \frac{s}{2 b_o}\right)\left(1 - \frac{s}{2 h_o}\right)\left(1 - \frac{A_s}{b_o h_o}\right)^{-1} \tag{5.5}$$

where a_i is the distance between longitudinal reinforcement, b_o and h_o are the dimensions of confinement zones and A_s is the total longitudinal reinforcement area.

X parameters used in Equation 5.1 is calculated according to Equation 5.6 (Equation 5A.5 of TBSC 2018)

$$X = \frac{\varepsilon_C}{\varepsilon_{CC}} \tag{5.6}$$

where ε_c is a variable and ε_{cc} is calculated by Equation 5.7 (Equation 5A.5 of TBSC 2018)

$$\varepsilon_{cc} = 0.002\,[1 + 5(\lambda_c - 1)] \tag{5.7}$$

R parameter used in Equation 5.1 is calculated by Equation 5.8 (Equation 5A.6 of TBSC (2018))

$$r = \frac{E_c}{E_c - E_{sec}} \tag{5.8}$$

where E_c and E_{sec} are modulus of elasticity and secant modulus of elasticity respectively and they are calculated by Equation 5.9 (Equation 5A.6 of TSC (2018))

$$E_c = 5000\sqrt{f_{co}}\ \text{(MPa)} \qquad E_{sec} = \frac{f_{cc}}{\varepsilon_{cc}} \tag{5.9}$$

5.1.2 Material Model for Reinforcement Steel

Turkish Seismic Code (2018) gives a reinforcement model with strain hardening to be used in nonlinear analysis. It is calculated according to Equation 5.10 (Equation 5A.7 of TBSC 2018).

$$\begin{aligned} f_s &= E_s\varepsilon_s && \varepsilon_s \le \varepsilon_{sy} \\ f_s &= f_y && \varepsilon_{sy} < \varepsilon_s \le \varepsilon_{sh} \\ f_s &= f_{su} - \left(f_{su} - f_{sy}\right)\frac{(\varepsilon_{su} - \varepsilon_s)^2}{(\varepsilon_{su} - \varepsilon_{sh})^2} && \varepsilon_{sh} < \varepsilon_s \le \varepsilon_{su} \end{aligned} \tag{5.10}$$

Modulus of elasticity of reinforcement steel is taken as $2x10^5$ MPa. In Figure 5.2 the original material model for S420 grade reinforcement and the elastic perfectly plastic idealized version are given.

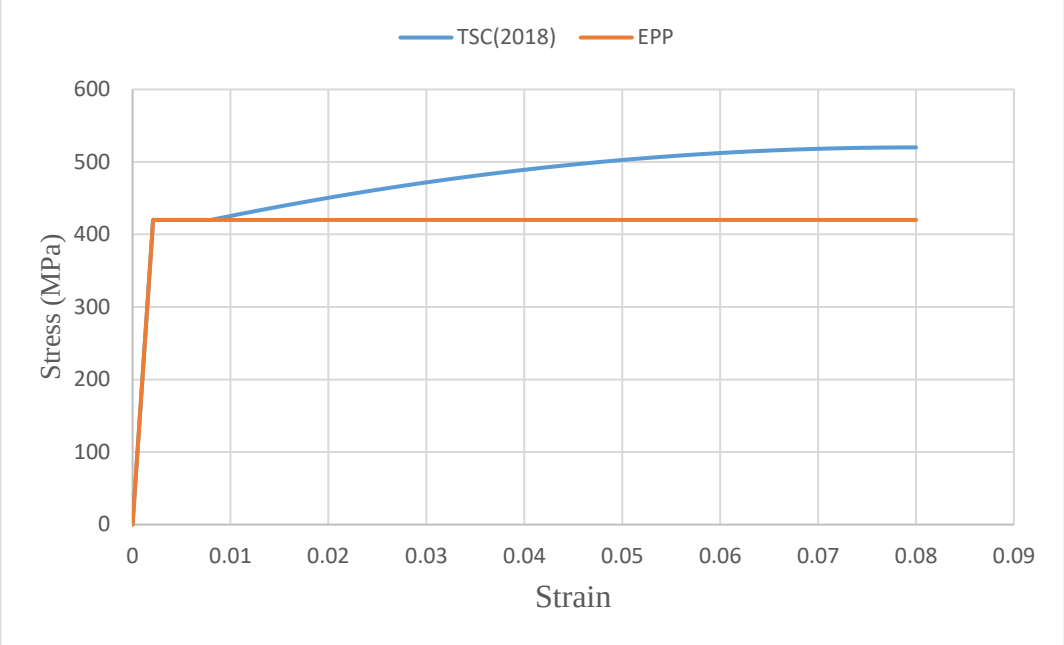

Figure 5.3. Reinforcement Steel Material Model

The parameter used in calculation of reinforcement steel material model is given in Table 5.1.

Table 5.1. Information About Reinforcement Steels

Grade	f_{sy} (MPa)	ε_{sy}	ε_{sh}	ε_{su}	f_{su} / f_{sy}
S220	220	0.0011	0.011	0.12	1.20
S420	420	0.0021	0.008	0.08	1.15-1.35
B420C	420	0.0021	0.008	0.08	1.15-1.35
B500C	500	0.0025	0.008	0.08	1.15-1.35

5.2 Beam Elements

Beam elements are modelled such that at the two ends of a beam plastic hinges are located to model inelastic behavior and in between them linear elastic elements are used. As a first step to model beams material models explained in the above section obtained by considering detailing of beams. Afterwards, moment rotation relationships for each type of beam are obtained. Then the moment rotation model is idealized by using a trilinear approximation method. In Figure 5.3, a sample moment rotation relationship for a beam is given.

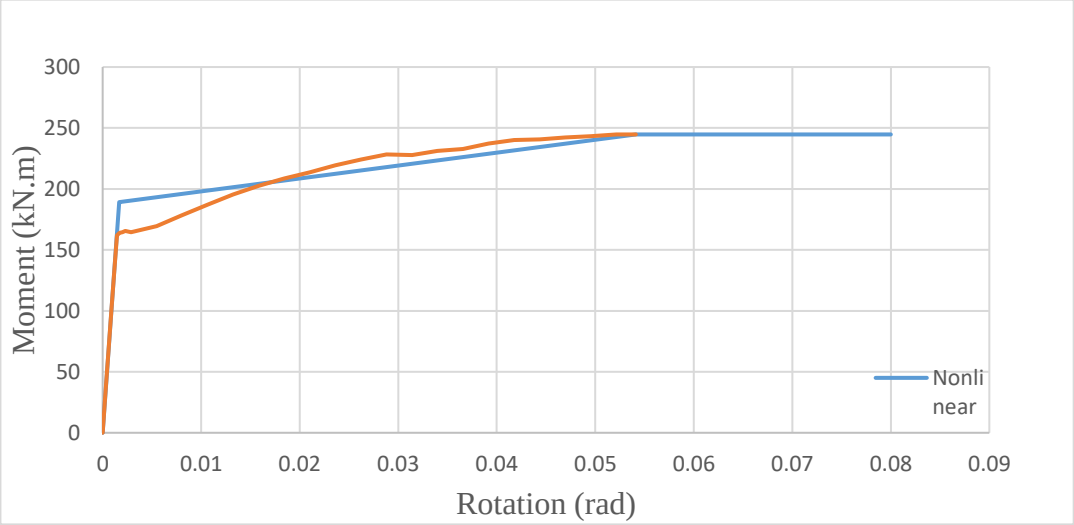

Figure 5.4. Moment Rotation Relationship for a Beam

The location of the plastic hinges has been selected according to provision 5.4.2.3 of Turkish Seismic Code (2018). In this provision, it is stated that plastic hinges can be placed next to beam column connection joints.

5.3 Column Elements

Column elements are also modeled as plastic hinges. However, in columns there is coupling between axial force and moments. Thus , PMM hinges will be used which is a coupled type of hinge. Location of the hinges will be similar to beam elements. In other words, hinges will be located next to beam column joints.

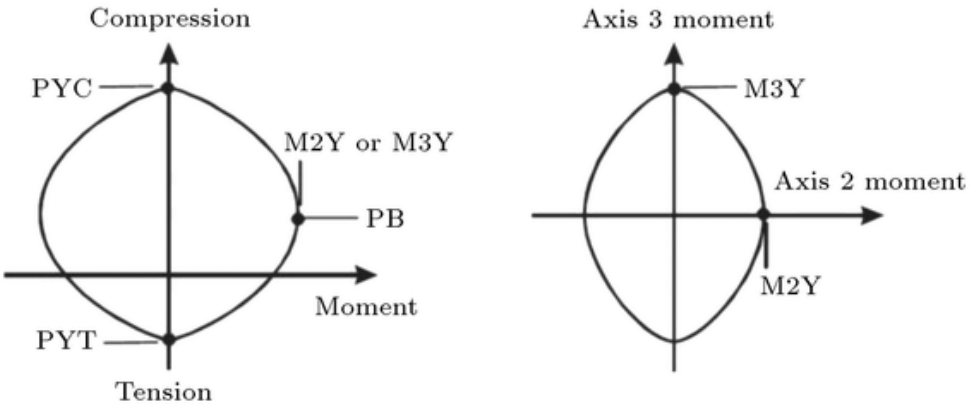

Figure 5.5. Yield Surface of a Column (Khaloo and Dehcheshmeh,2016)

Due to the existence of vertical ground motions, second order effects may be important and thus are taken into account in the analyses.

CHAPTER 6

ANALYSIS RESULTS

In this Chapter, two case study buildings located on two different soil classes were analyzed under the scaled ground motions. Each building was analyzed under 44 ground motions from four different earthquake design classes. The building with nine stories was investigated under the ground motions recorded on soil class C and the building with four stories was investigated under ground motion records from soil Class D.

For each ground motion in an earthquake design class, three different analyses were conducted. In the first scenario, the analyses are done by using the record of which horizontal and vertical components are scaled with the same scaling factor. In the second scenario, the analyses are conducted by using the records of which horizontal and vertical components are scaled with separate scaling factors. In the final scenario, the vertical components of ground motions were not included.

For each scenario defined in above paragraph two analyses were conducted by changing the orientation of the earthquake. In other words, in the first case the North-South component of ground motion is applied in the X direction of the building under consideration and in the second case the East-West component of ground motion is applied.

To sum up, for each building three methods, four earthquake design classes, eleven ground motions in each earthquake design class and two orientations are considered. Thus, for a building 264 time history analyses were conducted and in total 528 time history analyses were conducted. The summary of the analyses described above is given in Table 6.1.

Table 6.1. Number of Analyses for Different Scenarios

		Nine Story Building						Four Story Building					
		SC 1		SC 2		SC 3		SC 1		SC 2		SC3	
		NS	EW	NS	EW	NS	EW	NS	EW	NS	EW	NS	EW
Soil Class C	DC1	11	11	11	11	11	11						
	DC2	11	11	11	11	11	11						
	DC3	11	11	11	11	11	11						
	DC3	11	11	11	11	11	11						
Soil Class D	DC1							11	11	11	11	11	11
	DC2							11	11	11	11	11	11
	DC3							11	11	11	11	11	11
	DC4							11	11	11	11	11	11

Results obtained from time history analyses were investigated by using seven structural indicators. These indicators are as follows;

- Base shear
- Overturning moment
- Roof displacement
- Maximum drift
- Maximum axial force on the bottom floor
- Minimum axial force on the bottom floor
- Tip displacement of consoles in the buildings.

In Table 6.2, results are presented. The results obtained from Method 1 and Method 2 are presented as the ratio of results obtained from the analyses in which the vertical component of ground motions is disregarded. By presenting the results this way, it is possible to observe whether the indicator is affected by the vertical component of ground motions or not.

The ratio for base shear, overturning moment, roof displacement, maximum drift and tip displacement of the consoles is calculated as follows;

$$\text{Ratio} = \frac{Result(V+H)_{max}}{Result(H)_{max}} \qquad 6.1$$

The ratio for maximum and minimum axial force is calculated as follows;

$$\text{Ratio} = \frac{Result(V+H)_{max} - Result(H)_{max}}{Result(H)_{max}} \qquad 6.2$$

The analyses defined previous pages are firstly conducted on the same buildings without consoles. The results obtained from these analyses show very similar results in between the two-scaling method except axial loads. That's why, two consoles are added to each plan to have an asymmetric plan and another indicator that is expected to have different results in between the two scaling methods.

Table 6.2. Time History Analyses Results

EDC-EQ	Base Shear		Overturning Moment		Roof Displacement		Maximum Drift		Maximum Axial Force		Minimum Axial Force		Maximum Console Disp.	
	M1	M2	M1	M2	M1	M2	M1	M2	M1	M2	M1	M2	M1	M2
C1 33	1.01	1.03	1.00	1.02	1.01	0.97	0.97	0.97	0.59	1.03	0.33	-0.03	1.13	1.23
C1 164	1.00	1.01	1.02	1.05	1.04	1.06	1.00	1.01	0.66	0.89	0.23	0.00	2.85	3.22
C1 210	0.99	0.93	1.01	1.03	1.00	0.98	1.00	1.02	0.53	1.31	0.36	-0.39	1.20	1.82
C1 237	0.97	0.96	1.00	1.00	1.03	1.04	1.02	1.02	0.62	0.73	0.31	0.18	1.27	1.46
C1 238	0.93	0.89	1.01	1.00	0.96	0.96	1.03	1.00	0.55	0.76	0.32	0.10	1.75	2.03
C1 318	1.04	1.03	0.99	0.98	1.00	0.99	0.99	0.98	0.70	1.00	0.38	0.14	1.84	2.34
C1 454	0.95	0.98	0.94	0.94	1.00	0.98	1.03	0.99	0.60	0.84	0.25	0.03	1.53	1.76
C1 543	0.93	0.89	1.04	1.09	0.99	0.95	0.99	1.03	0.83	1.17	0.09	-0.23	1.55	1.93
C1 552	1.08	1.05	0.96	0.96	0.98	0.98	1.08	1.03	1.14	0.99	-0.20	-0.09	1.36	1.26

EDC-EQ	Base Shear		Overturning Moment		Roof Displacement		Maximum Drift		Maximum Axial Force		Minimum Axial Force		Maximum Console Disp.	
	M1	M2	M1	M2	M1	M2	M1	M2	M1	M2	M1	M2	M1	M2
C1 1148	1.01	1.03	1.07	1.08	1.02	1.05	0.99	0.99	0.34	0.53	0.66	0.50	1.22	1.38
C1 6057	0.91	0.90	1.02	1.00	0.98	0.97	0.93	0.90	0.75	0.83	0.21	0.15	1.86	2.05
C2 33	1.01	1.02	0.98	1.00	1.01	1.01	0.98	0.96	0.49	0.80	0.48	0.12	1.18	1.27
C2 164	0.99	0.98	1.00	1.00	1.05	1.07	1.01	1.01	0.54	0.68	0.35	0.17	2.84	3.16
C2 237	0.96	0.96	1.00	0.99	1.01	1.01	1.00	1.00	0.49	0.55	0.50	0.39	1.22	1.29
C2 238	0.95	0.93	1.00	1.01	0.97	0.97	0.97	0.95	0.47	0.59	0.43	0.25	1.68	2.09
C2 318	1.06	1.02	0.99	1.00	1.00	0.99	0.99	0.99	0.58	0.80	0.50	0.27	1.74	2.26
C2 454	0.94	0.98	0.94	0.94	1.01	0.99	1.06	0.99	0.45	0.61	0.49	0.33	2.00	1.07
C2 543	0.93	0.93	1.02	1.03	0.98	0.98	1.00	1.02	0.67	0.90	0.31	0.01	1.95	2.02

EDC-EQ	Base Shear		Overturning Moment		Roof Displacement		Maximum Drift		Maximum Axial Force		Minimum Axial Force		Maximum Console Disp.	
	M1	M2	M1	M2	M1	M2	M1	M2	M1	M2	M1	M2	M1	M2
C2 552	0.98	0.98	0.99	1.02	0.99	0.99	0.97	0.97	0.92	0.75	0.07	0.15	1.20	1.02
C2 1148	1.05	1.09	1.13	1.12	0.99	1.02	0.99	0.99	0.32	0.46	1.31	1.45	1.08	1.24
C2 1614	1.00	0.96	0.98	1.05	0.99	0.99	1.00	0.99	0.28	0.73	0.73	0.32	1.13	1.58
C2 6057	0.91	0.91	1.00	0.99	0.98	0.98	0.93	0.93	0.69	0.70	0.39	-0.08	1.74	1.78
C3 33	1.02	1.01	0.99	1.00	1.01	1.00	1.00	1.00	0.38	0.44	0.57	0.51	1.27	1.31
C3 164	1.00	1.00	1.02	1.01	1.00	1.00	1.01	1.00	0.44	0.40	0.51	0.56	2.57	2.29
C3 210	1.00	1.02	1.02	1.01	0.98	0.99	0.98	0.98	0.33	0.68	0.62	0.21	1.25	1.64
C3 237	0.97	0.98	0.99	0.98	1.00	1.00	0.99	0.99	0.38	0.30	0.60	0.69	1.19	1.13
C3 238	0.98	0.98	1.01	1.01	0.98	0.99	0.99	0.99	0.36	0.33	0.55	0.58	1.46	1.38

EDC-EQ	Base Shear		Overturning Moment		Roof Displacement		Maximum Drift		Maximum Axial Force		Minimum Axial Force		Maximum Console Disp.	
	M1	M2	M1	M2	M1	M2	M1	M2	M1	M2	M1	M2	M1	M2
C3 318	1.02	1.01	0.99	0.99	1.00	0.99	0.99	0.99	0.44	0.43	0.59	0.59	1.91	1.91
C3 552	1.02	1.02	0.99	0.98	0.99	1.00	0.97	0.99	0.71	0.43	0.22	0.53	1.13	0.91
C3 1148	0.98	0.97	1.05	1.06	0.97	0.97	0.96	0.96	0.26	0.30	0.74	0.70	1.29	1.32
C3 1633	0.98	0.98	0.99	0.99	1.01	1.01	0.98	0.97	0.56	0.64	0.51	0.45	1.97	2.27
C3 6057	0.92	0.95	0.98	1.00	0.98	0.99	0.96	0.98	0.58	0.41	0.45	0.59	1.61	1.42
C3 6059	1.00	1.00	0.97	0.98	0.98	0.98	0.99	0.99	0.20	0.21	0.79	0.78	1.36	1.40
C4 33	0.99	1.00	0.99	0.99	0.99	1.00	1.00	1.00	0.19	0.28	0.79	0.70	1.22	1.33
C4 164	1.02	1.02	1.00	0.99	0.96	0.97	0.92	0.93	0.25	0.28	0.71	0.67	2.48	2.52
C4 237	1.01	1.01	1.00	1.00	1.00	1.00	1.00	1.00	0.18	0.18	0.81	0.81	1.11	1.11

EDC-EQ	Base Shear		Overturning Moment		Roof Displacement		Maximum Drift		Maximum Axial Force		Minimum Axial Force		Maximum Console Disp.	
	M1	M2	M1	M2	M1	M2	M1	M2	M1	M2	M1	M2	M1	M2
C4 238	0.98	0.99	0.99	0.99	0.99	0.99	0.99	0.98	0.18	0.21	0.78	0.74	1.21	1.27
C4 318	0.99	0.99	1.00	1.00	1.00	0.99	0.99	0.99	0.21	0.27	1.04	1.06	1.43	1.75
C4 543	0.97	0.97	1.00	1.00	0.99	0.98	0.99	0.99	0.24	0.31	0.74	0.67	1.75	1.99
C4 552	0.96	0.98	0.99	1.00	0.98	0.99	0.97	0.98	0.36	0.27	0.63	0.73	1.09	1.00
C4 1148	1.02	1.02	1.01	1.01	1.00	1.01	1.00	1.00	0.15	0.20	0.85	0.80	1.26	1.36
C4 1633	0.98	0.97	0.99	0.98	1.00	1.00	1.00	0.99	0.29	0.40	0.74	0.64	1.45	1.89
C4 4137	0.95	0.96	0.97	0.98	0.98	0.98	0.98	0.99	0.26	0.19	0.78	0.84	1.89	1.32
C4 6057	1.02	1.01	0.99	1.00	0.99	0.99	0.99	0.98	0.28	0.27	0.69	0.71	1.44	1.37

EDC-EQ	Base Shear		Overturning Moment		Roof Displacement		Maximum Drift		Maximum Axial Force		Minimum Axial Force		Maximum Console Disp.	
	M1	M2	M1	M2	M1	M2	M1	M2	M1	M2	M1	M2	M1	M2
D1 10	1.00	0.99	1.00	1.01	0.99	0.98	1.00	0.99	0.18	0.90	-0.23	-1.09	1.06	1.70
D1 31	0.98	0.96	1.01	1.00	1.00	1.00	0.98	0.96	0.57	0.92	-0.62	-1.01	1.11	1.27
D1 167	0.99	0.98	1.00	1.00	1.00	1.01	0.99	0.98	0.57	0.96	-0.55	-1.09	1.06	1.27
D1 266	1.02	1.06	1.00	1.01	0.99	0.99	1.02	1.06	0.30	0.83	-0.38	-1.03	1.06	1.89
D1 314	0.99	0.99	1.01	1.00	1.00	1.00	0.99	0.99	0.46	0.91	-0.51	-0.96	1.48	2.71
D1 848	1.00	0.99	0.99	1.03	1.01	1.04	1.00	0.99	0.27	0.90	-0.32	-1.00	1.13	2.27
D1 850	0.97	0.99	1.01	1.00	0.98	0.98	0.97	0.99	0.57	0.95	-0.55	-0.95	1.35	2.35
D1 1158	1.00	1.01	1.00	1.02	1.00	1.01	1.00	1.01	0.23	0.65	-0.36	-0.96	1.06	1.74
D1 1602	1.02	1.03	0.99	1.01	1.02	1.00	1.02	1.03	0.17	0.86	-0.21	-1.06	1.05	1.82

EDC-EQ	Base Shear		Overturning Moment		Roof Displacement		Maximum Drift		Maximum Axial Force		Minimum Axial Force		Maximum Console Disp.	
	M1	M2	M1	M2	M1	M2	M1	M2	M1	M2	M1	M2	M1	M2
D1 1748	1.04	1.04	1.01	1.01	0.94	0.94	1.04	1.04	1.74	1.73	-2.08	-2.07	1.68	1.67
D1 4125	0.99	0.99	0.98	0.98	1.01	1.01	0.99	0.99	0.88	0.32	-1.21	-0.80	1.12	1.01
D2 31	0.99	0.98	1.00	1.00	1.01	1.01	0.99	0.98	0.46	0.63	-0.49	-0.68	1.10	1.18
D2 167	0.99	0.98	1.00	1.00	1.00	1.00	0.99	0.98	0.44	0.70	-0.44	-0.70	1.05	1.19
D2 266	1.00	1.02	1.01	1.01	1.00	1.00	1.00	1.02	0.22	0.47	-0.26	-0.56	1.05	1.41
D2 458	1.00	1.00	0.99	0.99	1.02	1.02	1.00	1.00	0.63	0.65	-0.53	-0.32	2.05	1.40
D2 848	1.00	1.00	0.99	1.01	1.00	1.01	1.00	1.00	0.19	0.46	-0.22	-0.52	1.09	1.48
D2 850	1.00	0.99	1.00	1.00	0.98	0.98	1.00	0.99	0.42	0.60	-0.39	-0.55	1.48	2.07
D2 900	1.00	1.00	0.99	0.97	1.00	1.00	1.00	1.00	0.23	0.55	-0.23	-0.55	1.00	1.58

EDC-EQ	Base Shear		Overturning Moment		Roof Displacement		Maximum Drift		Maximum Axial Force		Minimum Axial Force		Maximum Console Disp.	
	M1	M2	M1	M2	M1	M2	M1	M2	M1	M2	M1	M2	M1	M2
D2 1158	1.00	1.00	1.00	0.99	0.99	0.99	1.00	1.00	0.15	0.34	-0.24	-0.51	1.03	1.80
D2 1602	1.00	0.99	1.01	1.02	1.00	0.99	1.00	0.99	0.14	0.52	-0.16	-0.60	1.07	1.35
D2 1748	0.93	0.97	1.01	1.00	1.00	0.98	0.93	0.97	1.54	1.21	-1.62	-1.34	1.74	1.40
D2 4125	0.99	1.00	1.01	0.99	1.00	1.00	0.99	1.00	0.75	0.20	-0.95	-0.22	1.12	0.96
D3 31	0.99	0.99	1.00	1.00	1.00	1.00	0.99	0.99	0.43	0.45	-0.46	-0.49	1.12	1.13
D3 167	0.99	0.99	1.00	1.00	1.00	1.00	0.99	0.99	0.43	0.52	-0.42	-0.51	1.06	1.10
D3 266	1.01	1.01	1.01	1.00	1.00	1.00	1.01	1.01	0.18	0.31	-0.21	-0.37	1.03	1.11
D3 458	1.00	1.00	0.91	0.91	1.00	1.00	1.00	1.00	0.56	0.24	-0.50	-0.21	2.00	1.20
D3 848	1.00	1.00	1.00	1.00	1.00	1.00	1.00	1.00	0.17	0.27	-0.21	-0.34	1.04	1.10

EDC-EQ	Base Shear		Overturning Moment		Roof Displacement		Maximum Drift		Maximum Axial Force		Minimum Axial Force		Maximum Console Disp.	
	M1	M2	M1	M2	M1	M2	M1	M2	M1	M2	M1	M2	M1	M2
D3 850	0.99	0.99	1.00	1.00	1.00	1.00	0.99	0.99	0.36	0.43	-0.32	-0.38	1.20	1.49
D3 900	1.00	1.00	1.00	1.00	1.00	1.00	1.00	1.00	0.21	0.42	-0.20	-0.40	0.96	1.10
D3 1158	0.99	0.99	1.00	1.00	1.00	1.00	0.99	0.99	0.13	0.23	-0.19	-0.34	1.00	1.23
D3 1602	1.00	0.99	1.01	1.01	1.00	1.00	1.00	0.99	0.12	0.36	-0.13	-0.41	1.07	1.30
D3 1748	0.99	0.98	0.97	0.99	0.98	1.01	0.99	0.98	0.92	0.86	-1.41	-0.96	1.58	1.67
D3 4125	1.00	1.00	1.01	1.00	1.01	1.00	1.00	1.00	0.46	0.11	-0.98	-0.61	1.08	0.96
D4 31	1.00	1.00	1.00	1.00	1.00	1.00	1.00	1.00	0.32	0.30	-0.35	-0.32	1.17	1.15
D4 167	0.99	0.99	1.00	1.00	1.00	1.00	0.99	0.99	0.34	0.38	-0.32	-0.36	1.04	1.04
D4 266	1.00	1.00	1.00	1.00	1.00	1.00	1.00	1.00	0.14	0.20	-0.15	-0.23	1.02	1.04

EDC-EQ	Base Shear		Overturning Moment		Roof Displacement		Maximum Drift		Maximum Axial Force		Minimum Axial Force		Maximum Console Disp.	
	M1	M2	M1	M2	M1	M2	M1	M2	M1	M2	M1	M2	M1	M2
D4 314	1.00	1.00	1.00	1.00	1.00	1.00	1.00	1.00	0.36	0.26	-0.35	-0.25	1.60	1.31
D4 848	0.99	0.99	1.01	1.01	1.01	1.01	0.99	0.99	0.16	0.20	-0.17	-0.21	1.12	1.16
D4 850	1.00	1.00	1.00	1.00	1.00	1.00	1.00	1.00	0.27	0.27	-0.24	-0.24	0.98	0.98
D4 900	1.00	1.00	1.00	1.00	1.00	1.00	1.00	1.00	0.14	0.26	-0.14	-0.25	0.97	0.97
D4 1158	1.00	1.00	1.00	1.00	1.00	0.99	1.00	1.00	0.11	0.01	-0.14	-0.40	1.00	1.57
D4 1602	1.00	1.00	1.00	1.01	1.00	1.00	1.00	1.00	0.06	0.16	-0.06	-0.16	1.01	1.10
D4 1748	1.00	1.00	0.99	0.99	1.00	1.00	1.00	1.00	0.45	0.60	-0.47	-0.63	1.00	1.00
D4 4125	1.00	1.00	1.03	1.00	0.96	0.98	1.00	1.00	0.30	-0.02	-0.59	-0.06	1.04	1.03

Next, results are discussed in terms of each indicator.

6.1 Base Shear Results

To make the results more understandable, a simplified representation of them is presented in Table 6.3.

Table 6.3. Base Shear Results

Soil Class	Earthquake Design Class	Max		Average		Normalized Standard Deviation	
		M1	M2	M1	M2	M1	M2
C	1	1.08	1.05	0.98	0.97	0.21	0.23
C	2	1.05	1.09	0.98	0.98	0.18	0.19
C	3	1.02	1.02	0.99	0.99	0.20	0.20
C	4	1.02	1.02	0.99	0.99	0.17	0.17
D	1	1.04	1.04	1.00	1.00	0.24	0.24
D	2	1.00	1.02	0.99	0.99	0.25	0.25
D	3	1.01	1.01	1.00	1.00	0.26	0.26
D	4	1.00	1.00	1.00	1.00	0.32	0.32

The results shows that in Method 1, maximum increase in the base shear due to vertical load is 8 % on soil class C and 4 % soil class D. In both of the soil classes, average results are almost identical to the case without vertical ground motions.

In method 2, maximum increase in the base shear is 9 % on soil class C and 4 % on soil class D. In this method as well, average results are the same with the case where vertical components of ground motions were not included.

The normalized standard deviations are almost the same in both of the methods.

In the light of this information, it can be easily said that the vertical components of ground motions do not affect the base shear and no comparison can be made between the two scaling methods.

6.2 Overturning Moment Results

The results for overturning moment are presented in Table 6.4 in a simplified manner.

Table 6.4. Overturning Moment Results

Soil Class	Earthquake Design Class	Max		Average		Normalized Standard Deviation	
		M1	M2	M1	M2	M1	M2
C	1	1.04	1.05	1.01	1.01	0.09	0.09
C	2	1.13	1.12	1.00	1.01	0.09	0.11
C	3	1.05	1.06	1.00	1.00	0.10	0.10
C	4	1.01	1.01	0.99	1.00	0.13	0.13
D	1	1.01	1.03	1.00	1.01	0.04	0.04
D	2	1.01	1.02	1.00	1.00	0.03	0.03
D	3	1.01	1.01	0.99	0.99	0.03	0.03
D	4	1.03	1.01	1.00	1.00	0.08	0.08

Maximum increase in both of the methods is around 5 %. The average results obtained from both of the scaling methods do not deviate from the results obtained analysis without considering the vertical component of ground motions. The scatters of the results are identical in both of the methods. Similar to the base shear, the overturning moment is also not affected by the vertical component of ground motions.

6.3 Roof Displacement Results

The roof displacement results for each soil class and each design classes are presented in Table 6.5

Table 6.5. Roof Displacement Results

Soil Class	Earthquake Design Class	Max		Average		Normalized Standard Deviation	
		M1	M2	M1	M2	M1	M2
C	1	1.04	1.06	1.00	0.99	0.34	0.36
C	2	1.05	1.07	1.00	1.00	0.29	0.30
C	3	1.01	1.01	0.99	0.99	0.30	0.30
C	4	1.00	1.01	0.99	0.99	0.16	0.16
D	1	1.01	1.00	1.00	1.00	0.44	0.43
D	2	1.02	1.02	1.00	1.00	0.17	0.17
D	3	1.01	1.01	1.00	1.00	0.41	0.41
D	4	1.01	1.01	1.00	1.00	0.40	0.40

The results in Table 6.5 show that both of the maximum increase and normalized deviations are similar in both of the methods. Also, the average response ratio is around unity in both of the methods. Thus, roof displacement is also not affected by the vertical component of ground motions and no difference between the two scaling methods can be observed.

6.4 Maximum Drift

The maximum drifts occurred in the buildings exposed to ground motions scaled with the two scaling methods are presented in Table 6.6.

Table 6.6. Maximum Drift Results

Soil Class	Earthquake Design Class	Max		Average		Normalized Standard Deviation	
		M1	M2	M1	M2	M1	M2
C	1	1.03	1.03	1.00	0.99	0.31	0.31
C	2	1.01	1.02	0.99	0.98	0.21	0.22
C	3	1.01	1.00	0.98	0.99	0.28	0.28
C	4	1.00	1.00	0.98	0.98	0.17	0.17
D	1	1.01	1.02	0.99	0.99	0.28	0.28
D	2	1.02	1.02	0.99	0.99	0.23	0.24
D	3	1.00	1.00	0.99	1.00	0.27	0.28
D	4	1.01	1.00	1.00	1.00	0.34	0.34

The results presented show that maximum drift is also not affected by the vertical component of ground motions.

The base shear, overturning moment, roof displacement and maximum drift are not affected by the vertical components of ground motions. Since the buildings are almost symmetrical and there is no irregularity in the load bearing system of the buildings, it is expected that they are not affected by the vertical ground motions.

6.5 Maximum Axial Force

This structural indicator expresses the total maximum compressive force occurring at the base floor level. The change in the maximum compressive force level is shown in Table 6.7

Table 6.7. Maximum Axial Load Results

Soil Class	Earthquake Design Class	Max		Average		Normalized Standard Deviation	
		M1	M2	M1	M2	M1	M2
C	1	0.92	1.17	0.69	0.97	0.13	0.11
C	2	0.92	0.90	0.54	0.69	0.12	0.07
C	3	0.71	0.68	0.42	0.42	0.11	0.10
C	4	0.36	0.40	0.23	0.26	0.05	0.05
D	1	1.74	1.73	0.54	0.90	0.35	0.20
D	2	1.54	1.21	0.47	0.58	0.32	0.13
D	3	0.92	0.86	0.36	0.38	0.22	0.12
D	4	0.45	0.60	0.24	0.24	0.15	0.11

The results obtained from the two scaling methods deviate from the analysis without vertical ground motion. This observation indicates that the axial load level is dependent on the vertical component of ground motions as expected.

The results show that the average results obtained from the analysis using ground motion records scaled with Method 2 is significantly higher than the analysis results obtained by using ground motion records scaled with Method 1 in both of the buildings.

In the literature it is stated that the significance of the vertical component of ground motions increases as the ratio of peak ground acceleration of vertical component to peak ground acceleration of horizontal component increases. It is also known that ground motions recorded five kilometers away from the epicenter of an earthquake mostly have a $PGA_{Vertical}$ / $PGA_{Horizontal}$ ratio less than 0.67. (Shrestha, 2009) In the Turkish Seismic Code (2018), the vertical response spectrum is approximately eighty percent of the horizontal response spectrum. In another words, Turkish Seismic Code specifies to the $PGA_{Vertical}$ / $PGA_{Horizontal}$ ratio to be 0.8. In the study to eliminate near

fault effects ground motions, ground motions selected such that they are at least ten kilometers away from the epicenter. In other words, the ground motions selected for this study have a $PGA_{Vertical}$ / $PGA_{Horizontal}$ ratio less than 0.67. As a result, a ground motion scaled by the Method1 will have a $PGA_{Vertical}$ / $PGA_{Horizontal}$ ratio less than 0.67. However, if the vertical component of ground motion is scaled by using Method 2, the ground motion will have a $PGA_{Vertical}$ / $PGA_{Horizontal}$ ratio approximately 0.8. Thus, the scale factor for the vertical components determined using Method 2 will be larger than the scale factor determined using Method 1. This explains the higher results in Method 2. In Figure 6.1, $PGA_{Vertical}$ / $PGA_{Horizontal}$ ratio for soil class C and earthquake design class 1 are shown.

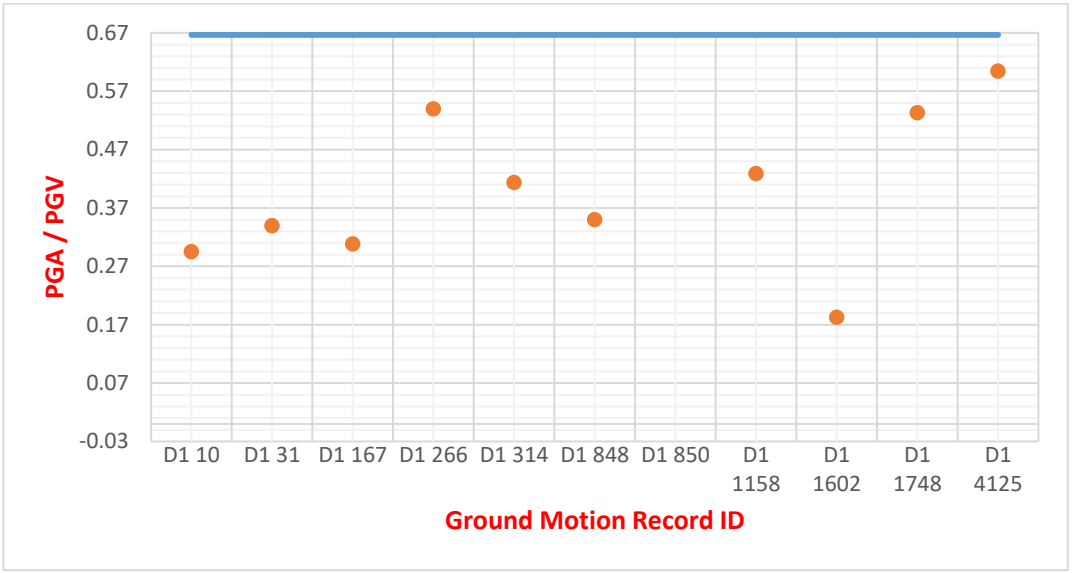

Figure 6.1. $PGA_{Vertical}$ / $PGA_{Horizontal}$ ratios for Soil Class D and EDC 1

It needs to be noted that the difference between the results obtained from Method 1 and Method 2 decreases as the earthquake design class increases. This is anticipated because as the earthquake design class increases, seismic load decreases and loses its importance compared to the other loads.

The results obtained from Method 2 have less normalized standard deviation than the results obtained from Method 1. This is expected because in Method 2, vertical components of all ground motions in a set are scaled to a target level. However, in

Method 1 the levels of vertical components are modified depending on horizontal components and no adjustment made for vertical components. Thus, it is expected that the results obtained from Method 1 are more scattered.

It needs to be noted that magnitude of scaling factors did not cause any difference compared to ground motions with smaller scale factors. However, as the ratio of scale factors of vertical components and horizontal components increases, the difference between the two scaling methods increases.

6.6 Minimum Axial Force

This structural indicator is used to represent the total maximum tensile or minimum compressive force occurring at the base floor level. Minimum axial load results obtained from the analyses are shown in Table 6.8.

Table 6.8. Minimum Axial Load Results

Soil Class	Earthquake Design Class	Min		Average		Normalized Standard Deviation	
		M1	M2	M1	M2	M1	M2
C	1	-1.20	-1.39	-0.73	-0.97	0.77	7.26
C	2	-0.93	-1.08	-0.49	-0.69	0.63	1.33
C	3	-0.78	-0.79	-0.44	-0.44	0.27	0.27
C	4	-0.31	-0.33	-0.22	-0.24	0.08	0.08
D	1	-2.08	-2.07	-0.64	-1.09	1.56	-3.98
D	2	-1.62	-1.34	-0.50	-0.59	0.88	0.68
D	3	-1.41	-0.96	-0.46	-0.46	0.73	0.34
D	4	-0.35	-0.36	-0.27	-0.28	0.26	0.18

The results show that decrease in the axial load level higher in Method 2. The reasons explained in the maximum axial load part are still applicable for the minimum load level.

The normalized standard deviation results show dispersion. The reason for this situation is that since some results are in tension and some results in compression, they cancel each other in calculation of the mean value.

6.7 Tip Displacement of Consoles

The maximum console displacement results obtained from the analyses are presented in a simplified manner in Table 6.9.

Table 6.9. Results for Tip Displacement of Consoles

Soil Class	Earthquake Design Class	Max		Average		Normalized Standard Deviation	
		M1	M2	M1	M2	M1	M2
C	1	2.85	3.22	1.60	1.86	0.20	0.15
C	2	2.00	2.02	1.61	1.71	0.38	0.21
C	3	2.57	2.27	1.55	1.54	0.27	0.27
C	4	2.48	2.52	1.50	1.53	0.25	0.23
D	1	1.68	2.71	1.20	1.79	0.48	0.28
D	2	2.05	2.07	1.25	1.44	0.68	0.48
D	3	2.00	1.67	1.19	1.22	0.73	0.70
D	4	1.60	1.57	1.09	1.12	0.72	0.67

The results show that in both of the buildings, average console displacement responses obtained from Method 2 are greater than the Method 1 responses as it was

observed in axial forces. Thus, it can be generalized that any parameter affected by the vertical component of ground motions in this study gave more critical results when Method 2 is used. However, it should be noted that if the selected ground motion records were in near fault region, different results could be obtained.

The normalized standard deviation in both of the buildings is also smaller when the ground motions are scaled with the Method 2. In another words, Method 2 indicates less scatter.

CHAPTER 7

SUMMARY AND CONCLUSION

7.1 Summary

This study aimed to examine the two commonly used approaches to scale vertical components of ground motion records. In the first approach, vertical components of the records are scaled with the same scale factor determined for horizontal components of that record. In the second approach, vertical components are scaled with a scale factor that is different from the horizontal scale factor and determined according to the vertical response spectrum.

For case studies, two buildings with asymmetrical plan are selected. The first building has nine stories and it is located on local soil class C. The second building has four stories and it is located on soil class D. Next two different consoles are added to each building to study potential effects of the vertical component of ground motions.

For each soil class, four target spectra are selected from the Marmara region of Turkey.The These four spectra are selected such that each one of them corresponds to a different earthquake design class specified in Turkish Seismic Code (2018).

For each soil class, candidate ground motions are selected from PEER NGAWest2 ground motion database (https://ngawest2.berkeley.edu/). The ground motions are selected such that their fault mechanism is strike slip, their moment magnitude is at least equal to 5.0 and R_{JB} distances are in between 10 km and 30 km. Afterwards, by using the target spectra, ground motions for each target spectrum are selected. The selected ground motions are scaled with the two mentioned scaling methods.

Models describing the nonlinear behavior of the buildings are created by using the lumped plasticity approach. After that for each building three different sets of analyses are conducted. In the first set, records whose vertical components scaled with the same scaling factors are used. In the second set, records with different scaling factors are used. In the third set, vertical components of the records are excluded to see whether they have an effect on the results or not.

Finally, the results obtained from these three sets are compared by using the seven specified indicators.

7.2 Conclusions

The numerical results obtained in this study led to the following conclusions;

- The base shear developing during an earthquake is generally independent of the vertical components of the ground motions for regular buildings. In both of the building and both of the scaling methods, the variation in base shear values is negligible so the effect of vertical ground motion is insignificant.

- Similar to the base shear values, overturning moments are found to not deviate due to presence of vertical ground motion effects. However, it needs to be noted that the change in the axial load level changes the moment capacity of the columns.

- The results also show that the roof displacements and the maximum drift ratio are also independent of the vertical components of the ground motion records.

- The axial load levels and console displacements are found to be dependent on the vertical components of ground motions. In both of the buildings, the results obtained from Method 2 gave more critical results than Method 1. The maximum compressive and maximum tensile forces resulting from ground motions are higher in Method 2. The reason for this observation is partially due to the large amplification in the vertical component of ground motion resulting from independent scaling of components to corresponding spectra.

- The axial loads level and console displacements showed more scatter in Method 1. This is mostly because the independent scaling of the vertical spectrum in Method 2 causes a large variation in scale factors and thus the response due to the vertical ground motion effects.

- The amplitude of scaling factors did not affect the findings presented here. However, the ratio of vertical scale factor to horizontal scale factor increased the difference between results from the two methods.

- The results showed that as amplitude level of the target spectrum decreases, the difference between the results obtained from the two-scaling method decreases. Because influence of seismic load becomes insignificant compare to other loads acting on the structure.

- The findings showed that for any designer who wants to be conservative Method 2 is better option. However, it needs to be kept in mind that the scaling horizontal and vertical component with a different scale factor is not realistic as it changes the physical properties of the ground motions.

7.3 Recommendations for Future Studies

This study constitutes an initial attempt to study the differences of scaling approaches for the vertical ground motion components. In the future, the following further studies could be performed:

- In this study, the fault mechanism is specified to be strike slip, in the following studies different types of fault mechanism can be investigated.
- Only the local soil classes C and D are used in this study; the other soil classes can also be used to see the effect of different soil conditions on the scaling of the vertical components.
- The high-rise buildings on softer soil conditions and low-rise buildings on stiff soil and rock conditions can be studied to assess more critical cases.
- Buildings with further irregularities can be studied in future attempts to investigate vertical ground motion effects
- In the future studies, behavior of bridges can also be investigated since they have longer spans and they are more susceptible to vertical components of ground motions.
- In this study, global indicators are mostly used to assess the initial results. in the future studies, the changes in the element level responses can also be investigated.

REFERENCES

Applied Technology Council. (2009). Quantification of building seismic performance factors. US Department of Homeland Security, FEMA.

American Society of Civil Engineers (2005). ASCE/SEI 7-05: Minimum Design Loads for Buildings, Reston, VA.

American Society of Civil Engineers (2010). ASCE/SEI 7-10: Minimum Design Loads for Buildings, Reston, VA.

American Society of Civil Engineers (2016). ASCE/SEI 7-16: Minimum Design Loads for Buildings, Reston, VA.

Baker, J. W., & Allin Cornell, C. (2006). Spectral shape, epsilon and record selection. Earthquake Engineering & Structural Dynamics, 35(9), 1077-1095.

Bazzurro, P., Cornell, C. A., Shome, N., & Carballo, J. E. (1998). Three proposals for characterizing MDOF nonlinear seismic response. Journal of Structural Engineering, 124(11), 1281-1289.

Bommer, J. J., Scott, S. G., & Sarma, S. K. (2000). Hazard-consistent earthquake scenarios. Soil Dynamics and Earthquake Engineering, 19(4), 219-231.

Bozorgnia, Y., & Campbell, K. W. (2004). The vertical-to-horizontal response spectral ratio and tentative procedures for developing simplified V/H and vertical design spectra. Journal of Earthquake Engineering, 8(02), 175-207.

Chopra, A. (2011). Dynamic of Structures Chopra

Elnashai, A. S., & Papazoglou, A. J. (1997). Procedure and spectra for analysis of RC structures subjected to strong vertical earthquake loads. Journal of Earthquake Engineering, 1(01), 121-155.

European Committee for Standardization (1998). Eurocode 8: Design of Structures for earthquake resistance, Brussels, Belgium

Gülerce, Z., & Abrahamson, N. A. (2011). Site-specific design spectra for vertical ground motion. Earthquake Spectra, 27(4), 1023-1047.

Hancock, J., Bommer, J. J., & Stafford, P. J. (2008). Numbers of scaled and matched accelerograms required for inelastic dynamic analyses. Earthquake Engineering & Structural Dynamics, 37(14), 1585-1607.

Haselton, C. B., Baker, J. W., Bozorgnia, Y., Goulet, C. A., Kalkan, E., Luco, N., ... & Zareian, F. (2009). Evaluation of ground motion selection and modification methods: Predicting median interstory drift response of buildings. PEER report, 1, 1-288.

Heo, Y., Kunnath, S. K., & Abrahamson, N. (2011). Amplitude-scaled versus spectrum-matched ground motions for seismic performance assessment. Journal of Structural Engineering, 137(3), 278-288.

Jayaram, N., Lin, T., & Baker, J. W. (2011). A computationally efficient ground-motion selection algorithm for matching a target response spectrum mean and variance. Earthquake spectra, 27(3), 797-815.

Kalkan, E., & Chopra, A. K. (2011). Modal-pushover-based ground-motion scaling procedure. Journal of structural engineering, 137(3), 298-310.

Karakütük, Ö. (2015). Effect of ground motion selection on seismic response of buildings (Master's thesis, Middle East Technical University).

Keskin, E. (2020). Effect of vertical ground motion on the performance of high-rise buildings (Master's thesis, Fen Bilimleri Enstitüsü).

Kurama, Y. C., & Farrow, K. T. (2003). Ground motion scaling methods for different site conditions and structure characteristics. Earthquake engineering & structural dynamics, 32(15), 2425-2450.

Kwon, O. S., & Elnashai, A. (2006). The effect of material and ground motion uncertainty on the seismic vulnerability curves of RC structure. Engineering structures, 28(2), 289-303.

Kwong, N. S., & Chopra, A. K. (2020). Selecting, scaling, and orienting three components of ground motions for intensity-based assessments at far-field sites. Earthquake Spectra, 36(3), 1013-1037.

Mander, J. B., Priestley, M. J., & Park, R. (1988). Theoretical stress-strain model for confined concrete. Journal of structural engineering, 114(8), 1804-1826.

Najafi, L. H., & Tehranizadeh, M. (2015). Ground motion selection and scaling in practice. Periodica Polytechnica Civil Engineering, 59(2), 233-248.

Nau, J. M., & Hall, W. J. (1984). Scaling methods for earthquake response spectra. Journal of Structural Engineering, 110(7), 1533-1548.

Naumoski, N., Saatcioglu, M., & Amiri-Hormozaki, K. (2004, August). Effects of scaling of earthquake excitations on the dynamic response of reinforced concrete frame buildings. In 13th World Conference on Earthquake Engineering (Vol. 2917, p. 15).

Padgett, J. E., & DesRoches, R. (2007). Sensitivity of seismic response and fragility to parameter uncertainty. Journal of Structural Engineering, 133(12), 1710-1718.

Papazoglou, A. J., & Elnashai, A. S. (1996). Analytical and field evidence of the damaging effect of vertical earthquake ground motion. Earthquake Engineering & Structural Dynamics, 25(10), 1109-1137.

PEER, 2010. Seismic design guidelines for tall buildings. Report no. PEER-2010/05, PEER Center,University of California, Berkeley, CA.

Perform 3D, 2021. Nonlinear analysis and performance assessment of 3D structures. Software Version 8.0.0. Computers & Structures, Inc. (CSI), Berkeley, CA.

Shome, N., Cornell, C. A., Bazzurro, P., & Carballo, J. E. (1998). Earthquakes, records, and nonlinear responses. Earthquake spectra, 14(3), 469-500.

Shrestha, B. (2009, November). Vertical ground motions and its effect on engineering structures: a state-of-the-art review. In Proceeding of international seminar on hazard management for sustainable development in Kathmandu, Nepal (pp. 29-30).

Sucuoğlu, H., & Akkar, S. (2014). Basic Earthquake Engineering. In *Basic Earthquake Engineering*. https://doi.org/10.1007/978-3-319-01026-7

TBSC-2018. (2018). Deprem Etkisi Altında Binaların Tasarımı için Esaslar

TDY-2007. (2007). Deprem Bölgelerinde Yapılacak Binalar Hakkında Esaslar.

Tran, T. T., Hussan, M., Kim, D., & Nguyen, P. C. (2020). Distributed plasticity approach for the nonlinear structural assessment of offshore wind turbine. International Journal of Naval Architecture and Ocean Engineering, 12, 743-754.

Travasarou, T., Bray, J. D., & Abrahamson, N. A. (2003). Empirical attenuation relationship for Arias intensity. Earthquake engineering & structural dynamics, 32(7), 1133-1155.

TS-498. (1997). Design Loads for Buildings

TS-500. (2000). Requirements for Design and Construction of Reinforced Concrete Structures

Heo, Y., Kunnath, S. K., & Abrahamson, N. (2011). Amplitude-scaled versus spectrum-matched ground motions for seismic performance assessment. Journal of Structural Engineering, 137(3), 278-288.

Jayaram, N., Lin, T., & Baker, J. W. (2011). A computationally efficient ground-motion selection algorithm for matching a target response spectrum mean and variance. Earthquake spectra, 27(3), 797-815.

Kalkan, E., & Chopra, A. K. (2011). Modal-pushover-based ground-motion scaling procedure. Journal of structural engineering, 137(3), 298-310.

Mander, J. B., Priestley, M. J., & Park, R. (1988). Theoretical stress-strain model for confined concrete. Journal of structural engineering, 114(8), 1804-1826.

Tran, T. T., Hussan, M., Kim, D., & Nguyen, P. C. (2020). Distributed plasticity approach for the nonlinear structural assessment of offshore wind turbine. International Journal of Naval Architecture and Ocean Engineering, 12, 743-754.

Sucuoğlu, H., & Akkar, S. (2014). Basic Earthquake Engineering. In *Basic Earthquake Engineering*. https://doi.org/10.1007/978-3-319-01026-7

TBSC-2018. (2018). Deprem Etkisi Altında Binaların Tasarımı için Esaslar.

TDY-2007. (2007). Deprem Bölgelerinde Yapılacak Binalar Hakkında Esaslar

TS-498. (1997). Design Loads for Buildings.

TS-500. (2000). Requirements for Design and Construction of Reinforced Concrete Structures

APPENDICES

A. SELECTED GROUND MOTIONS

In Appendix A response spectrum and acceleration graphs of the selected ground motions are presented.

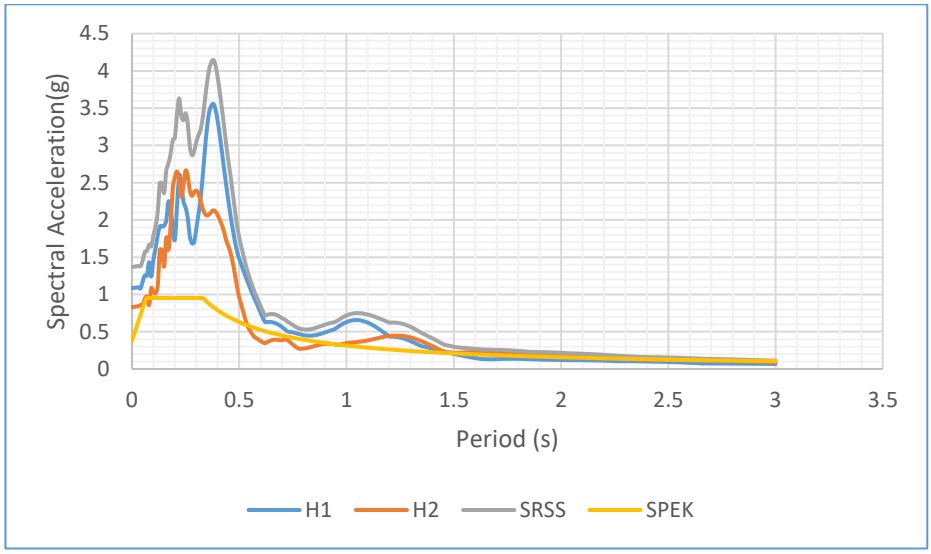

Figure A1. Scaled Horizontal Response Spectra of Parkfield(C1-33) Earthquake

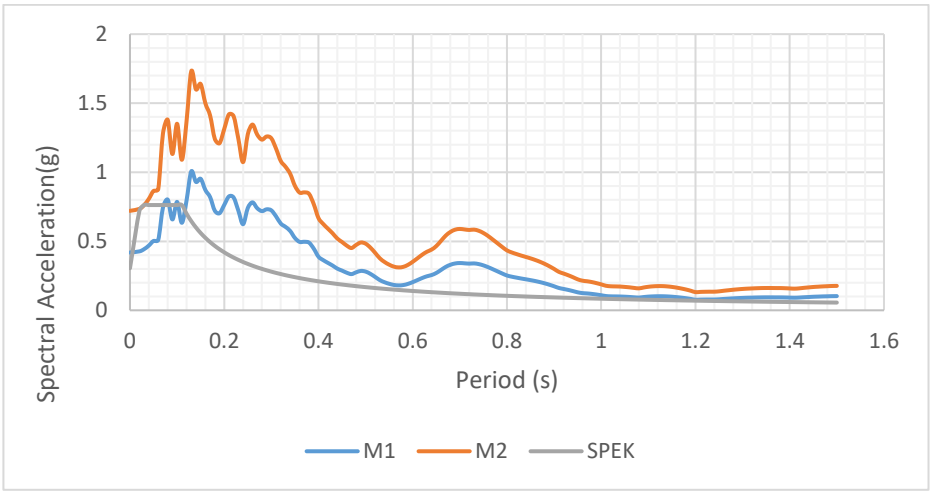

Figure A2. Scaled Vertical Response Spectra of Parkfield(C1–33) Earthquake

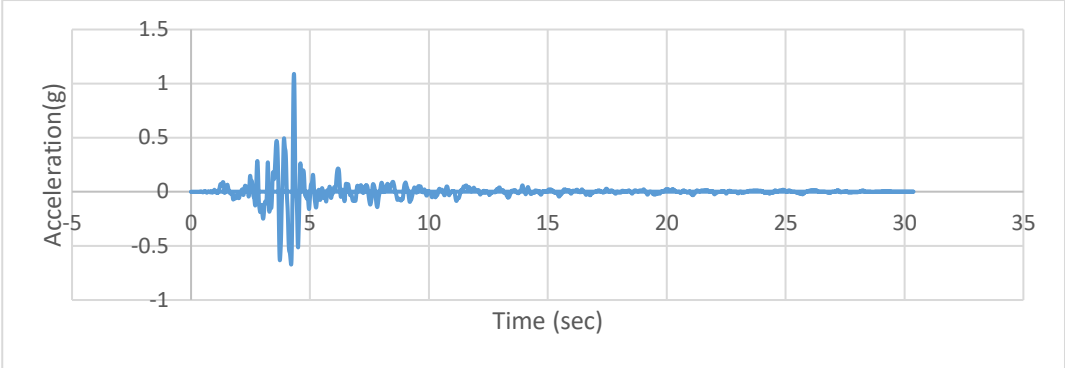

Figure A3. Scaled Acceleration Time Histories of Parkfield(C1–33X) Earthquake

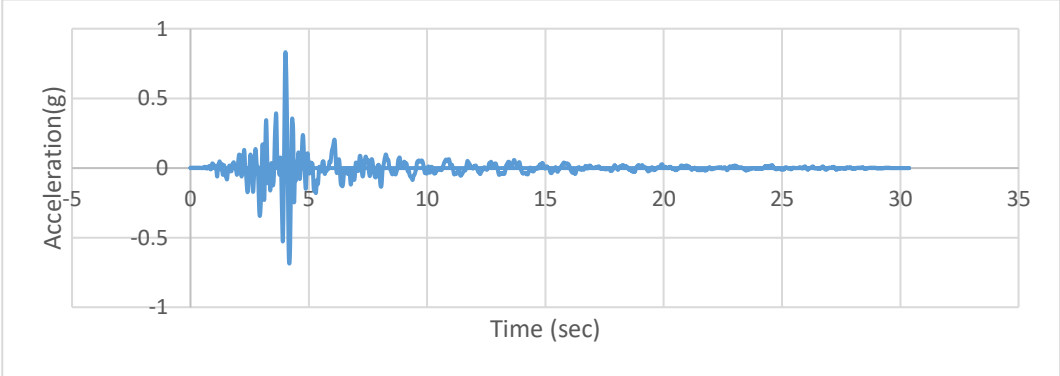

Figure A4. Scaled Acceleration Time Histories of Parkfield(C1–33Y) Earthquake

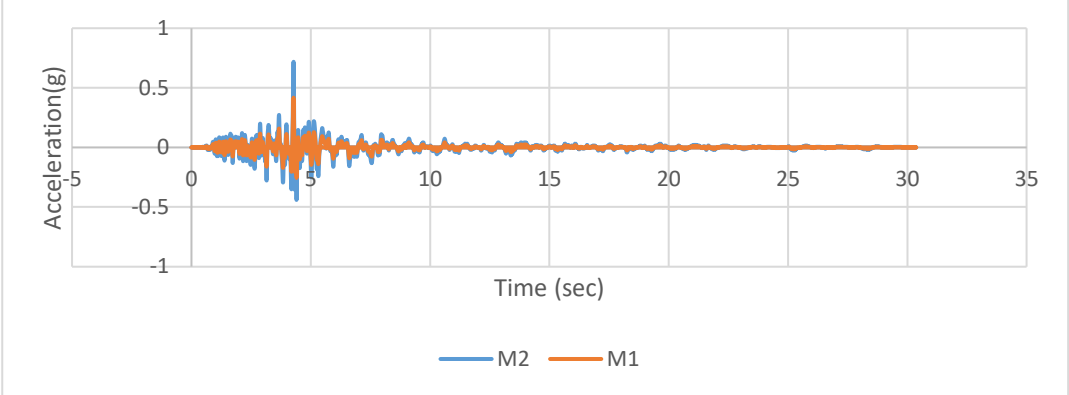

Figure A5. Scaled Acceleration Time Histories of Parkfield(C1–33Z) Earthquake

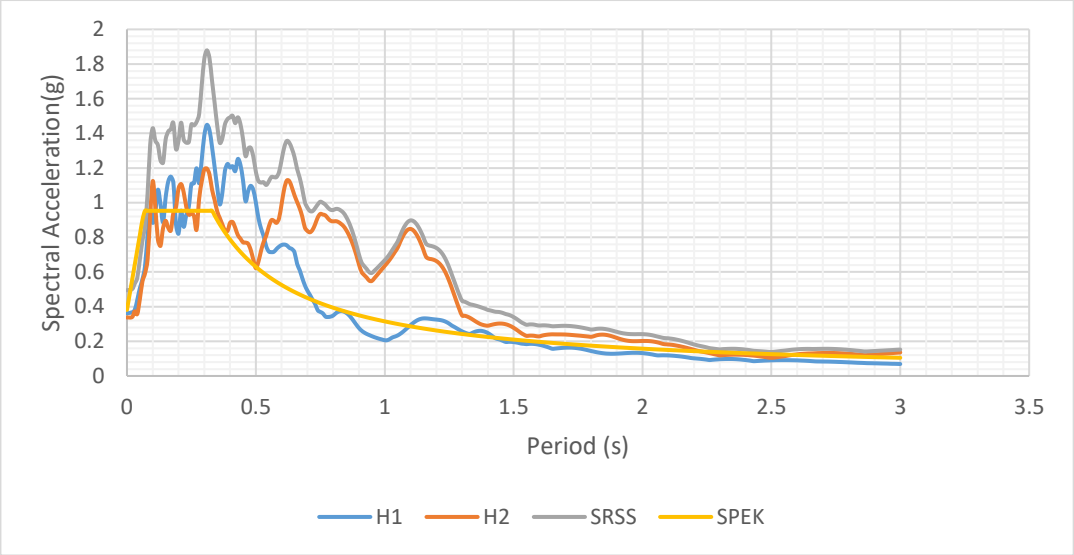

Figure A6. Scaled Horizontal Response Spectra of Imperial Valley-06(C1-164) Earthquake

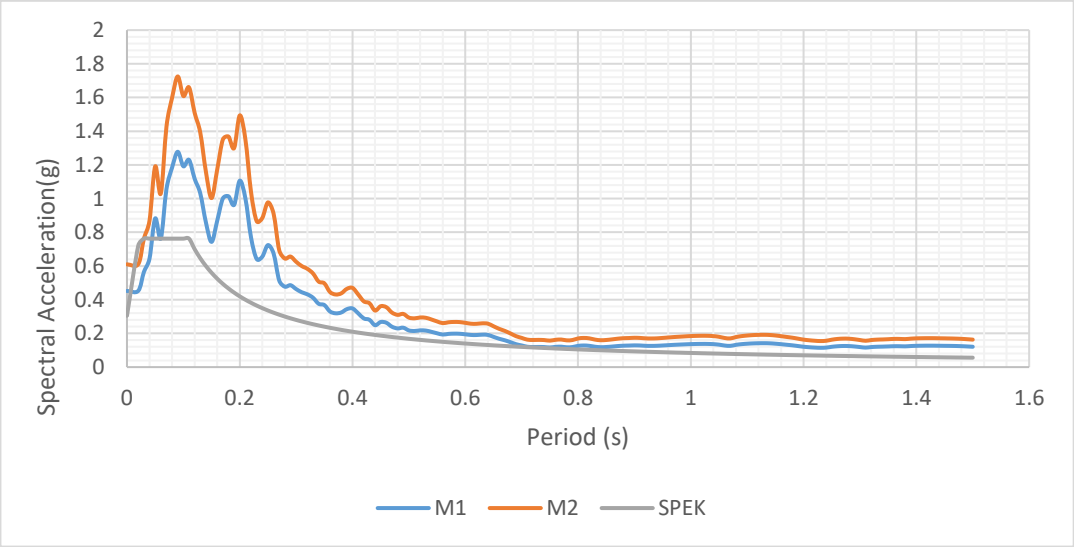

Figure A7. Scaled Vertical Response Spectra of Imperial Valley-06 (C1-164) Earthquake

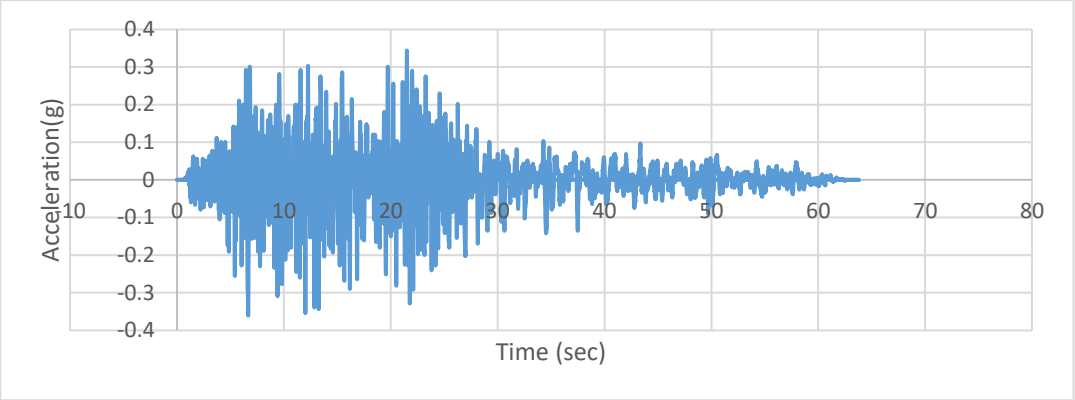

Figure A8. Scaled Acceleration Time Histories of Imperial Valley-06 (C1-164X) Earthquake

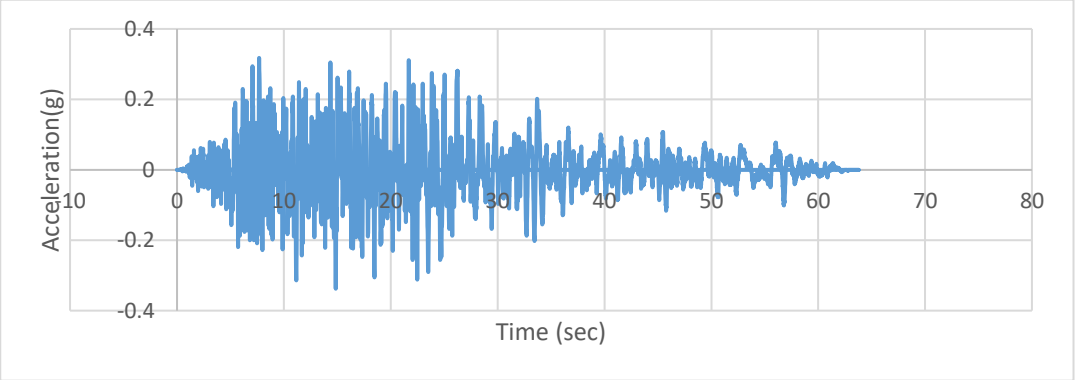

Figure A9. Scaled Vertical Response Spectra of Imperial Valley-06 (C1-164Y) Earthquake

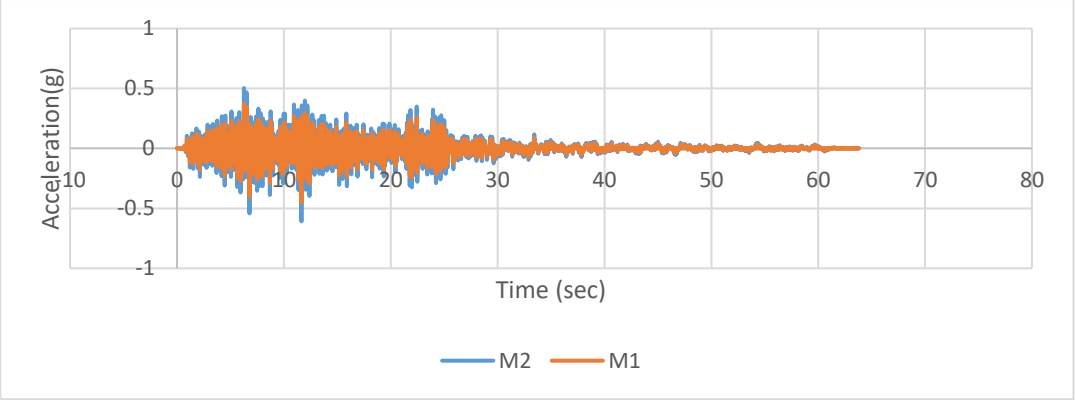

Figure A10. Scaled Vertical Response Spectra of Imperial Valley-06 (C1-164Z) Earthquake

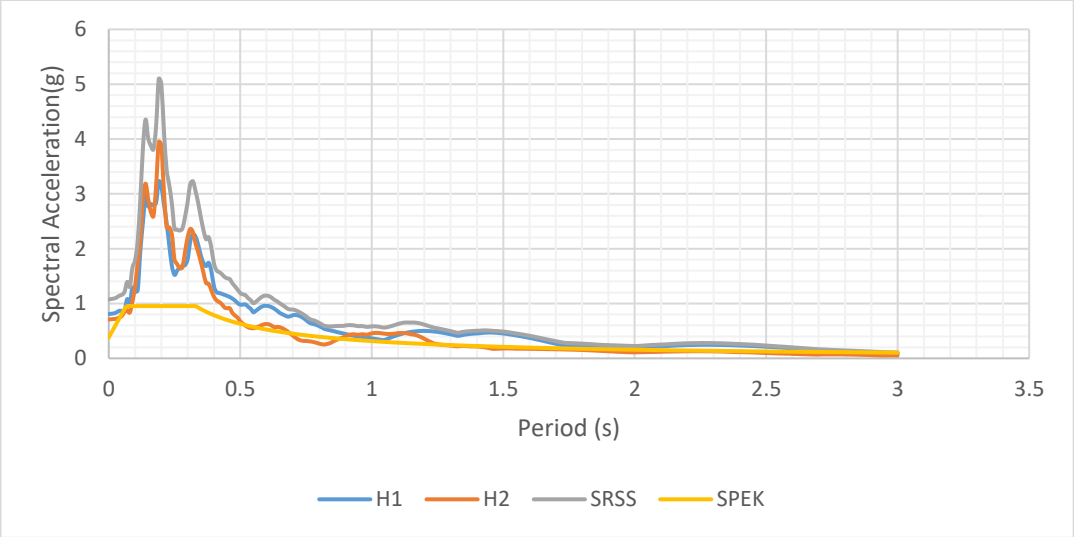

Figure A11. Scaled Horizontal Response Spectra of Livermore-01 (C1-210) Earthquake

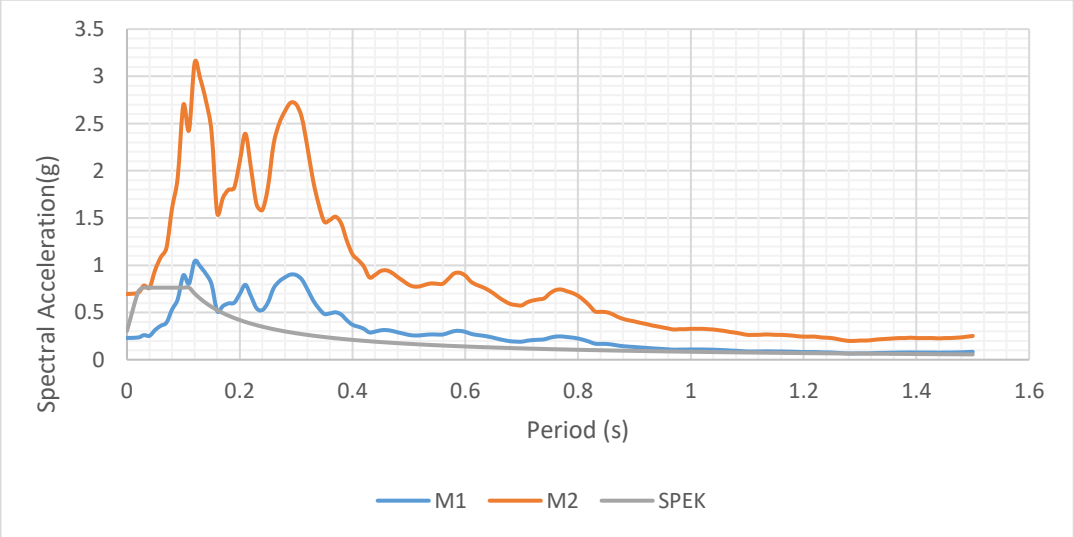

Figure A12. Scaled Vertical Response Spectra of Livermore-01 (C1-210) Earthquake

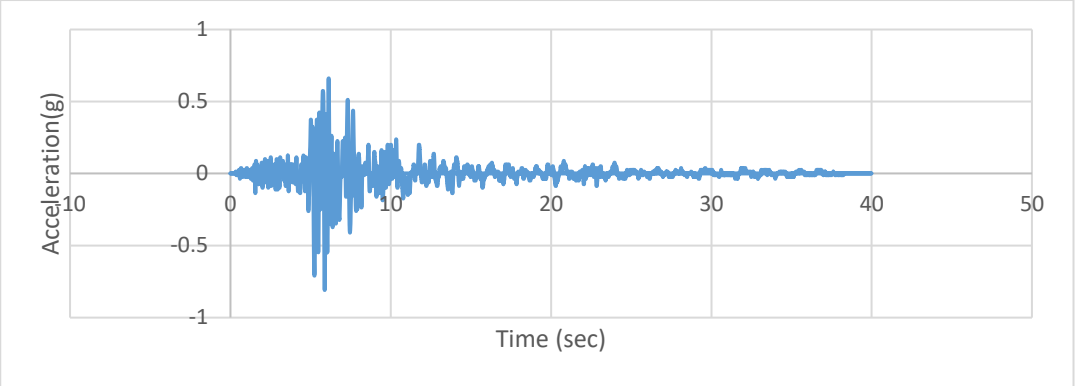

Figure A13. Scaled Acceleration Time Histories of Livermore-01 (C1-210X) Earthquake

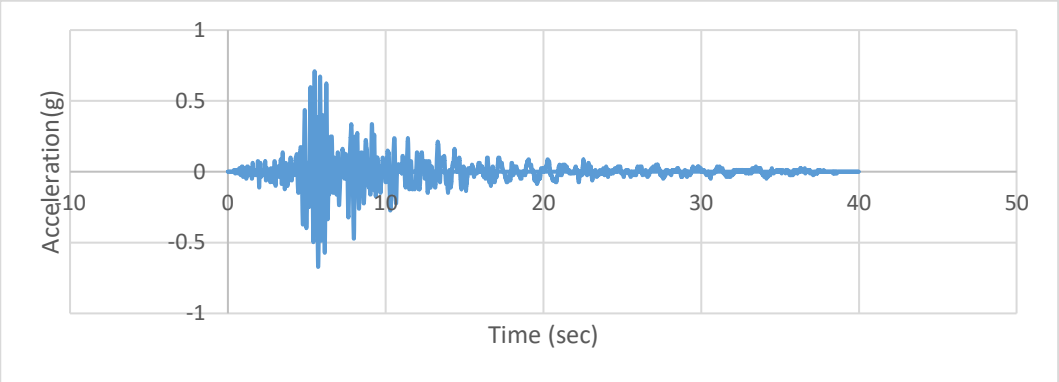

Figure A14. Scaled Acceleration Time Histories of Livermore-01 (C1-210Y) Earthquake

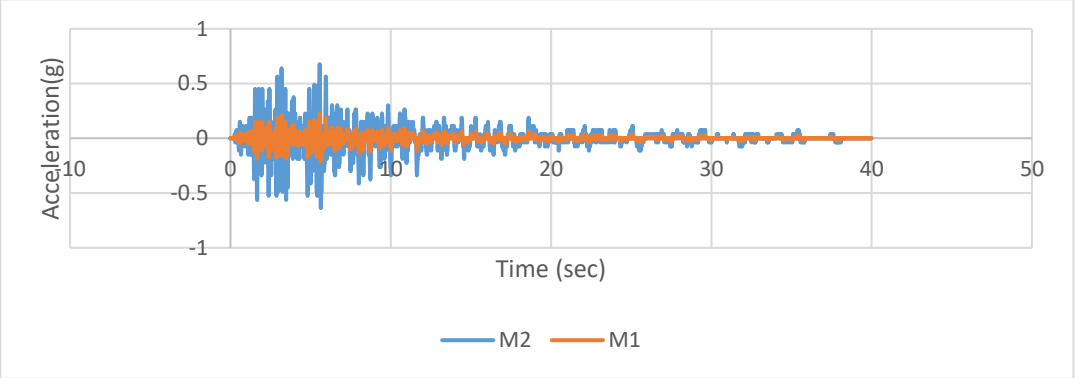

Figure A15. Scaled Acceleration Time Histories of Livermore-01 (C1-210Z) Earthquake

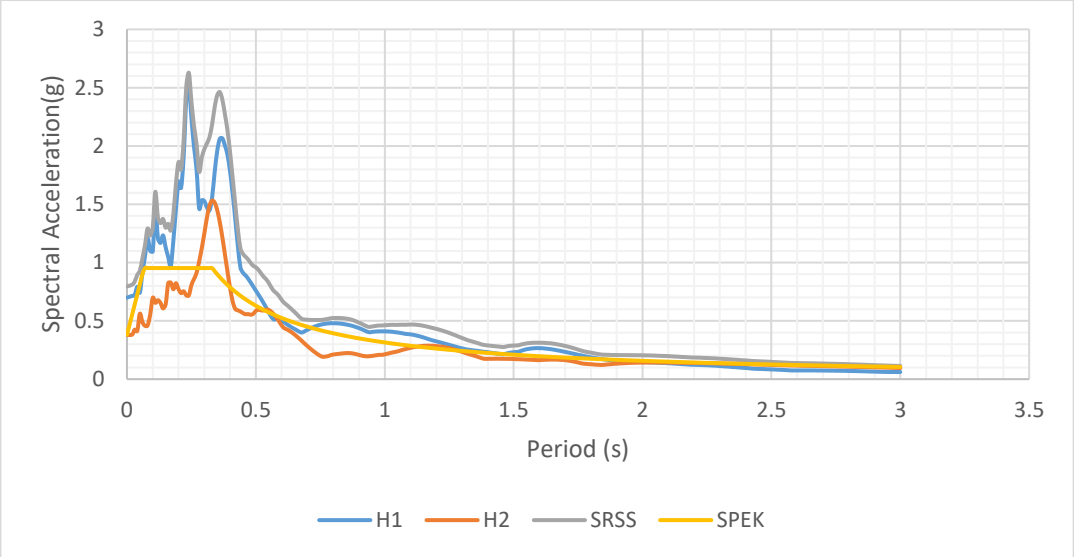

Figure A16. Scaled Horizontal Response Spectra of Mammoth Lakes-03 (C1-237) Earthquake

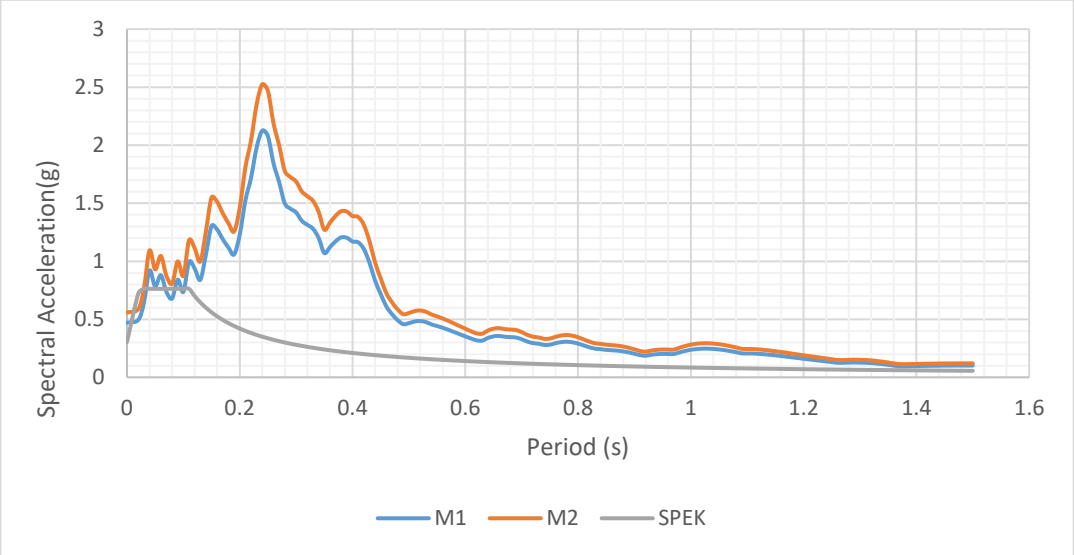

Figure A17. Scaled Acceleration Time Histories of Mammoth Lakes-03(C1-237) Earthquake

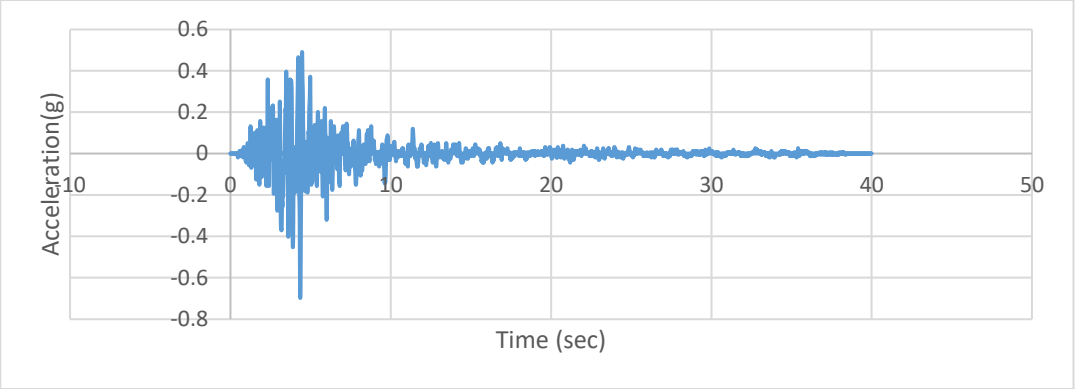

Figure A18. Scaled Vertical Response Spectra of Mammoth Lakes-03(C1-237X) Earthquake

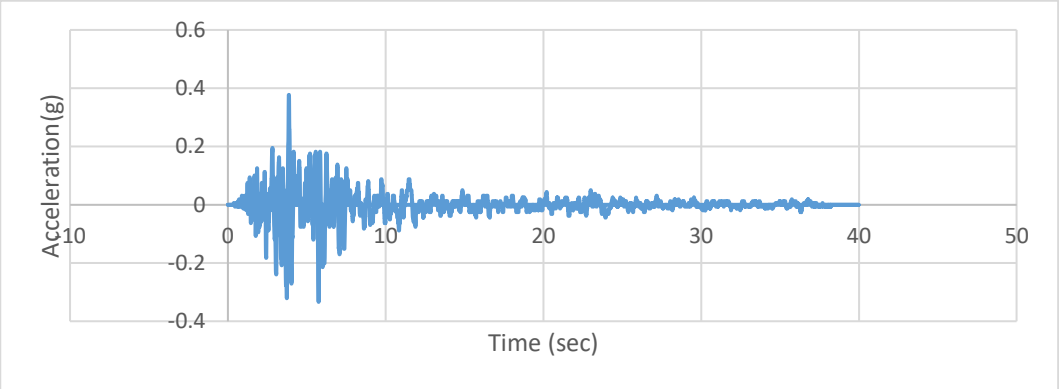

Figure A19. Scaled Vertical Response Spectra of Mammoth Lakes-03(C1-237Y) Earthquake

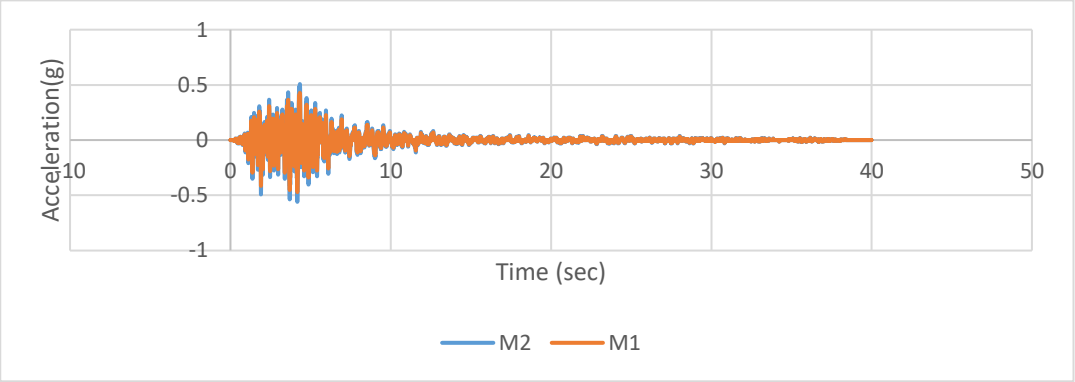

Figure A20. Scaled Vertical Response Spectra of Mammoth Lakes-03 (C1-237Z) Earthquake

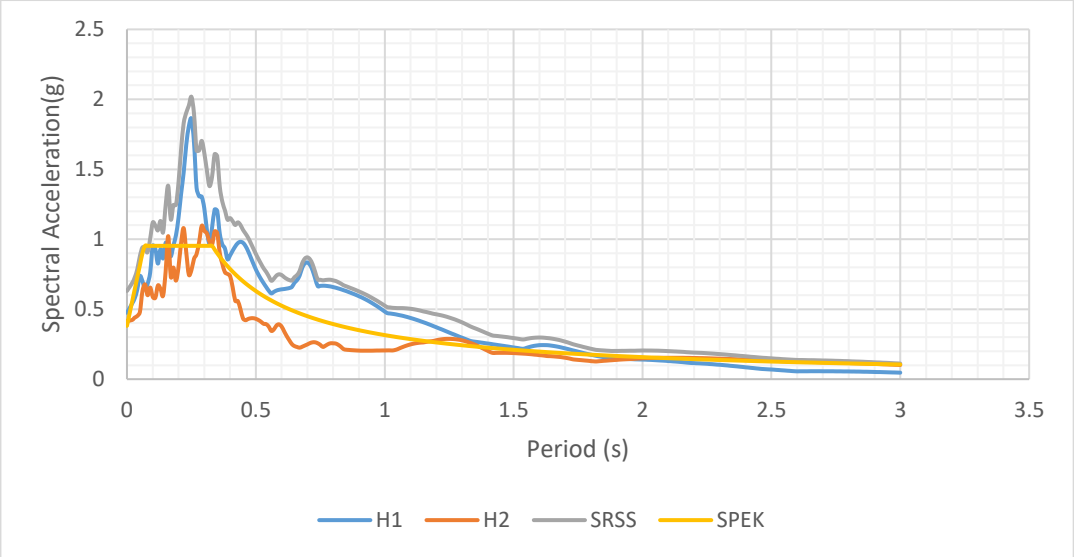

Figure A21. Scaled Horizontal Response Spectra of Mammoth Lakes-03 (C1-238) Earthquake

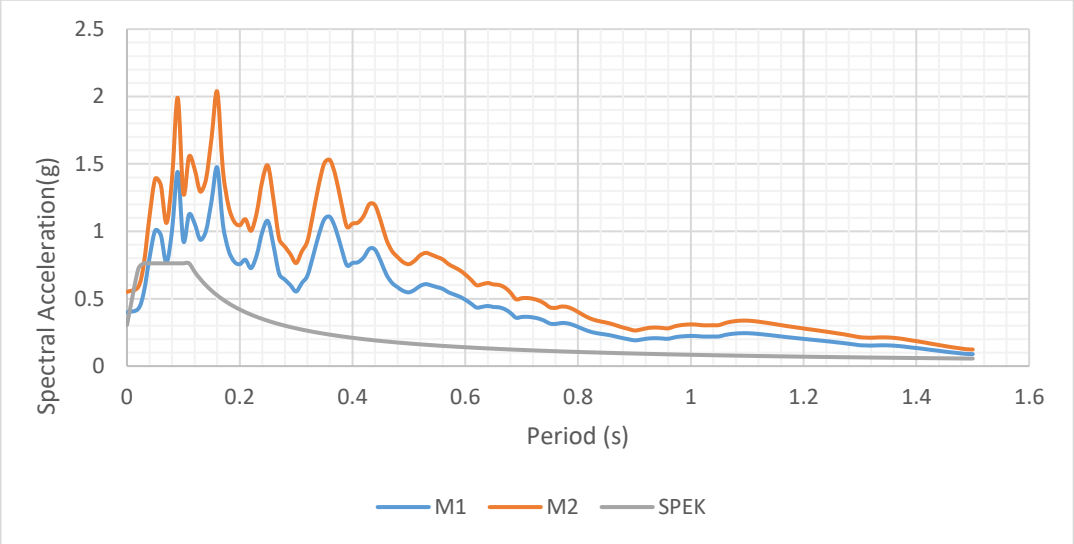

Figure A22. Scaled Acceleration Time Histories of Mammoth Lakes-03 (C1-238) Earthquake

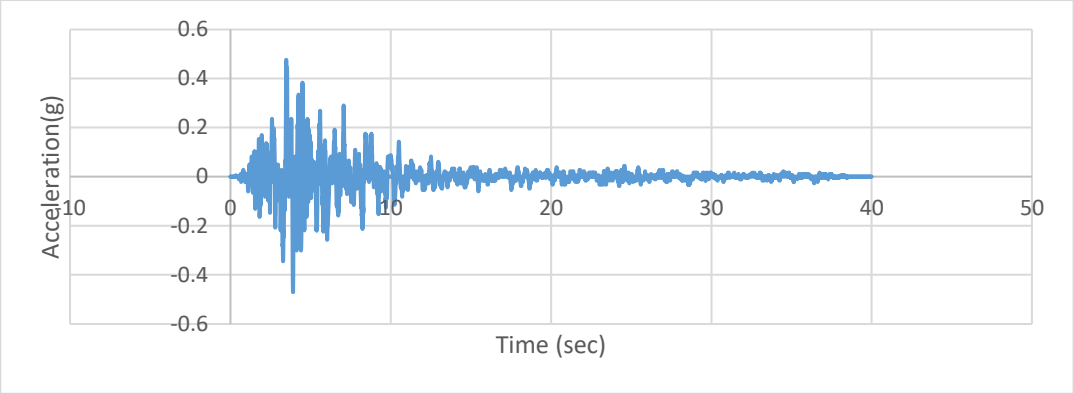

Figure A23. Scaled Vertical Response Spectra of Mammoth Lakes-03(C1-238X) Earthquake

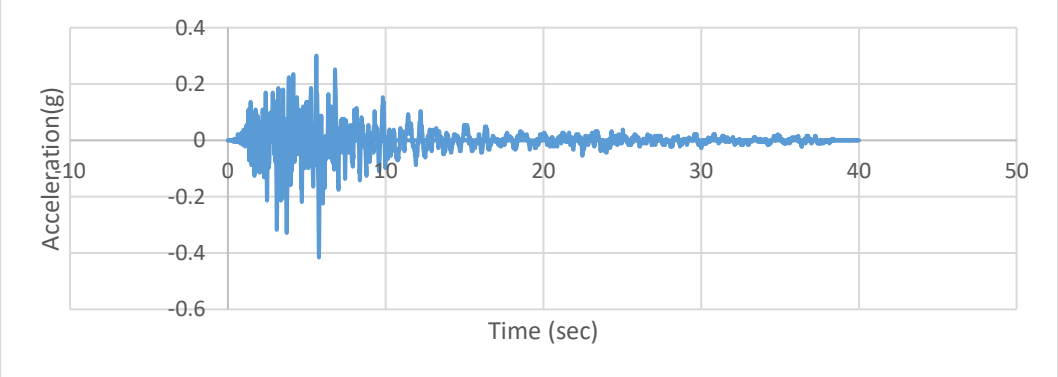

Figure A24. Scaled Vertical Response Spectra of Mammoth Lakes-03 (C1-238Y) Earthquake

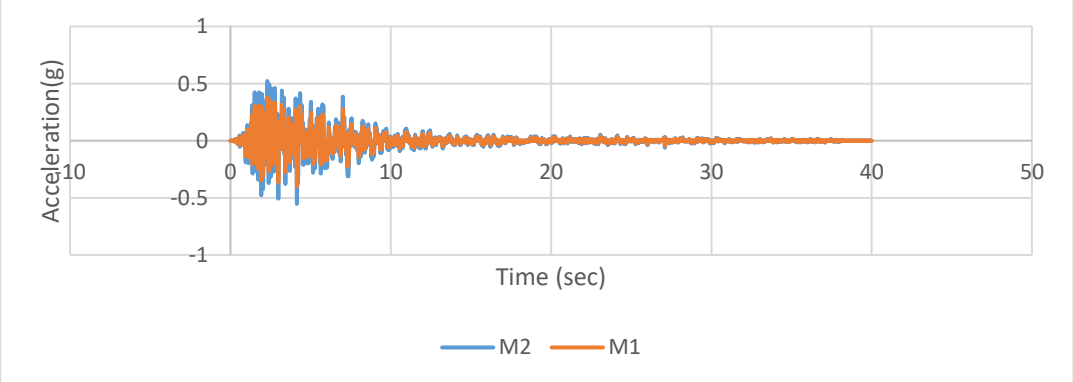

Figure A25. Scaled Vertical Response Spectra of Mammoth Lakes-03 (C1-238Z) Earthquake

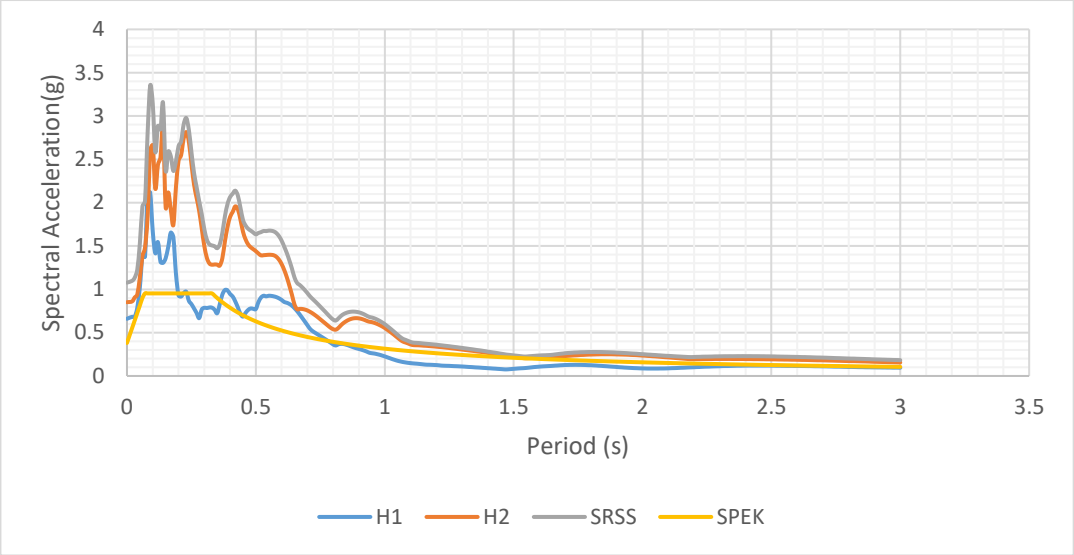

Figure A26. Scaled Horizontal Response Spectra of Westmorland (C1-318) Earthquake

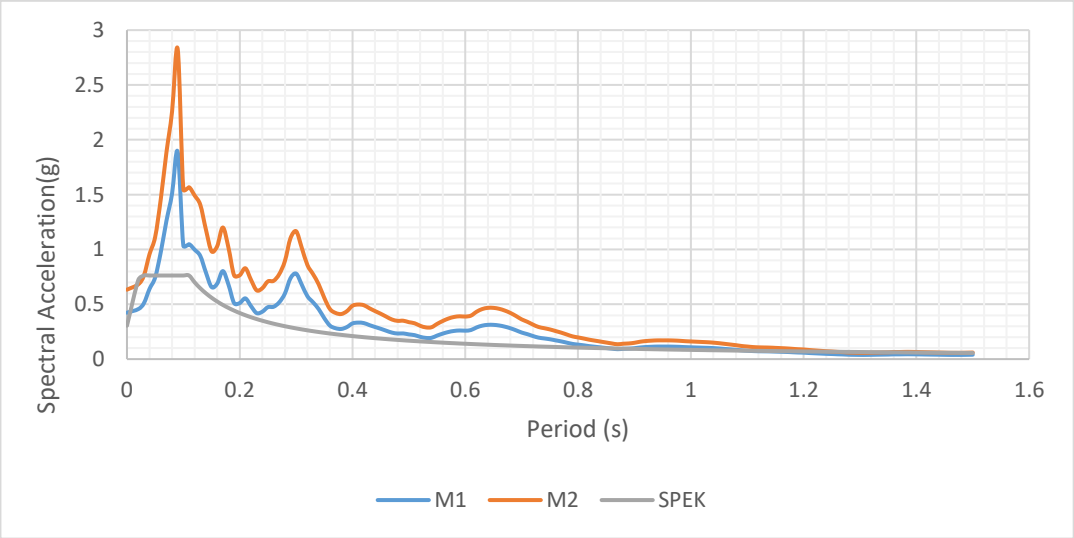

Figure A27. Scaled Vertical Response Spectra of Westmorland (C1-318) Earthquake

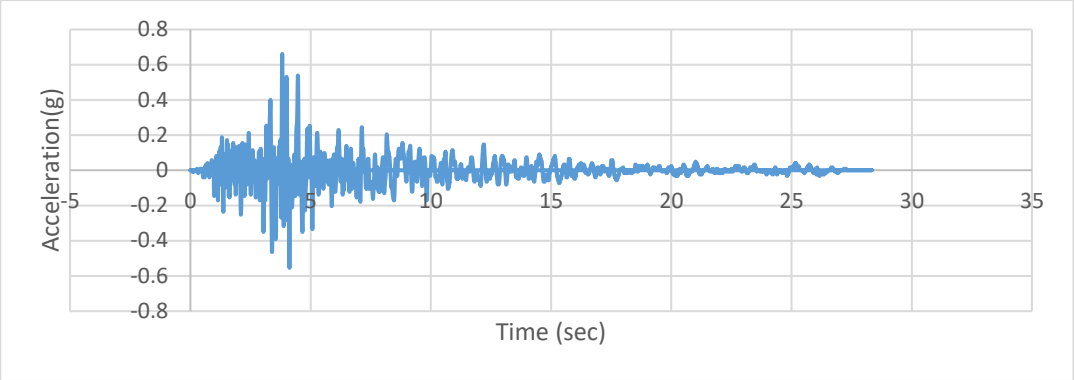

Figure A28. Scaled Acceleration Time Histories of Westmorland (C1-318X) Earthquake

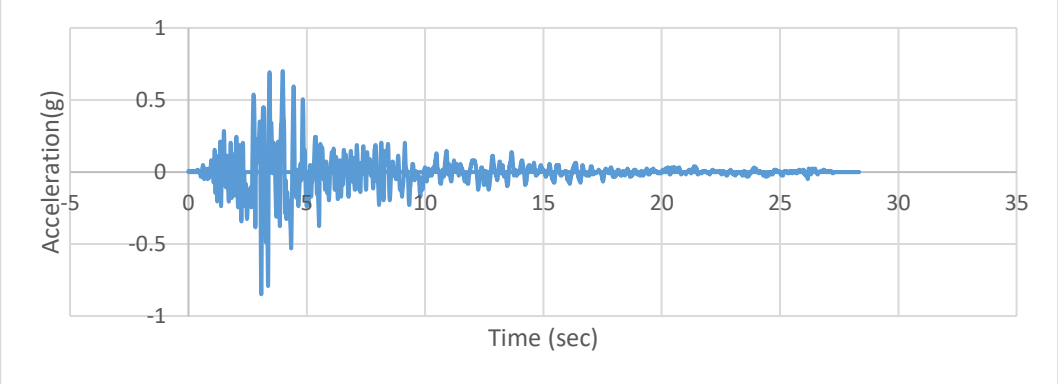

Figure A29. Scaled Acceleration Time Histories of Westmorland (C1-318Y) Earthquake

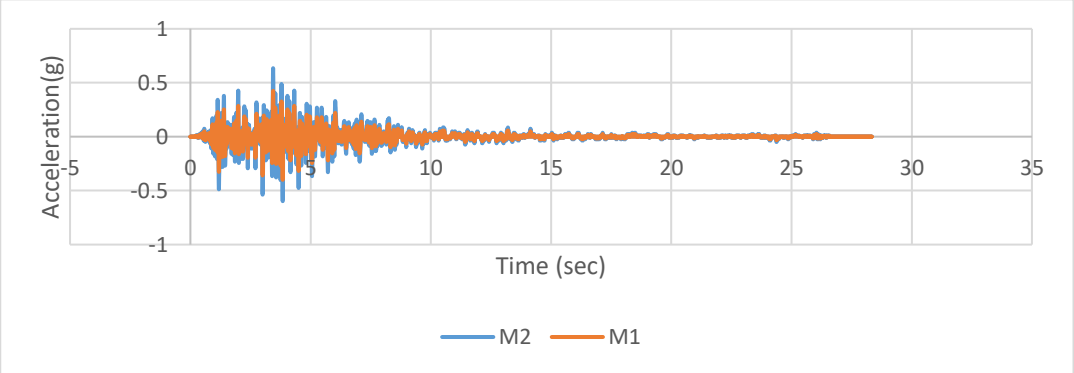

Figure A30. Scaled Acceleration Time Histories of Westmorland (C1-318Z) Earthquake

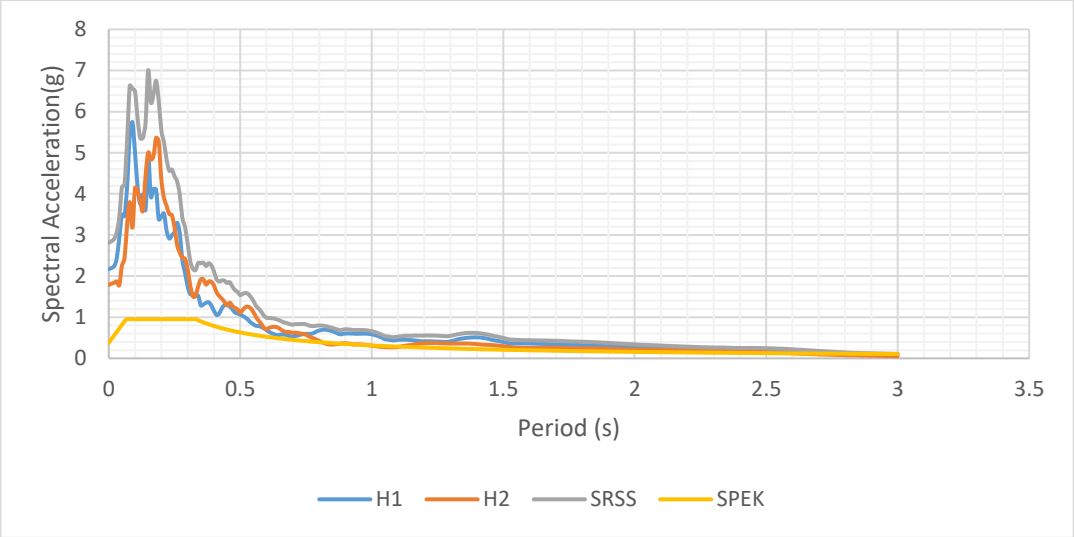

Figure A31. Scaled Horizontal Response Spectra of Morgan Hill (C1-454) Earthquake

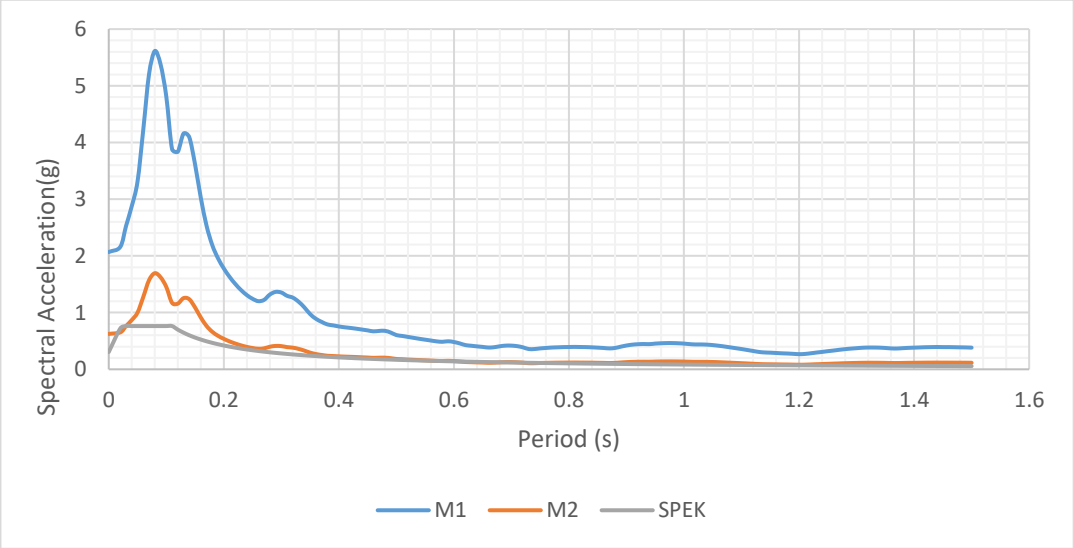

Figure A32. Scaled Vertical Response Spectra of Morgan Hill (C1-454) Earthquake

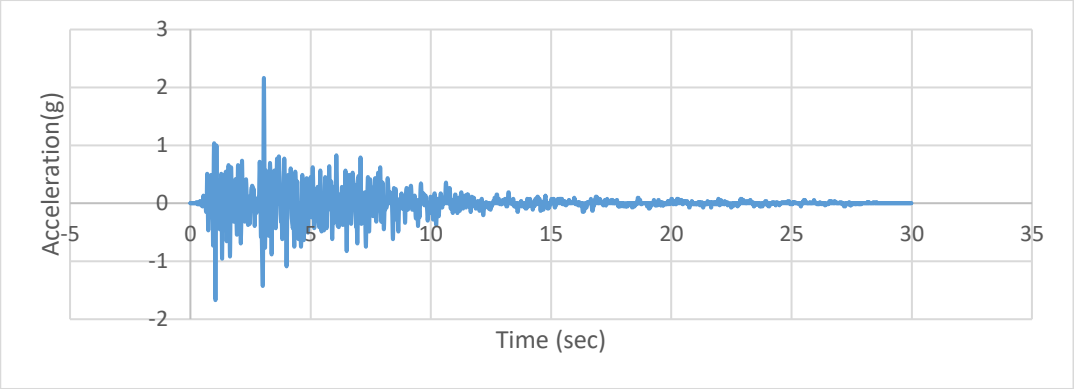

Figure A33. Scaled Acceleration Time Histories of Morgan Hill (C1-454X) Earthquake

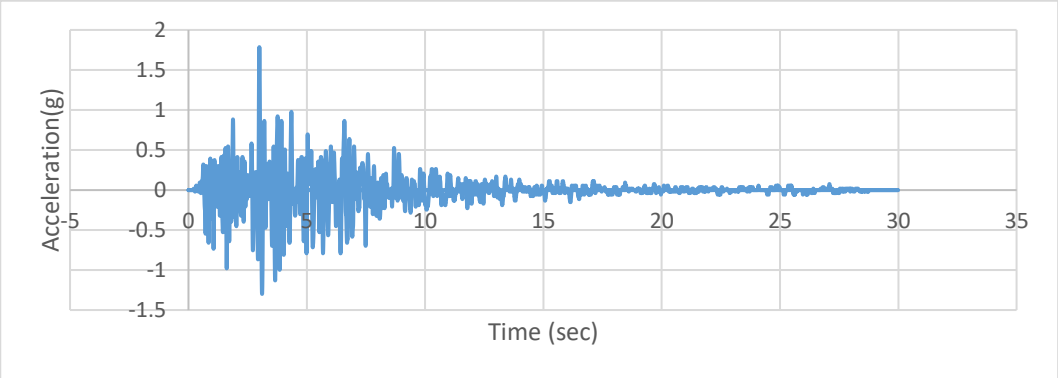

Figure A34. Scaled Acceleration Time Histories of Morgan Hill (C1-454Y) Earthquake

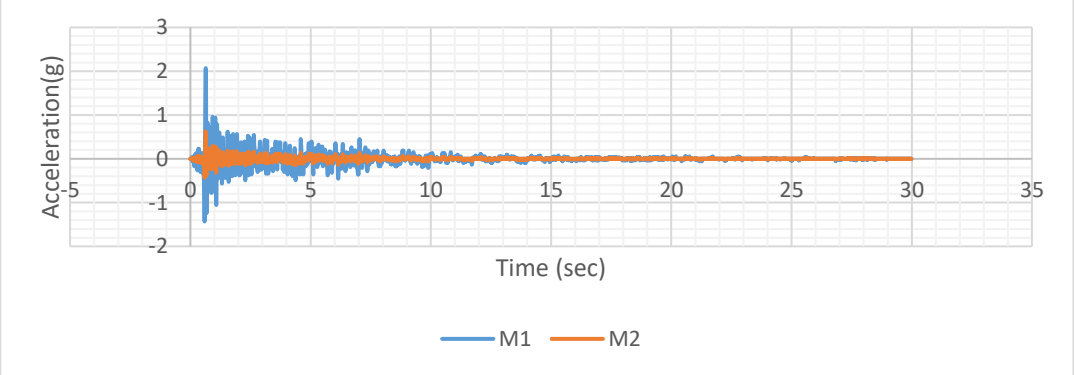

Figure A35. Scaled Acceleration Time Histories of Morgan Hill (C1-454Z) Earthquake

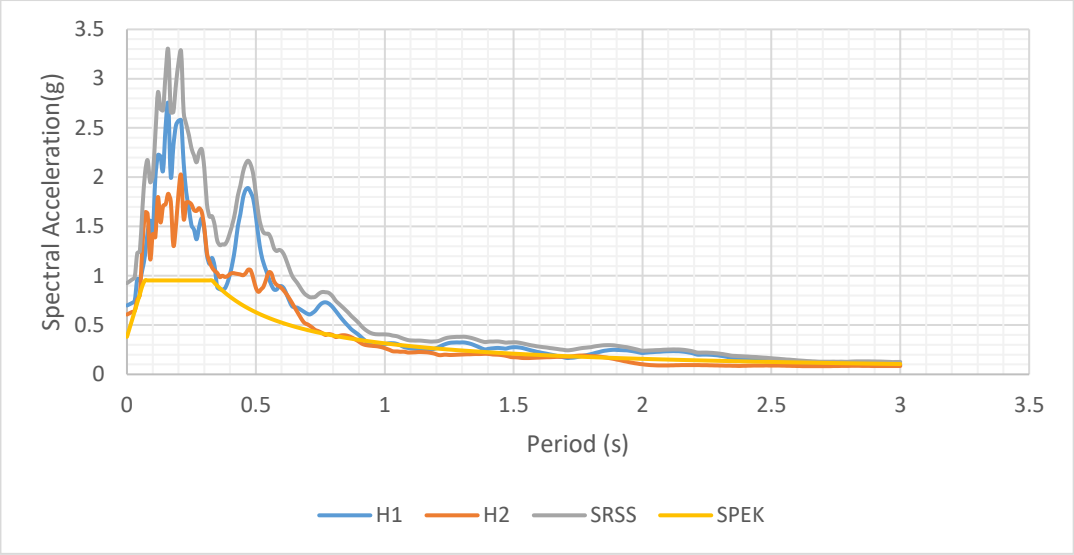

Figure A36. Scaled Horizontal Response Spectra of Chalfant Valley-01(C1-543) Earthquake

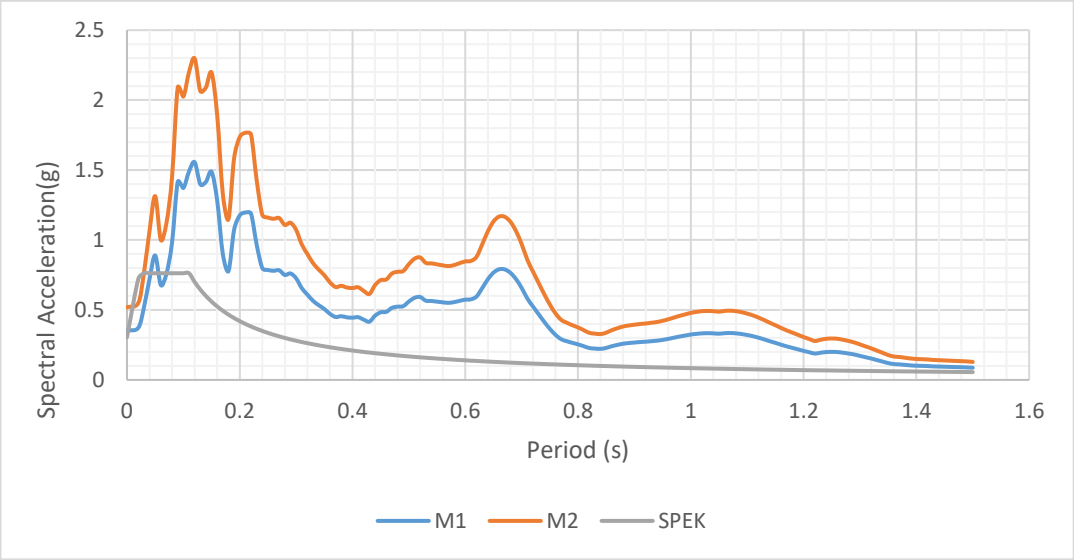

Figure A37. Scaled Vertical Response Spectra of Chalfant Valley-01(C1-543) Earthquake

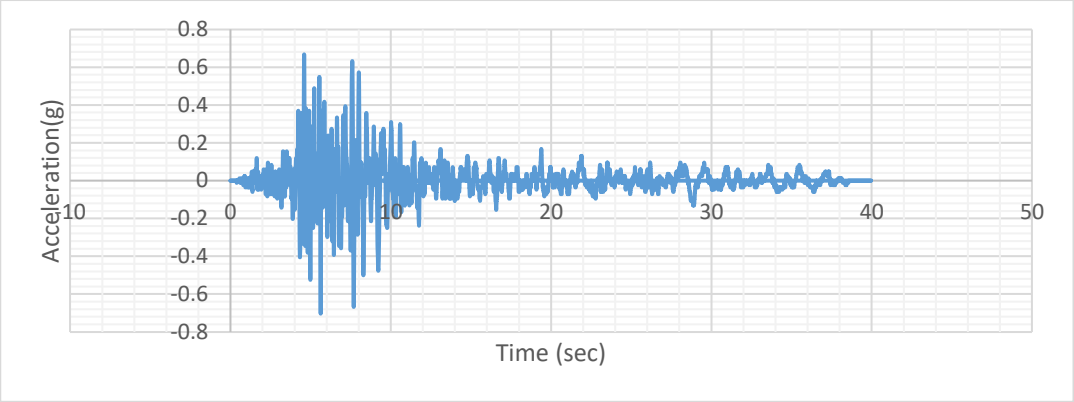

Figure A38. Scaled Acceleration Time Histories of Chalfant Valley-01(C1-543X) Earthquake

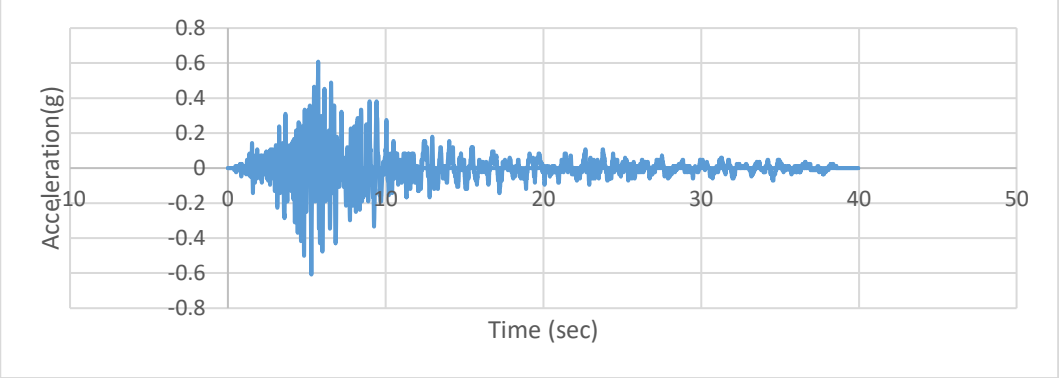

Figure A39. Scaled Acceleration Time Histories of Chalfant Valley-01 (C1-543Y) Earthquake

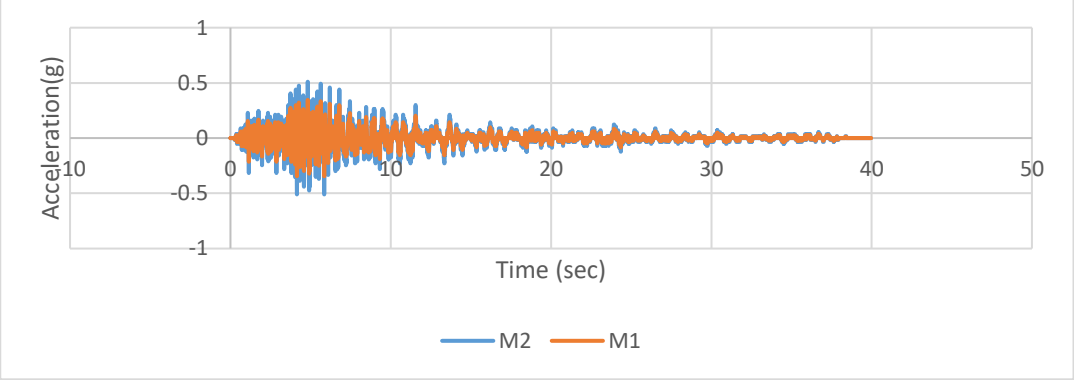

Figure A40. Scaled Acceleration Time Histories of Chalfant Valley-01(C1-543Z) Earthquake

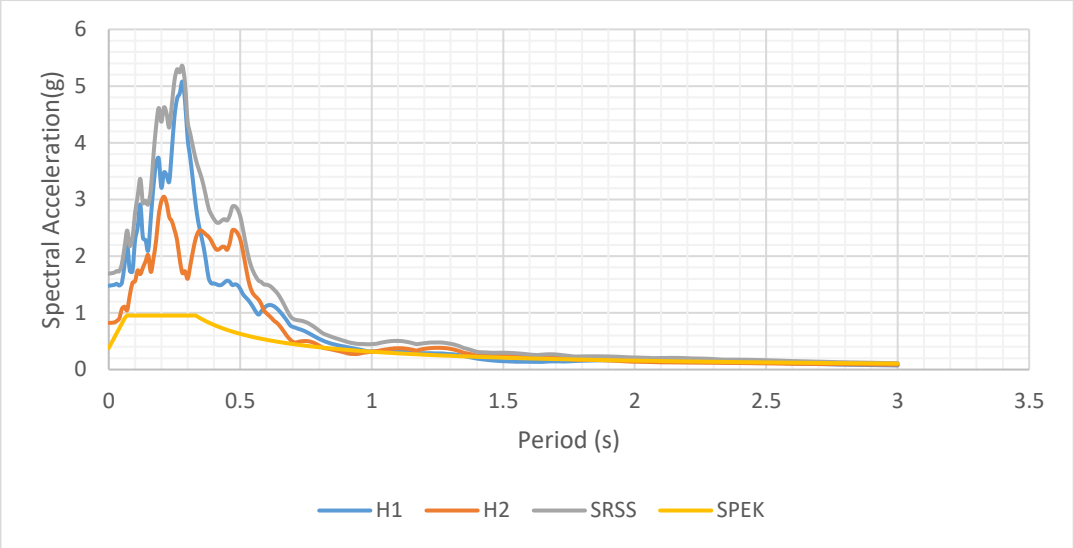

Figure A41. Scaled Horizontal Response Spectra of Chalfant Valley-02 (C1-552) Earthquake

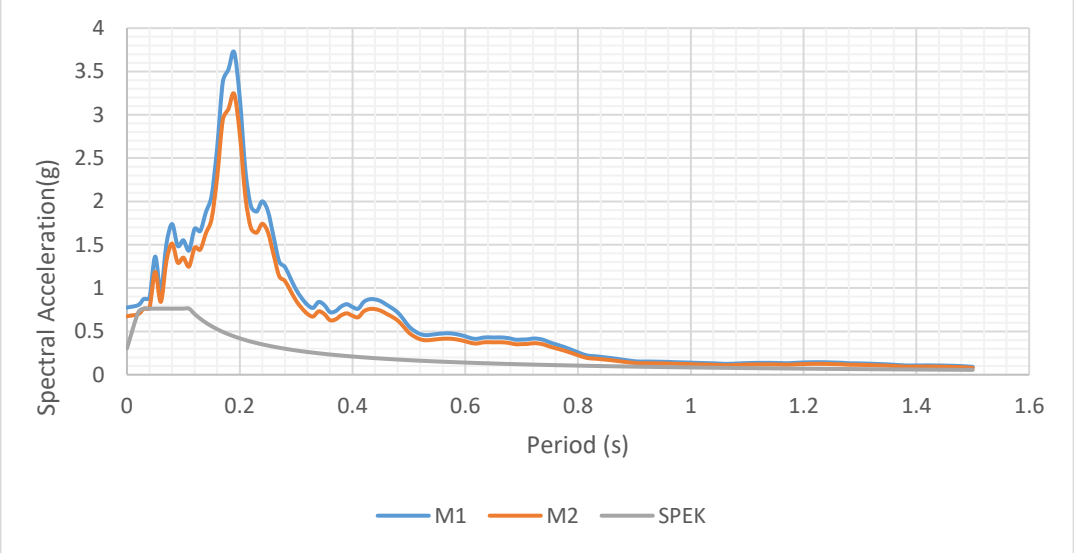

Figure A42. Scaled Vertical Response Spectra of Chalfant Valley-02 (C1-552) Earthquake

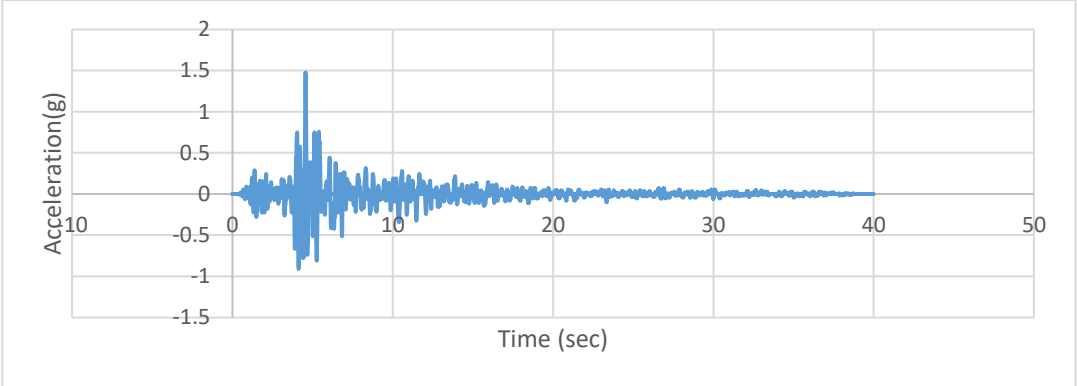

Figure A43. Scaled Acceleration Time Histories of Chalfant Valley-02 (C1-552X) Earthquake

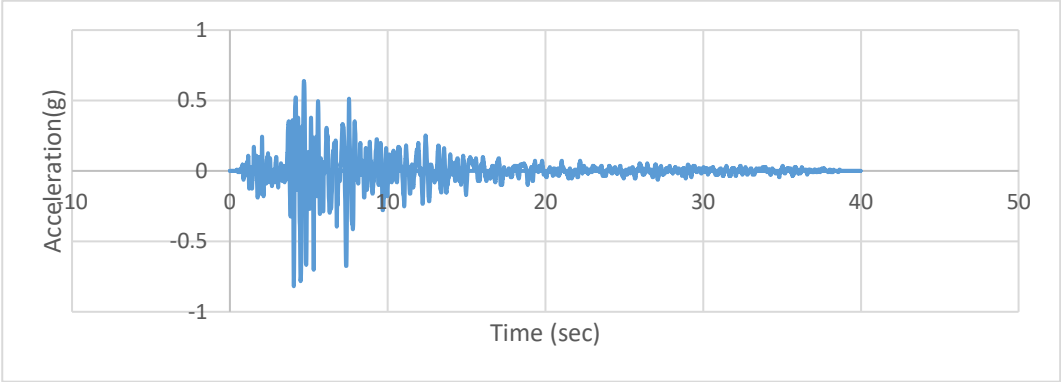

Figure A44. Scaled Acceleration Time Histories of Chalfant Valley-02 (C1-552Y) Earthquake

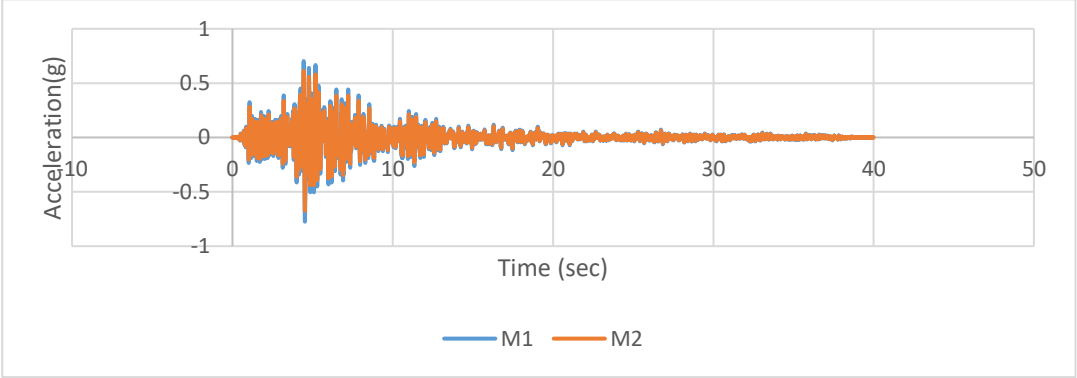

Figure A45. Scaled Acceleration Time Histories of Chalfant Valley-02 (C1-552Z) Earthquake

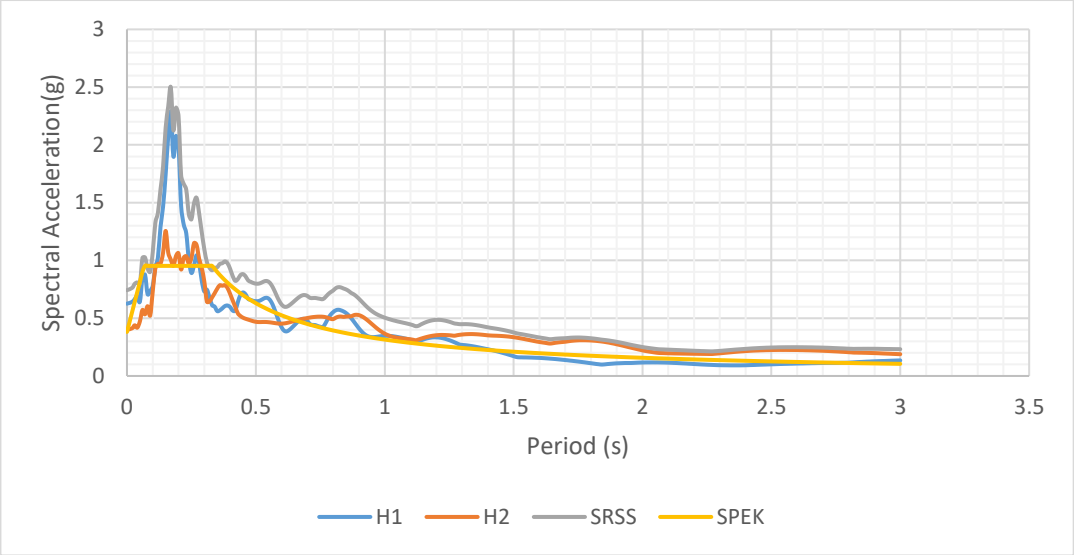

Figure A46. Scaled Horizontal Response Spectra of Kocaeli (C1-1148) Earthquake

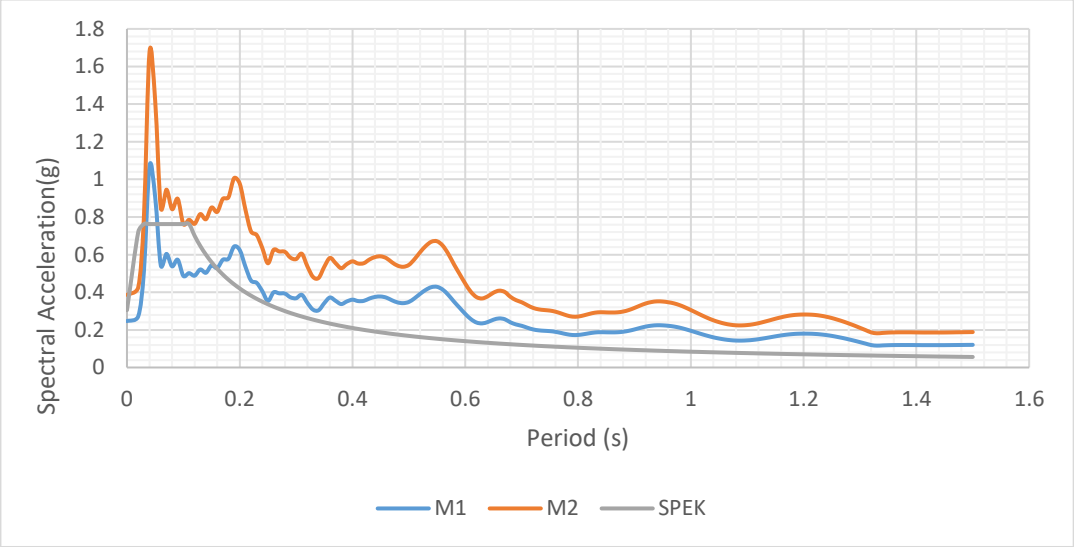

Figure A47. Scaled Vertical Response Spectra of Kocaeli (C1-1148) Earthquake

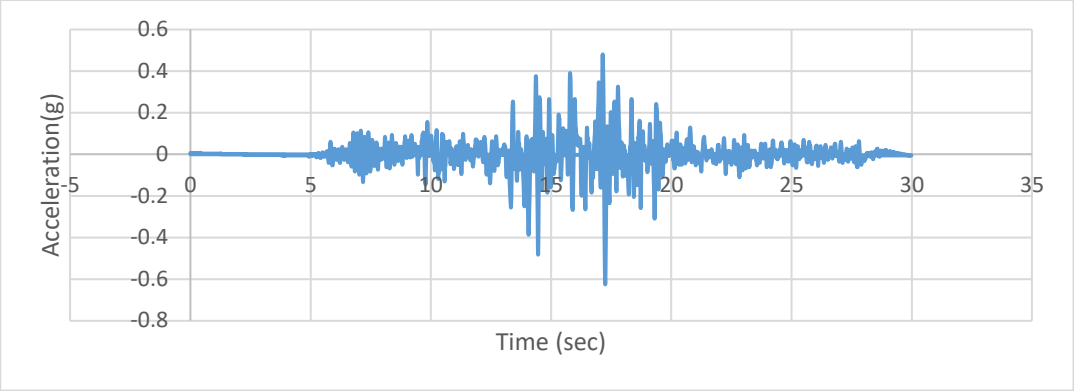

Figure A48. Scaled Acceleration Time Histories of Kocaeli (C1-1148X) Earthquake

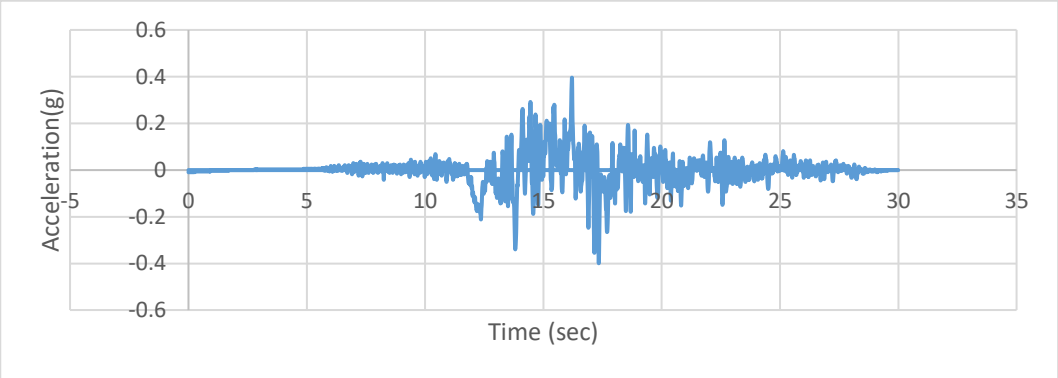

Figure A49. Scaled Acceleration Time Histories of Kocaeli (C1-1148Y) Earthquake

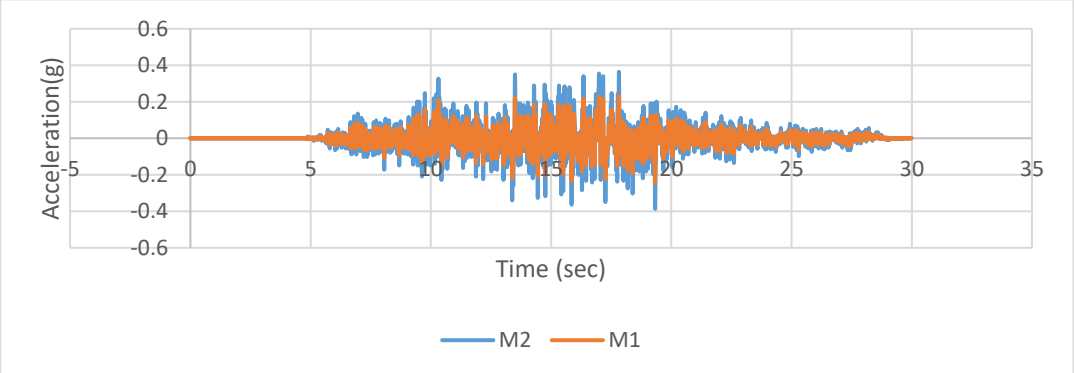

Figure A50. Scaled Acceleration Time Histories of Kocaeli (C1-1148Z) Earthquake

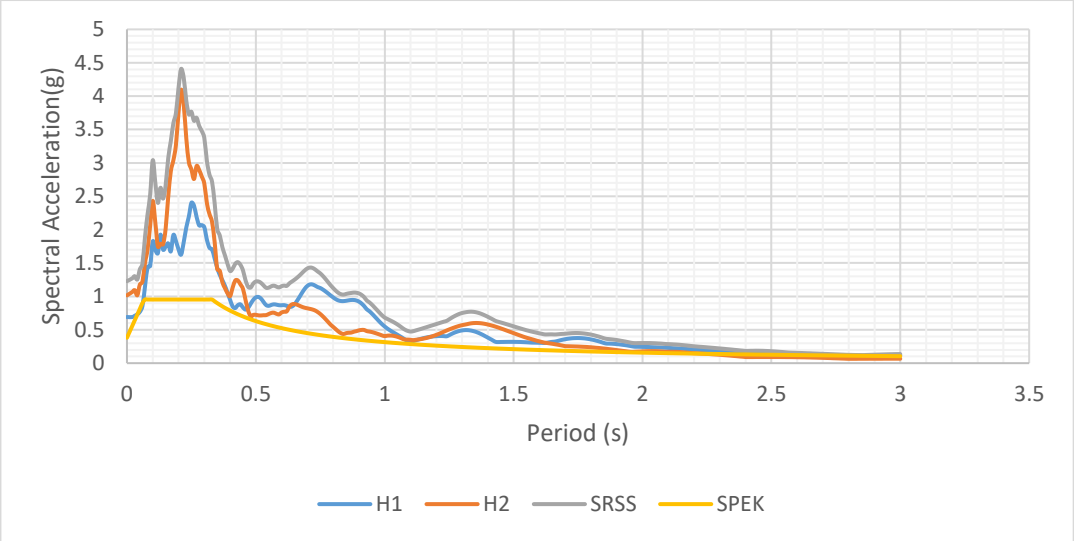

Figure A51.Scaled Horizontal Response Spectra of Big Bear-01 (C1-6057) Earthquake

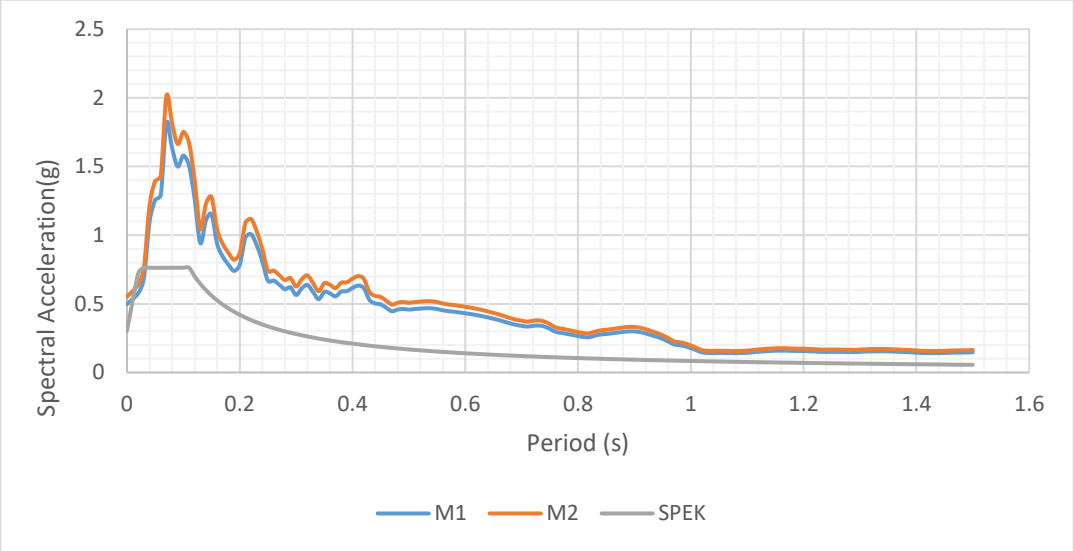

Figure A52. Scaled Vertical Response Spectra of Big Bear-01 (C1-6057) Earthquake

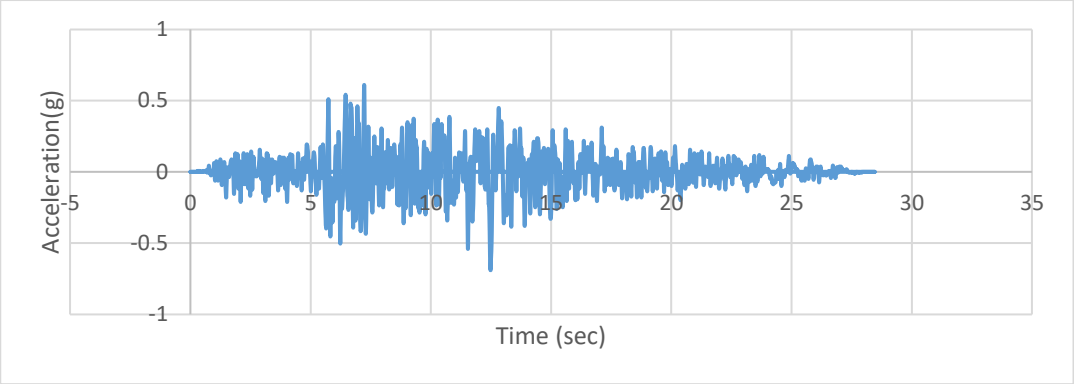

Figure A53.Scaled Acceleration Time Histories of Big Bear-01 (C1-6057X) Earthquake

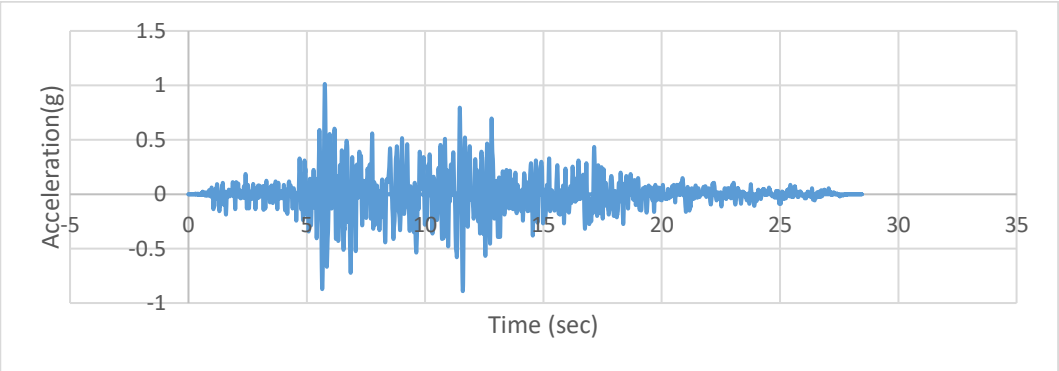

Figure A54. Scaled Acceleration Time Histories of Big Bear-01 (C1-6057Y) Earthquake

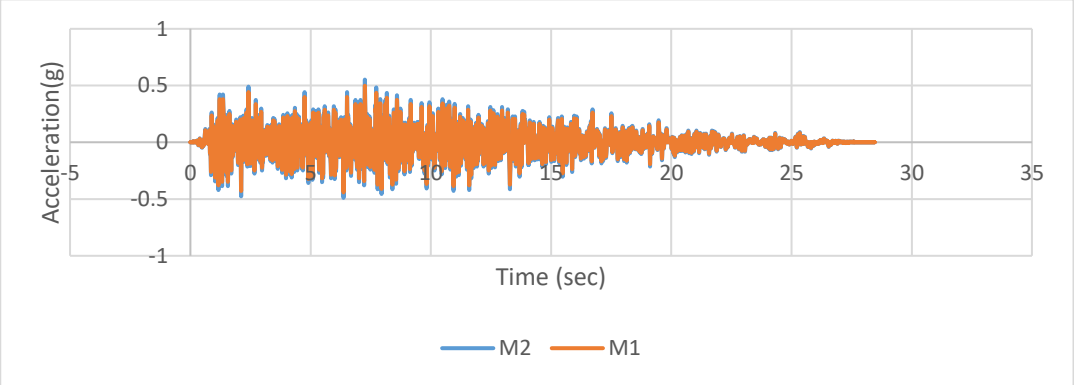

Figure A55. Scaled Acceleration Time Histories of Big Bear-01 (C1-6057Z) Earthquake

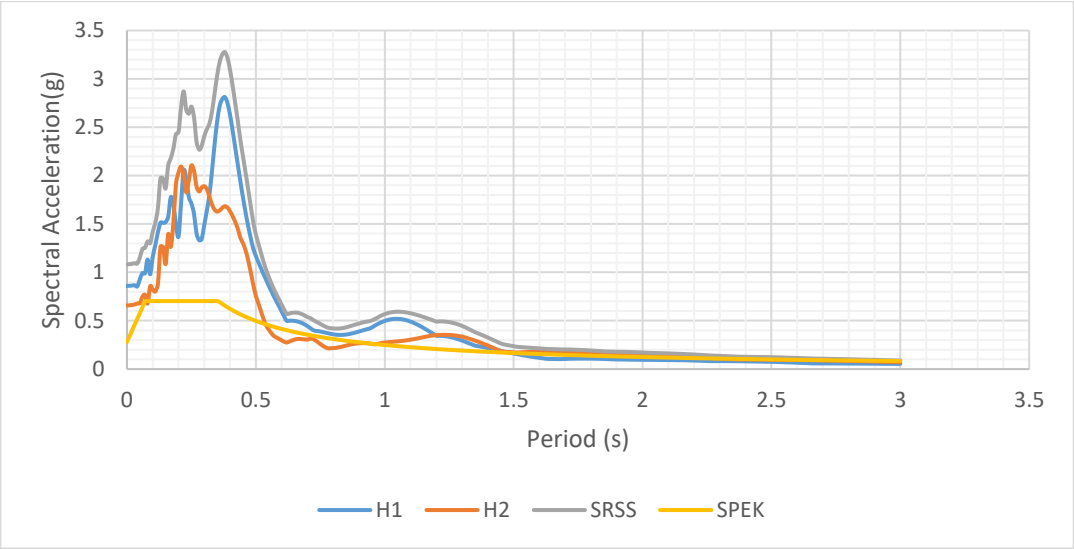

Figure A56. Scaled Horizontal Response Spectra of Parkfield (C2 -33) Earthquake

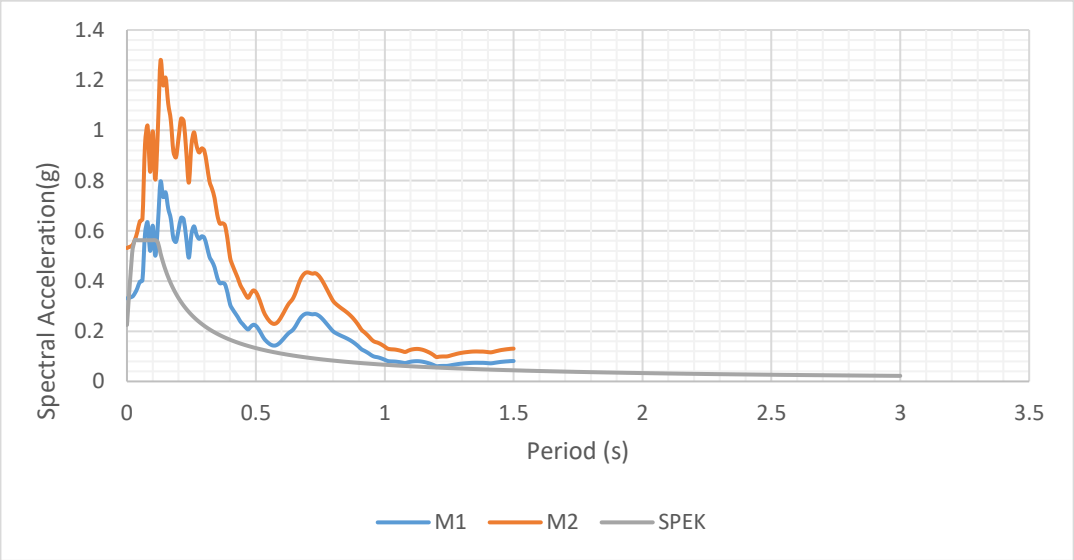

Figure A57. Scaled Vertical Response Spectra of Parkfield (C2 -33) Earthquake

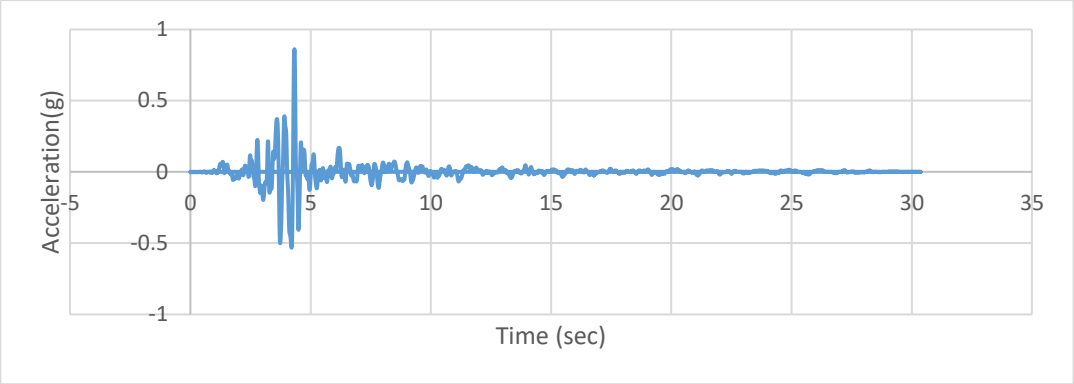

Figure A58. Scaled Acceleration Time Histories of Parkfield (C2 -33X) Earthquake

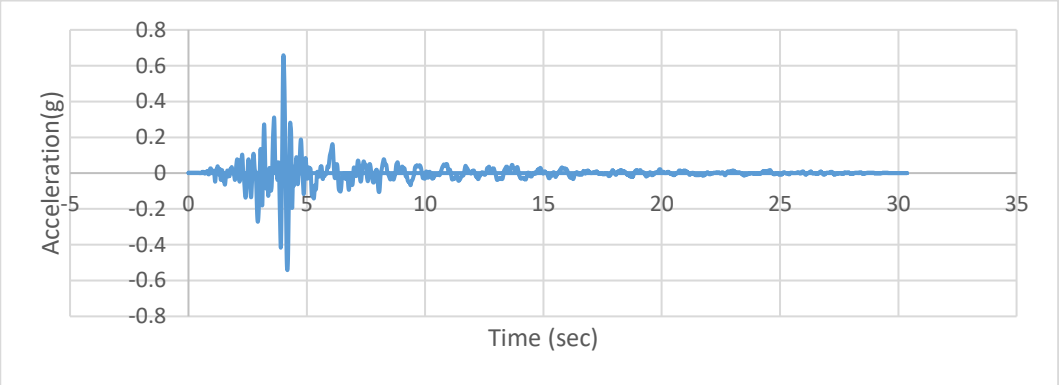

Figure A59. Scaled Acceleration Time Histories of Parkfield (C2 -33Y) Earthquake

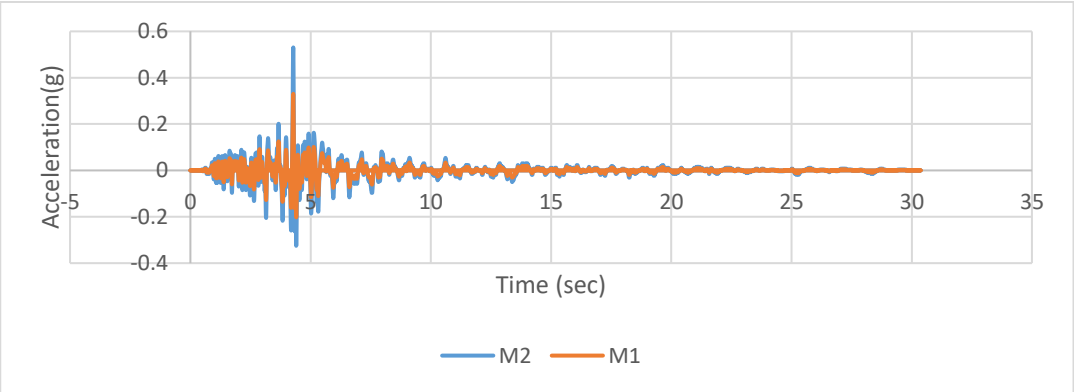

Figure A60. Scaled Acceleration Time Histories of Parkfield (C2 -33Z) Earthquake

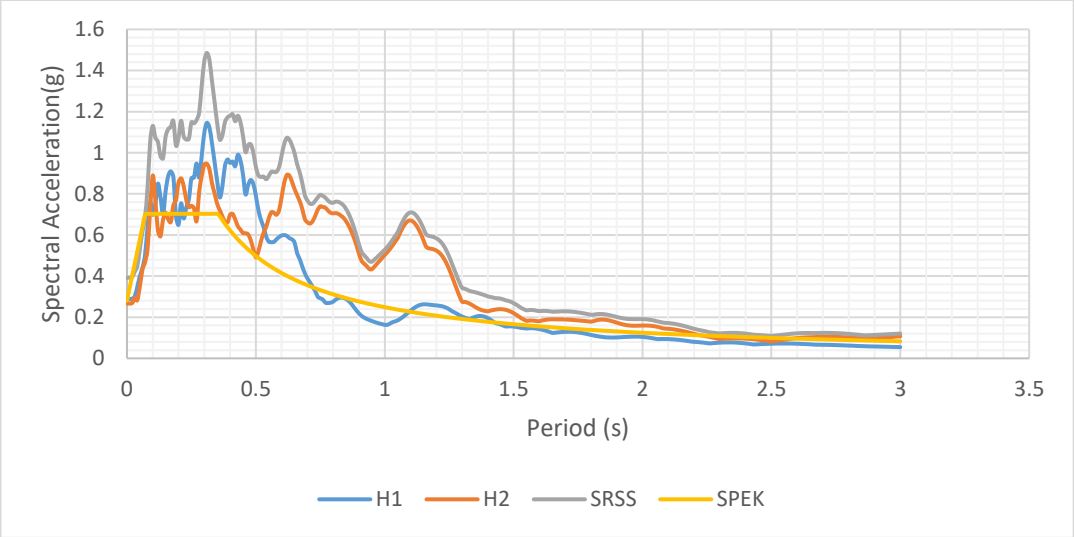

Figure A61. Scaled Horizontal Response Spectra of Imperial Valley-06 (C2-164) Earthquake

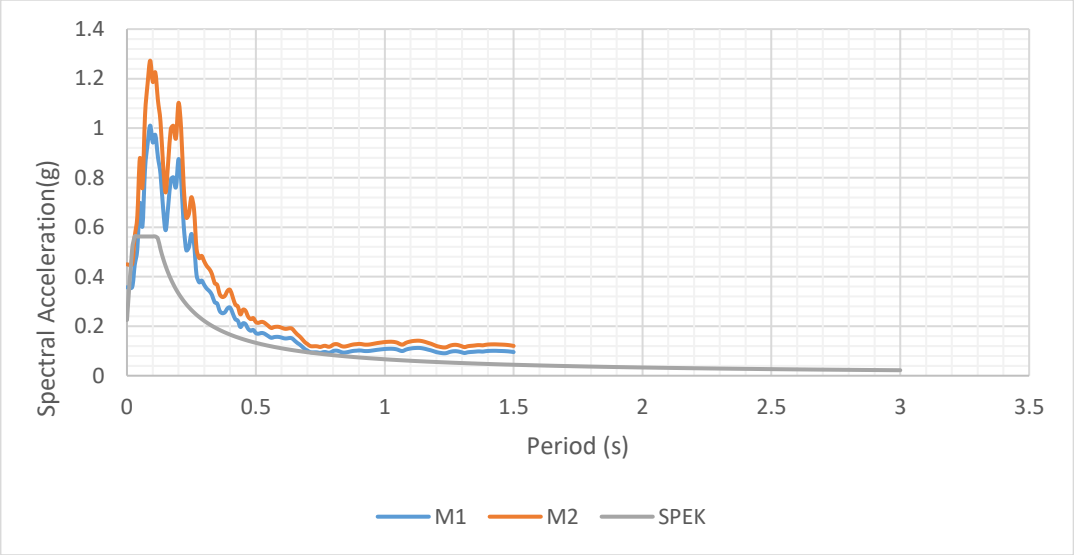

Figure A62. Scaled Vertical Response Spectra of Imperial Valley-06 (C2-164) Earthquake

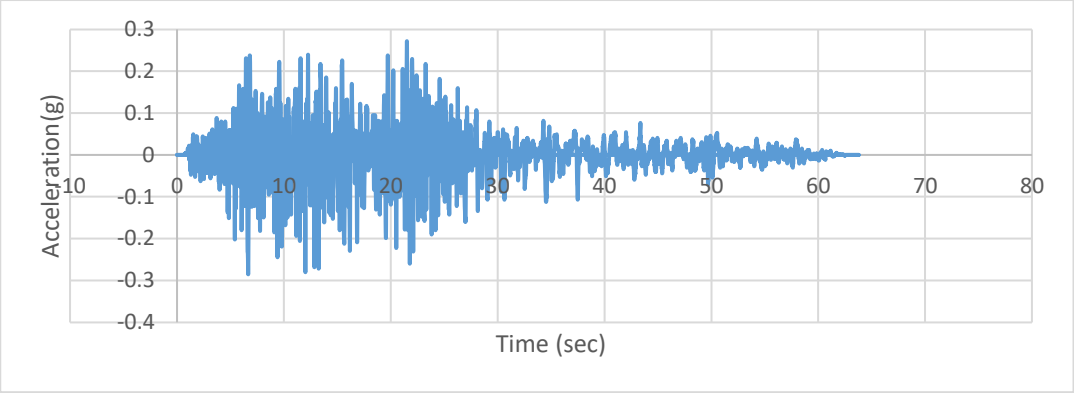

Figure A63. Scaled Acceleration Time Histories of Imperial Valley-06 (C2-164X) Earthquake

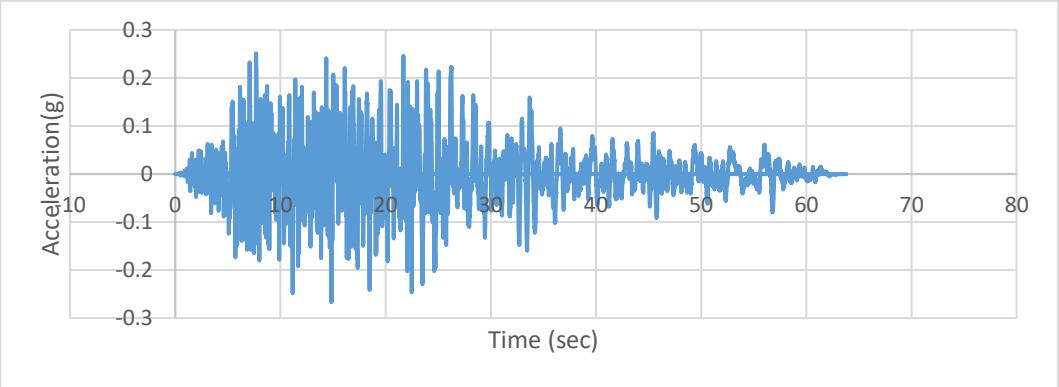

Figure A64. Scaled Acceleration Time Histories of Imperial Valley-06 (C2-164Y) Earthquake

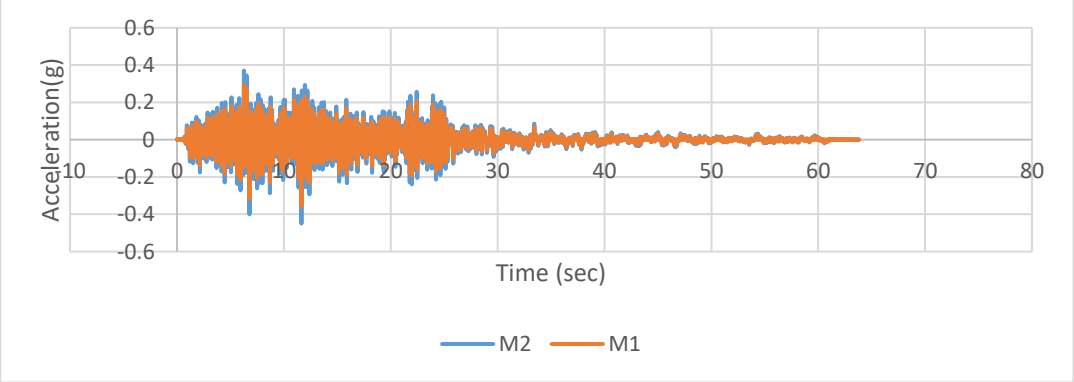

Figure A65. Scaled Acceleration Time Histories of Imperial Valley-06 (C2-164Z) Earthquake

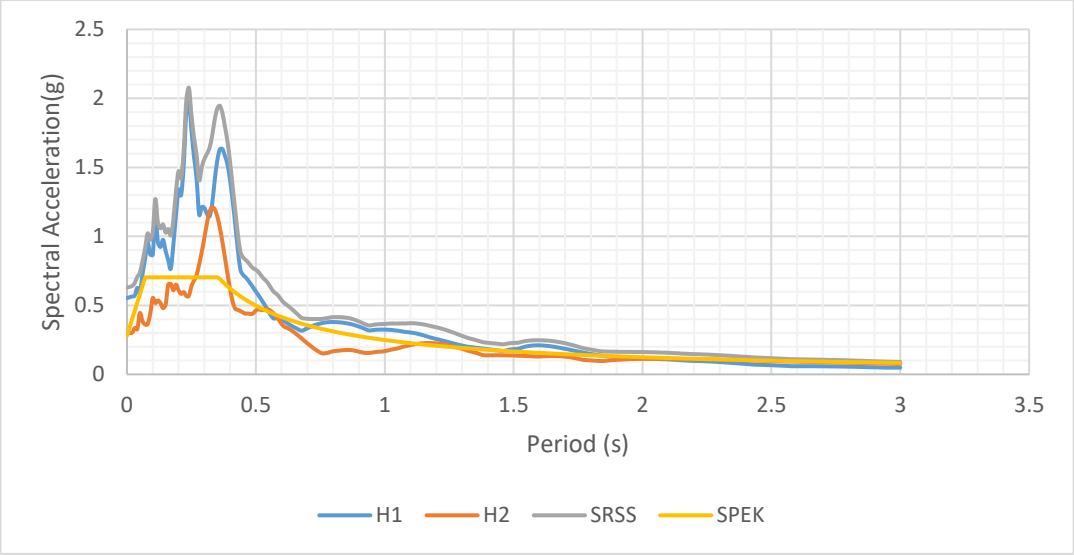

Figure A66. Scaled Horizontal Response Spectra of Mammoth Lakes-03 (C2-237) Earthquake

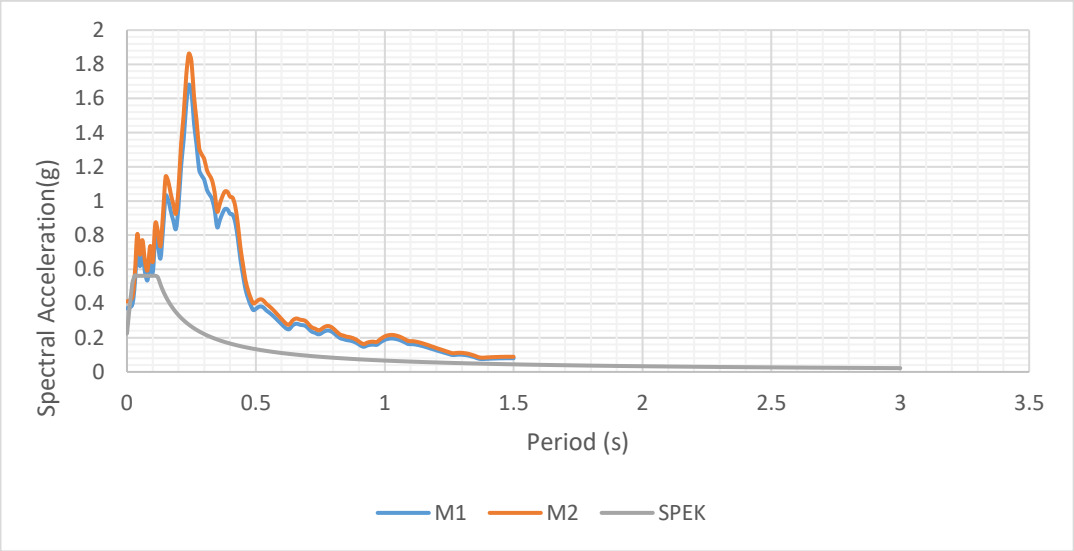

Figure A67. Scaled Vertical Response Spectra of Mammoth Lakes-03 (C2-237) Earthquake

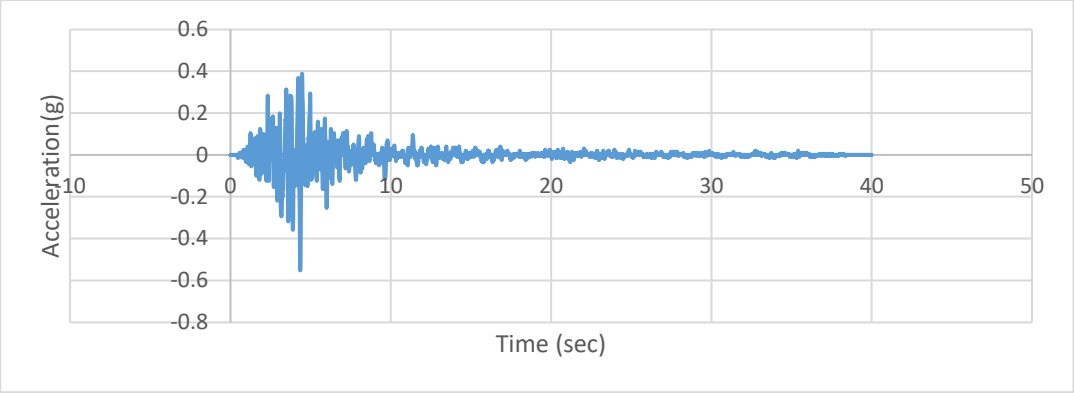

Figure A68. Scaled Acceleration Time Histories of Mammoth Lakes-03 (C2-237X) Earthquake

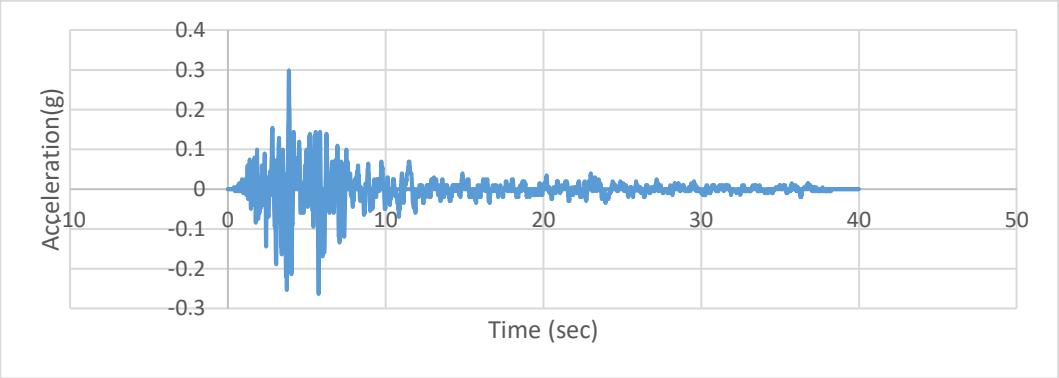

Figure A69. Scaled Acceleration Time Histories of Mammoth Lakes-03 (C2-237Y) Earthquake

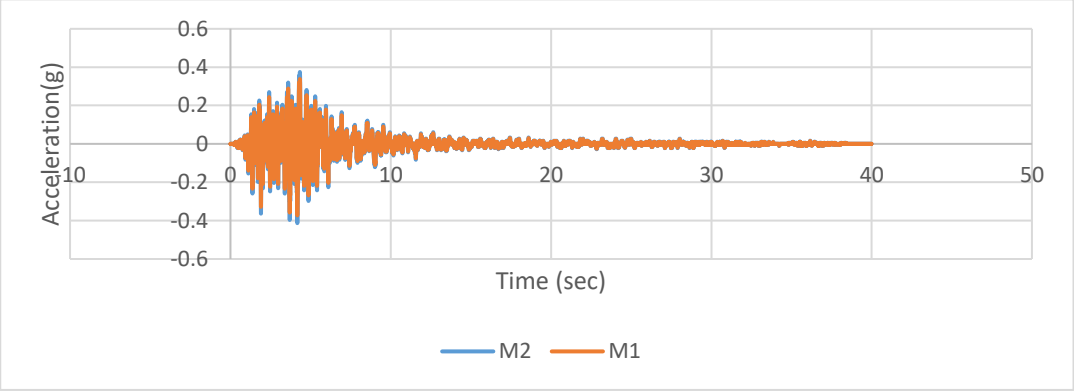

Figure A70. Scaled Acceleration Time Histories of Mammoth Lakes-03 (C2-237Z) Earthquake

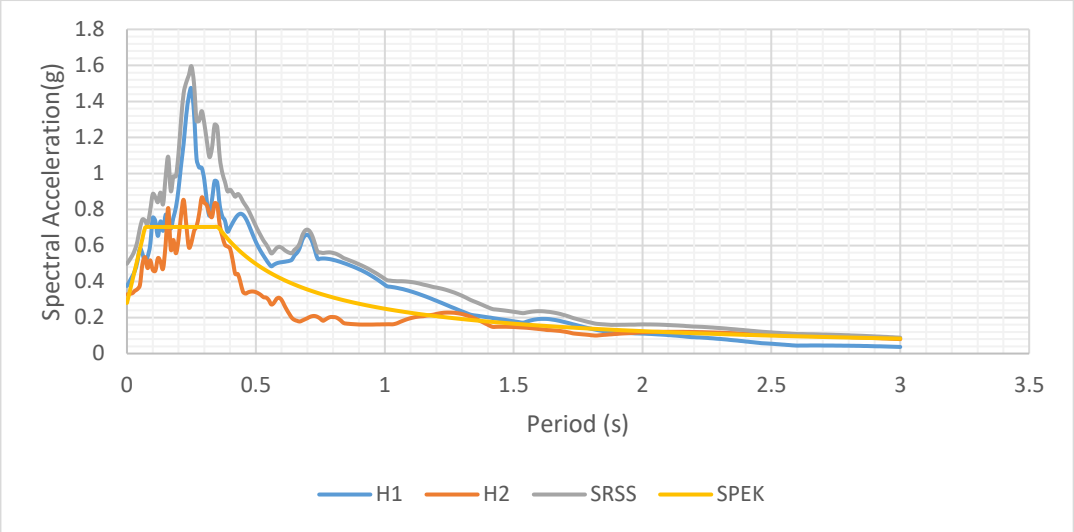

Figure A71. Scaled Horizontal Response Spectra of Mammoth Lakes-03 (C2-238) Earthquake

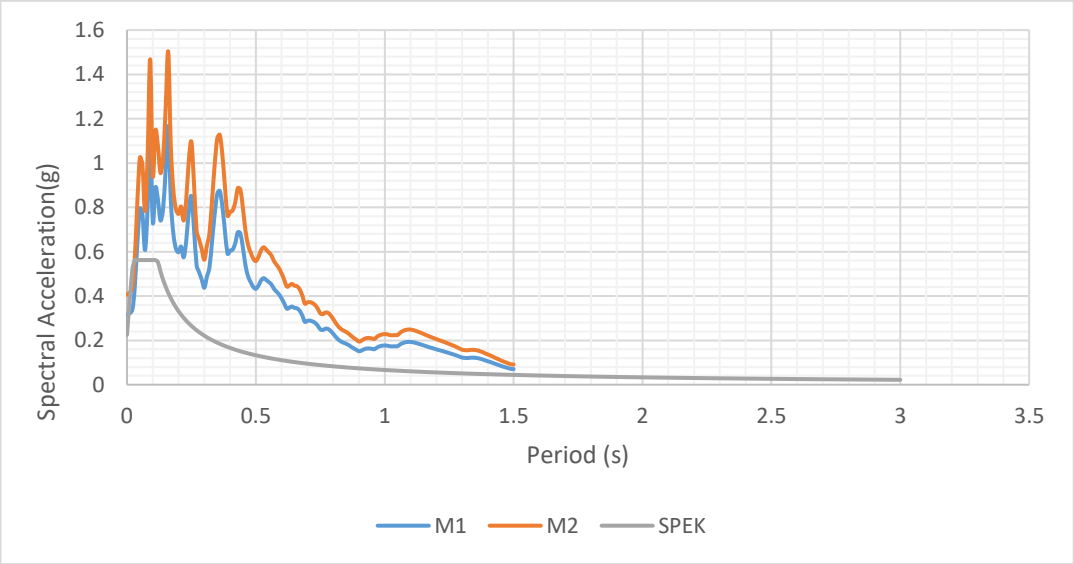

Figure A72. Scaled Vertical Response Spectra of Mammoth Lakes-03 (C2-238) Earthquake

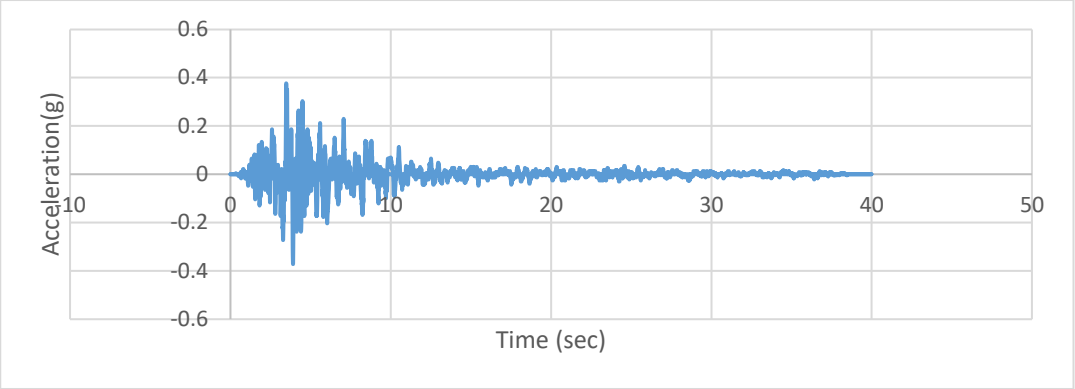

Figure A73.Scaled Acceleration Time Histories of Mammoth Lakes-03 (C2-238X) Earthquake

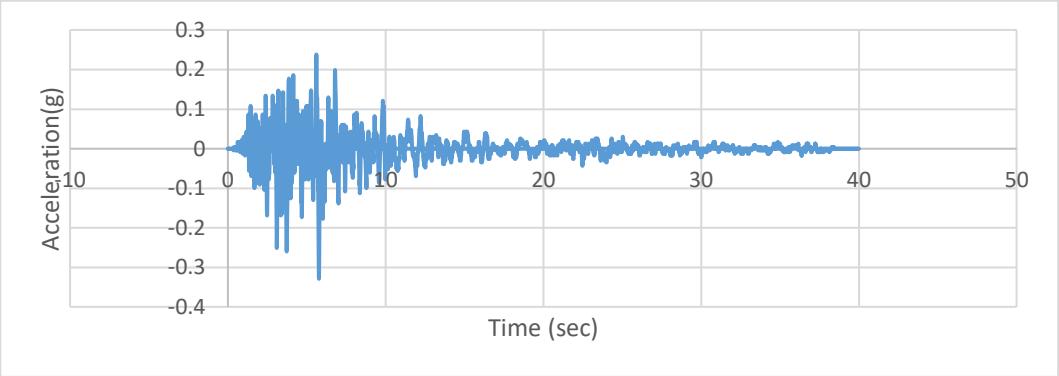

Figure A74. Scaled Acceleration Time Histories of Mammoth Lakes-03 (C2-238Y) Earthquake

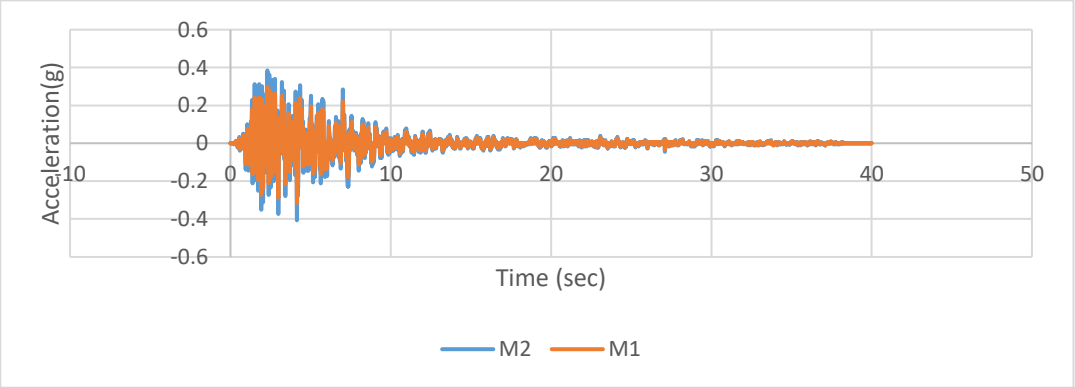

Figure A75. Scaled Acceleration Time Histories of Mammoth Lakes-03 (C2-238Z) Earthquake

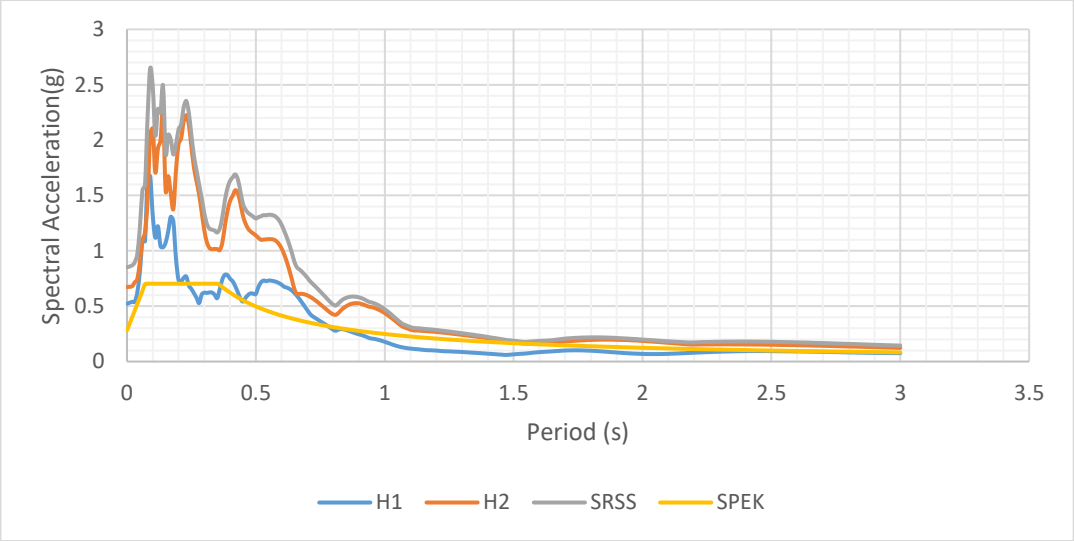

Figure A76. Scaled Horizontal Response Spectra of Westmorland (C2-318) Earthquake

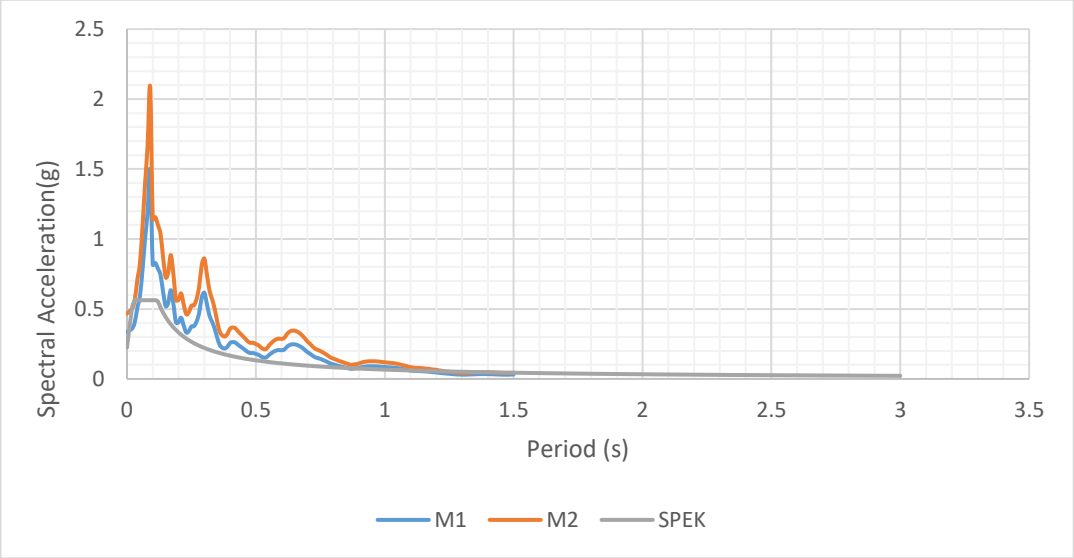

Figure A77. Scaled Vertical Response Spectra of Westmorland (C2-318) Earthquake

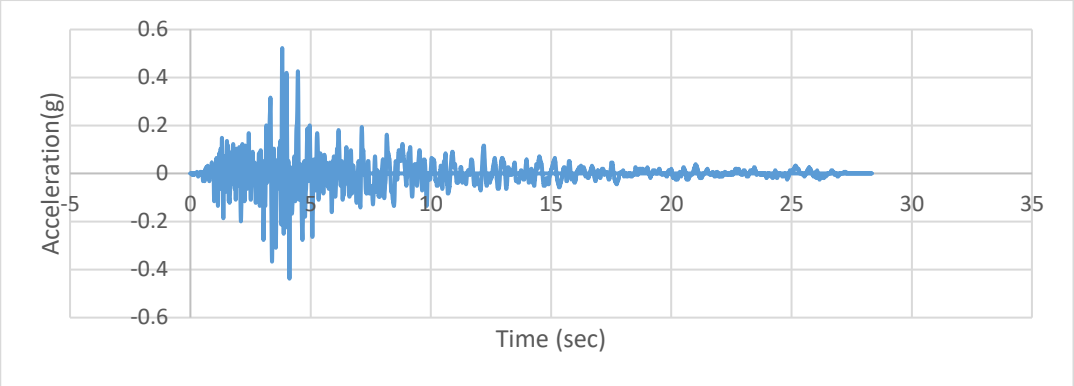

Figure A78. Scaled Acceleration Time Histories of Westmorland (C2-318X) Earthquake

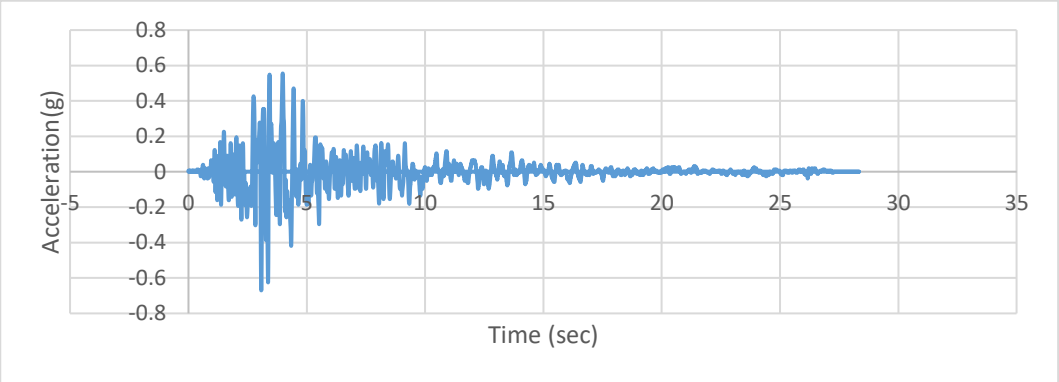

Figure A79. Scaled Acceleration Time Histories of Westmorland (C2-318Y) Earthquake

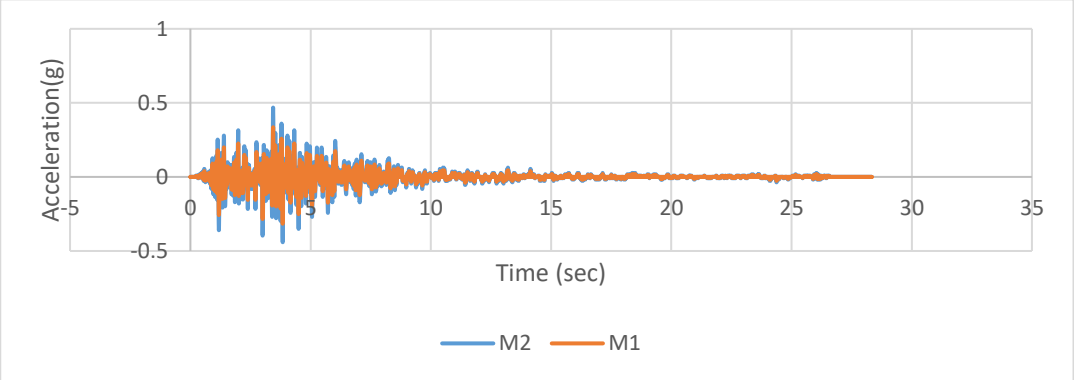

Figure A80. Scaled Acceleration Time Histories of Westmorland (C2-318Z) Earthquake

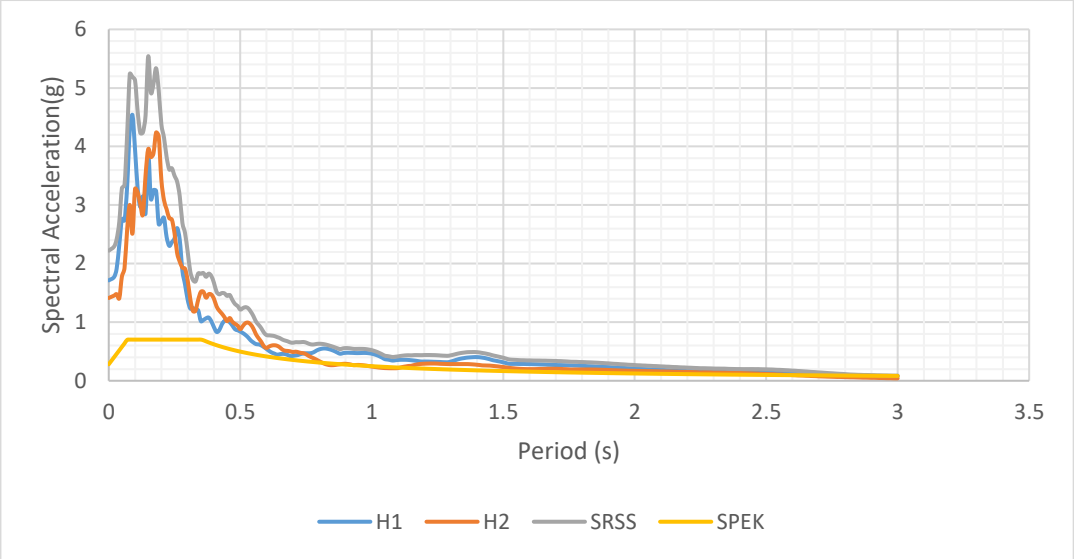

Figure A81. Scaled Horizontal Response Spectra of Morgan Hill (C2-454) Earthquake

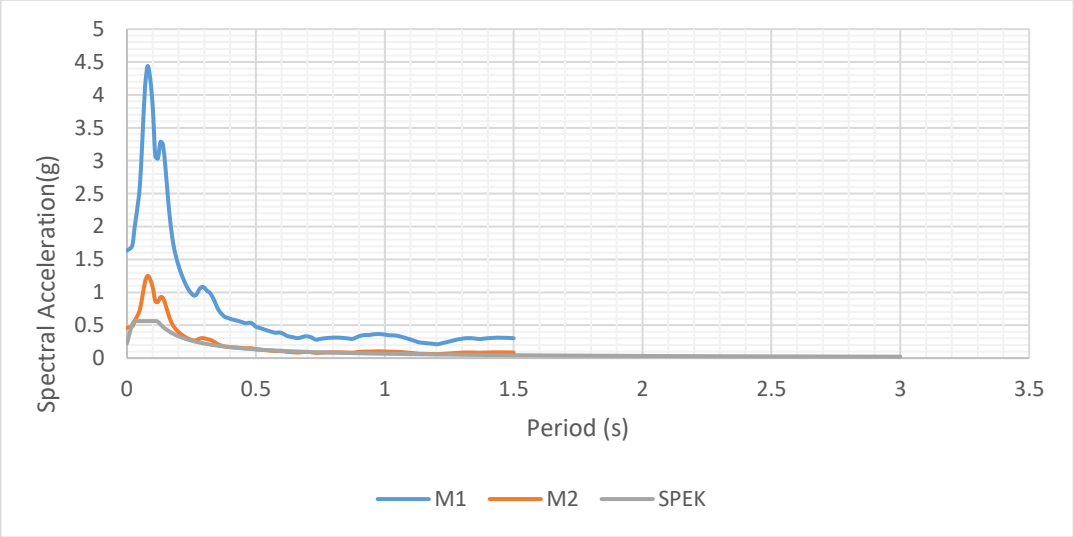

Figure A82. Scaled Vertical Response Spectra of Morgan Hill (C2-454) Earthquake

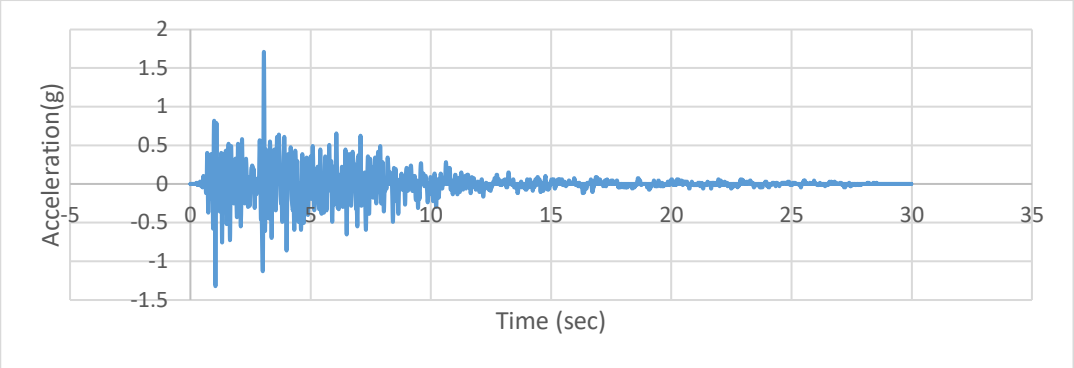

Figure A83. Scaled Acceleration Time Histories of Morgan Hill (C2-454X) Earthquake

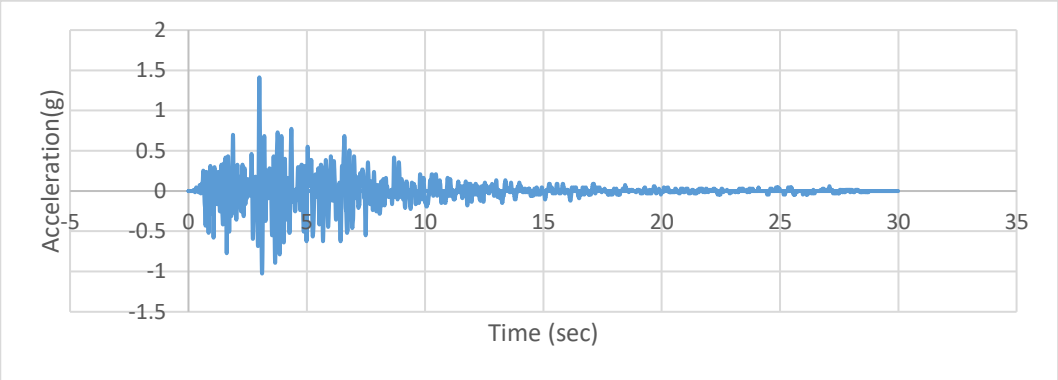

Figure A84. Scaled Acceleration Time Histories of Morgan Hill (C2-454Y) Earthquake

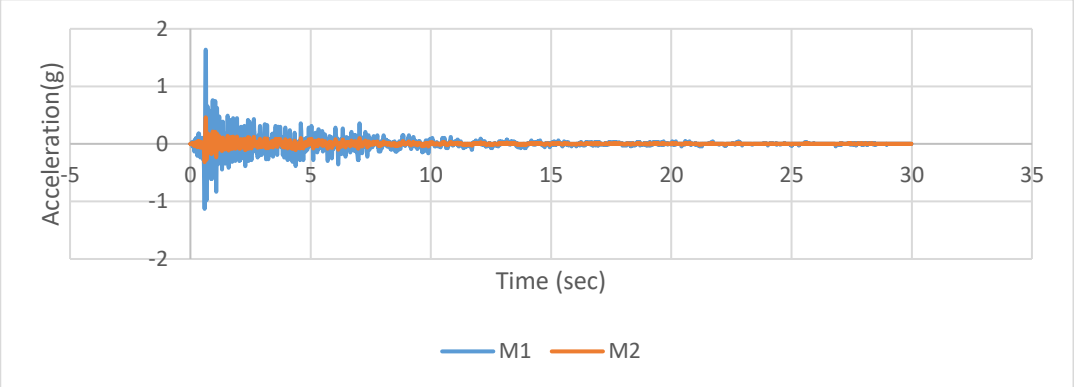

Figure A85. Scaled Acceleration Time Histories of Morgan Hill (C2-454Z) Earthquake

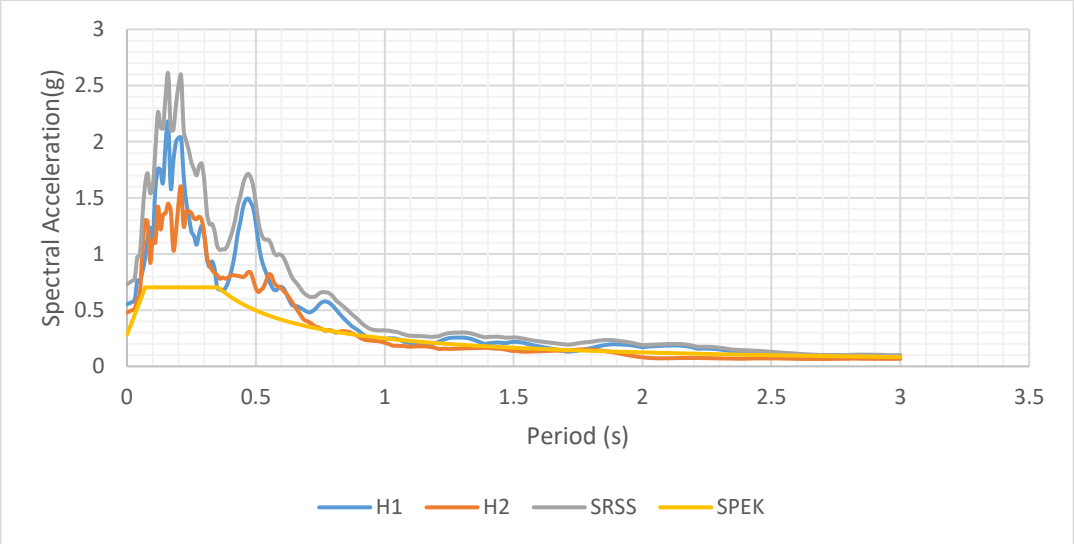

Figure A86. Scaled Horizontal Response Spectra of Chalfant Valley-01 (C2-543) Earthquake

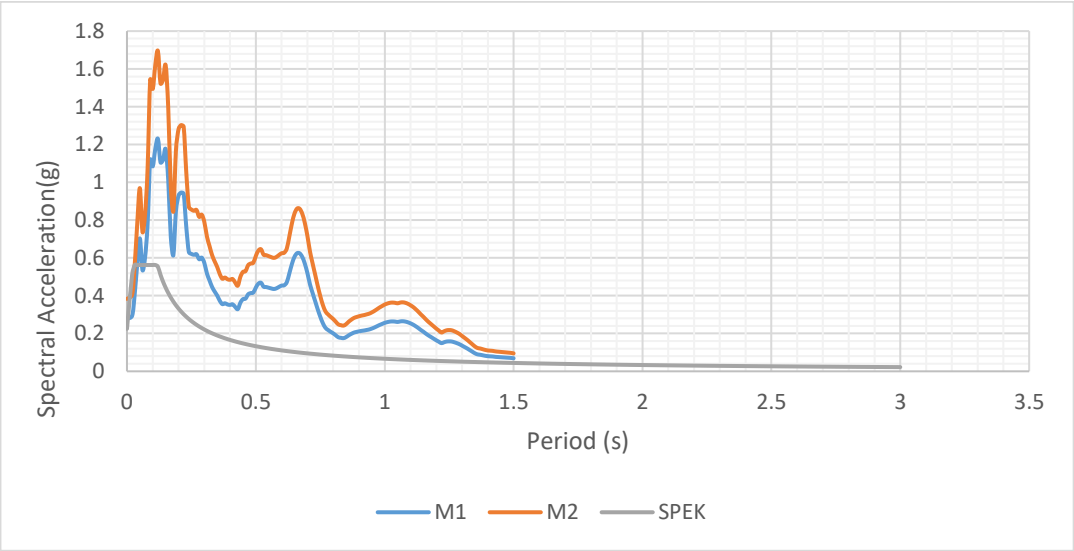

Figure A87. Scaled Vertical Response Spectra of Chalfant Valley-01 (C2-543) Earthquake

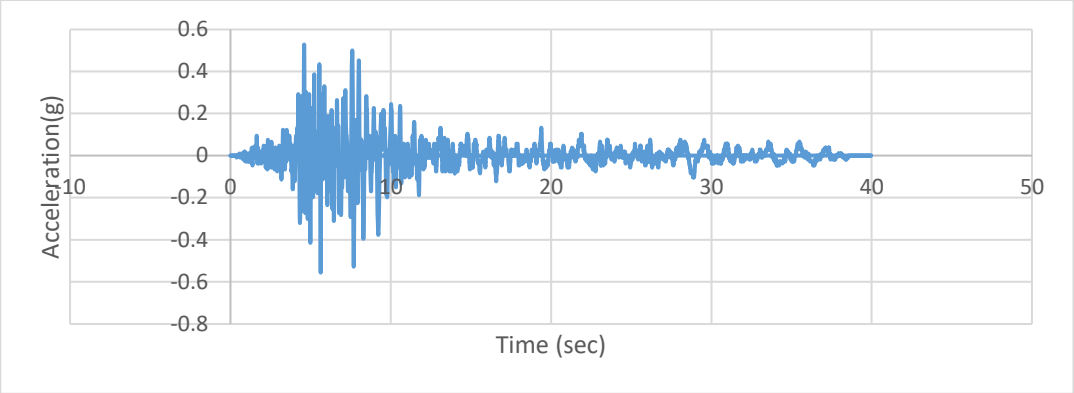

Figure A88. Scaled Acceleration Time Histories of Chalfant Valley-01 (C2-543X) Earthquake

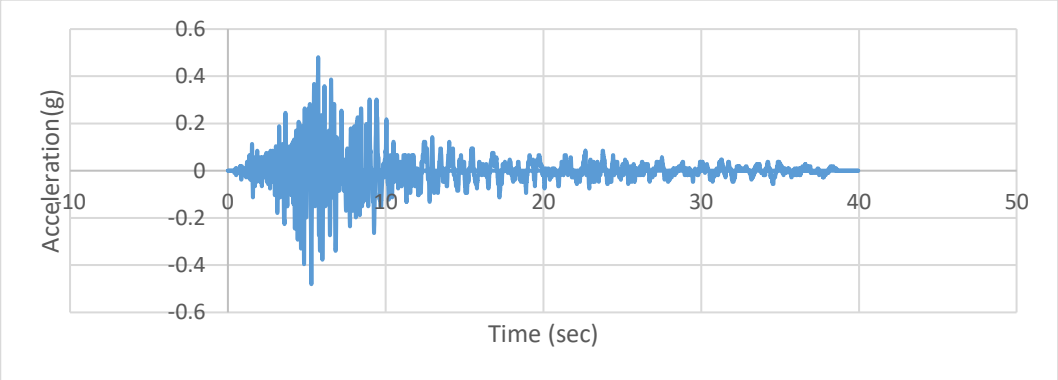

Figure A89. Scaled Acceleration Time Histories of Chalfant Valley-01 (C2-543Y) Earthquake

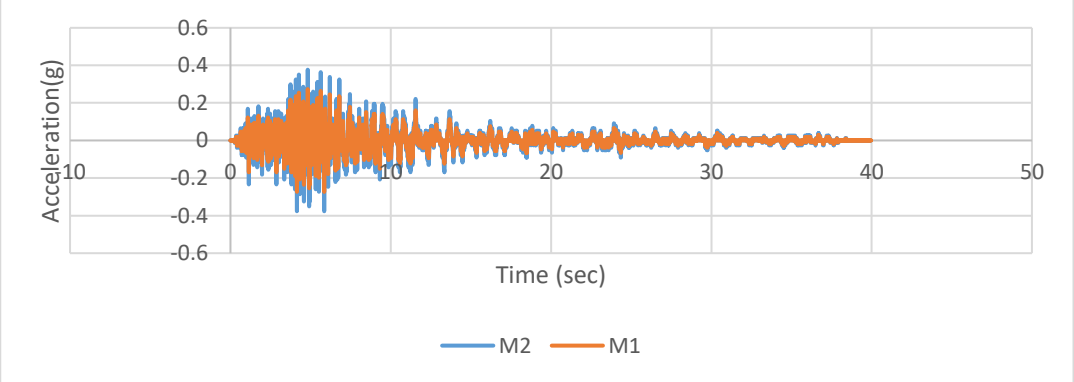

Figure A90. Scaled Acceleration Time Histories of Chalfant Valley-01 (C2-543Z) Earthquake

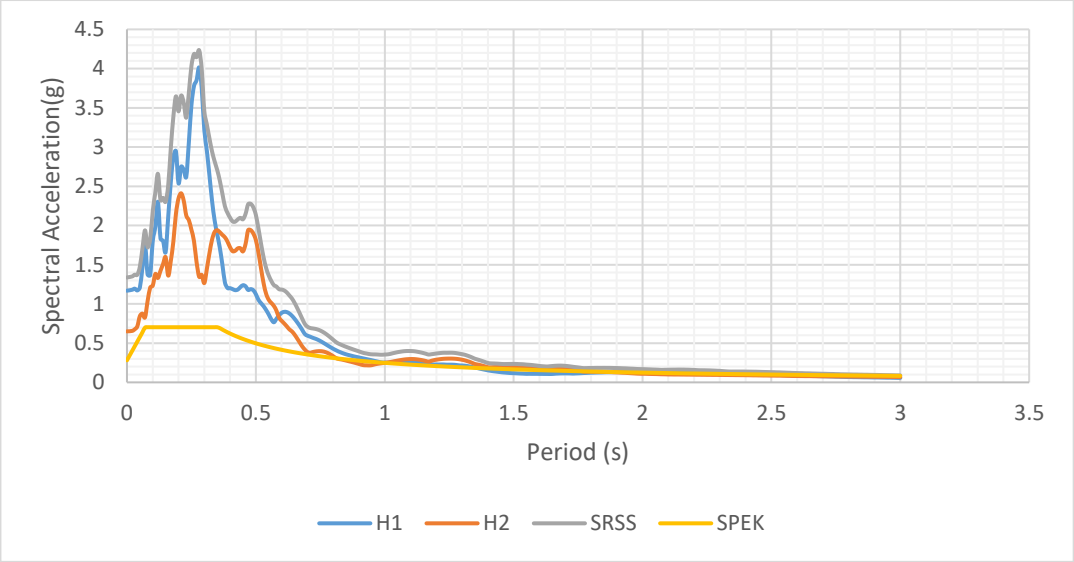

Figure A91. Scaled Horizontal Response Spectra of Chalfant Valley-02 (C2-552) Earthquake

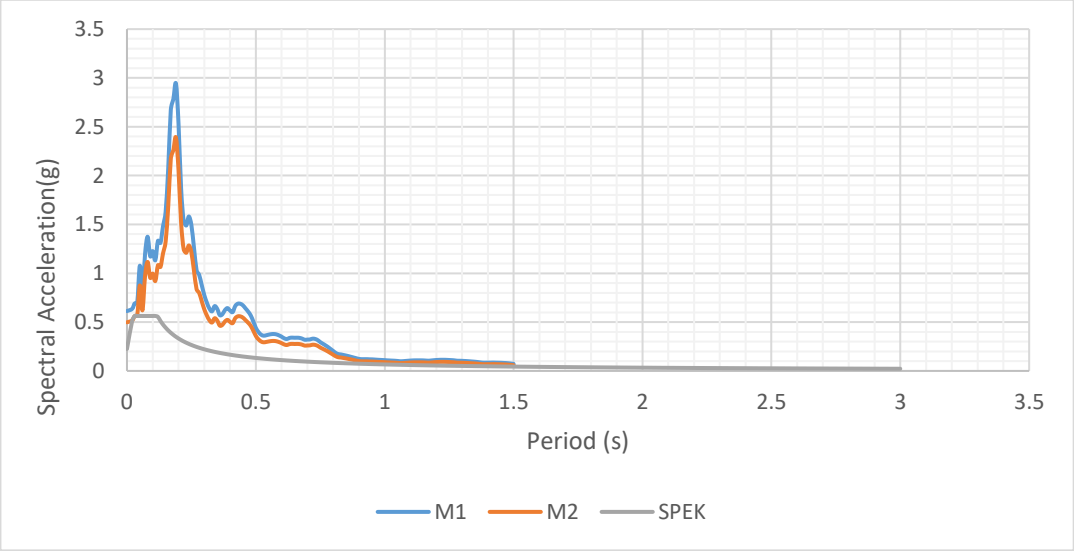

Figure A92. Scaled Vertical Response Spectra of Chalfant Valley-02 (C2-552) Earthquake

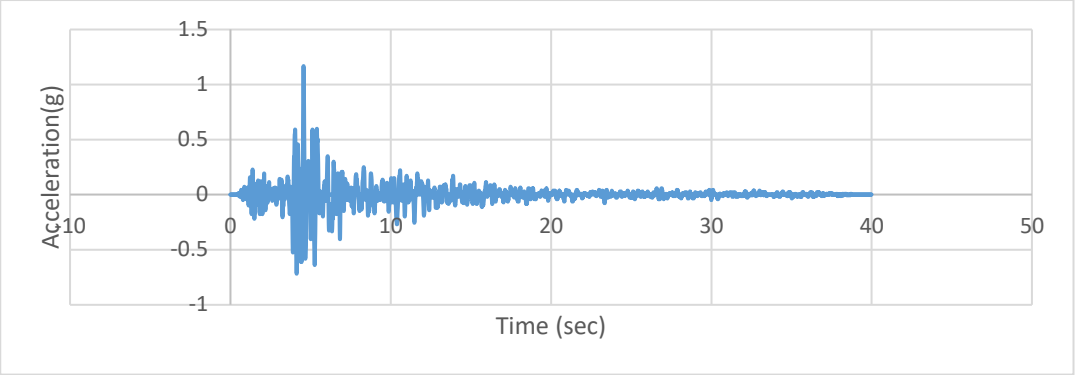

Figure A93. Scaled Acceleration Time Histories of Chalfant Valley-02 (C2-552X) Earthquake

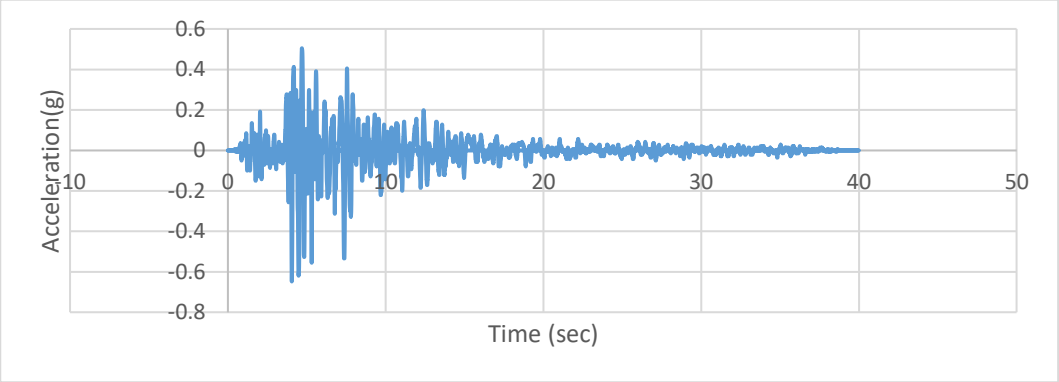

Figure A94. Scaled Acceleration Time Histories of Chalfant Valley-02 (C2-552Y) Earthquake

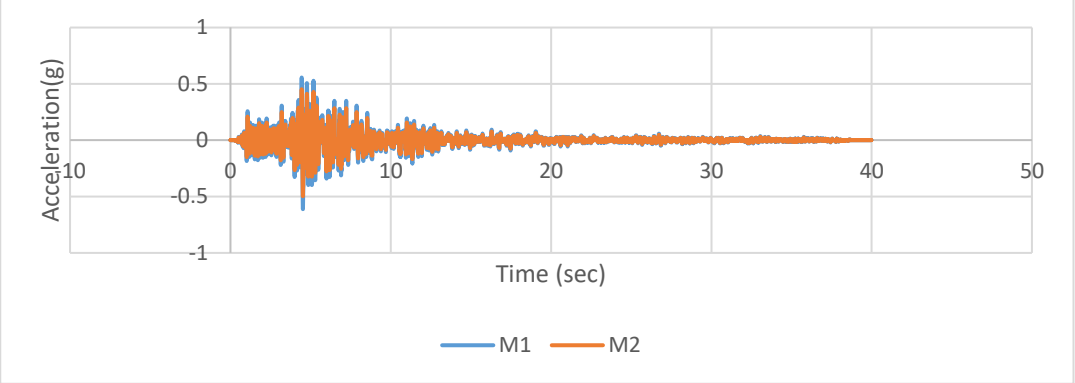

Figure A95. Scaled Acceleration Time Histories of Chalfant Valley-02 (C2-552Z) Earthquake

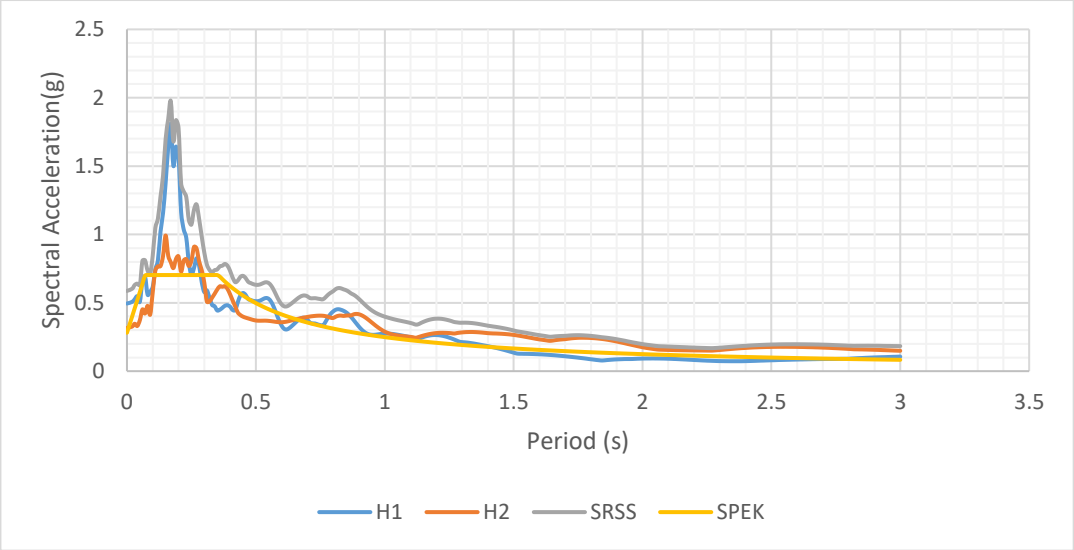

Figure A96. Scaled Horizontal Response Spectra of Kocaeli (C2-1148) Earthquake

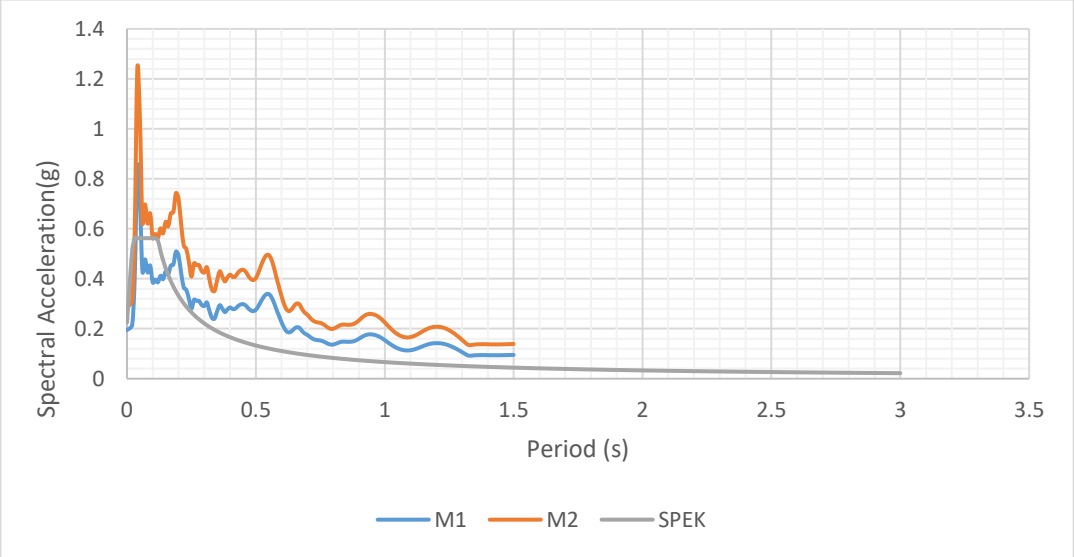

Figure A97. Scaled Vertical Response Spectra of Kocaeli (C2-1148) Earthquake

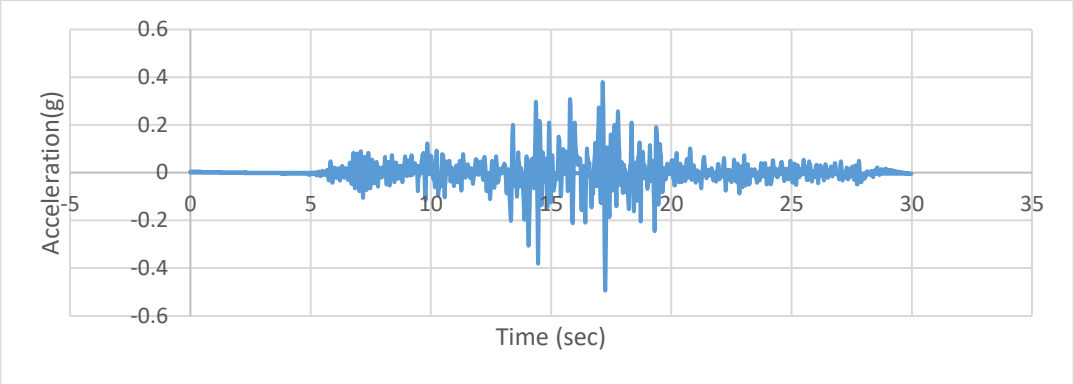

Figure A98. Scaled Acceleration Time Histories of Kocaeli (C2-1148X) Earthquake

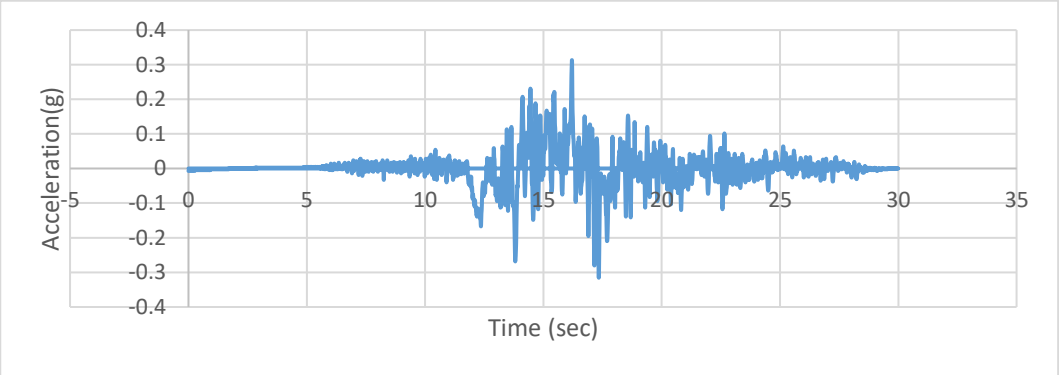

Figure A99. Scaled Acceleration Time Histories of Kocaeli (C2-1148Y) Earthquake

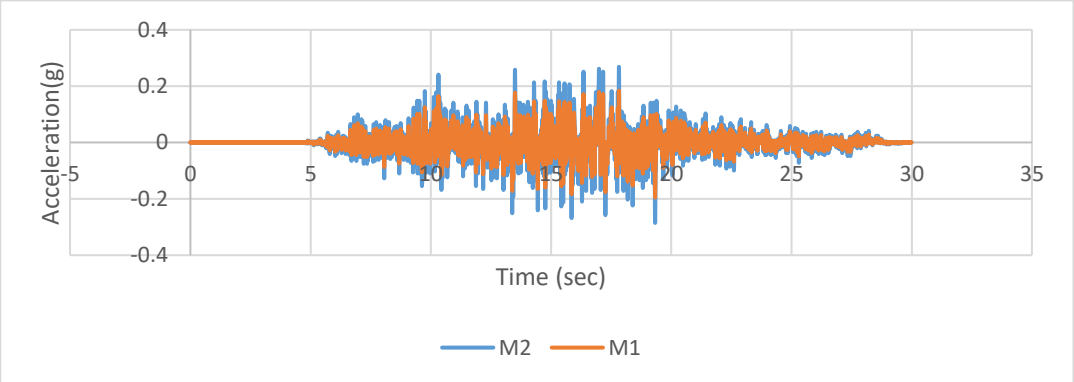

Figure A100. Scaled Acceleration Time Histories of Kocaeli (C2-1148Y) Earthquake

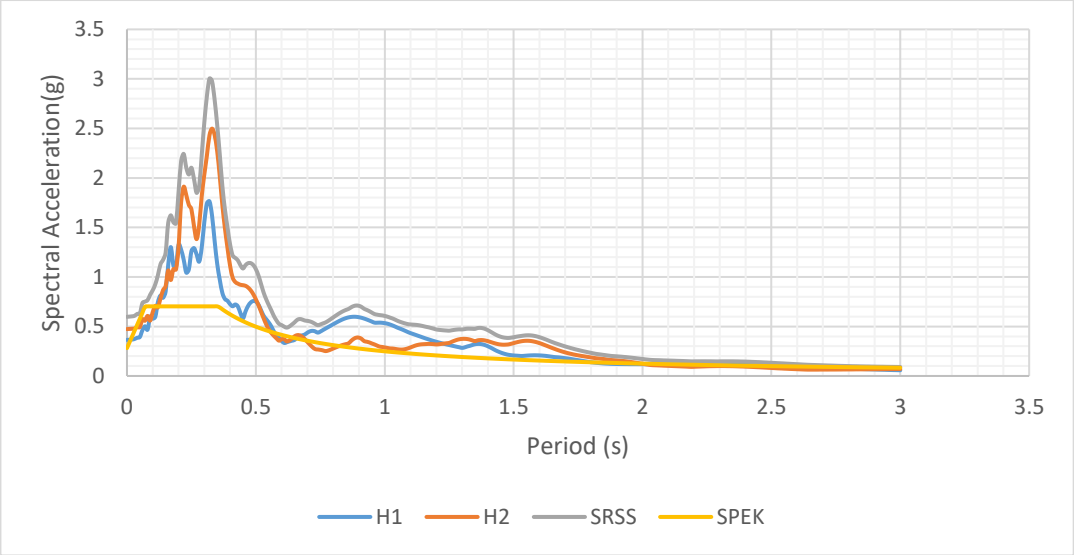

Figure A101. Scaled Horizontal Response Spectra of Duzce (C2-1614) Earthquake

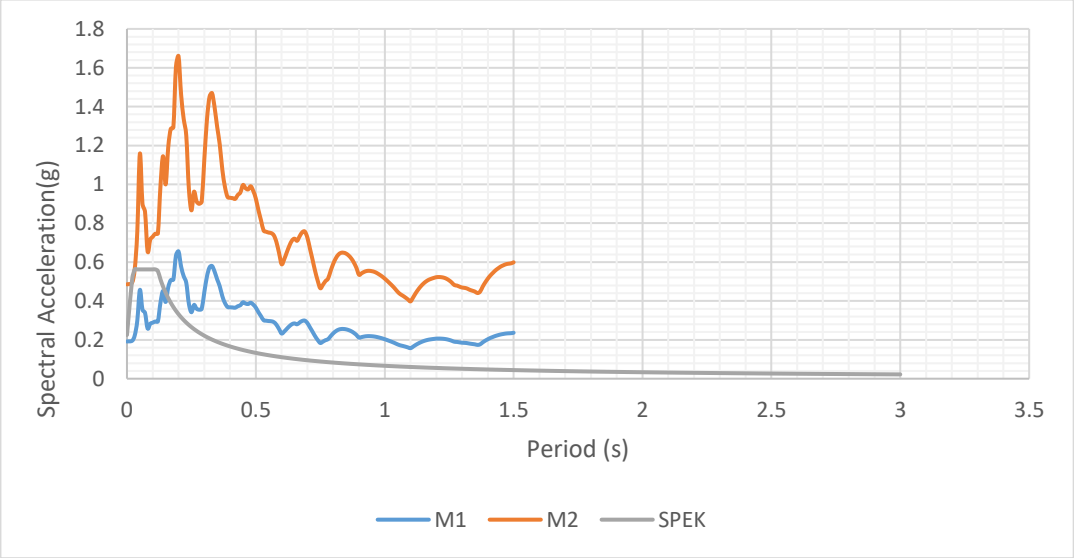

Figure A102. Scaled Vertical Response Spectra of Duzce (C2-1614) Earthquake

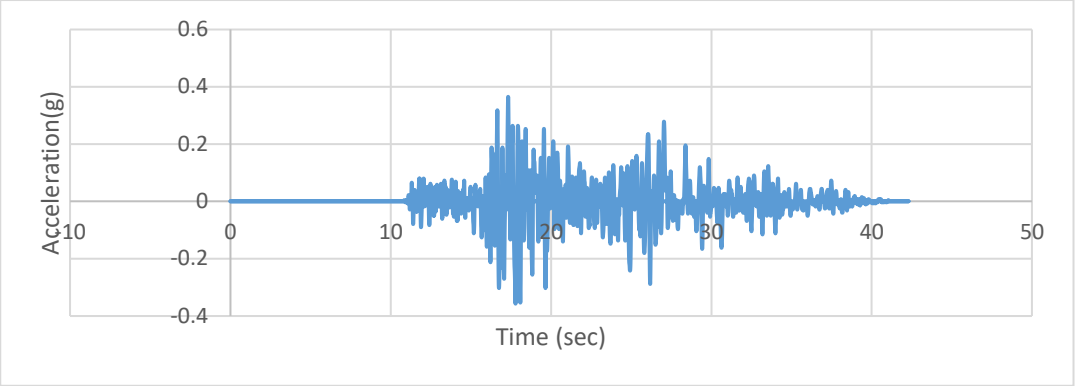

Figure A103. Scaled Acceleration Time Histories of Duzce (C2-1614X) Earthquake

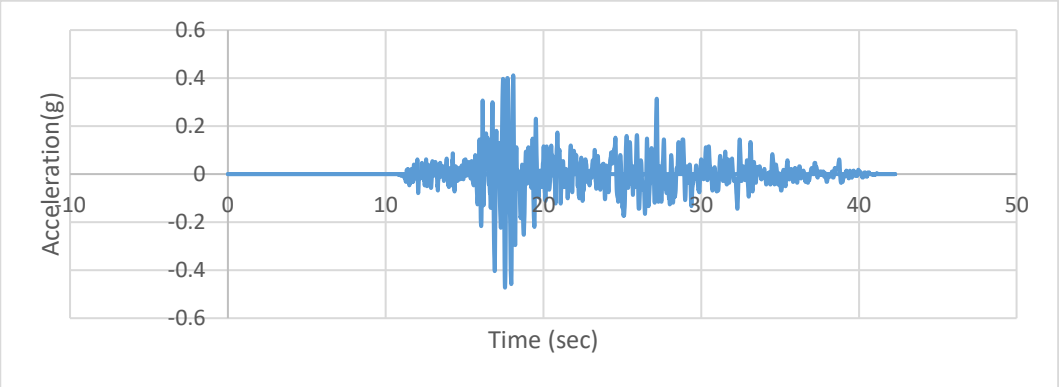

Figure A104. C2 1614Y Scaled Acceleration Time Histories of Duzce (C2-1614Y) Earthquake

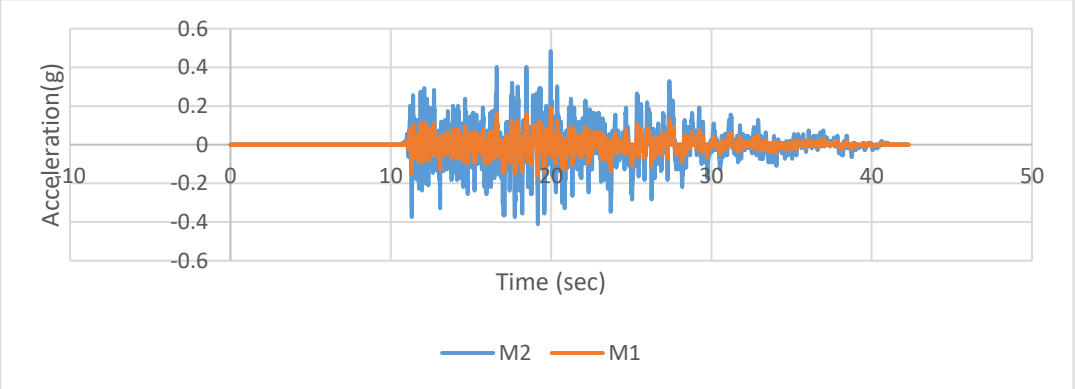

Figure A105. Scaled Acceleration Time Histories of Duzce (C2-1614Z) Earthquake

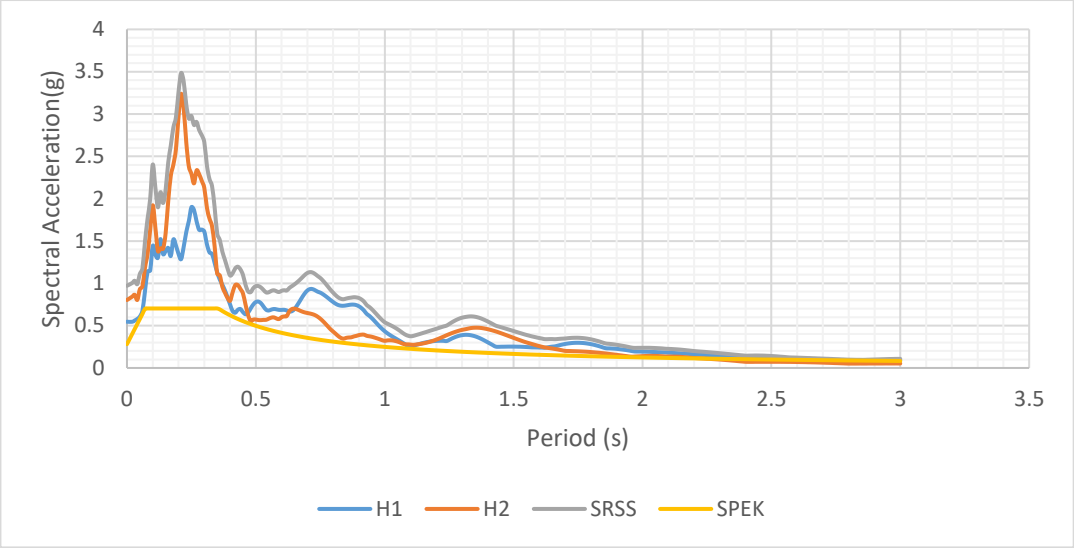

Figure A106. Scaled Horizontal Response Spectra of Big Bear-01 (C2-6057) Earthquake

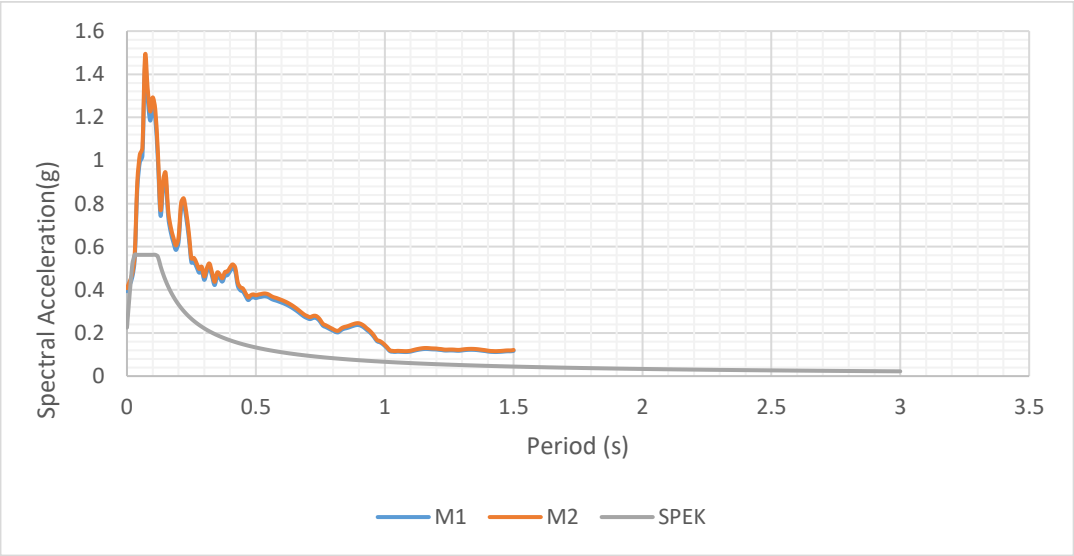

Figure A107. Scaled Vertical Response Spectra of Big Bear-01 (C2-6057) Earthquake

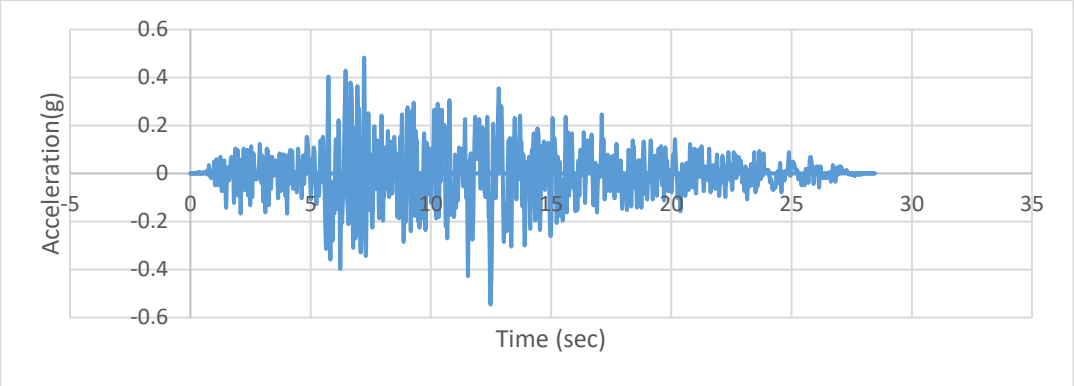

Figure A108. Scaled Acceleration Time Histories of Big Bear-01 (C2 6057X) Earthquake

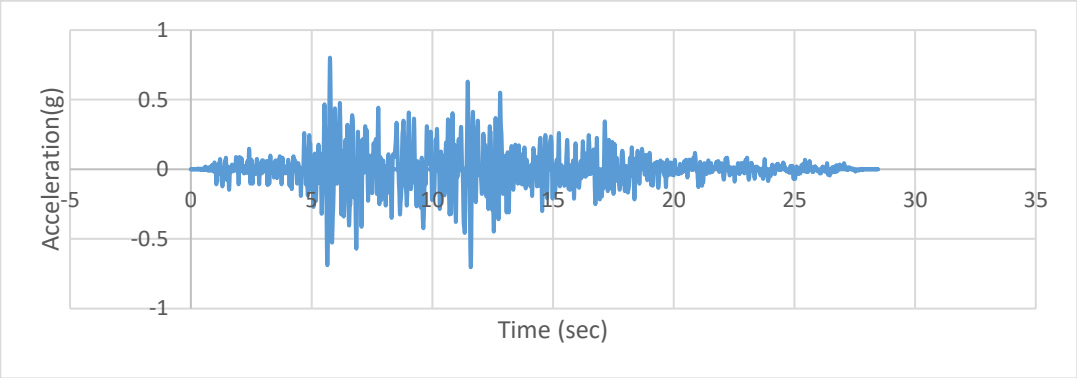

Figure A109. Scaled Acceleration Time Histories of Big Bear-01 (C2 6057Y) Earthquake

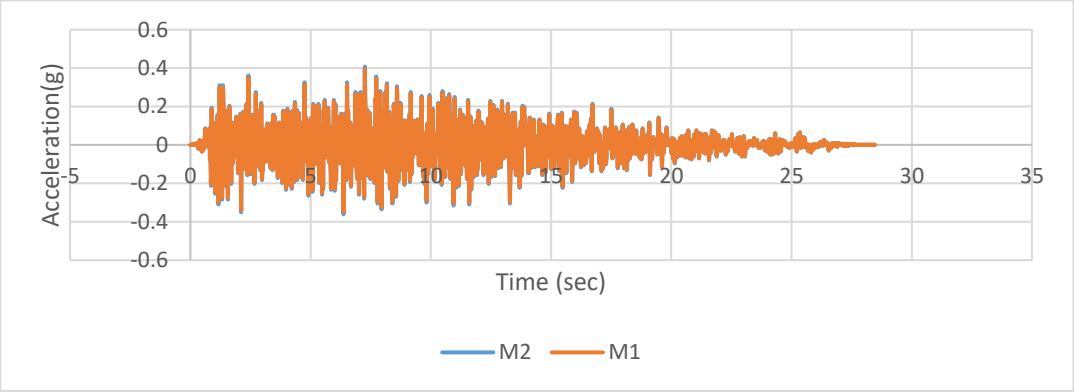

Figure A110. Scaled Acceleration Time Histories of Big Bear-01 (C2 6057Z) Earthquake

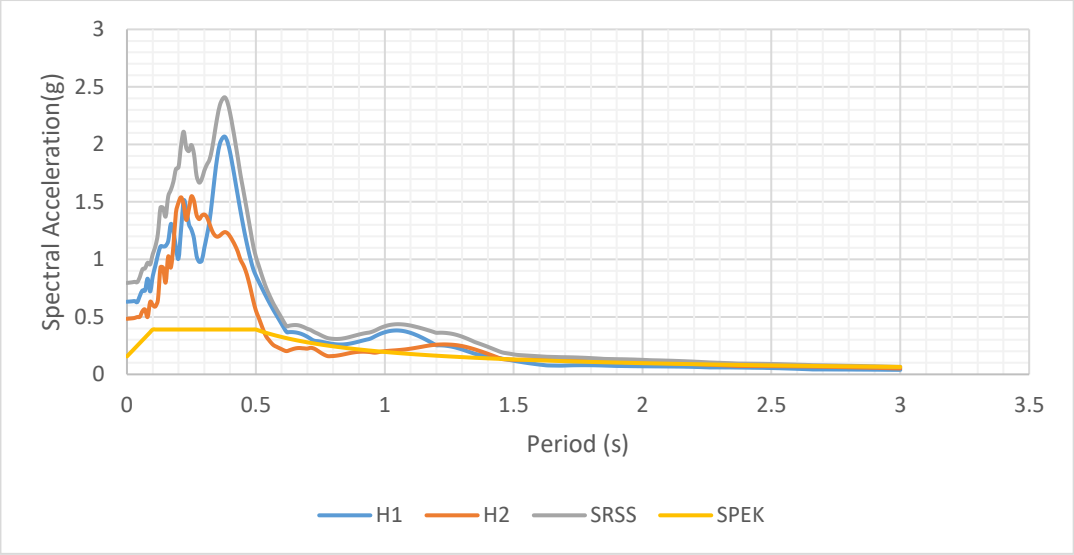

Figure A111. Scaled Horizontal Response Spectra of Parkfield (C3-33) Earthquake

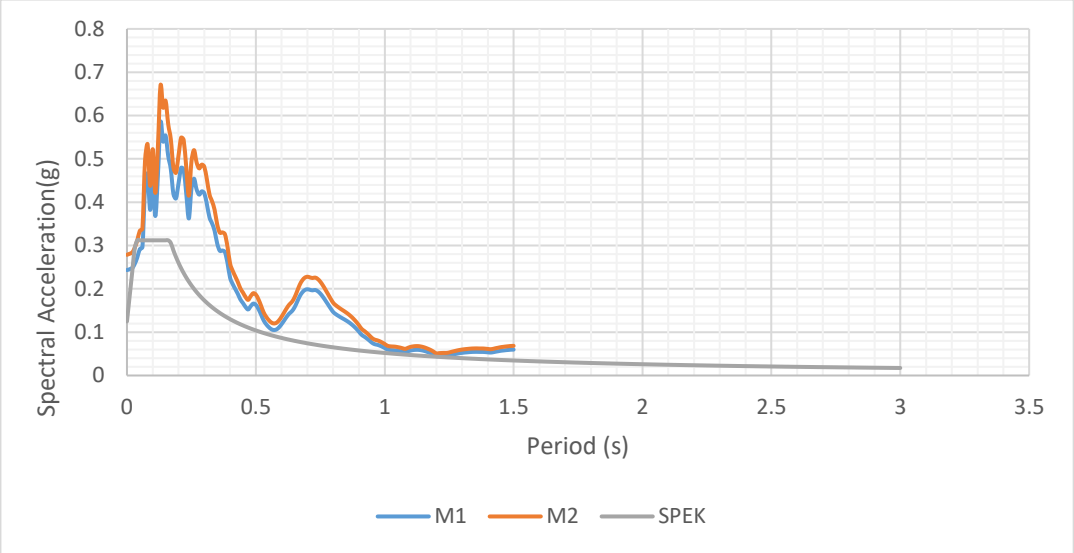

Figure A112. Scaled Vertical Response Spectra of Parkfield (C3-33) Earthquake

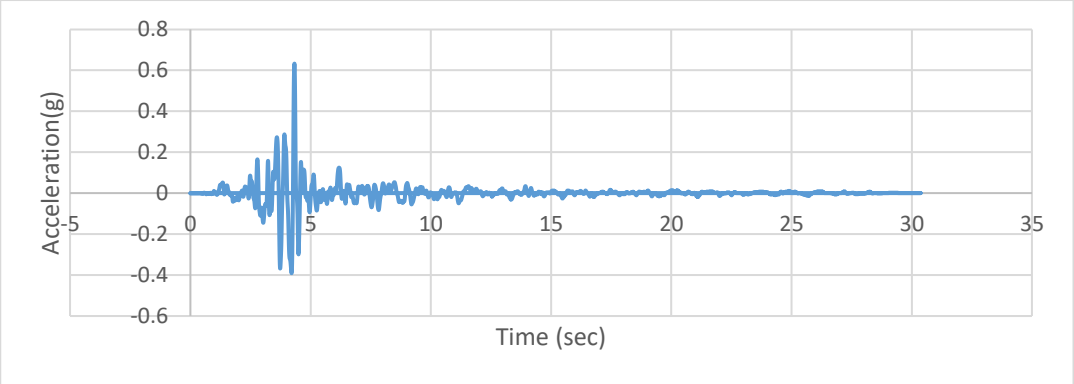

Figure A113.Scaled Acceleration Time Histories of Parkfield (C3-33X) Earthquake

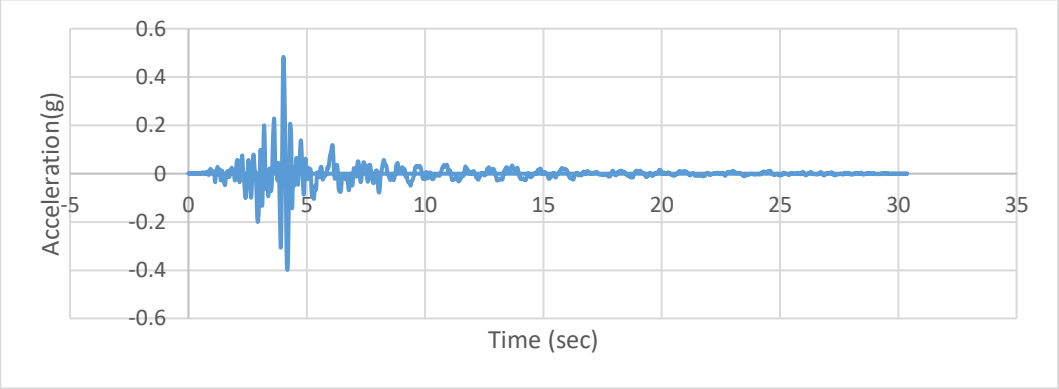

Figure A114. Scaled Acceleration Time Histories of Parkfield (C3-33Y) Earthquake

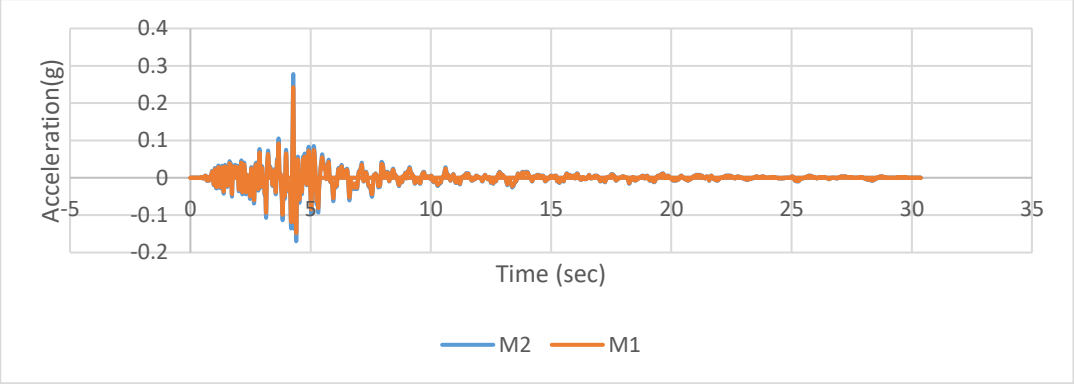

Figure A115. Scaled Acceleration Time Histories of Parkfield (C3-33Z) Earthquake

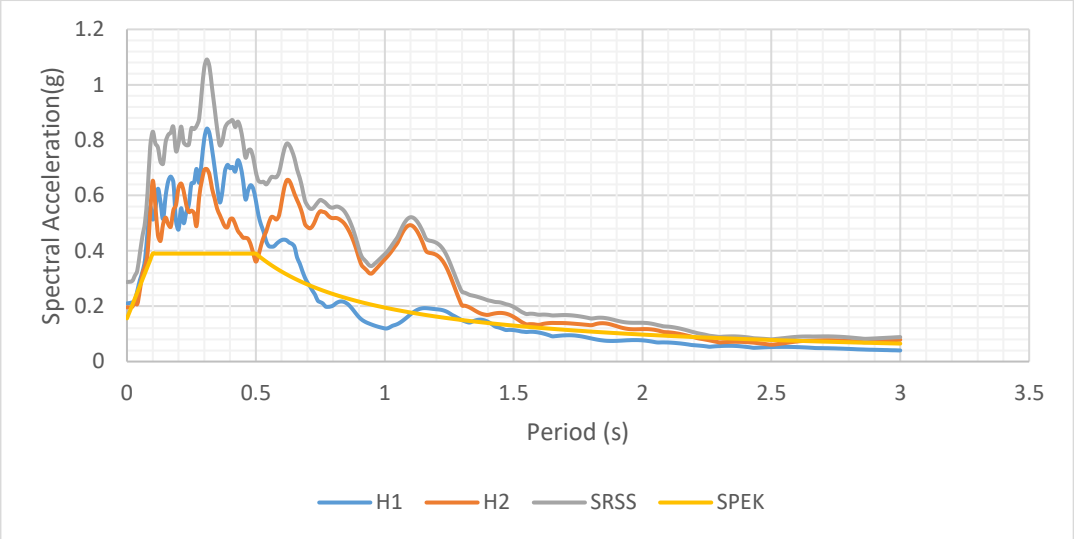

Figure A116. Scaled Horizontal Response Spectra of Imperial Valley-06 (C3-164) Earthquake

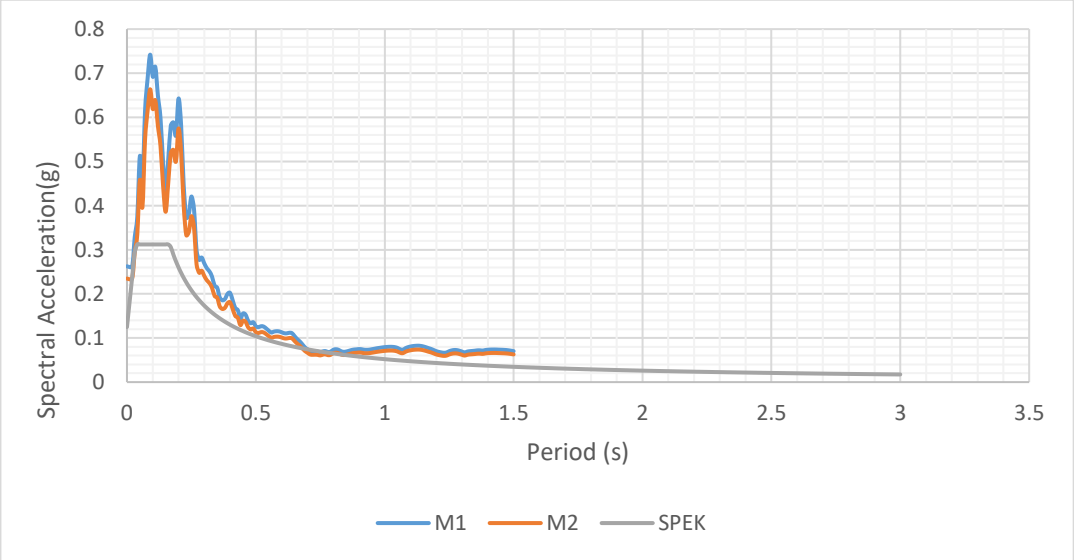

Figure A117. Scaled Vertical Response Spectra of Imperial Valley-06 (C3-164) Earthquake

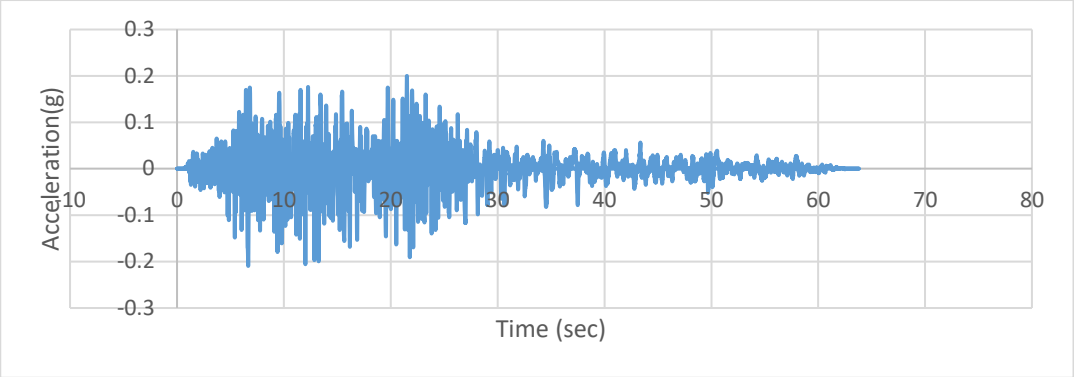

Figure A118. Scaled Acceleration Time Histories of Imperial Valley-06 (C3-164X) Earthquake

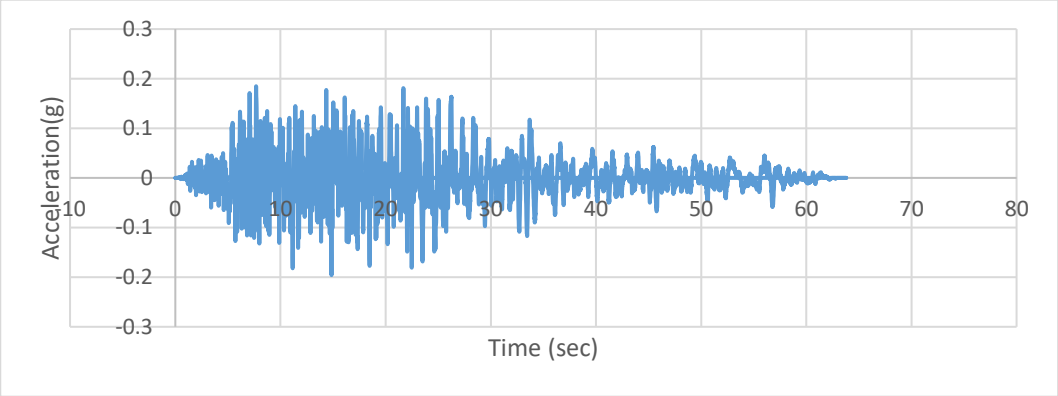

Figure A119. Scaled Acceleration Time Histories of Imperial Valley-06 (C3-164Y) Earthquake

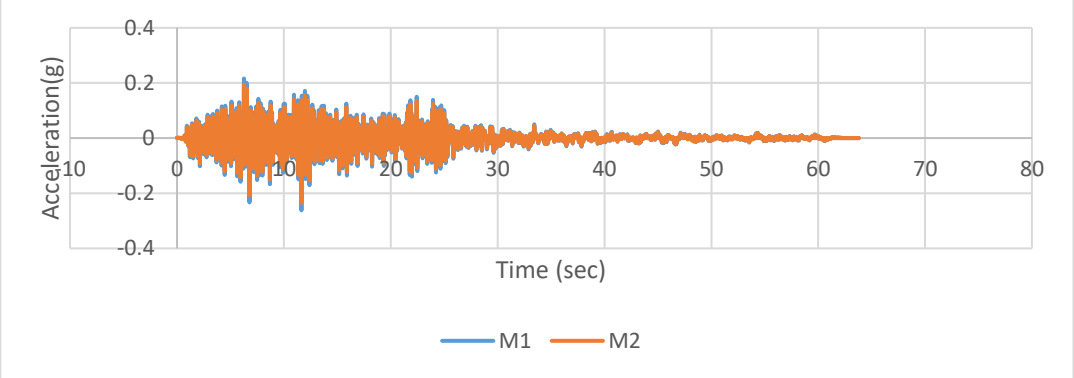

Figure A120. Scaled Acceleration Time Histories of Imperial Valley-06 (C3-164Z) Earthquake

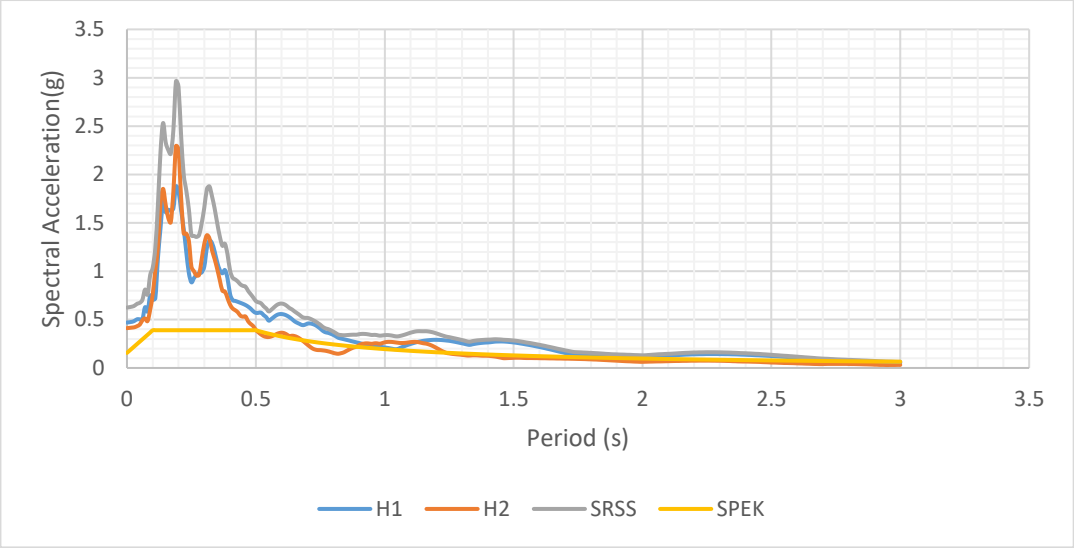

Figure A121. Scaled Horizontal Response Spectra of Livermore-01(C3-210) Earthquake

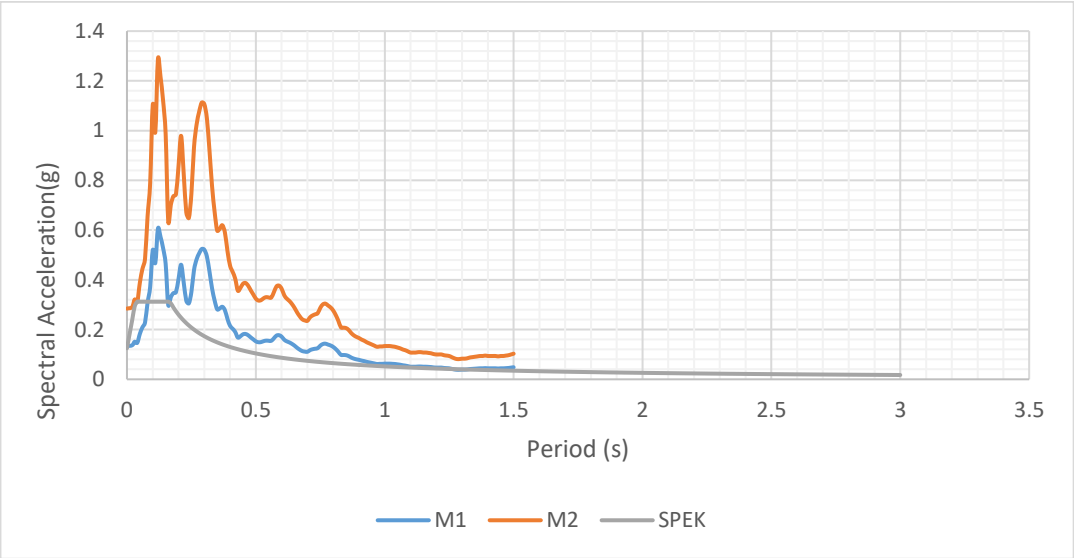

Figure A122. Scaled Vertical Response Spectra of Livermore-01(C3-210) Earthquake

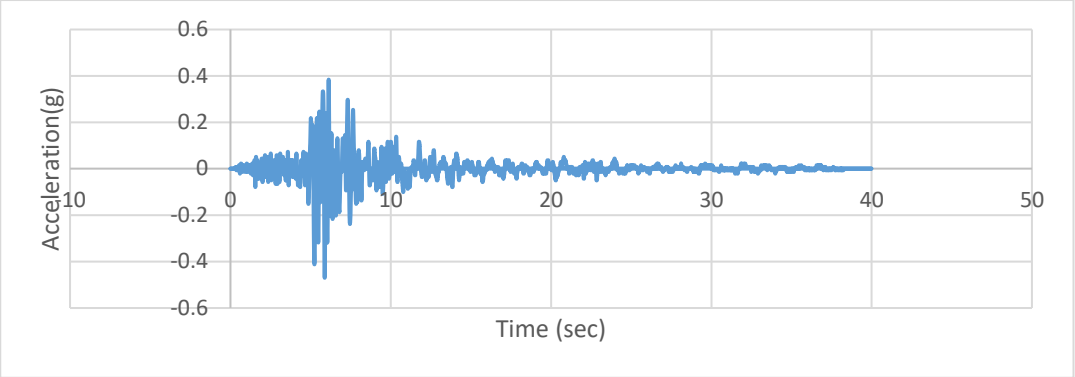

Figure A123. Scaled Acceleration Time Histories of Livermore-01(C3-210X) Earthquake

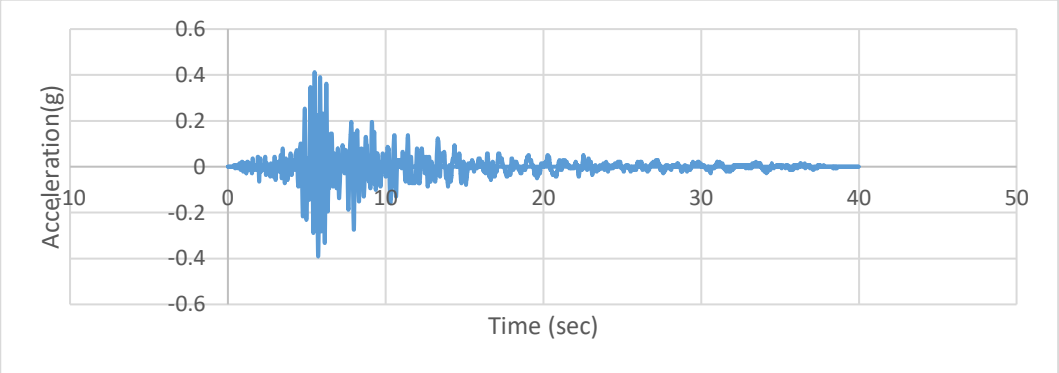

Figure A124. Scaled Acceleration Time Histories of Livermore-01(C3-210Y) Earthquake

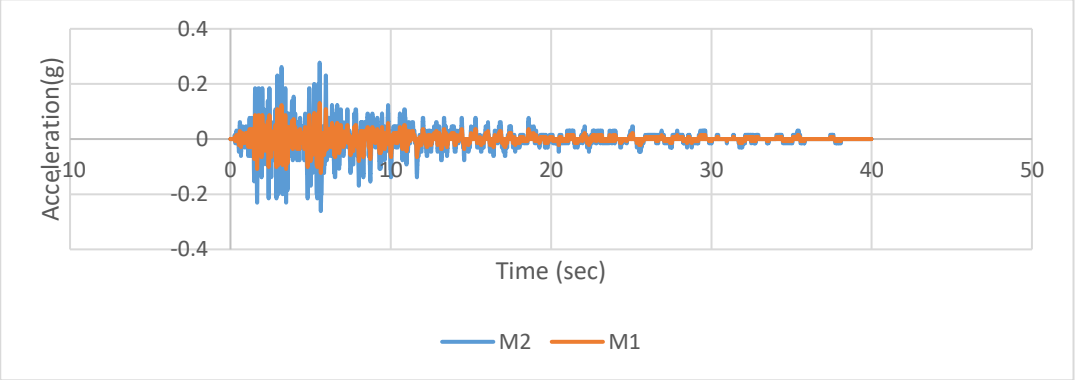

Figure A125. Scaled Acceleration Time Histories of Livermore-01(C3-210Z) Earthquake

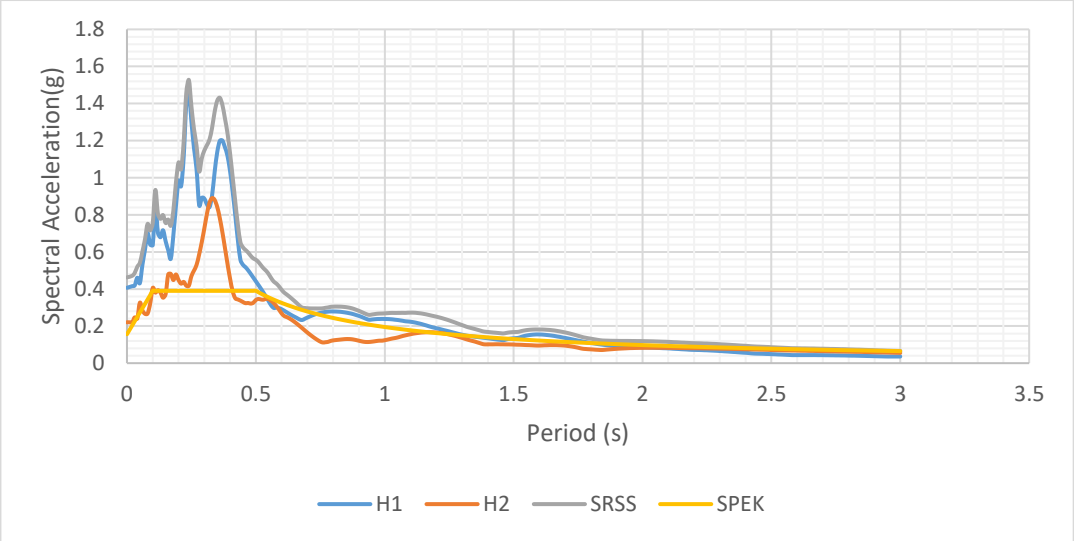

Figure A126. Scaled Horizontal Response Spectra of Mammoth Lakes-03 (C3-237) Earthquake

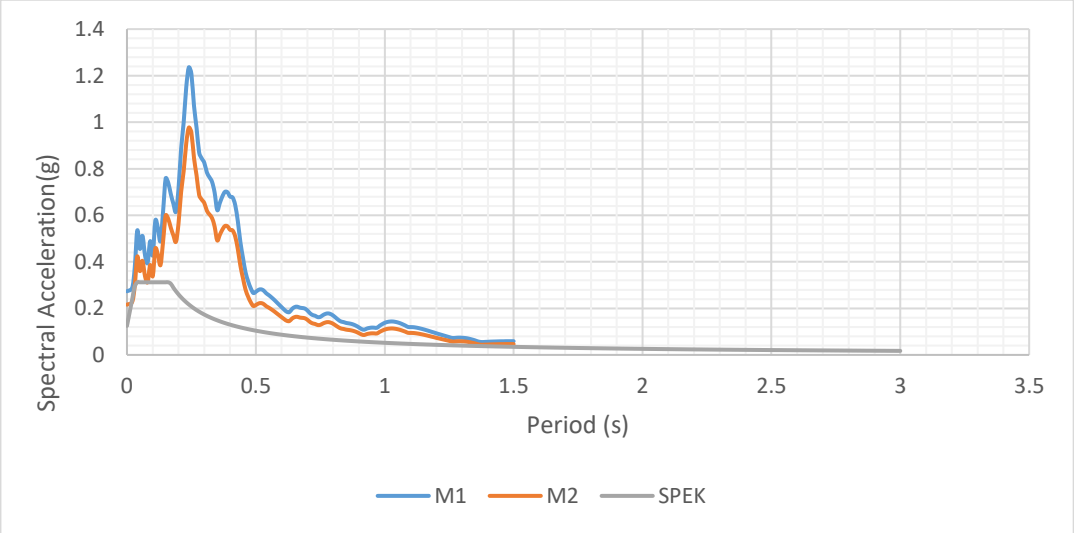

Figure A127. Scaled Vertical Response Spectra of Mammoth Lakes-03 (C3-237) Earthquake

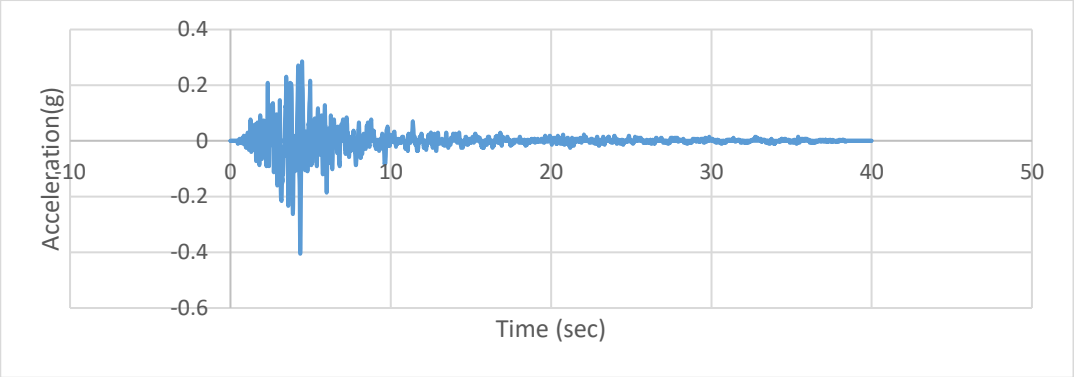

Figure A128. Scaled Acceleration Time Histories of Mammoth Lakes-03 (C3-237X) Earthquake

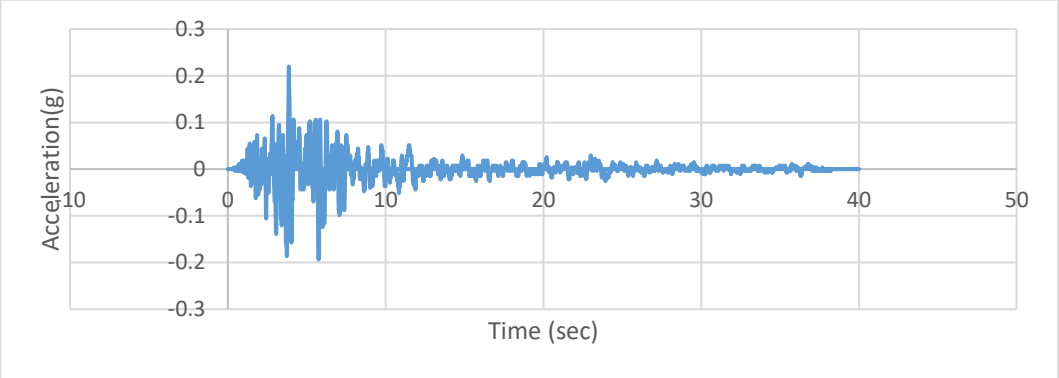

Figure A129. Scaled Acceleration Time Histories of Mammoth Lakes-03 (C3-237Y) Earthquake

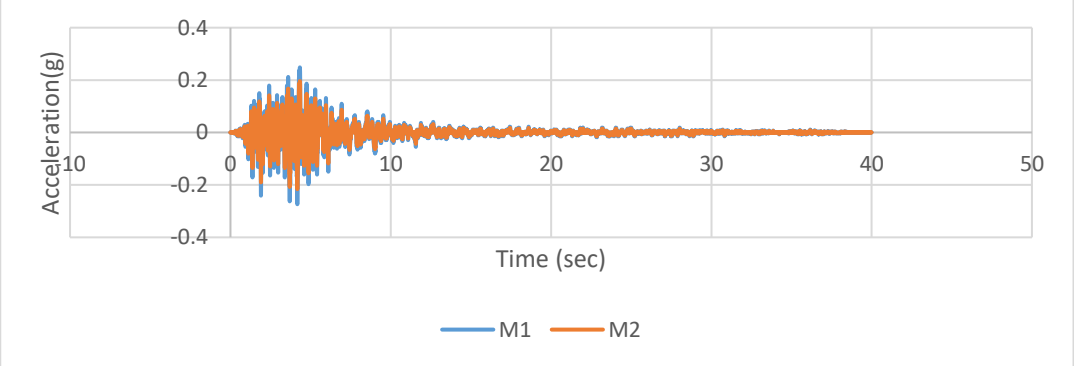

Figure A130. Scaled Acceleration Time Histories of Mammoth Lakes-03 (C3-237Z) Earthquake

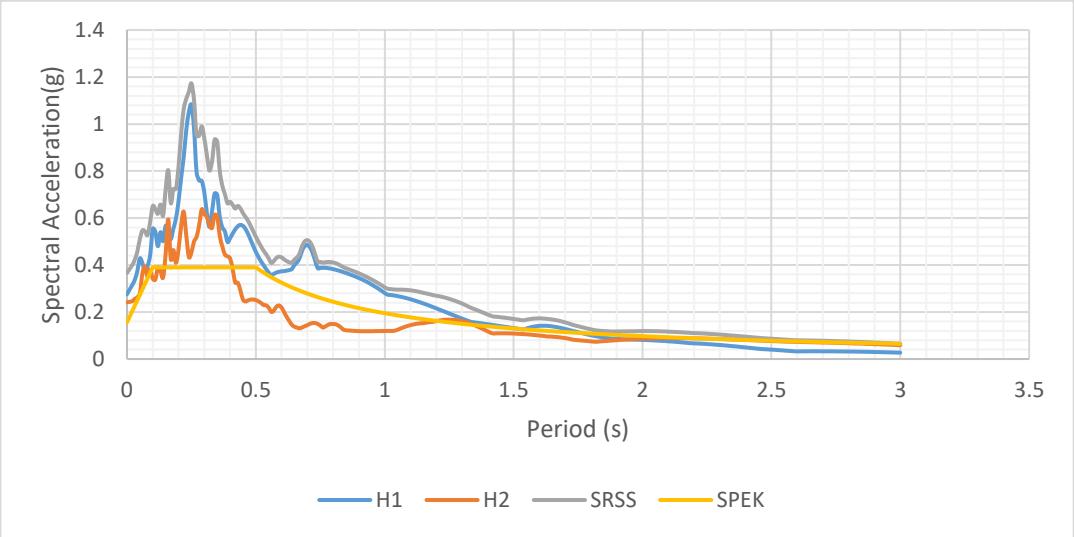

Figure A131. Scaled Horizontal Response Spectra of Mammoth Lakes-03 (C3-238) Earthquake

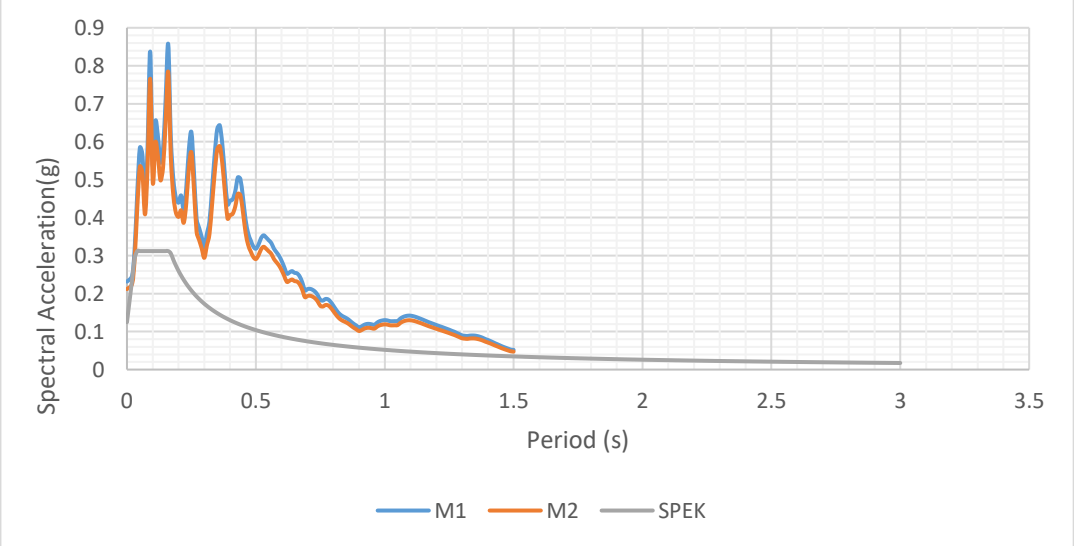

Figure A132. Scaled Vertical Response Spectra of Mammoth Lakes-03 (C3-238) Earthquake

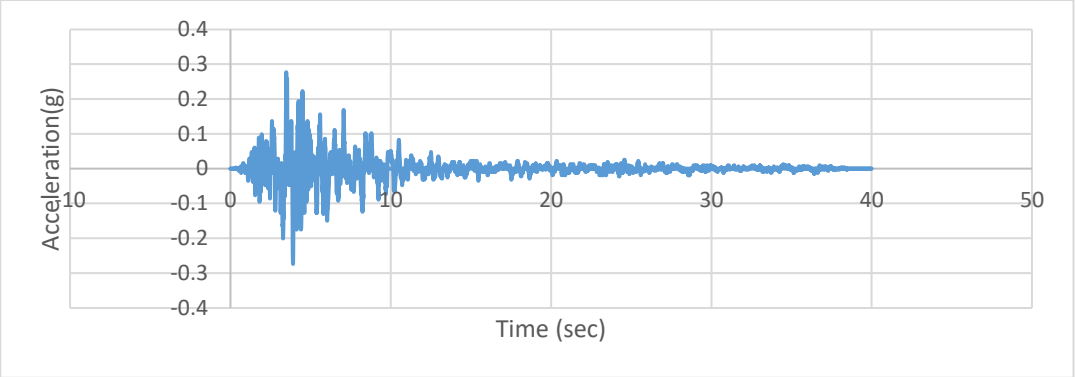

Figure A133. Scaled Acceleration Time Histories of Mammoth Lakes-03 (C3-238X) Earthquake

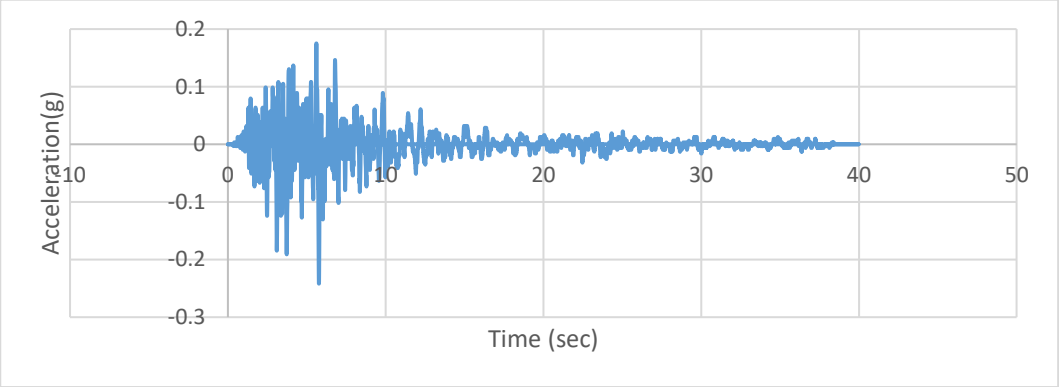

Figure A134. Scaled Acceleration Time Histories of Mammoth Lakes-03 (C3-238Y) Earthquake

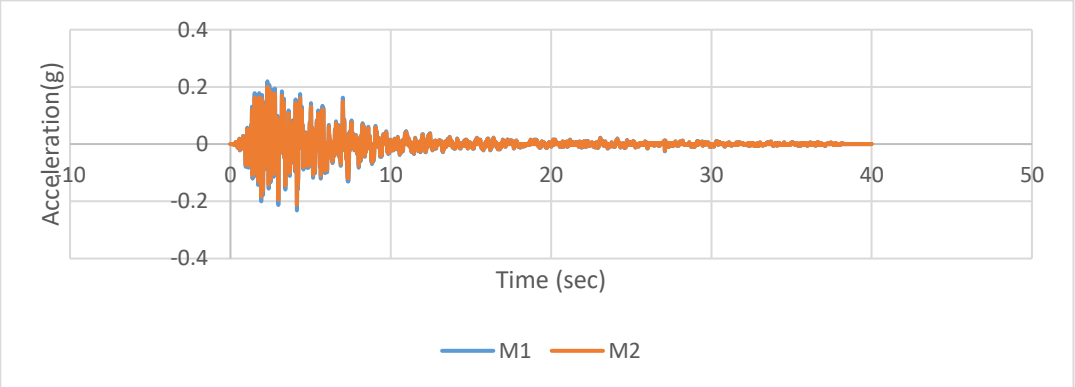

Figure A135. Scaled Acceleration Time Histories of Mammoth Lakes-03 (C3-238Z) Earthquake

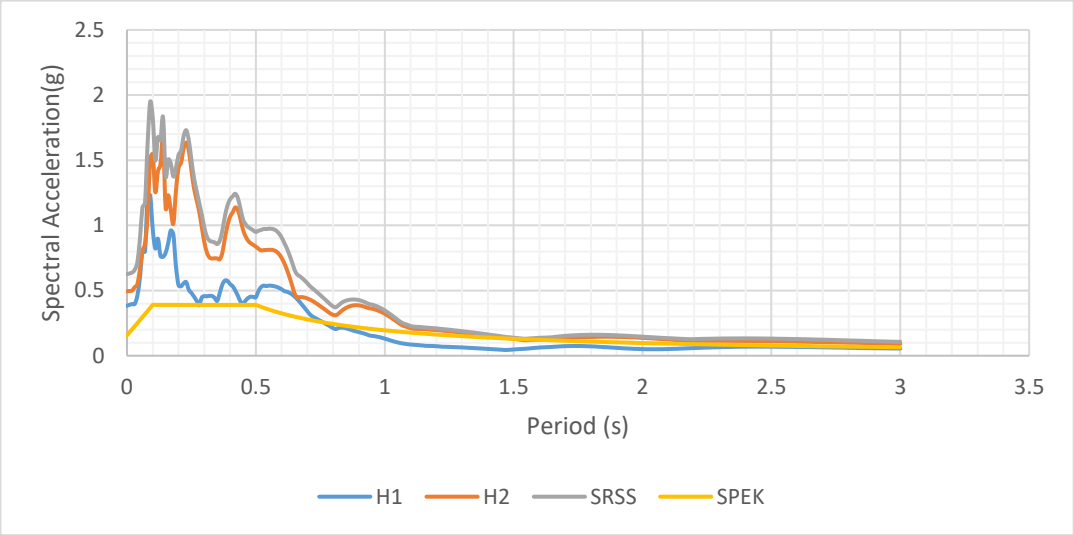

Figure A136.Scaled Horizontal Response Spectra of Westmorland (C3-318) Earthquake

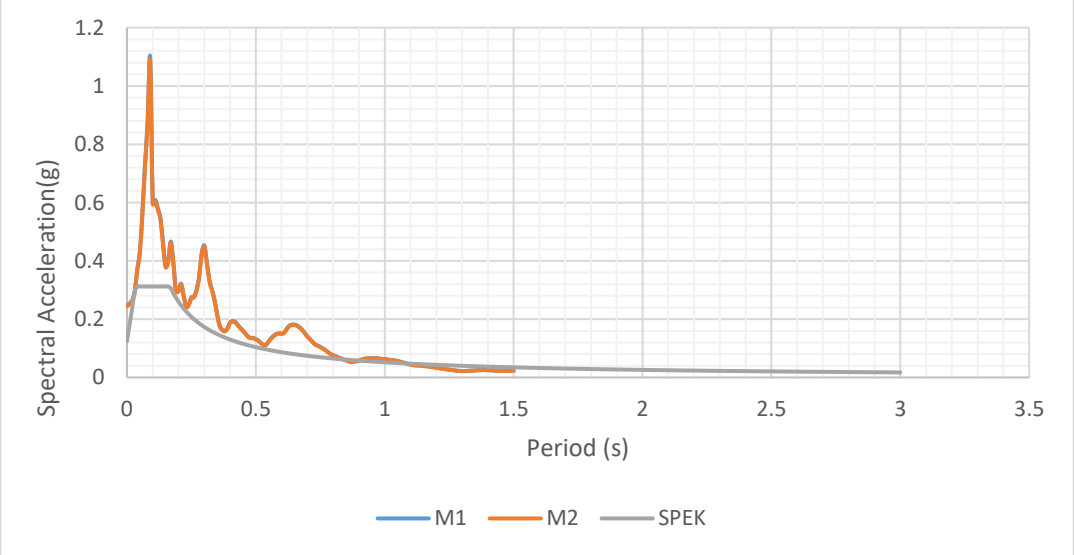

Figure A137. Scaled Vertical Response Spectra of Westmorland (C3-318) Earthquake

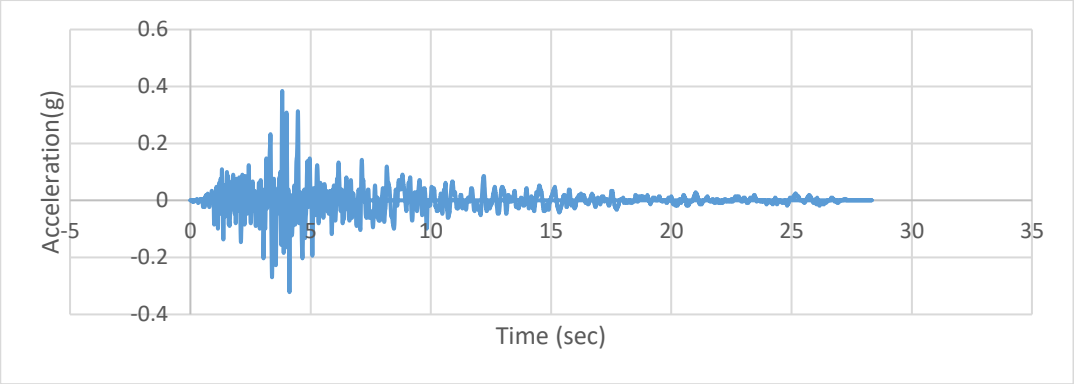

Figure A138. Scaled Acceleration Time Histories of Westmorland (C3-318X) Earthquake

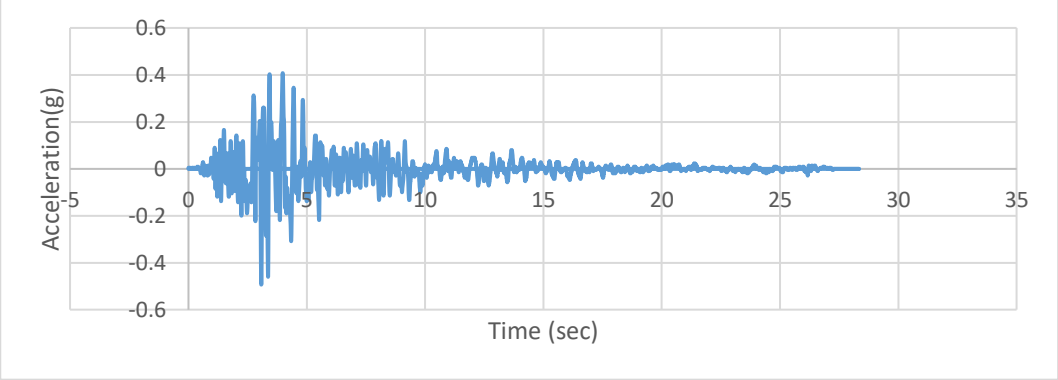

Figure A139. Scaled Acceleration Time Histories of Westmorland (C3-318Y) Earthquake

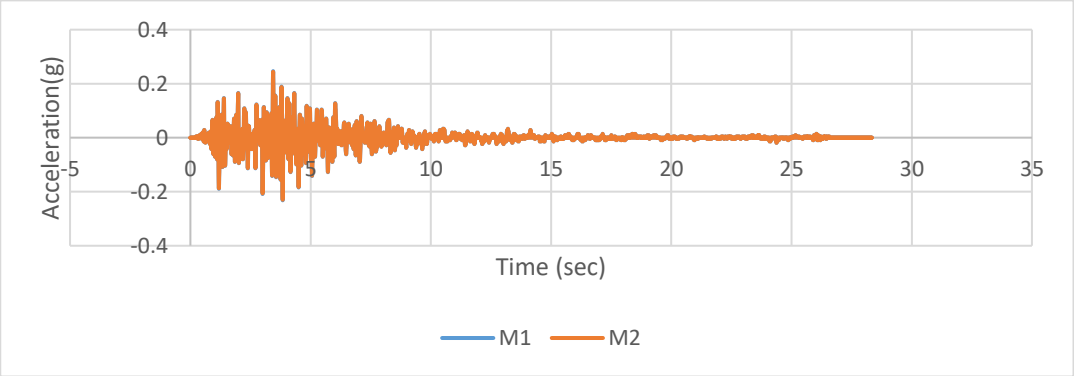

Figure A140. Scaled Acceleration Time Histories of Westmorland (C3-318Z) Earthquake

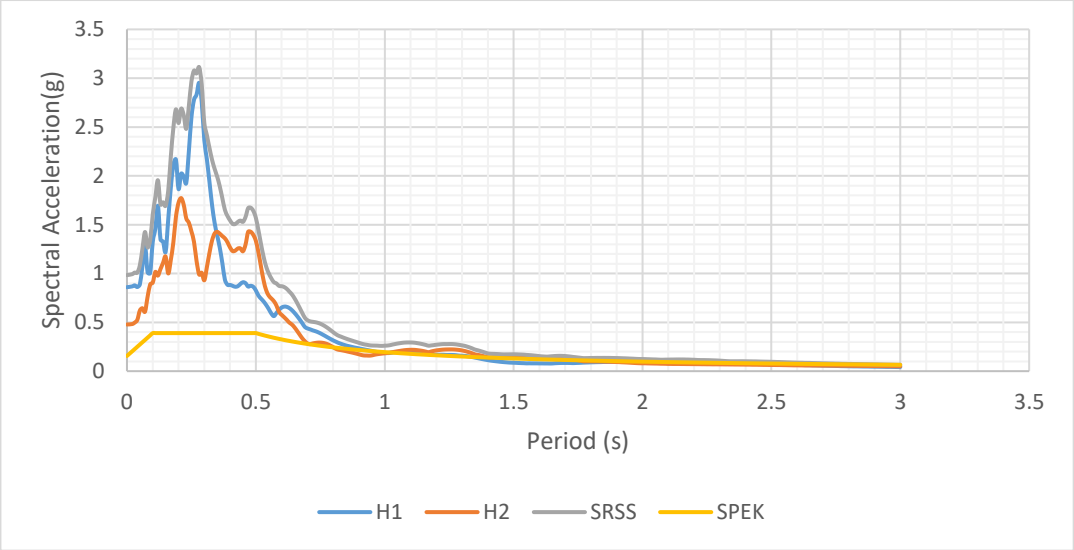

Figure A141. Scaled Horizontal Response Spectra of Chalfant Valley-02 (C3-552) Earthquake

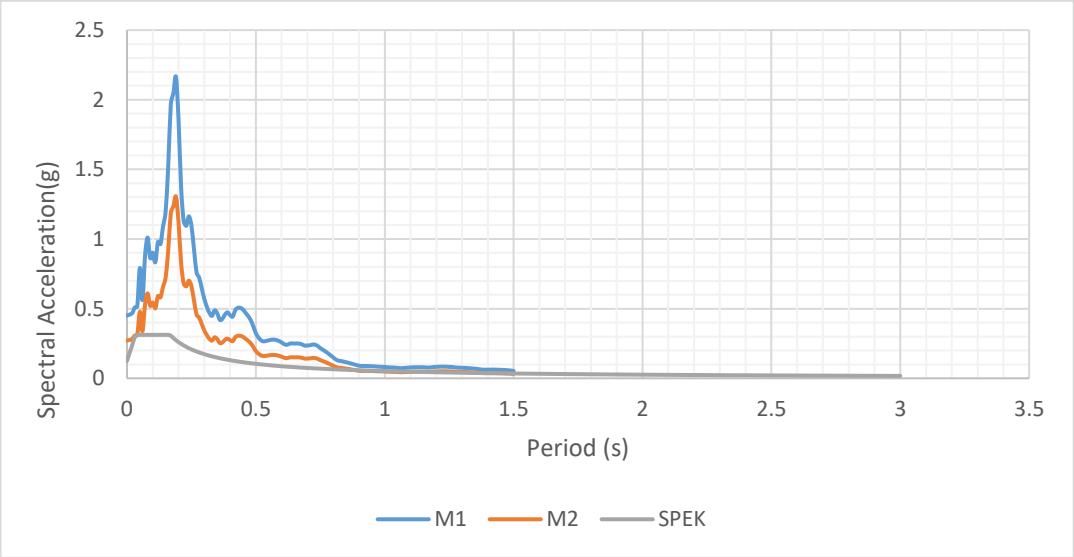

Figure A142. Scaled Vertical Response Spectra of Chalfant Valley-02 (C3-552) Earthquake

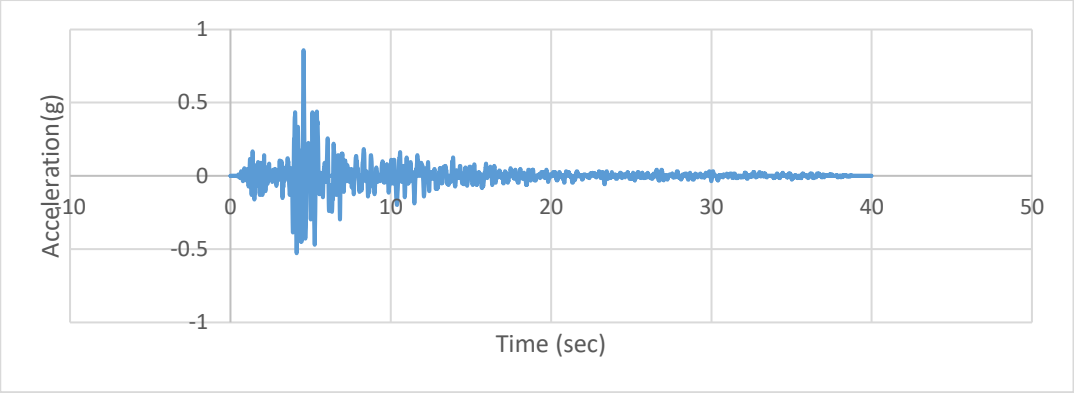

Figure A143. Scaled Acceleration Time Histories of Chalfant Valley-02 (C3-552X) Earthquake

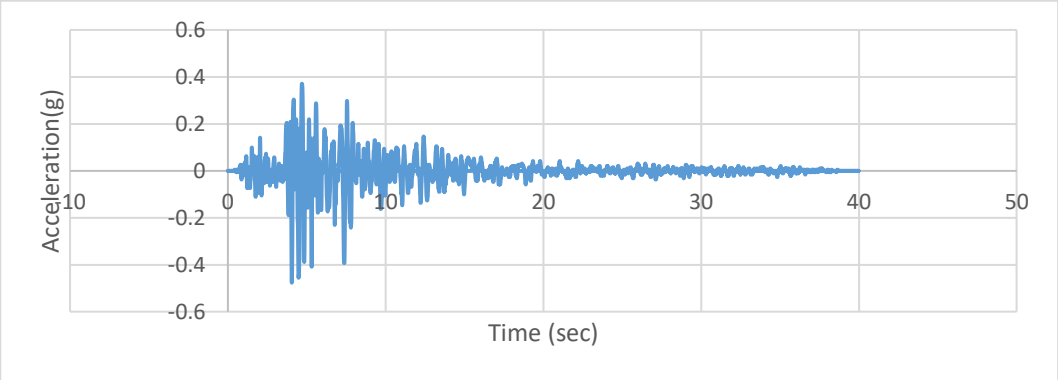

Figure A144. Scaled Acceleration Time Histories of Chalfant Valley-02 (C3-552Y) Earthquake

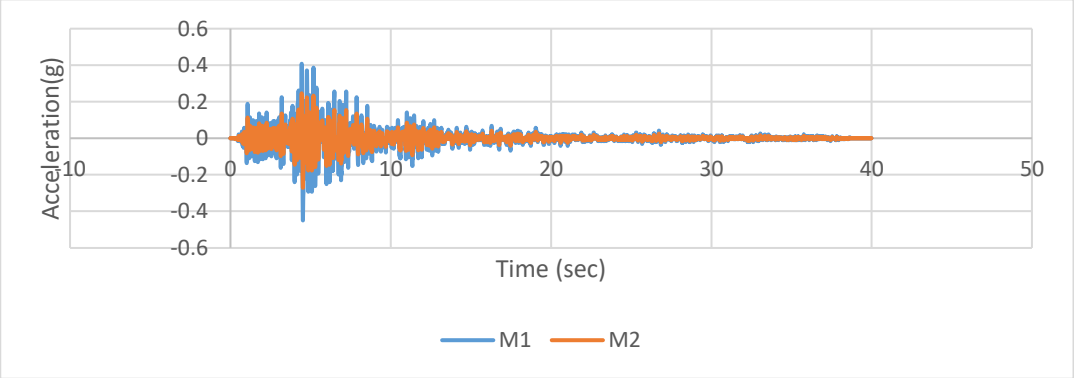

Figure A145. Scaled Acceleration Time Histories of Chalfant Valley-02 (C3-552Z) Earthquake

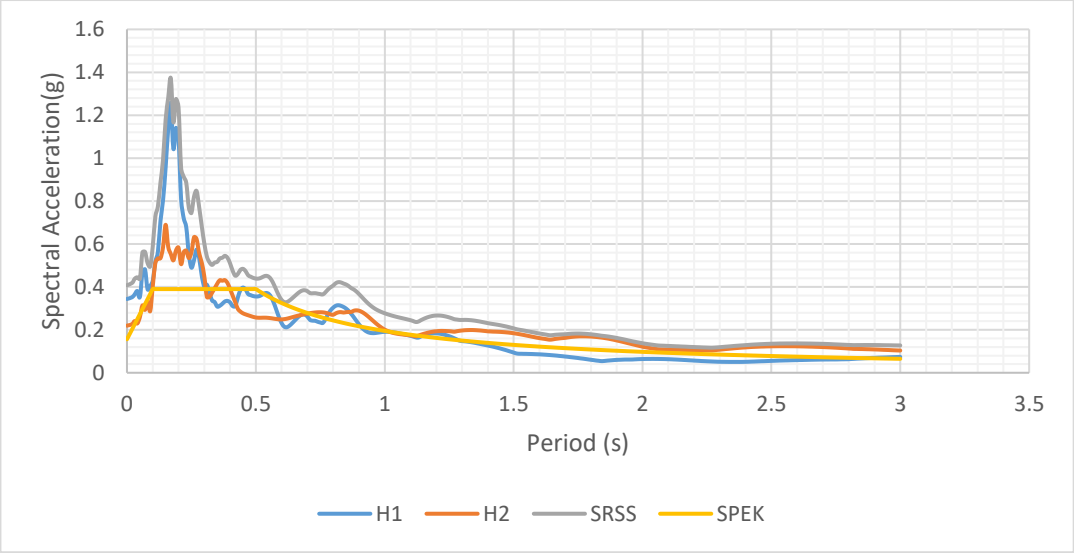

Figure A146. Scaled Horizontal Response Spectra of Kocaeli (C3-1148) Earthquake

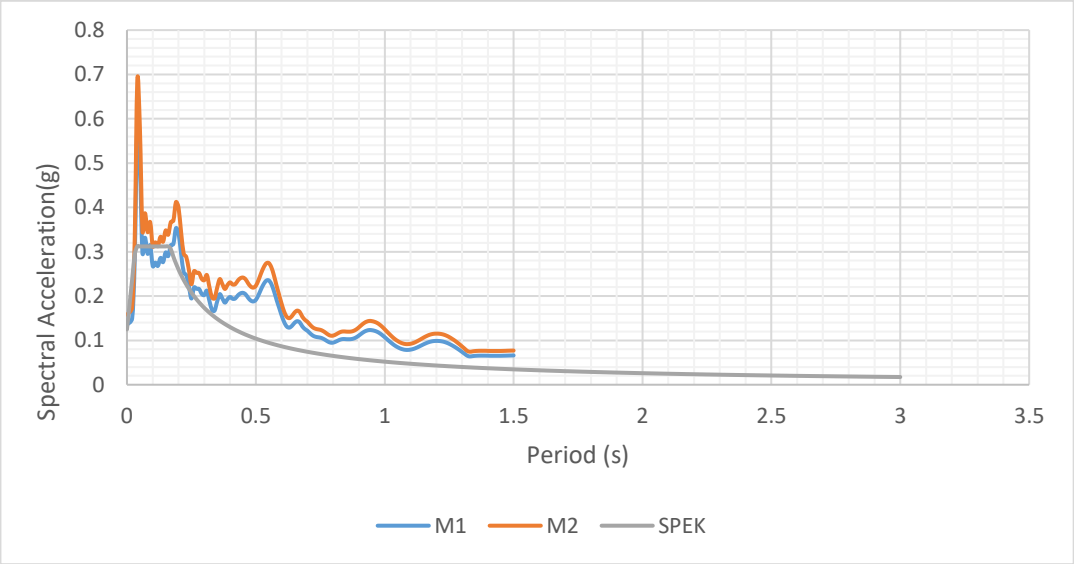

Figure A147. Scaled Vertical Response Spectra of Kocaeli (C3-1148) Earthquake

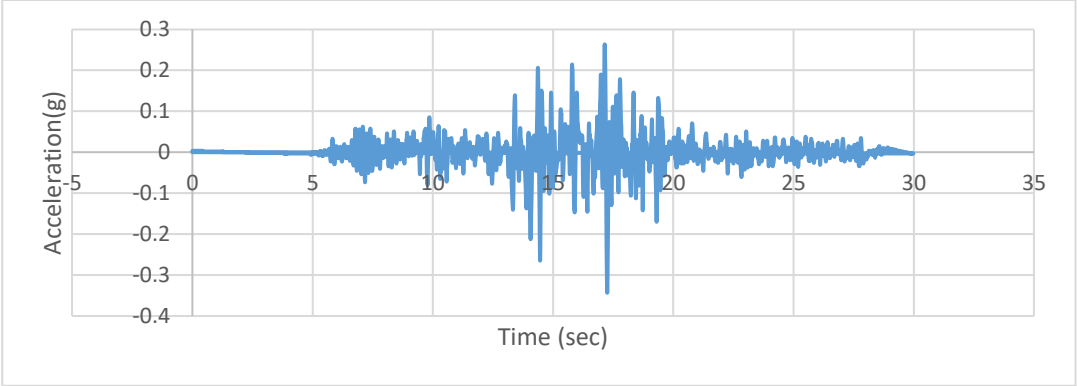

Figure A148. Scaled Acceleration Time Histories of Kocaeli (C3-1148X) Earthquake

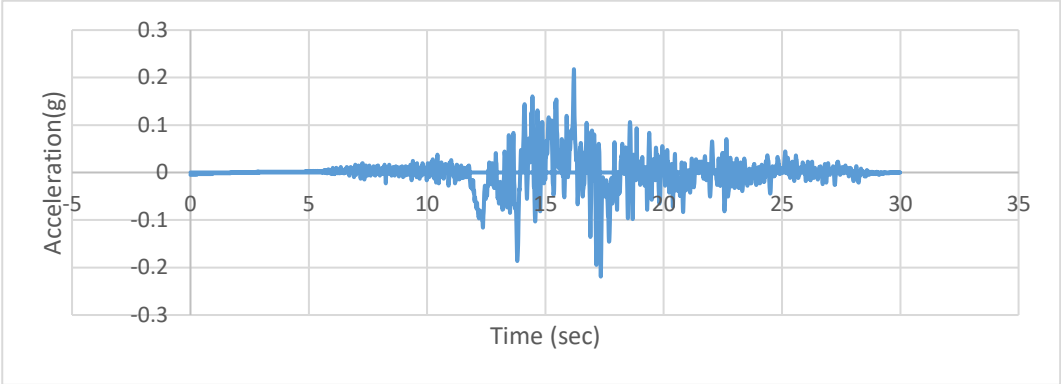

Figure A149. Scaled Acceleration Time Histories of Kocaeli (C3-1148Y) Earthquake

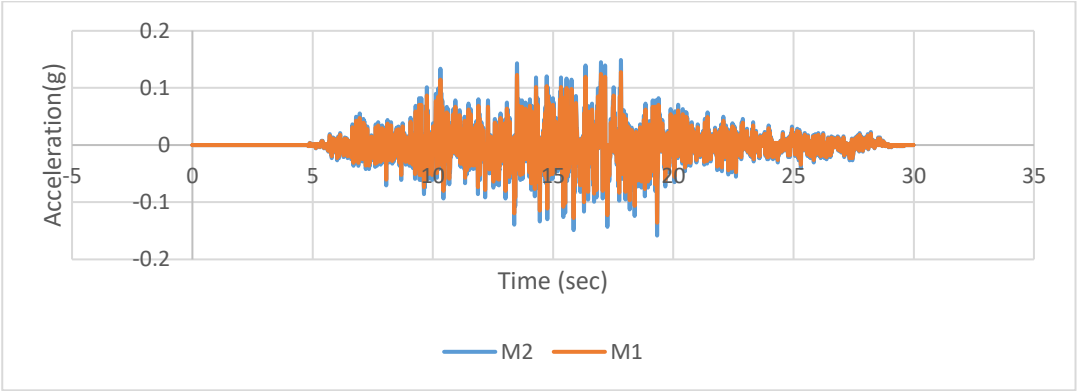

Figure A150. Scaled Acceleration Time Histories of Kocaeli (C3-1148Z) Earthquake

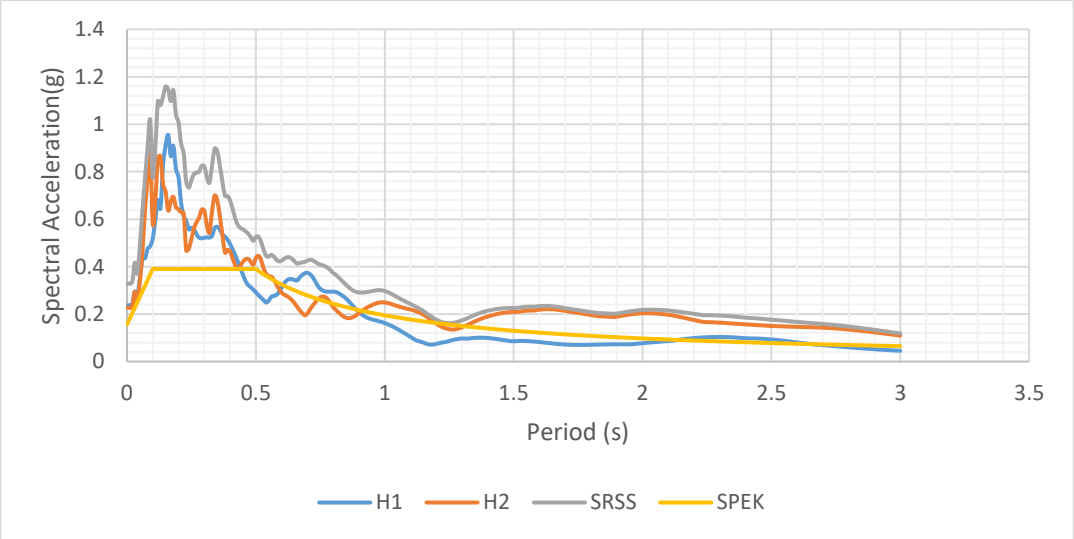

Figure A151. Scaled Horizontal Response Spectra of Manjil (C3-1633) Earthquake

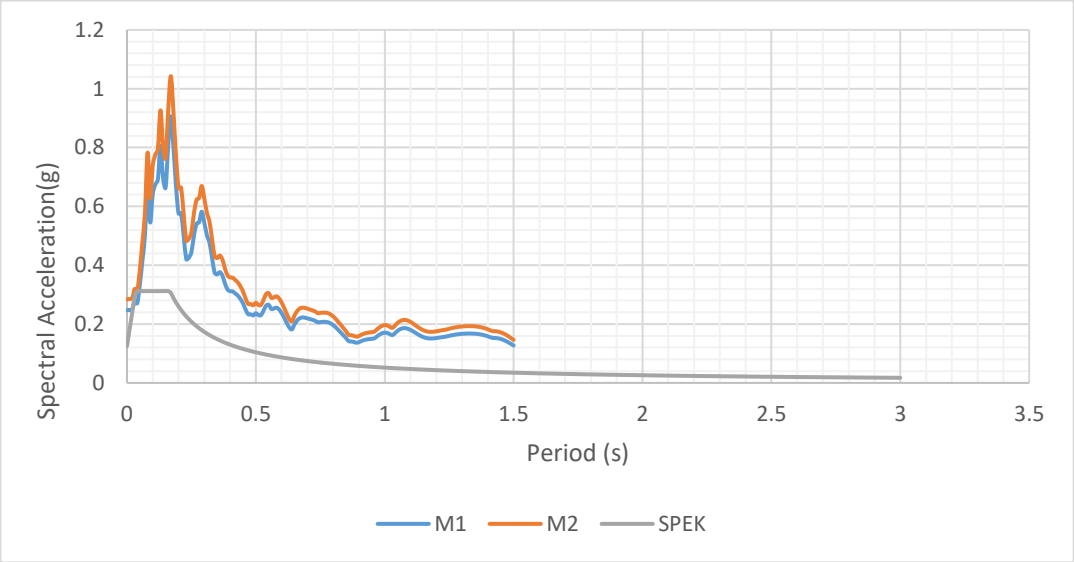

Figure A152. Scaled Vertical Response Spectra of Manjil (C3-1633) Earthquake

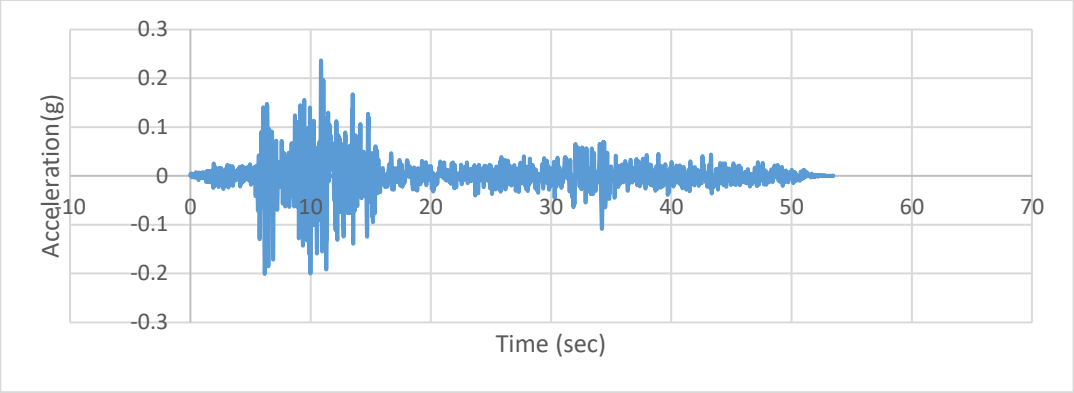

Figure A153. Scaled Acceleration Time Histories of Manjil (C3-1633X) Earthquake

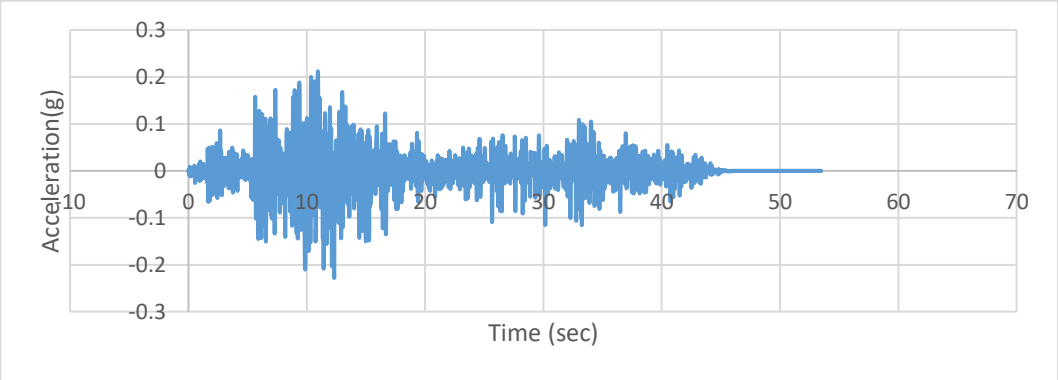

Figure A154. Scaled Acceleration Time Histories of Manjil (C3-1633Y) Earthquake

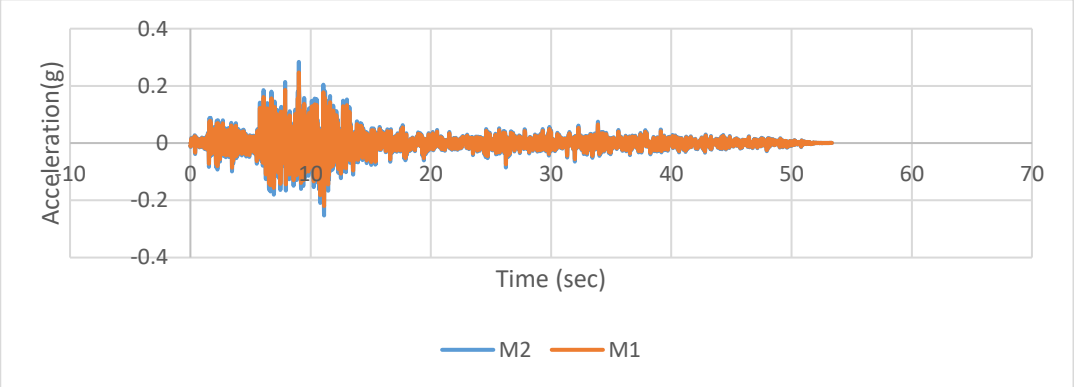

Figure A155. Scaled Acceleration Time Histories of Manjil (C3-1633Z) Earthquake

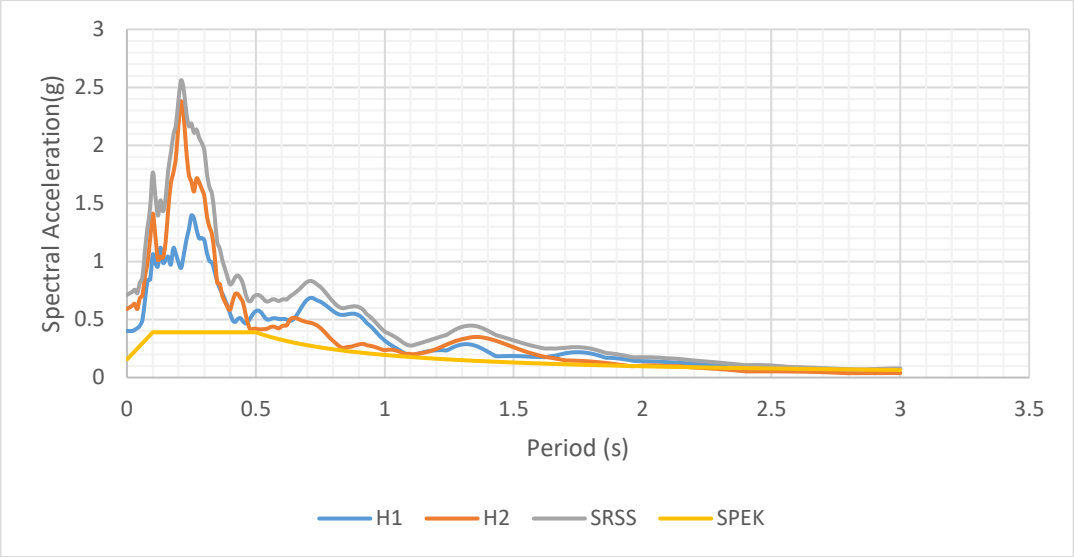

Figure A156. Scaled Horizontal Response Spectra of Big Bear-01 (C3-6057) Earthquake

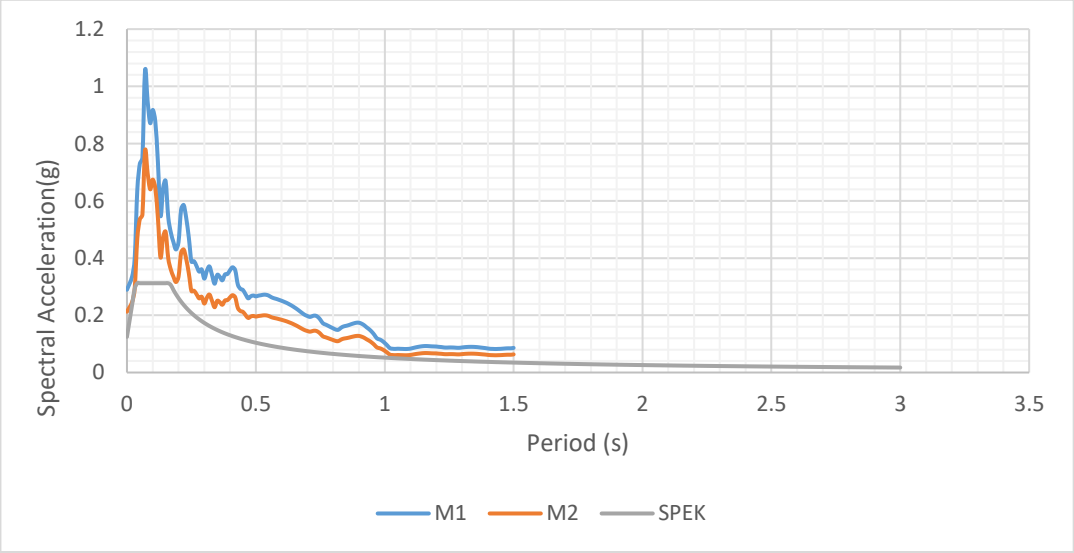

Figure A157. Scaled Vertical Response Spectra of Big Bear-01 (C3-6057) Earthquake

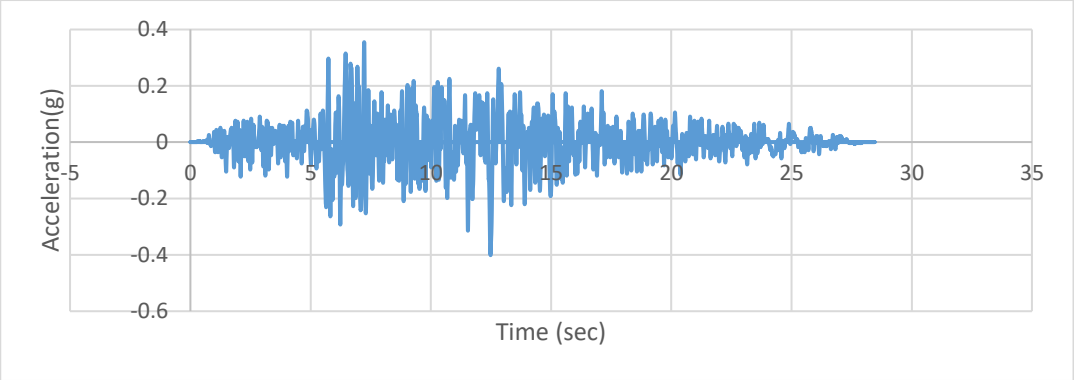

Figure A158.Scaled Acceleration Time Histories of Big Bear-01(C3-6057X) Earthquake

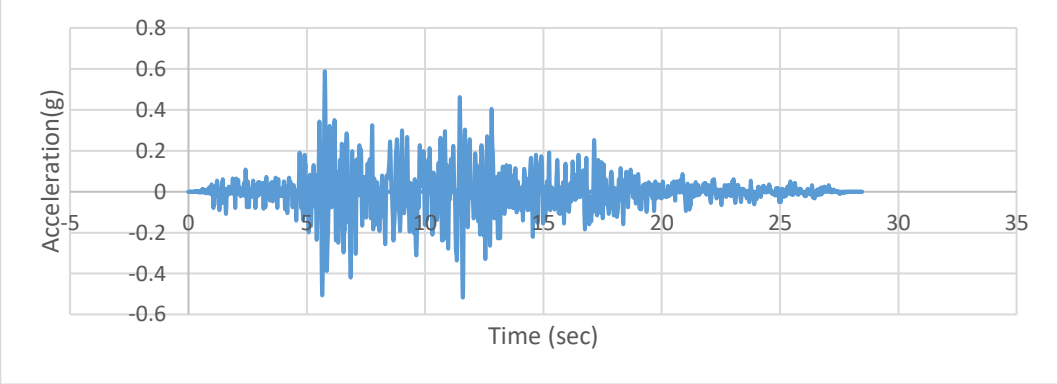

Figure A159. Scaled Acceleration Time Histories of Big Bear-01(C3-6057Y) Earthquake

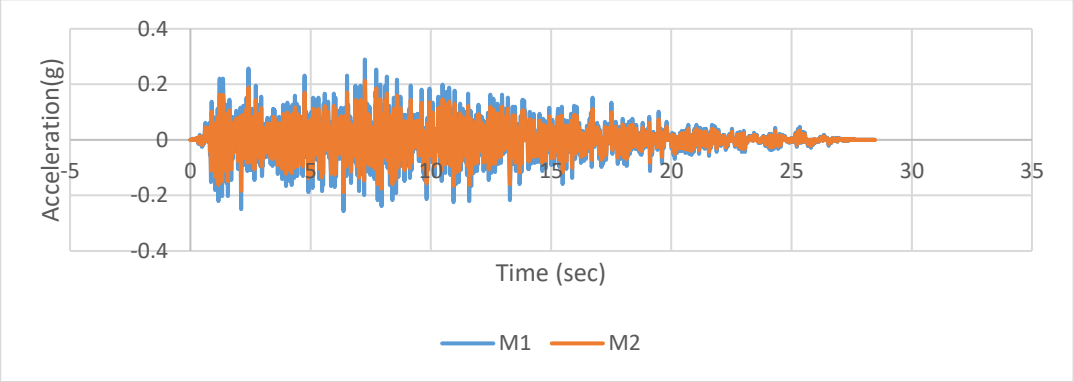

Figure A160. Scaled Acceleration Time Histories of Big Bear-01(C3-6057Y) Earthquake

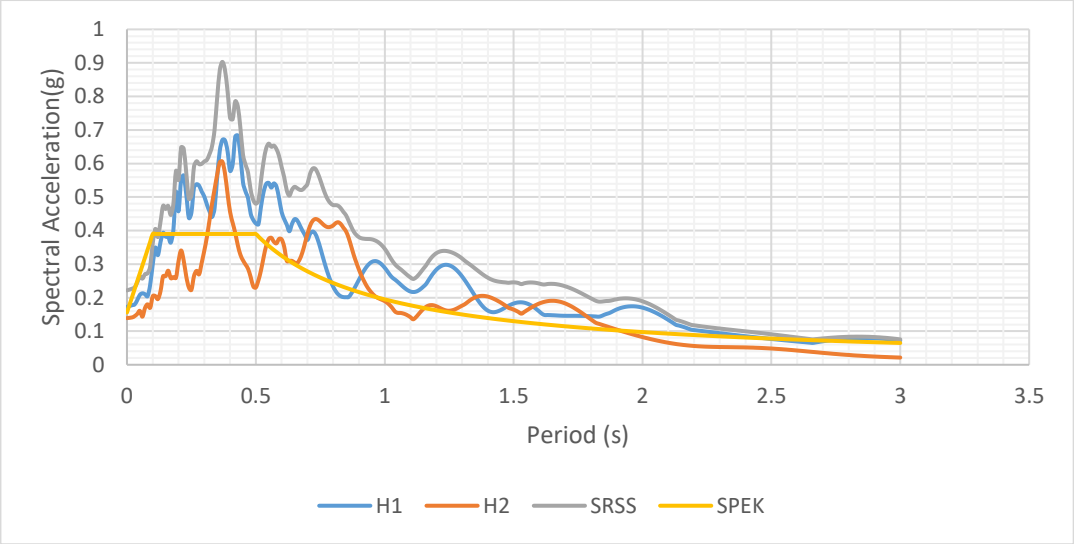

Figure A161. Scaled Horizontal Response Spectra of Big Bear-01 (C3-6059) Earthquake

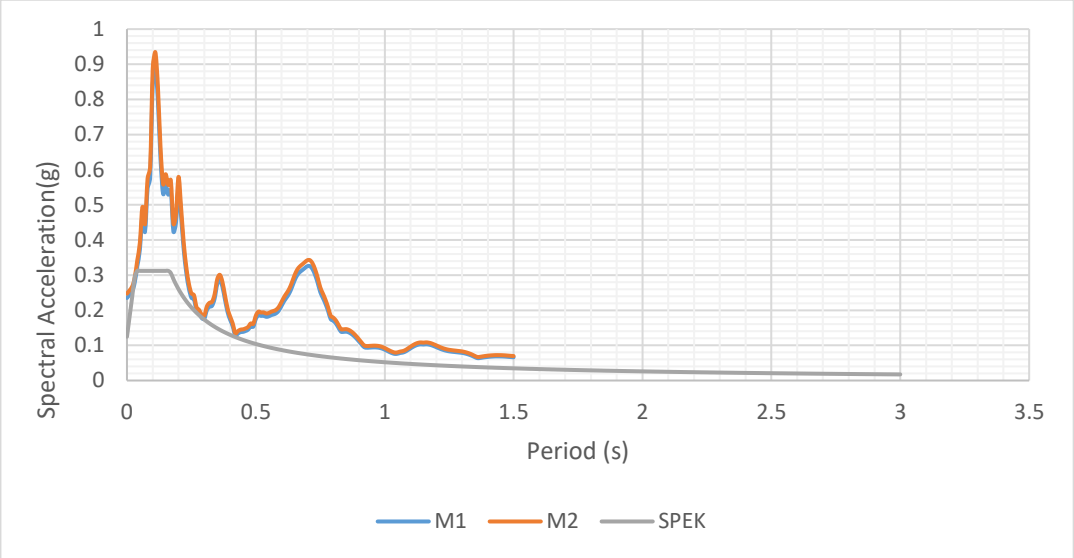

Figure A162. Scaled Vertical Response Spectra of Big Bear-01 (C3-6059) Earthquake

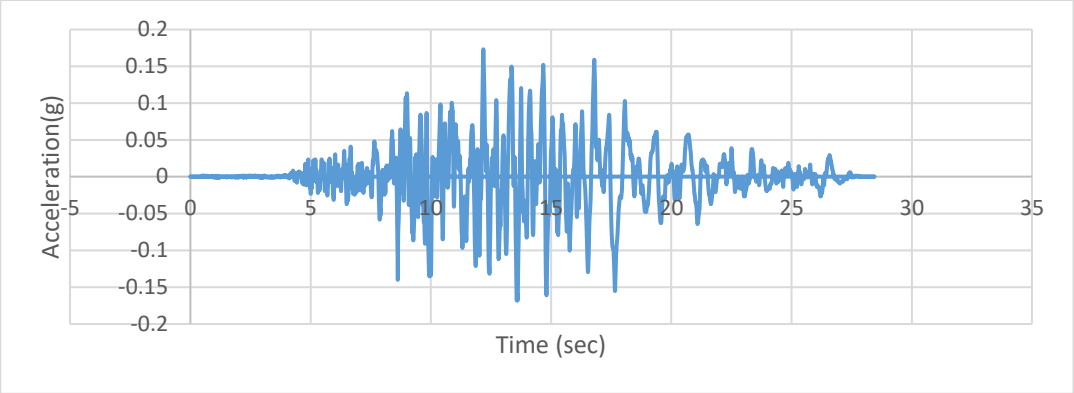

Figure A163. Scaled Acceleration Time Histories of Big Bear-01 (C3-6059X) Earthquake

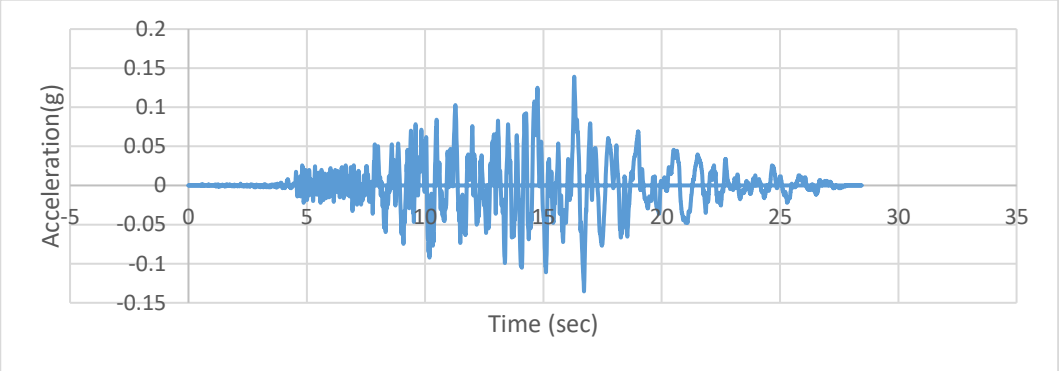

Figure A164. Scaled Acceleration Time Histories of Big Bear-01 (C3-6059Y) Earthquake

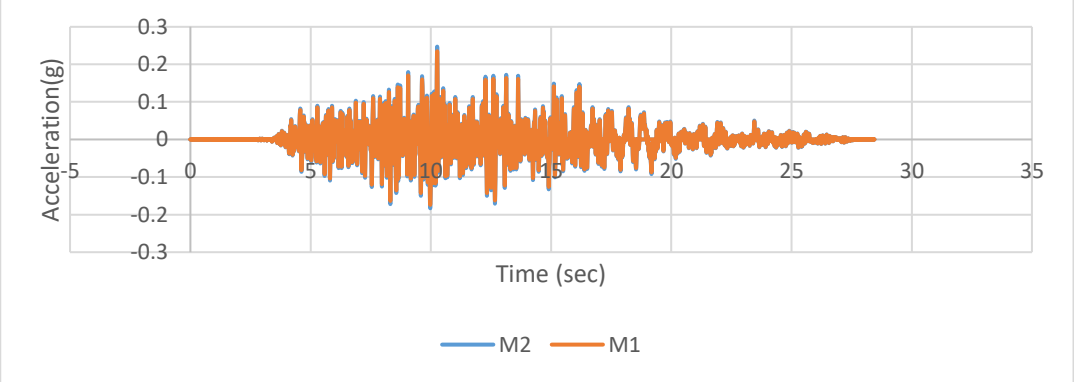

Figure A165. Scaled Acceleration Time Histories of Big Bear-01 (C3-6059Z) Earthquake

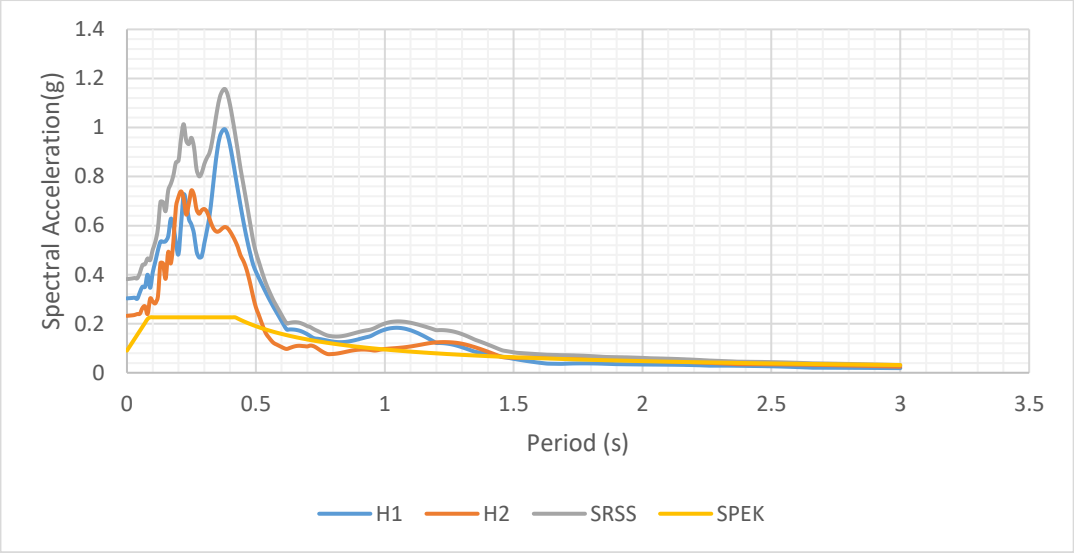

Figure A166. Scaled Horizontal Response Spectra of Parkfield (C4-33) Earthquake

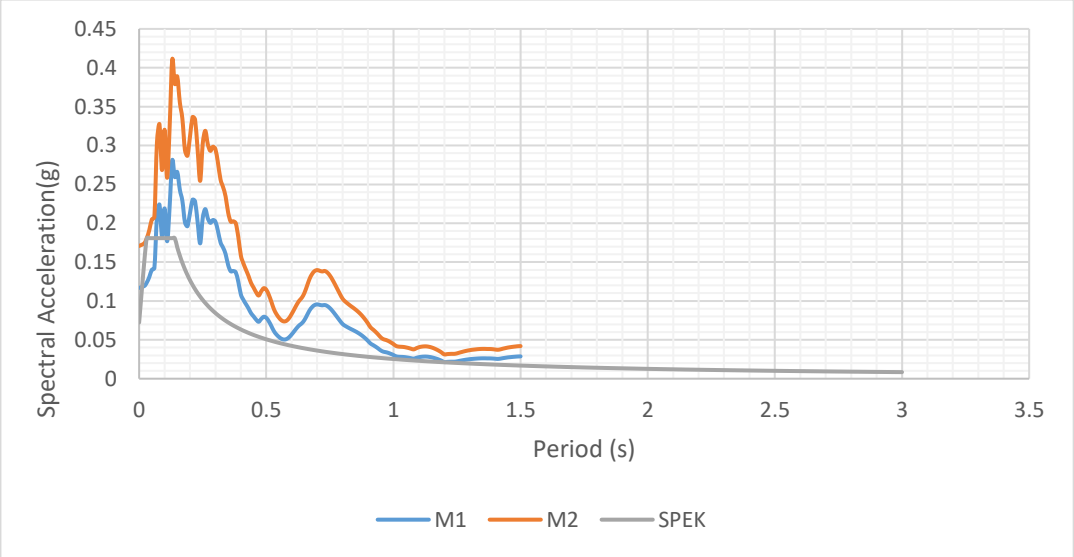

Figure A167. Scaled Vertical Response Spectra of Parkfield (C4-33) Earthquake

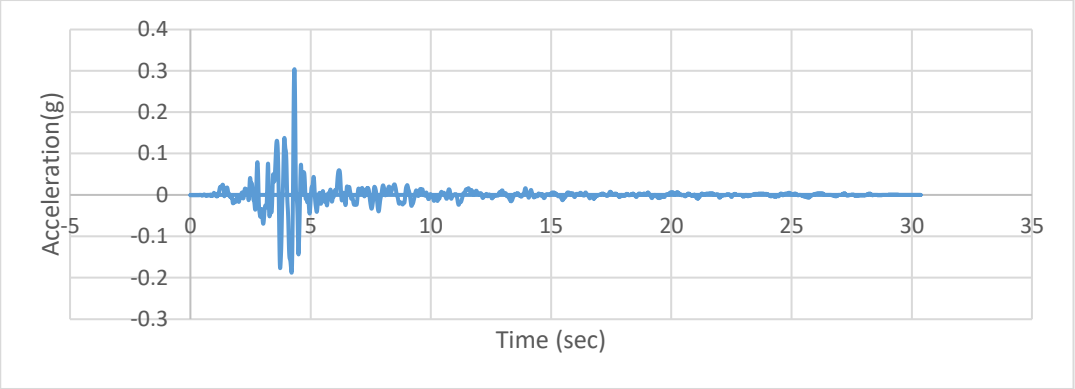

Figure A168. Scaled Acceleration Time Histories of Parkfield (C4-33X) Earthquake

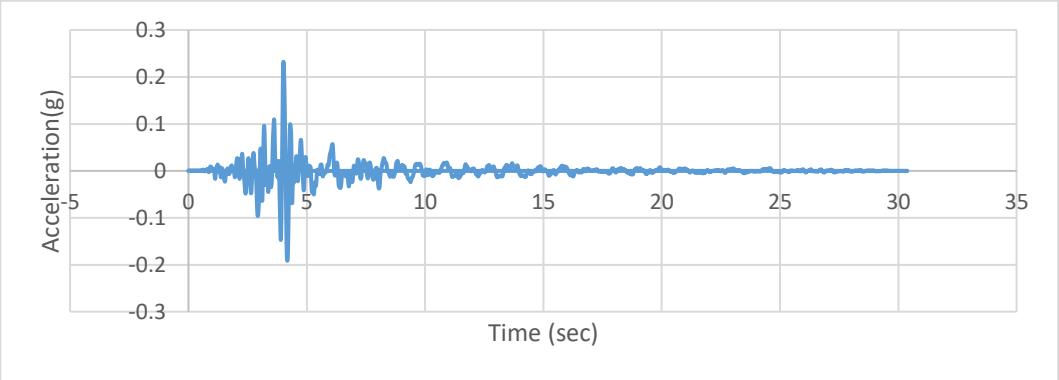

Figure A169. Scaled Acceleration Time Histories of Parkfield (C4-33Y) Earthquake

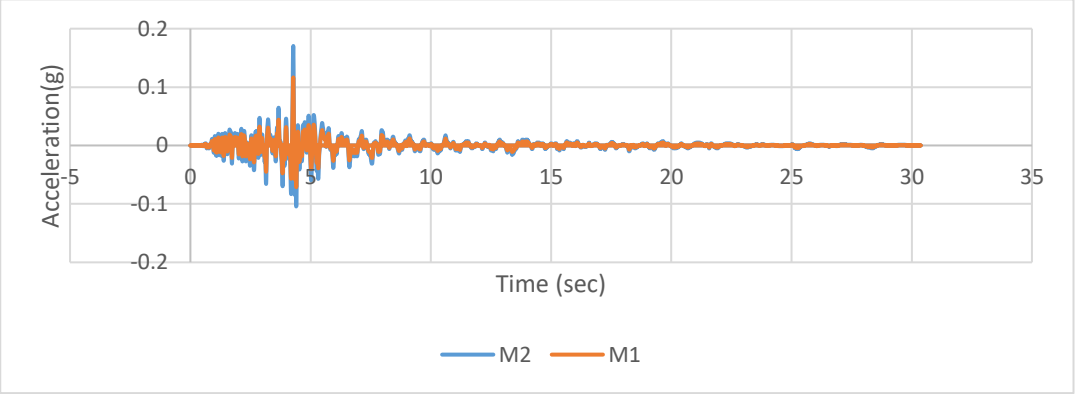

Figure A170. Scaled Acceleration Time Histories of Parkfield (C4-33Z) Earthquake

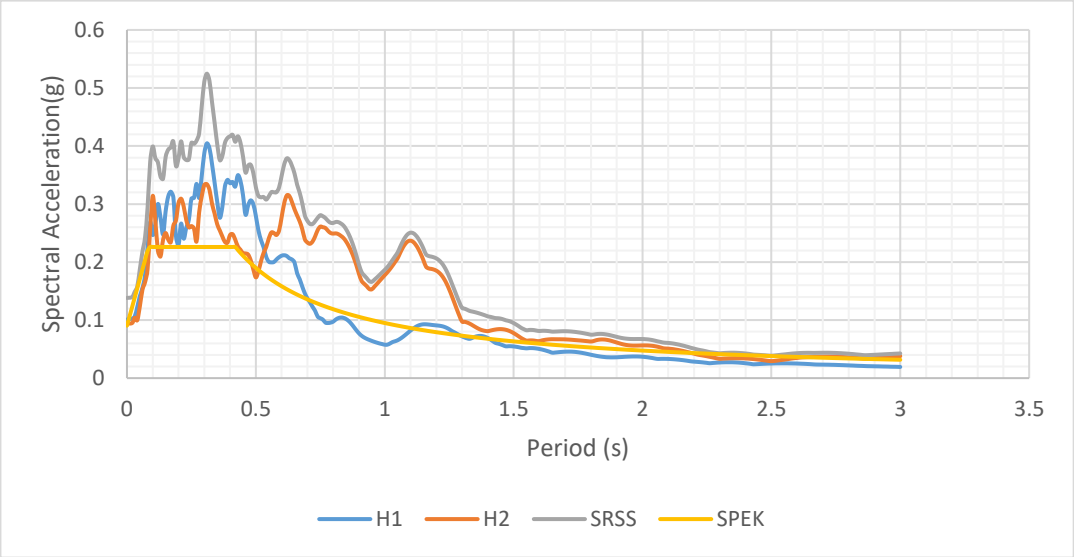

Figure A171. Scaled Horizontal Response Spectra of Imperial Valley-06 (C4-164) Earthquake

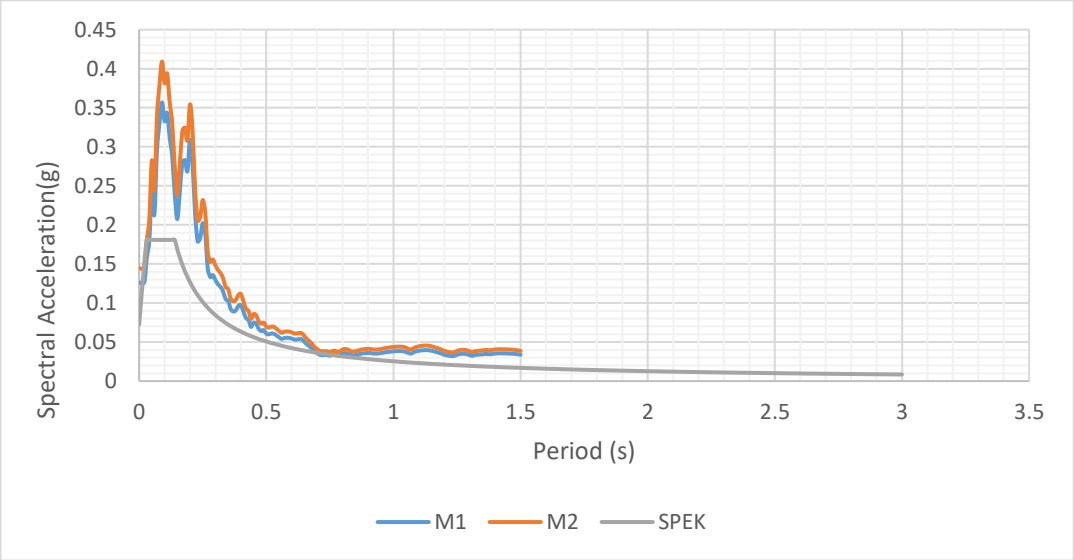

Figure A172. Scaled Vertical Response Spectra of Imperial Valley-06 (C4-164) Earthquake

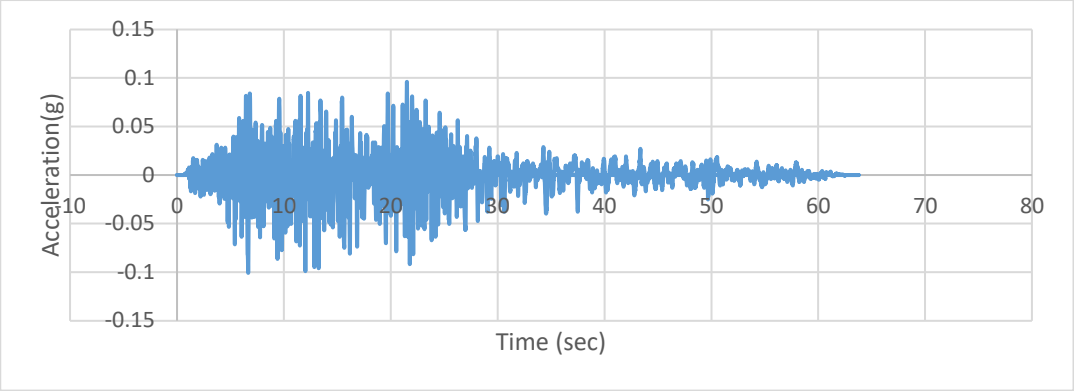

Figure A173. Scaled Acceleration Time Histories of Imperial Valley-06 (C4-164X) Earthquake

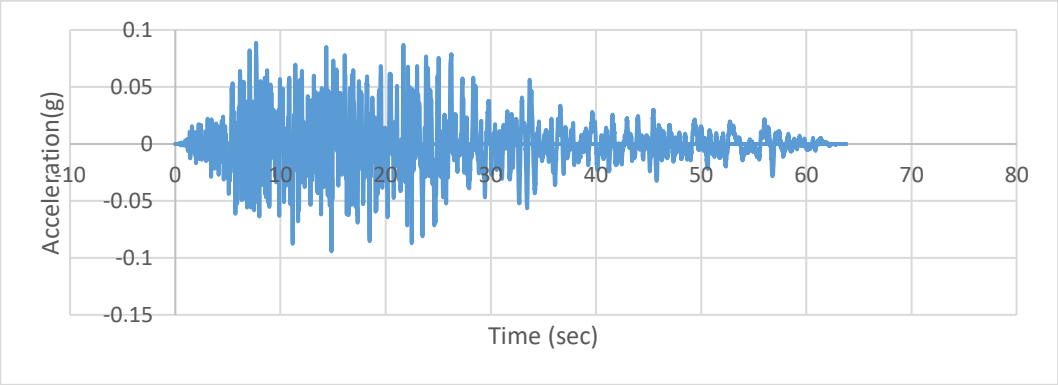

Figure A174. Scaled Acceleration Time Histories of Imperial Valley-06 (C4-164Y) Earthquake

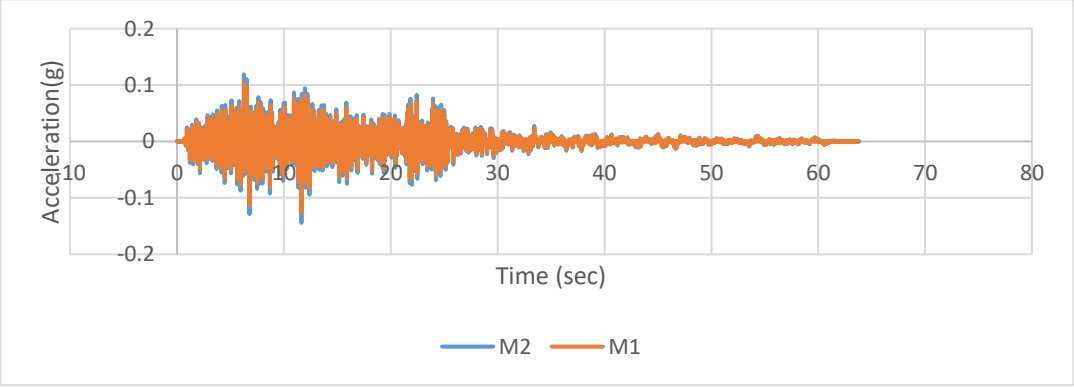

Figure A175. Scaled Acceleration Time Histories of Imperial Valley-06 (C4-164Z) Earthquake

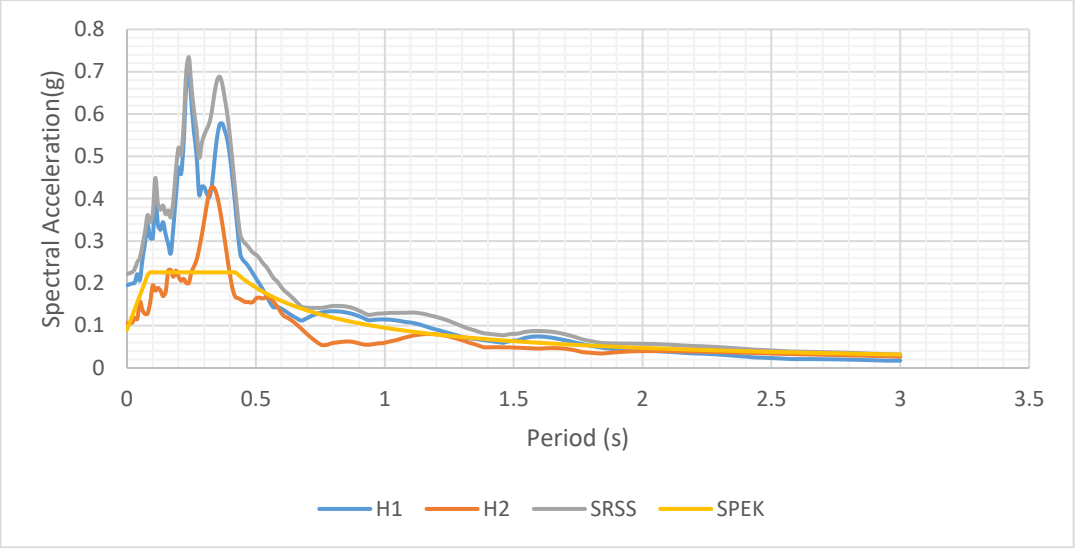

Figure A176.Scaled Horizontal Response Spectra of Mammoth Lakes-03 (C4-237) Earthquake

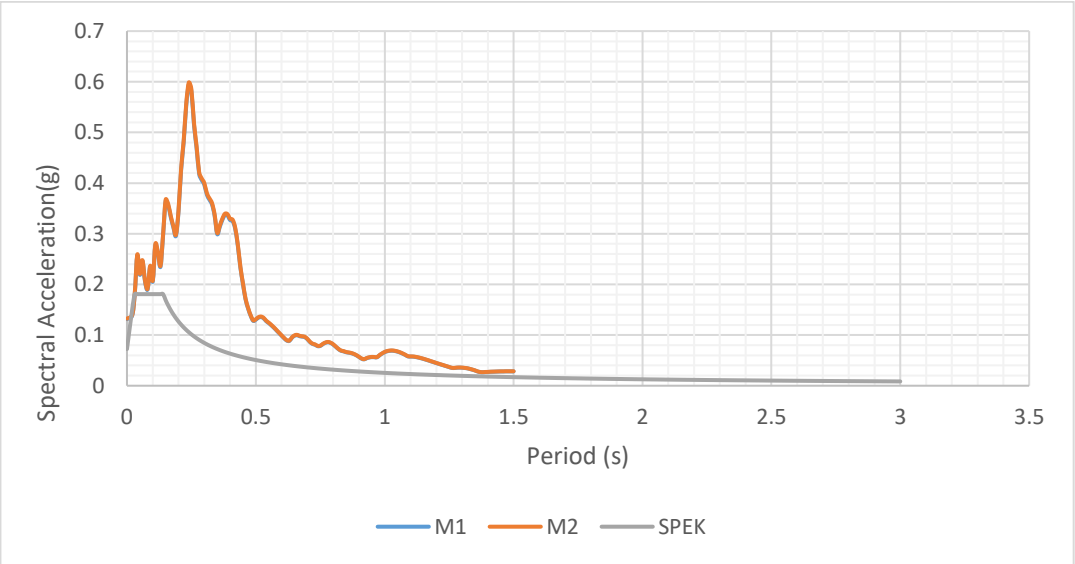

Figure A177. Scaled Vertical Response Spectra of Mammoth Lakes-03 (C4-237) Earthquake

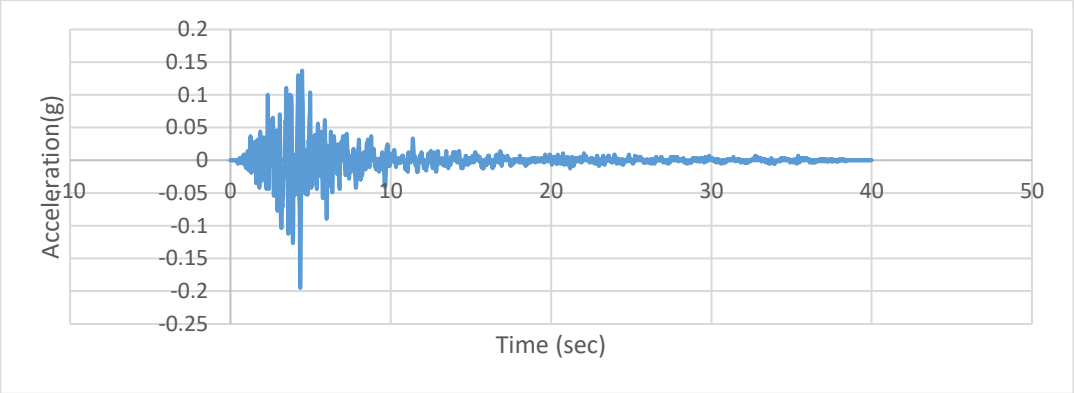

Figure A178.Scaled Acceleration Time Histories of Mammoth Lakes-03(C4-237X) Earthquake

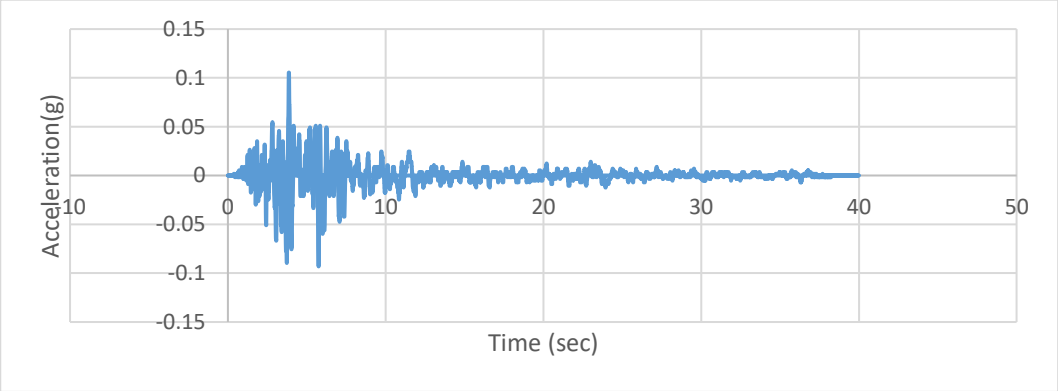

Figure A179.Scaled Acceleration Time Histories of Mammoth Lakes-03(C4-237Y) Earthquake

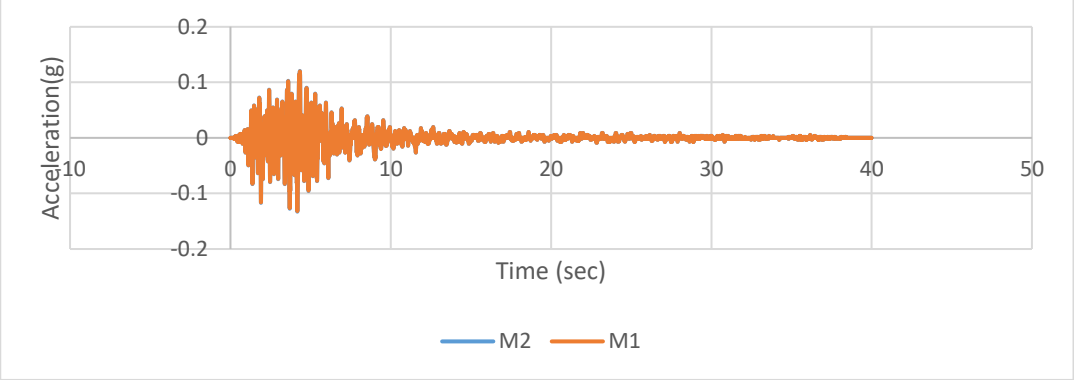

Figure A180.Scaled Acceleration Time Histories of Mammoth Lakes-03(C4-237Z) Earthquake

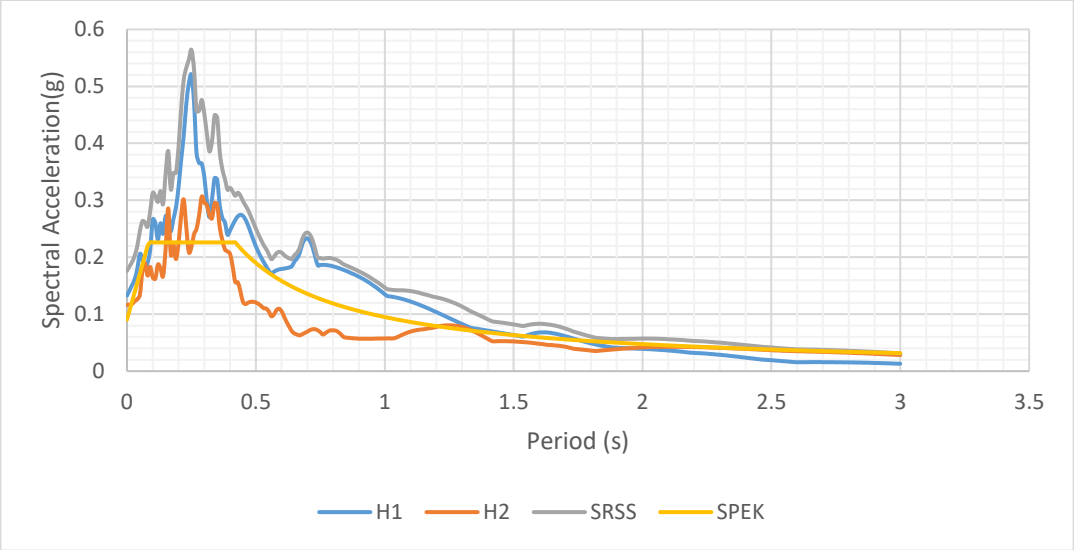

Figure A181.Scaled Horizontal Response Spectra of Mammoth Lakes-03 (C4-238) Earthquake

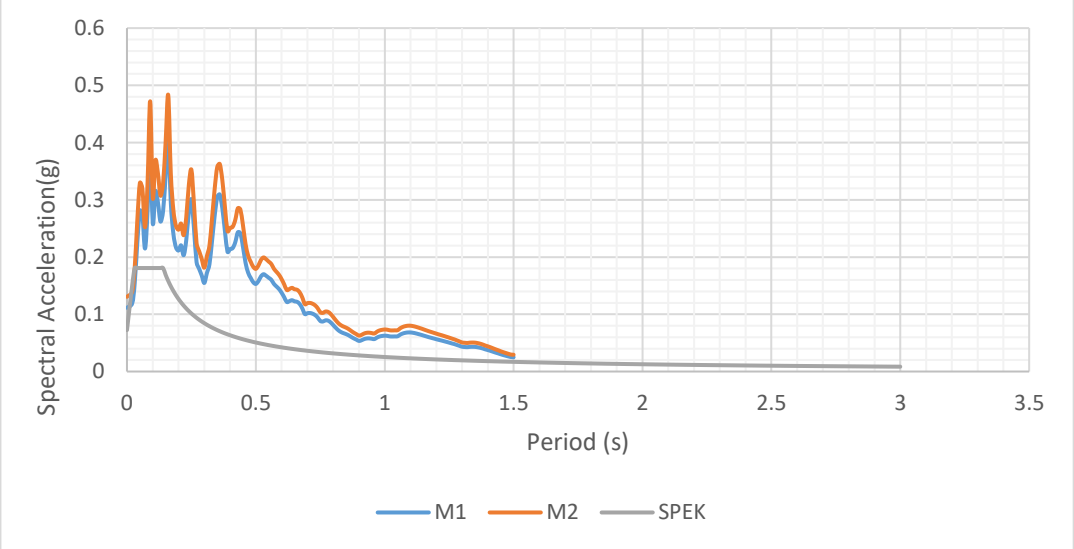

Figure A182.Scaled Vertical Response Spectra of Mammoth Lakes-03 (C4-238) Earthquake

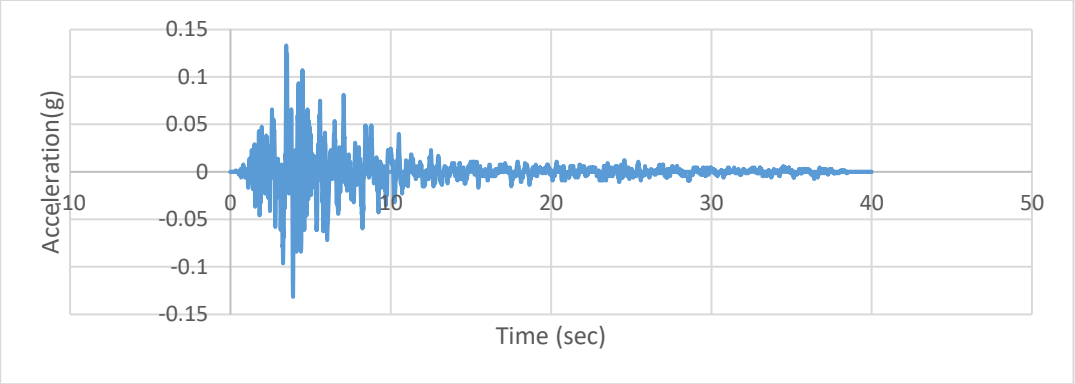

Figure A183.Scaled Acceleration Time Histories of Mammoth Lakes-03 (C4-238X) Earthquake

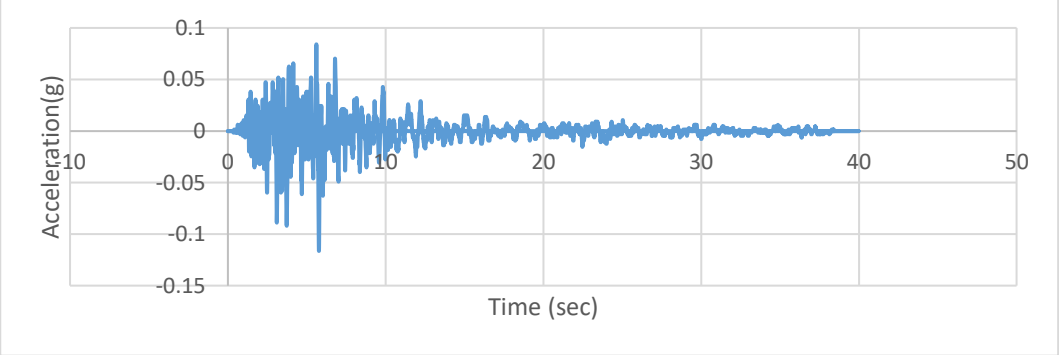

Figure A184. Scaled Acceleration Time Histories of Mammoth Lakes-03 (C4-238Y) Earthquake

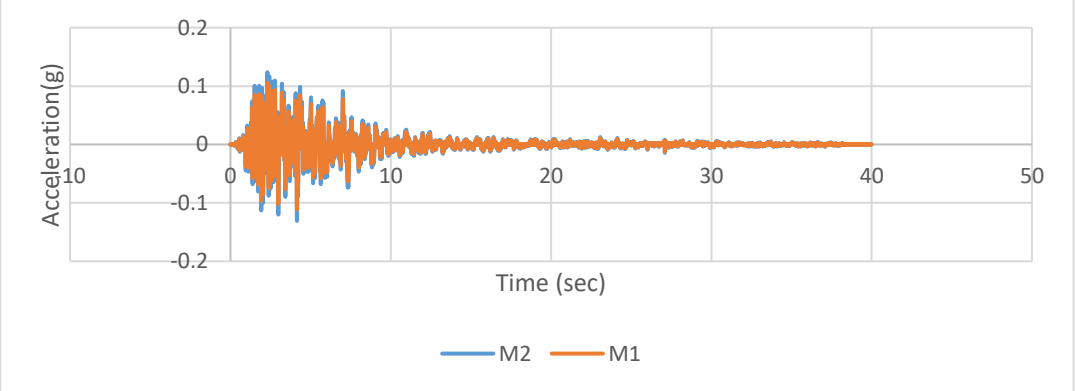

Figure A185. Scaled Acceleration Time Histories of Mammoth Lakes-03 (C4-238Z) Earthquake

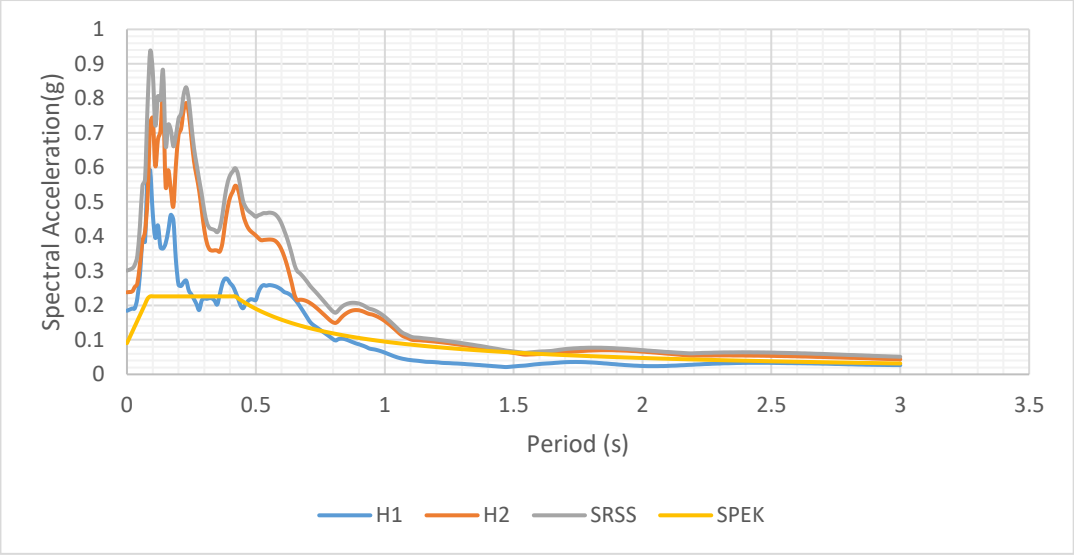

Figure A186.Scaled Horizontal Response Spectra of Westmorland (C4-318) Earthquake

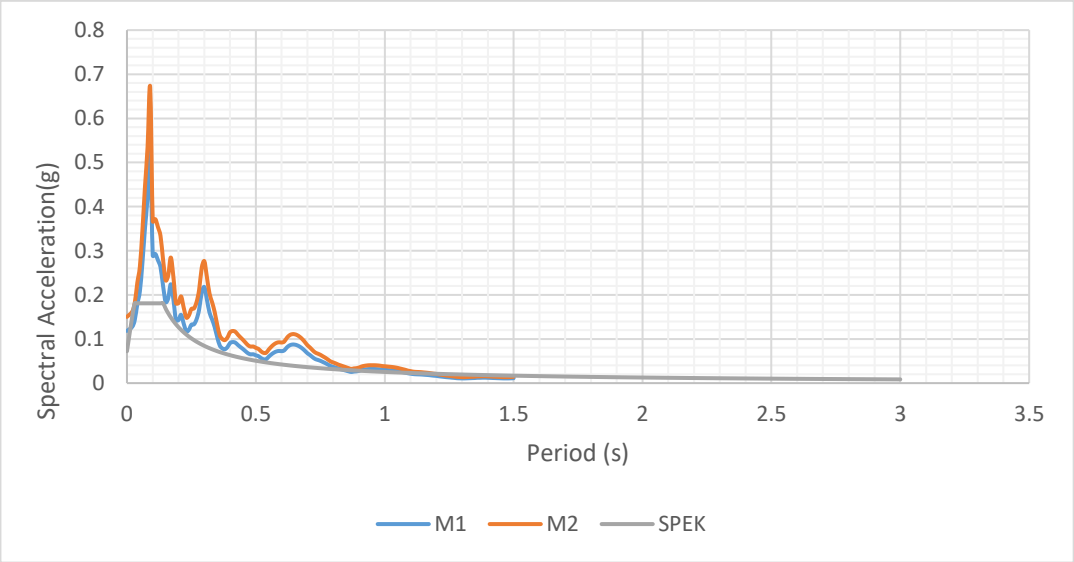

Figure A187. Scaled Vertical Response Spectra of Westmorland (C4-318) Earthquake

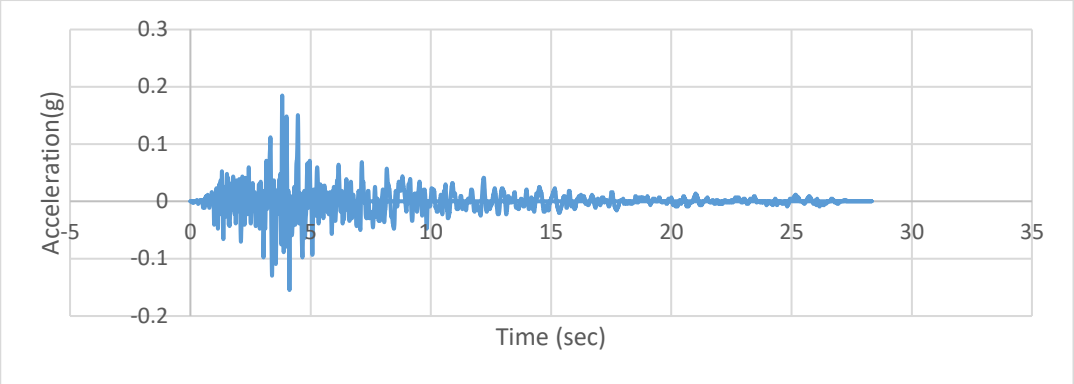

Figure A188.Scaled Acceleration Time Histories of Westmorland (C4-318X) Earthquake

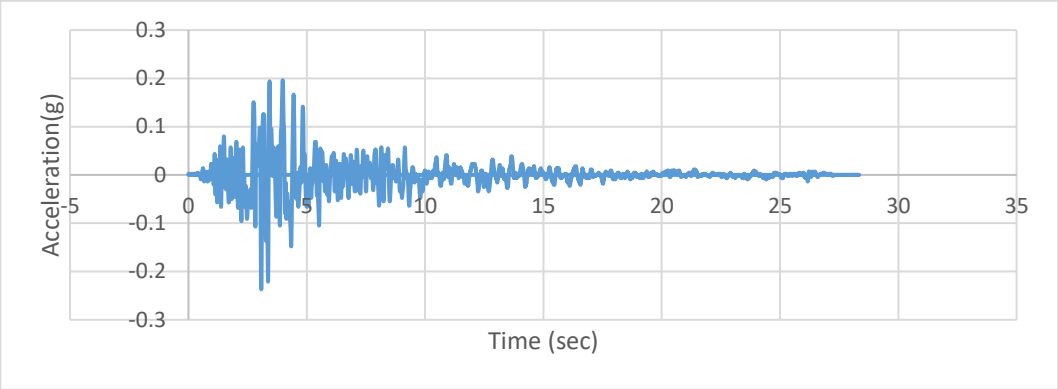

Figure A189.Scaled Acceleration Time Histories of Westmorland (C4-318Y) Earthquake

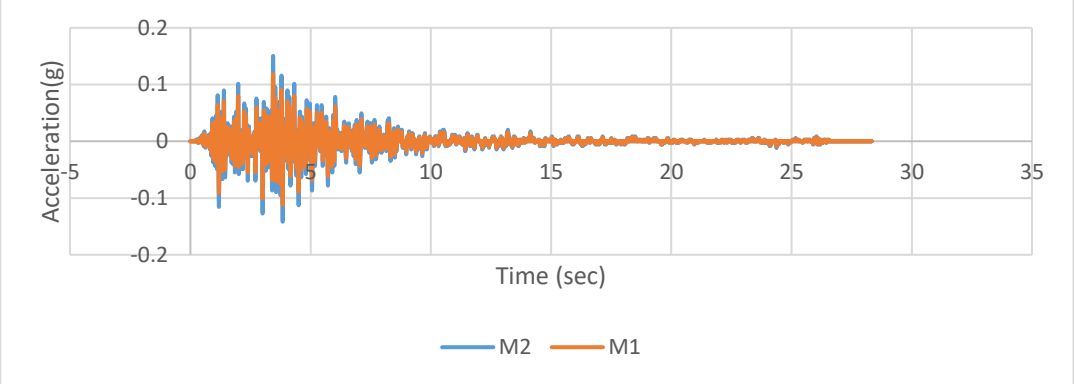

Figure A190. Scaled Acceleration Time Histories of Westmorland (C4-318Z) Earthquake

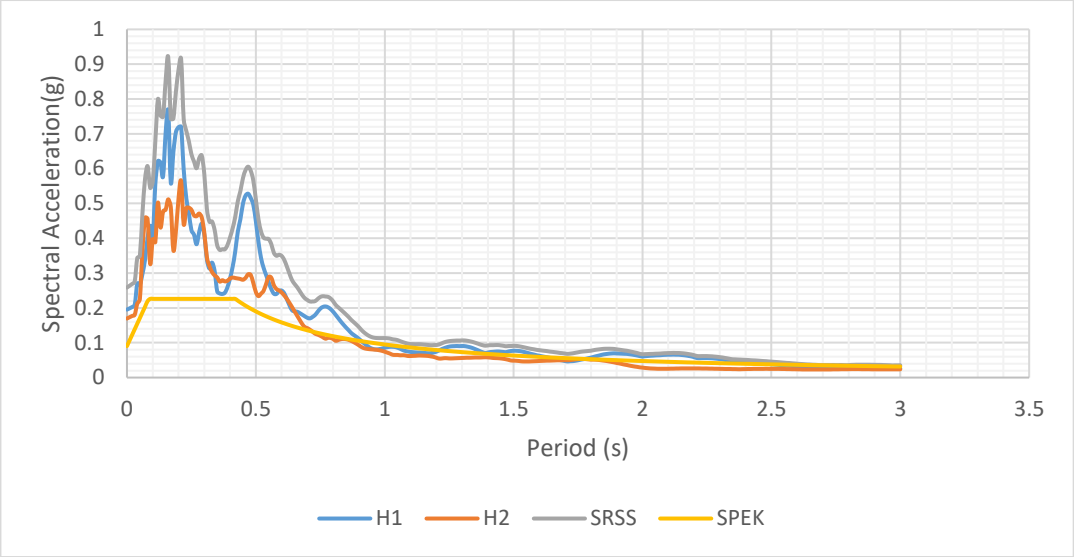

Figure A191.Scaled Horizontal Response Spectra of Chalfant Valley-01(C4-543) Earthquake

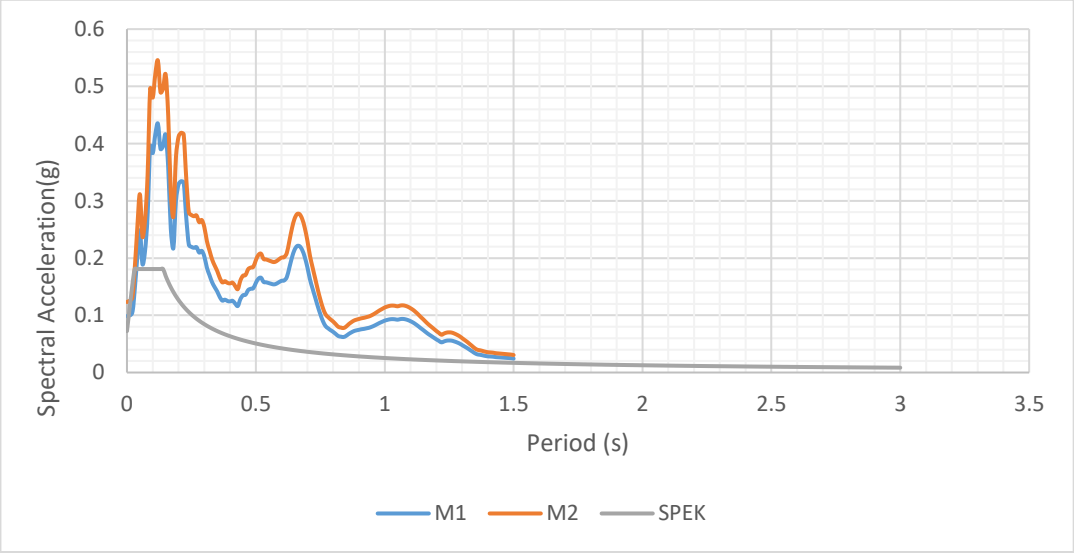

Figure A192. Scaled Vertical Response Spectra of Chalfant Valley-01(C4-543) Earthquake

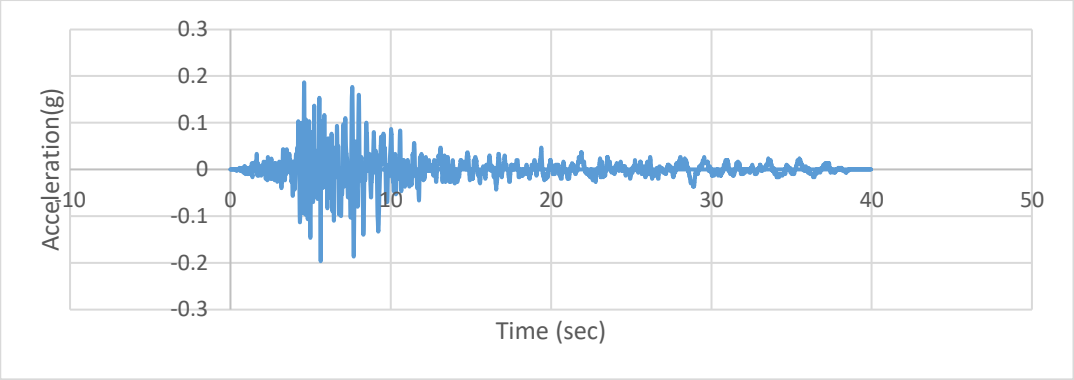

Figure A193. Scaled Acceleration Time Histories of Chalfant Valley-01(C4-543X) Earthquake

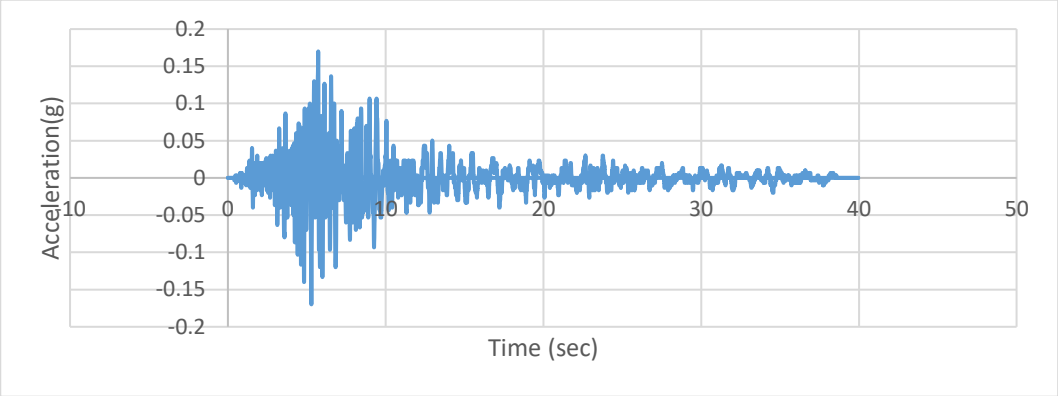

Figure A194. Scaled Acceleration Time Histories of Chalfant Valley-01(C4-543Y) Earthquake

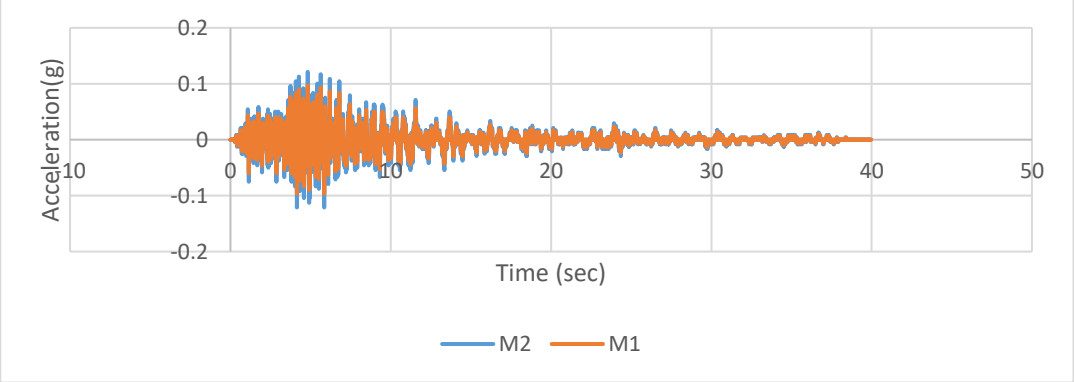

Figure A195. Scaled Acceleration Time Histories of Chalfant Valley-01(C4-543Z) Earthquake

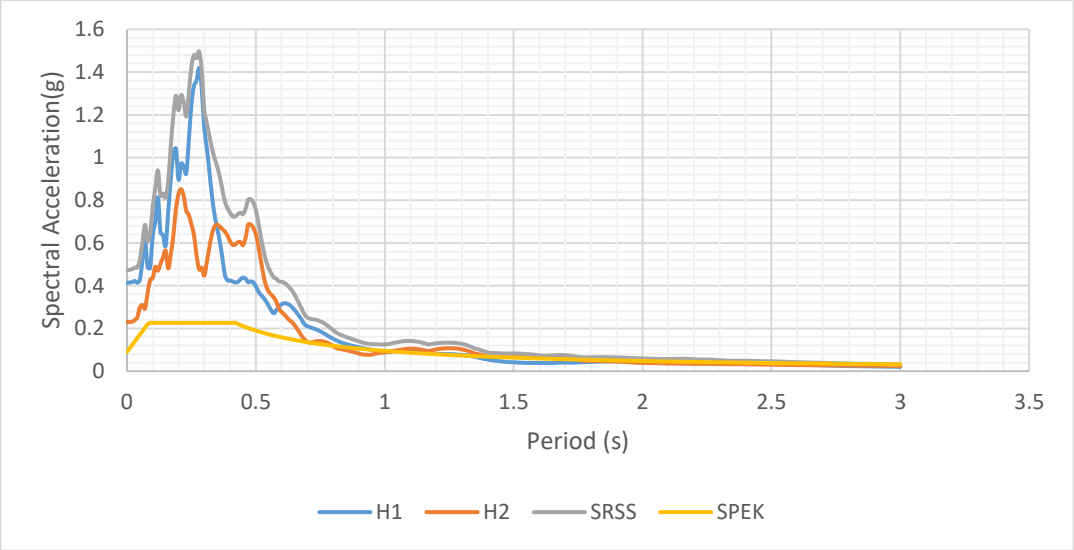

Figure A196. Scaled Horizontal Response Spectra of Chalfant Valley-02(C4-552) Earthquake

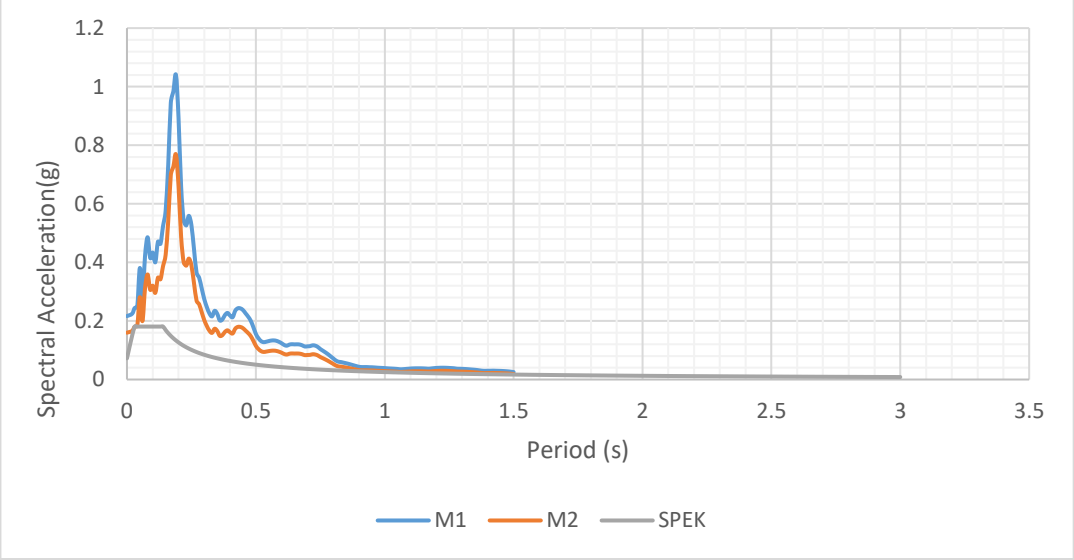

Figure A197. Scaled Vertical Response Spectra of Chalfant Valley-02 (C4-552) Earthquake

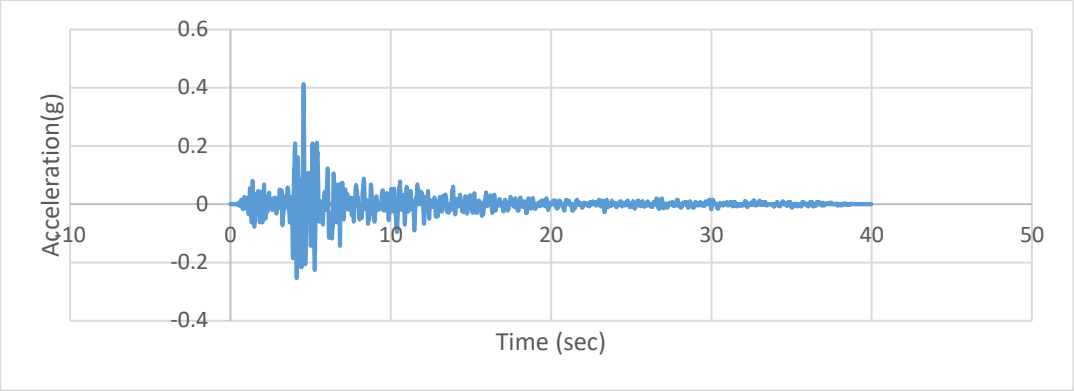

Figure A198. Scaled Acceleration Time Histories of Chalfant Valley-02 (C4-552X) Earthquake

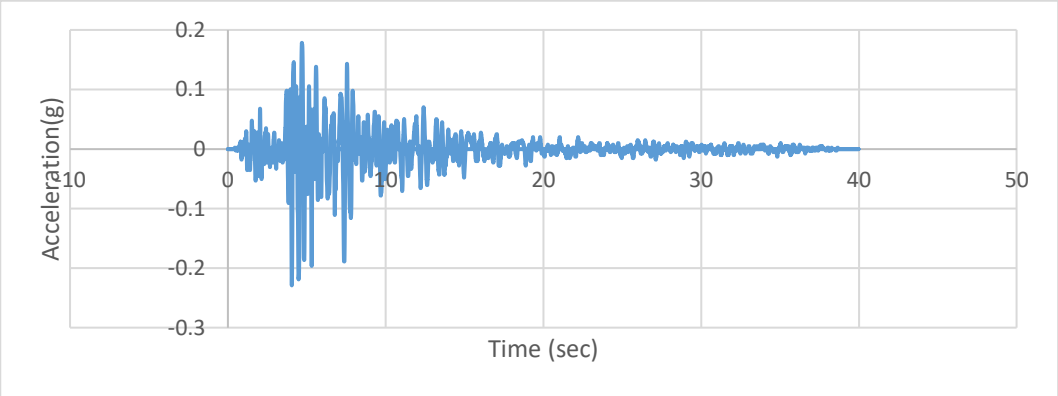

Figure A199. Scaled Acceleration Time Histories of Chalfant Valley-02 (C4-552Y) Earthquake

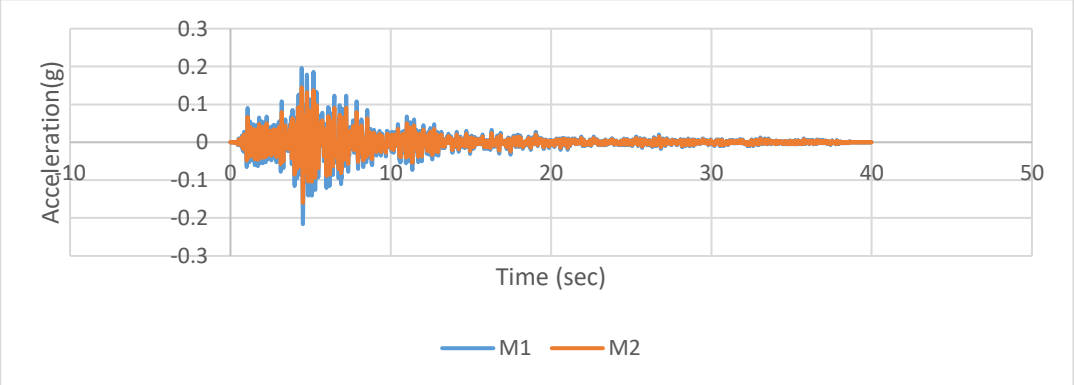

Figure A200. Scaled Acceleration Time Histories of Chalfant Valley-02 (C4-552Z) Earthquake

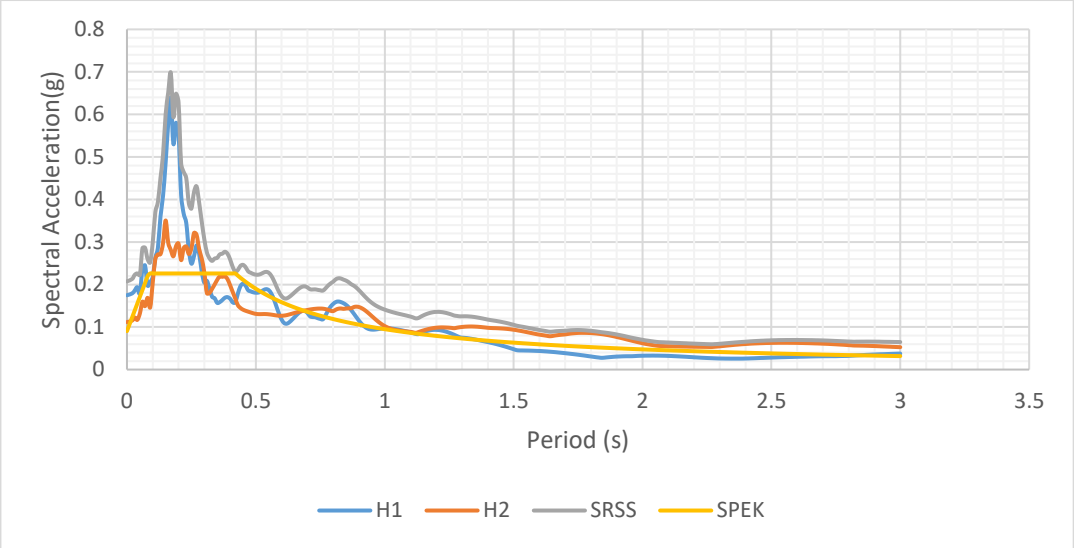

Figure A201. Scaled Horizontal Response Spectra of Kocaeli (C4-1148) Earthquake

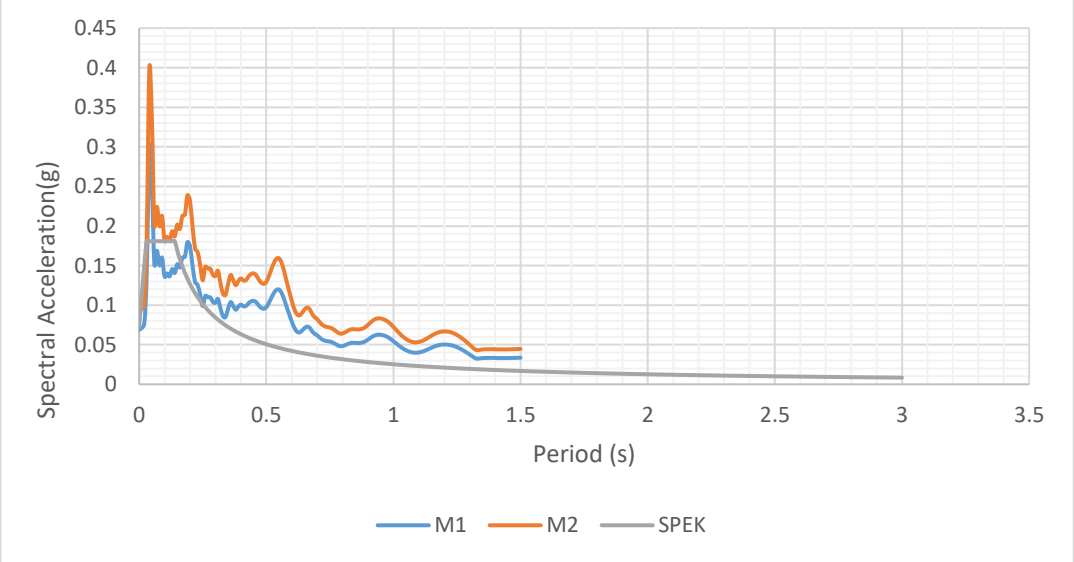

Figure A202. Scaled Vertical Response Spectra of Kocaeli (C4-1148) Earthquake

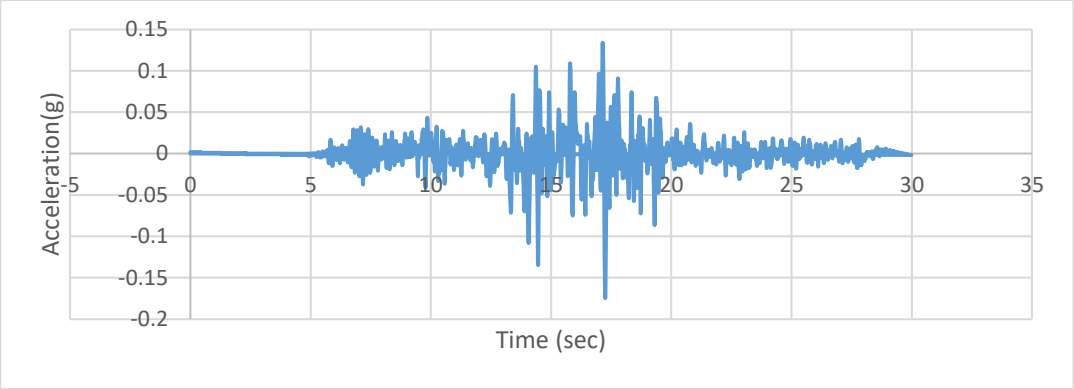

Figure A203. Scaled Acceleration Time Histories of Kocaeli (C4-1148X) Earthquake

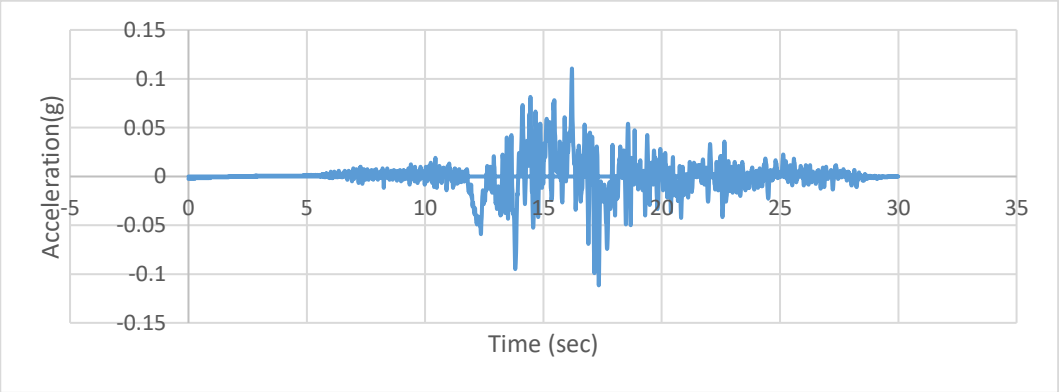

Figure A204. Scaled Acceleration Time Histories of Kocaeli (C4-1148Y) Earthquake

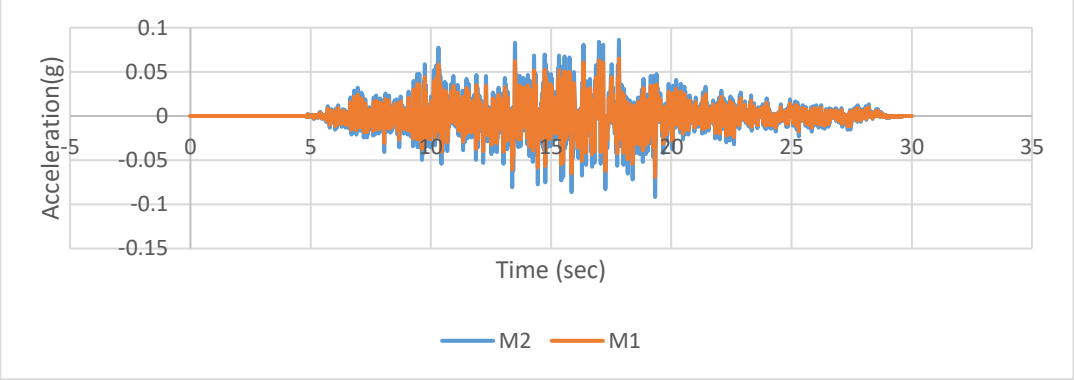

Figure A205. Scaled Acceleration Time Histories of Kocaeli (C4-1148Z) Earthquake

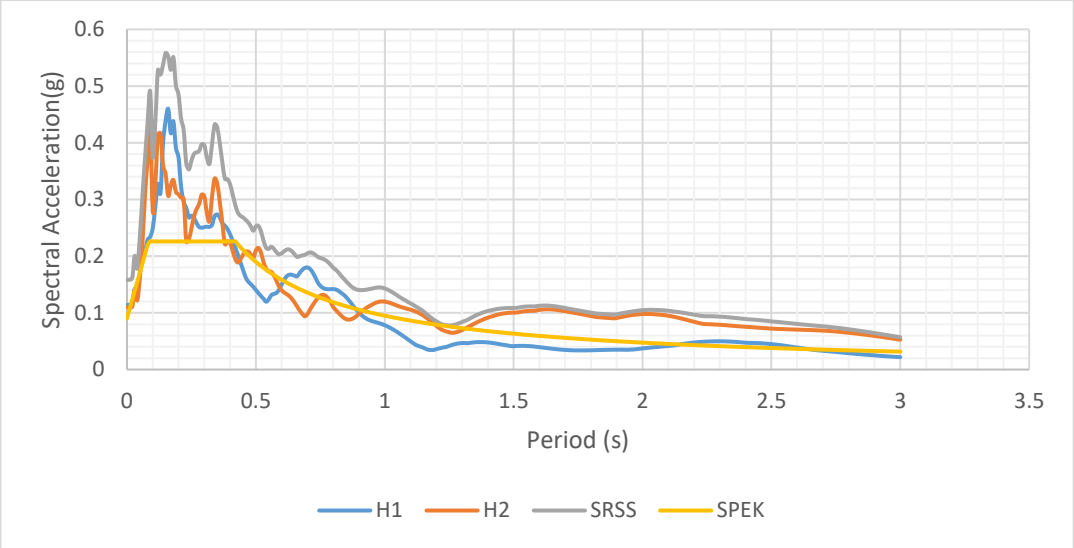

Figure A206. Scaled Horizontal Response Spectra of Manjil (C4-1633) Earthquake

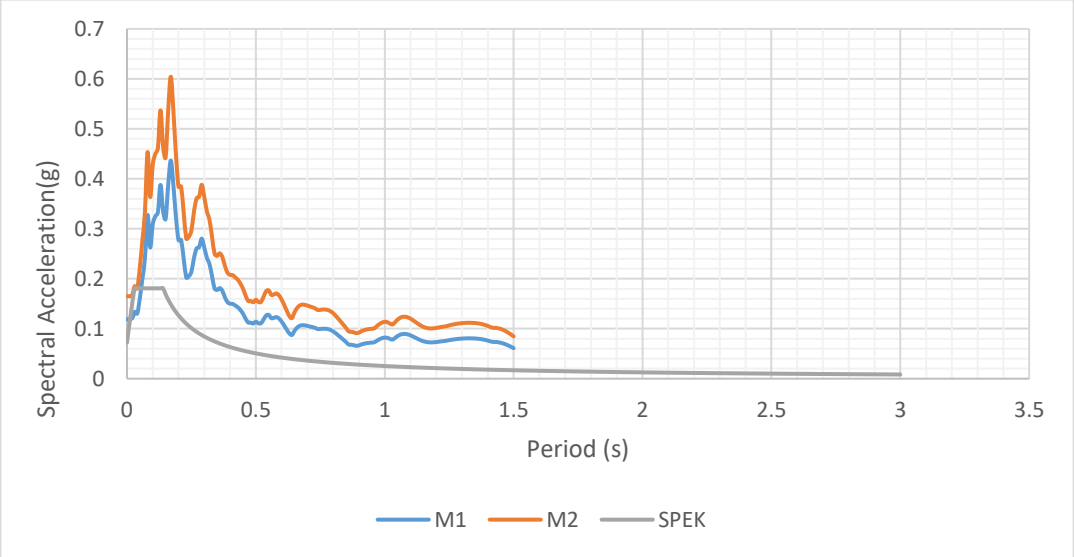

Figure A207. Scaled Vertical Response Spectra of Manjil (C4-1633) Earthquake

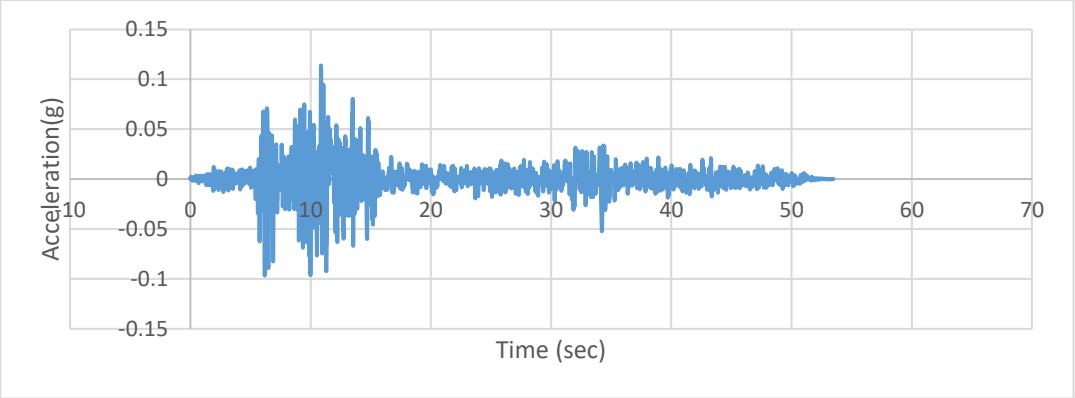

Figure A208. Scaled Acceleration Time Histories of Manjil(C4-1633X) Earthquake

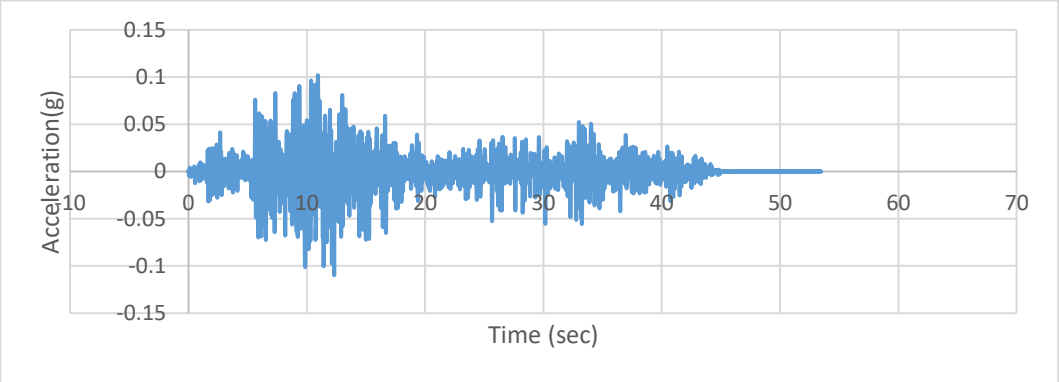

Figure A209. Scaled Acceleration Time Histories of Manjil(C4-1633Y) Earthquake

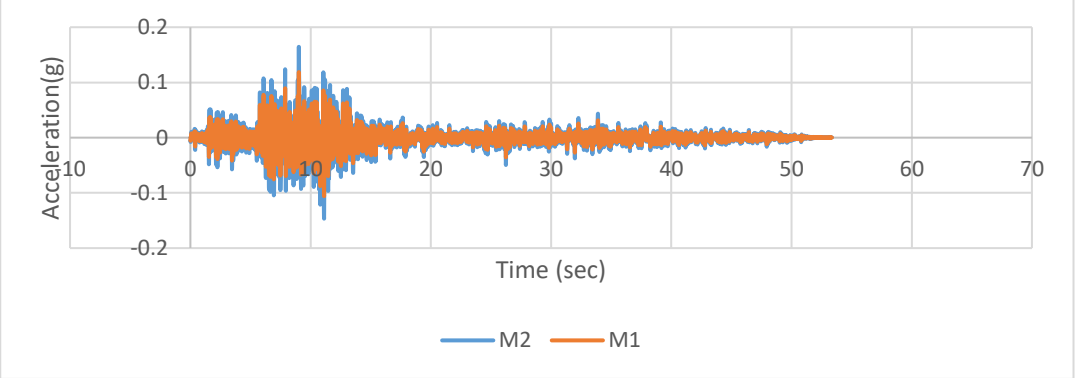

Figure A210. Scaled Acceleration Time Histories of Manjil(C4-1633Z) Earthquake

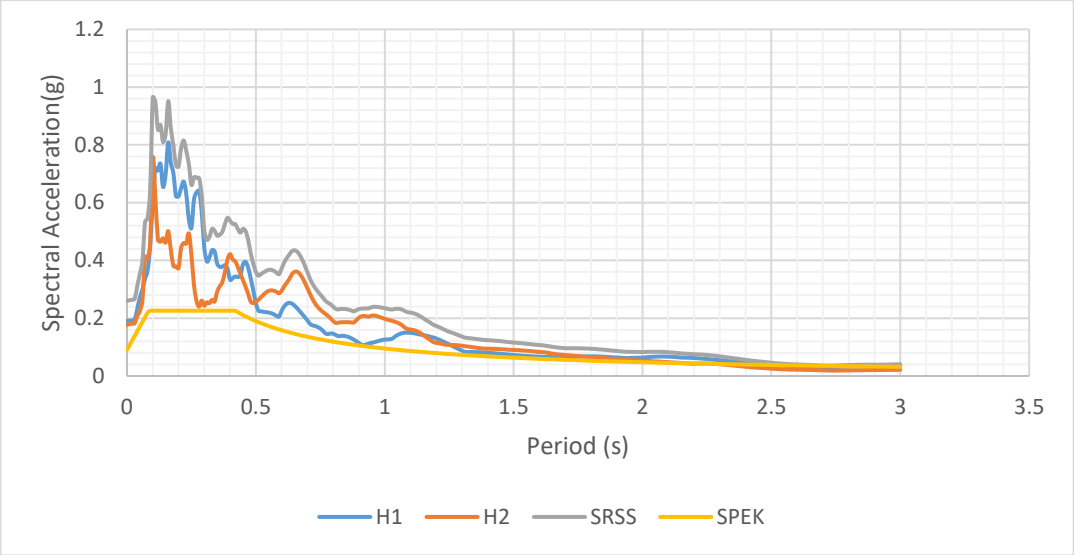

Figure A211.Scaled Horizontal Response Spectra of Parkfield-02(C4-4137) Earthquake

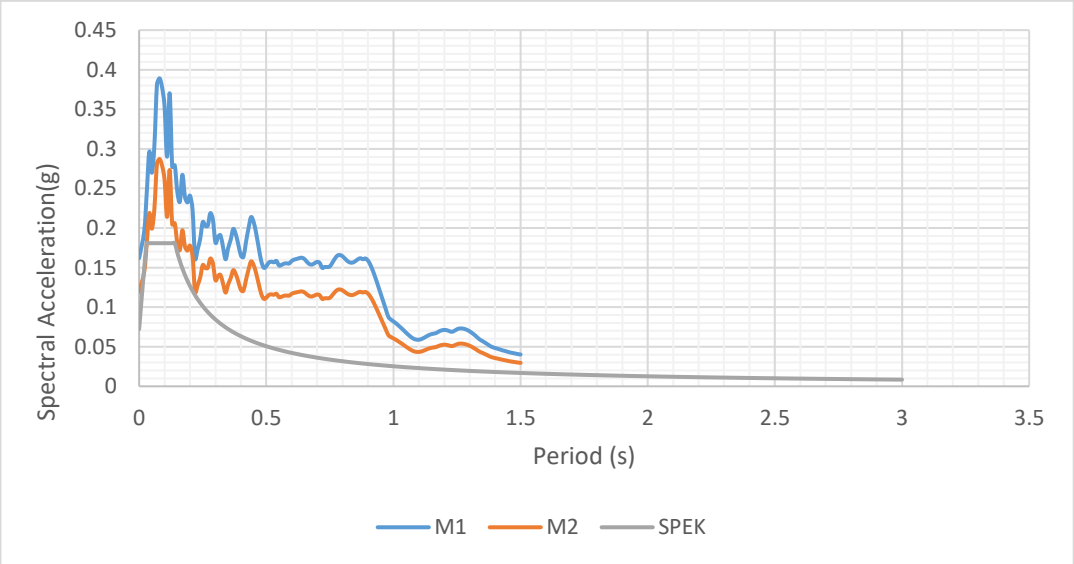

Figure A212. Scaled Vertical Response Spectra of Parkfield-02(C4-4137) Earthquake

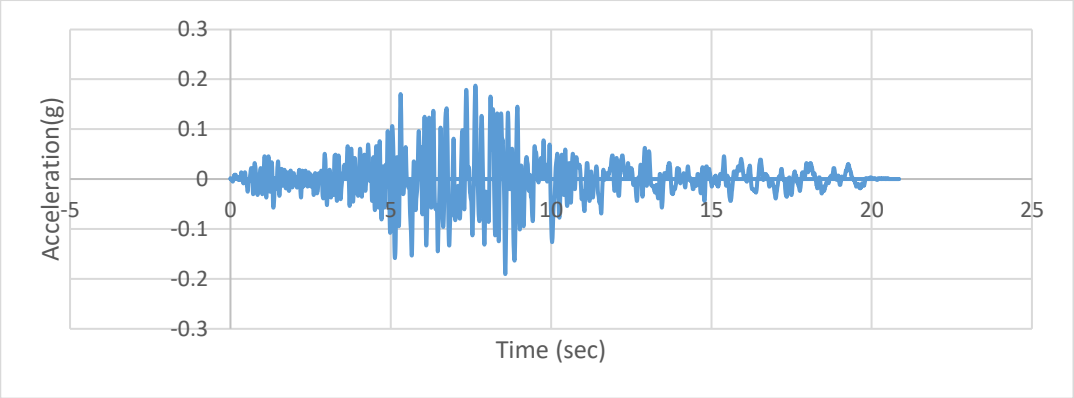

Figure A213. Scaled Acceleration Time Histories of Parkfield-02(C4-4137X) Earthquake

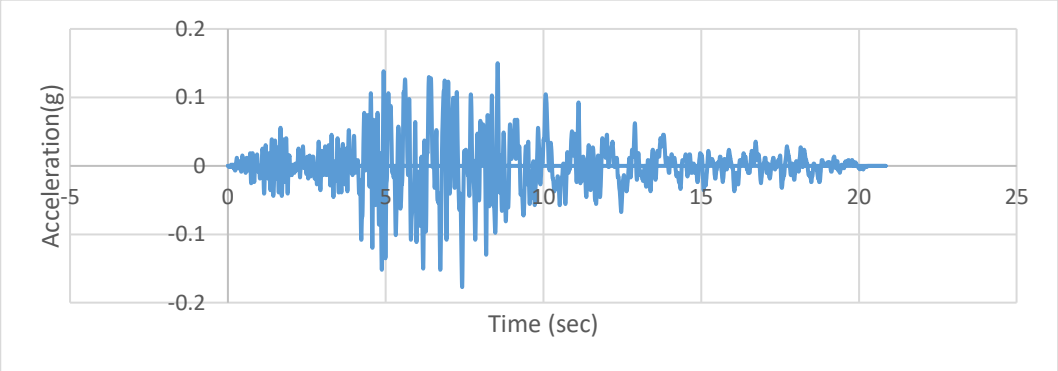

Figure A214.Scaled Acceleration Time Histories of Parkfield-02(C4-4137Y) Earthquake

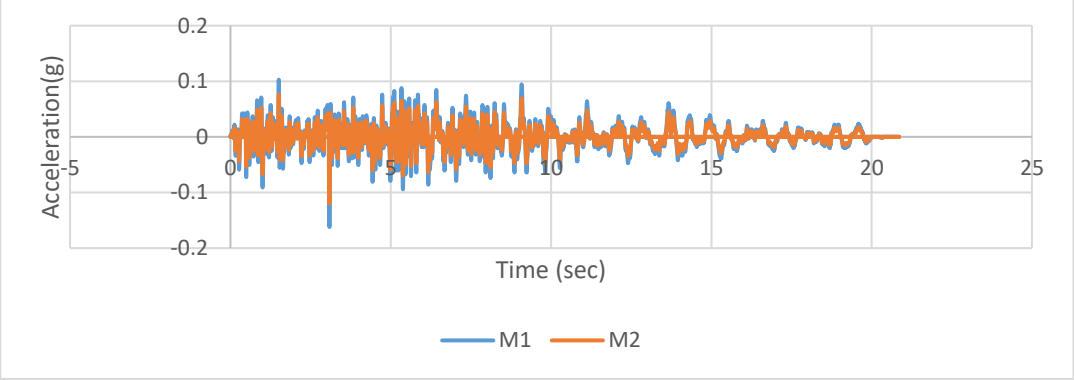

Figure A215. Scaled Acceleration Time Histories of Parkfield-02(C4-4137Z) Earthquake

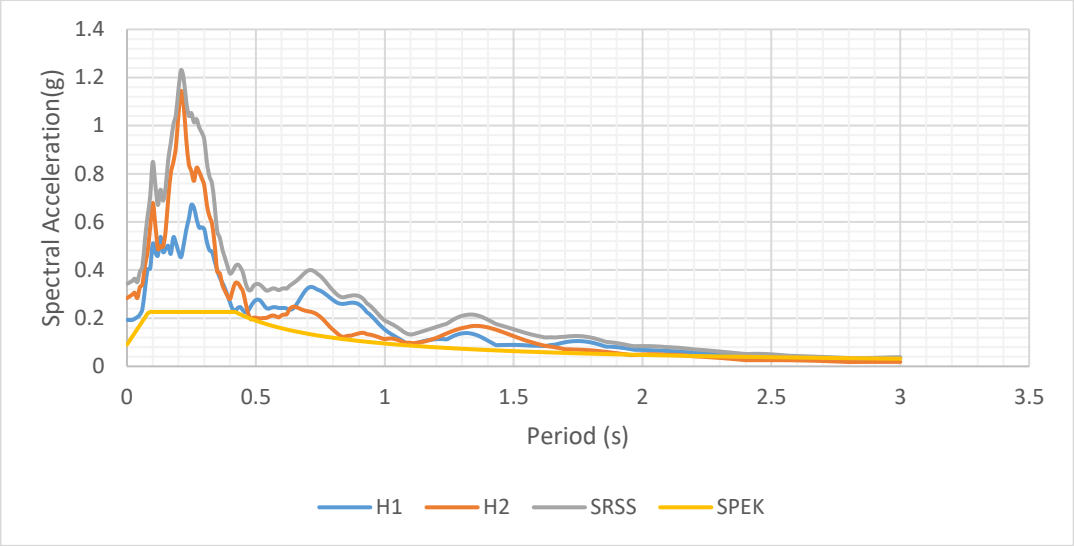

Figure A216.Scaled Horizontal Response Spectra of Big Bear-01 (C4-6057) Earthquake

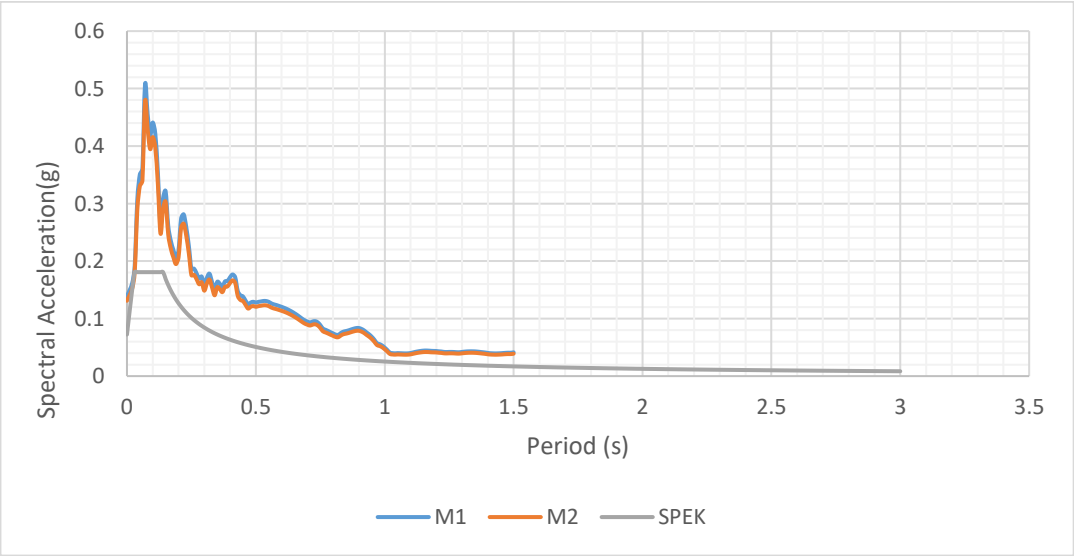

Figure A217. Scaled Vertical Response Spectra of Big Bear-01 (C4-6057) Earthquake

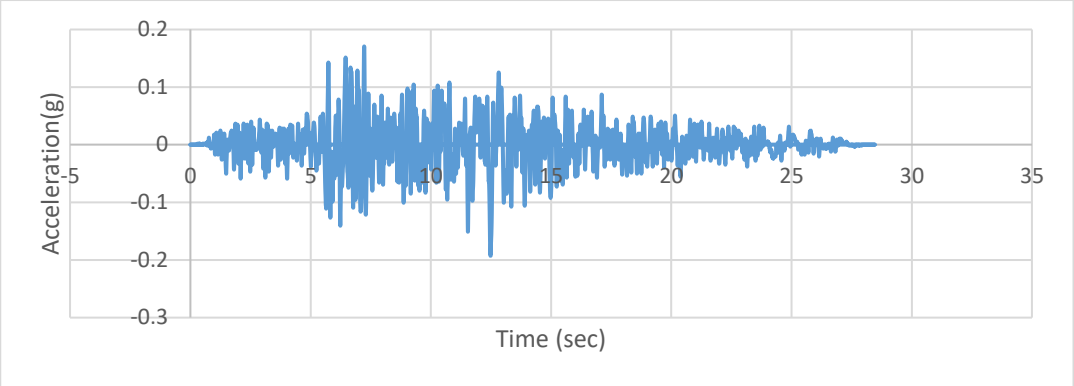

Figure A218. Scaled Acceleration Time Histories of Big Bear-01 (C4-6057X) Earthquake

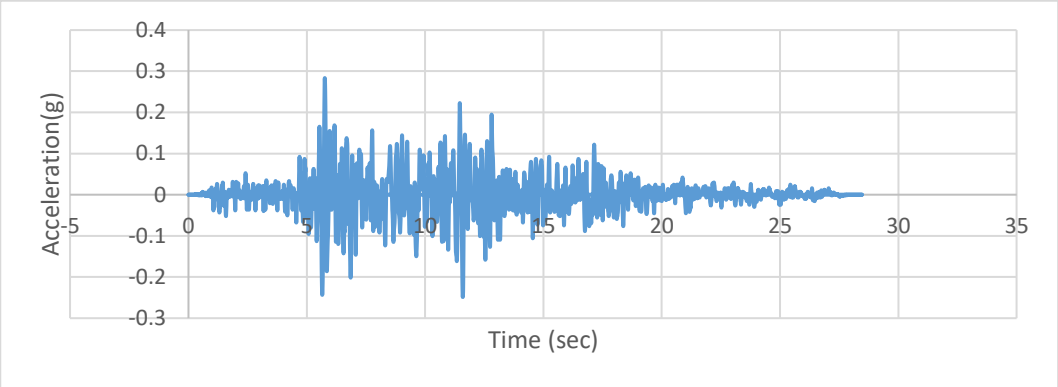

Figure A219. Scaled Acceleration Time Histories of Big Bear-01 (C4-6057Y) Earthquake

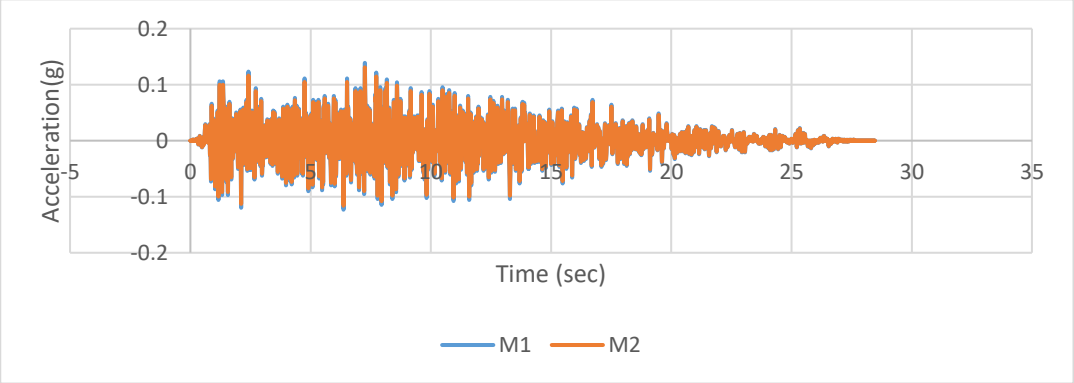

Figure A220. Scaled Acceleration Time Histories of Big Bear-01 (C4-6057Z) Earthquake

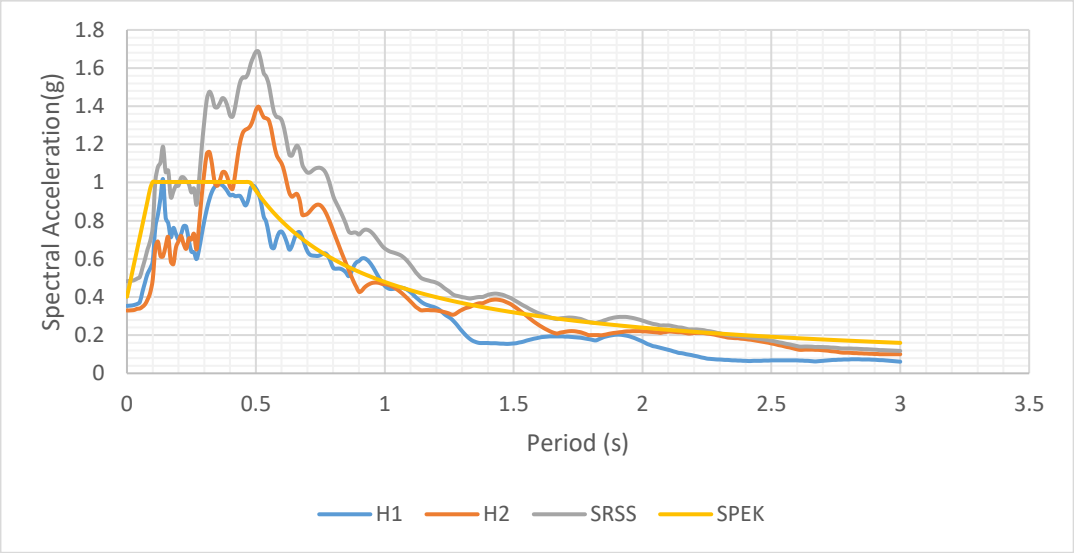

Figure A221.Horizontal Response Spectra of Imperial Valley-03 (D1-10) Earthquake

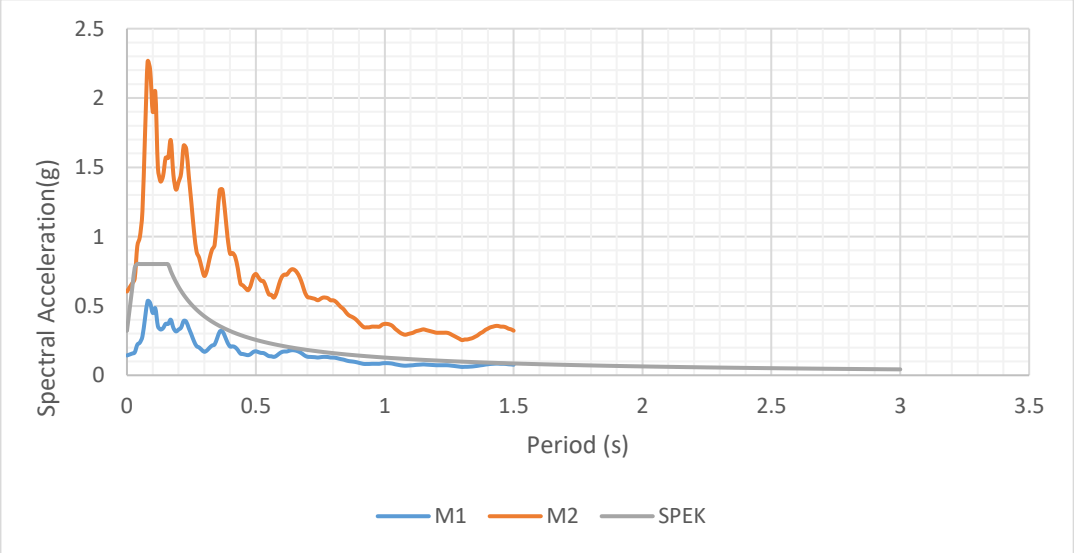

Figure A222. Scaled Vertical Response Spectra of Imperial Valley-03 (D1-10) Earthquake

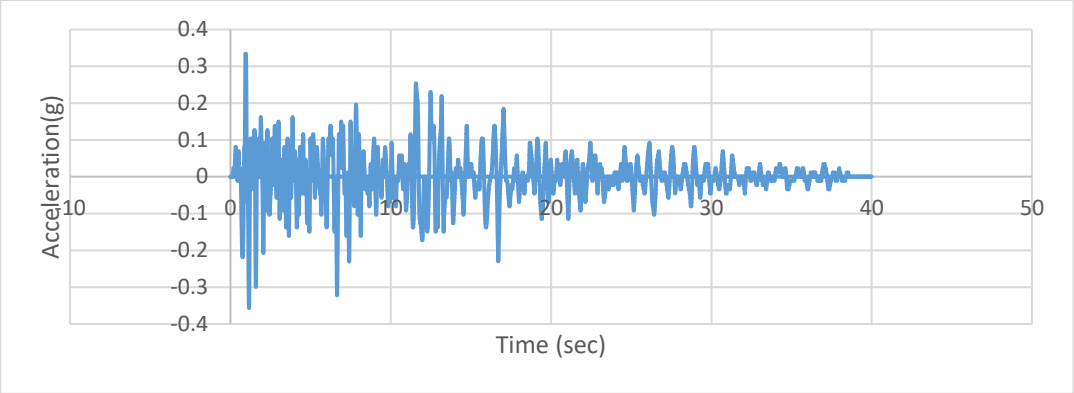

Figure A223. Scaled Acceleration Time Histories of Imperial Valley-03 (D1-10X) Earthquake

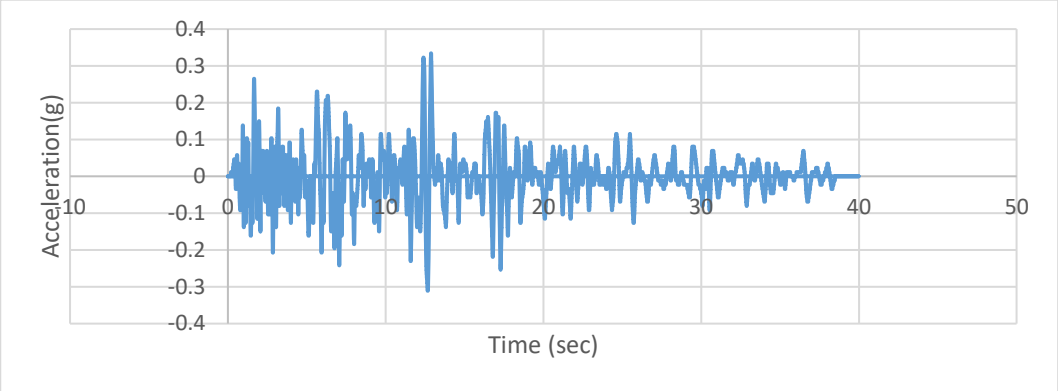

Figure A224.Scaled Acceleration Time Histories of Imperial Valley-03 (D1-10Y) Earthquake

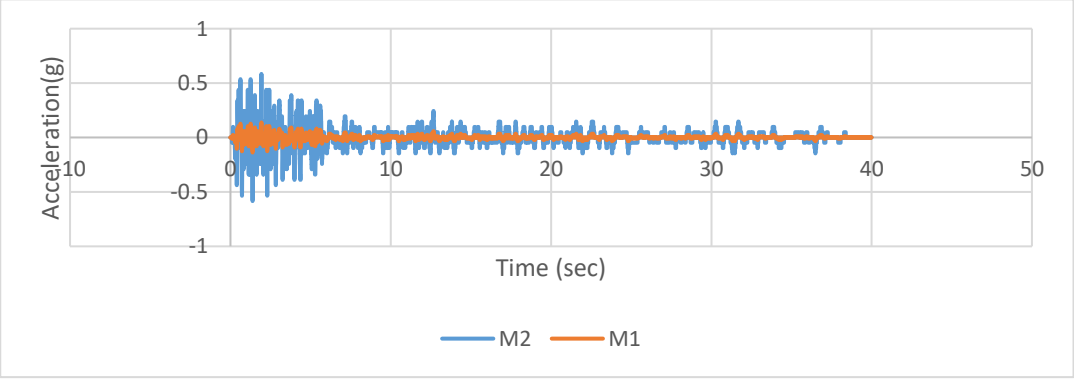

Figure A225. Scaled Acceleration Time Histories of Imperial Valley-03 (D1-10Z) Earthquake

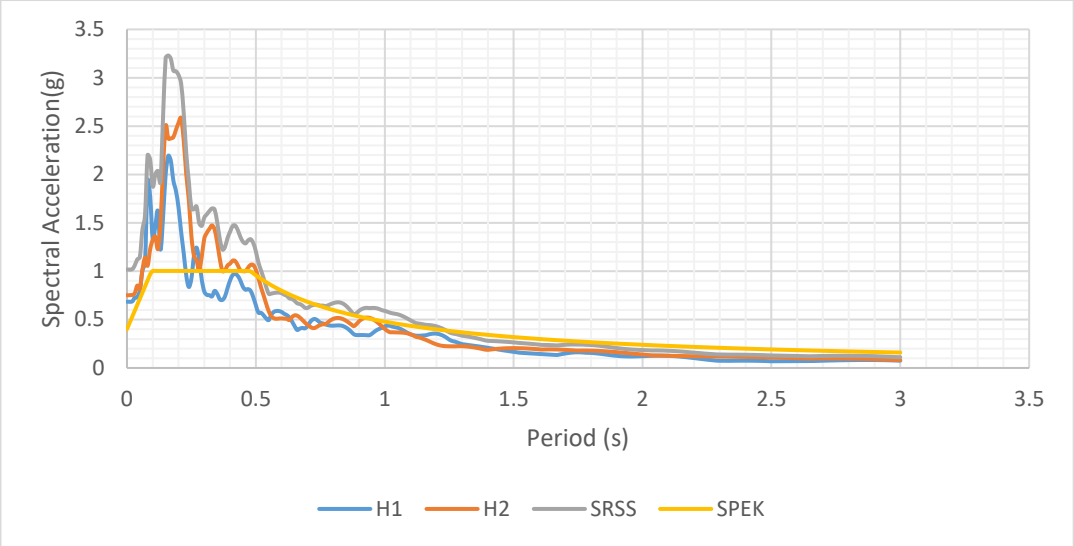

Figure A226. Scaled Horizontal Response Spectra of Parkfield (D1-31) Earthquake

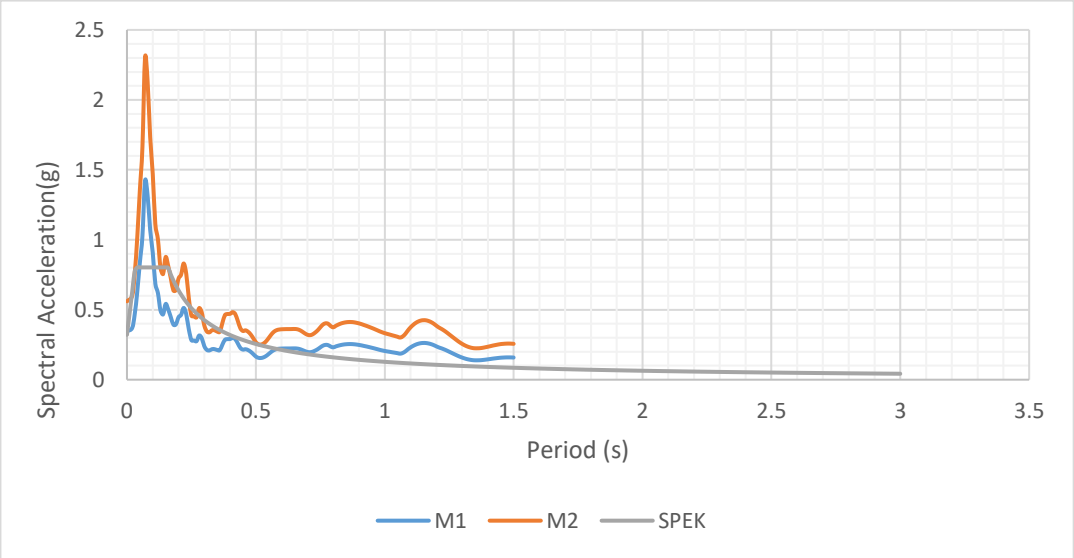

Figure A227.Scaled Vertical Response Spectra of Parkfield (D1-31) Earthquake

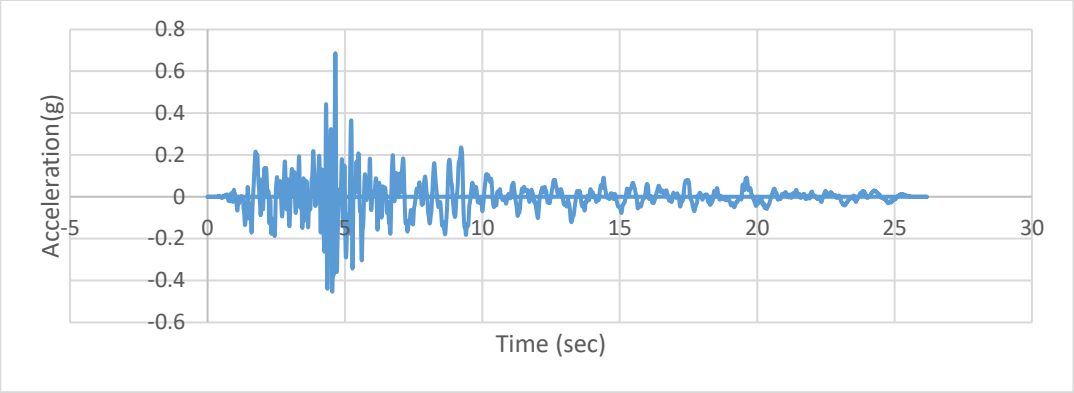

Figure A228. Scaled Acceleration Time Histories of Parkfield (D1-31X) Earthquake

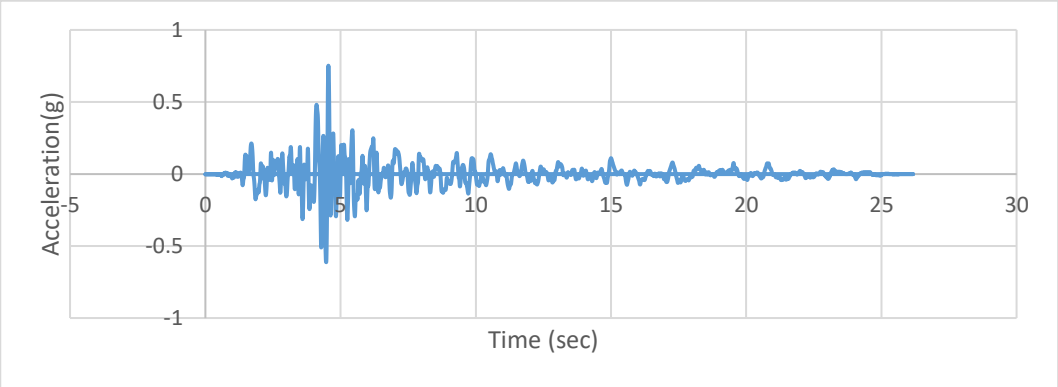

Figure A229. Scaled Acceleration Time Histories of Parkfield (D1-31Y) Earthquake

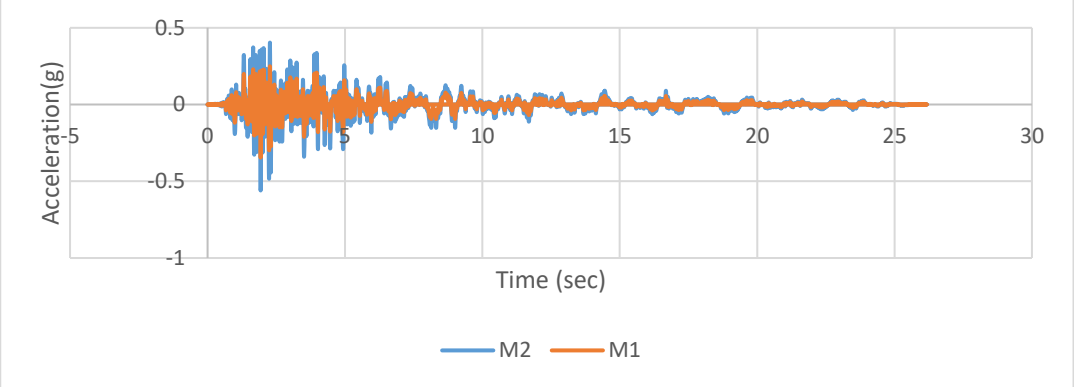

Figure A230. Scaled Acceleration Time Histories of Parkfield (D1-31Z) Earthquake

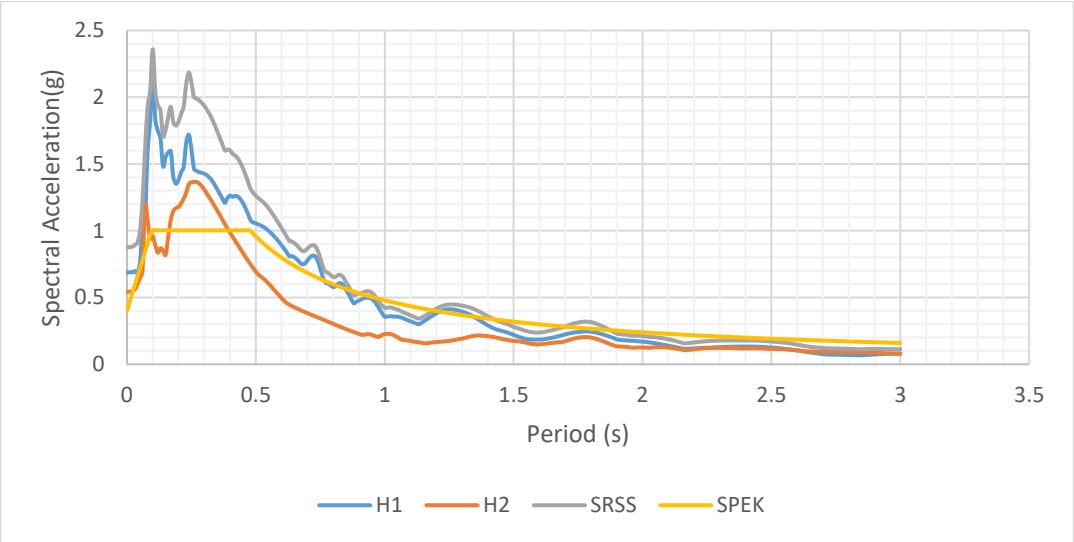

Figure A231. Scaled Horizontal Response Spectra of Imperial Valley-06 (D1-167) Earthquake

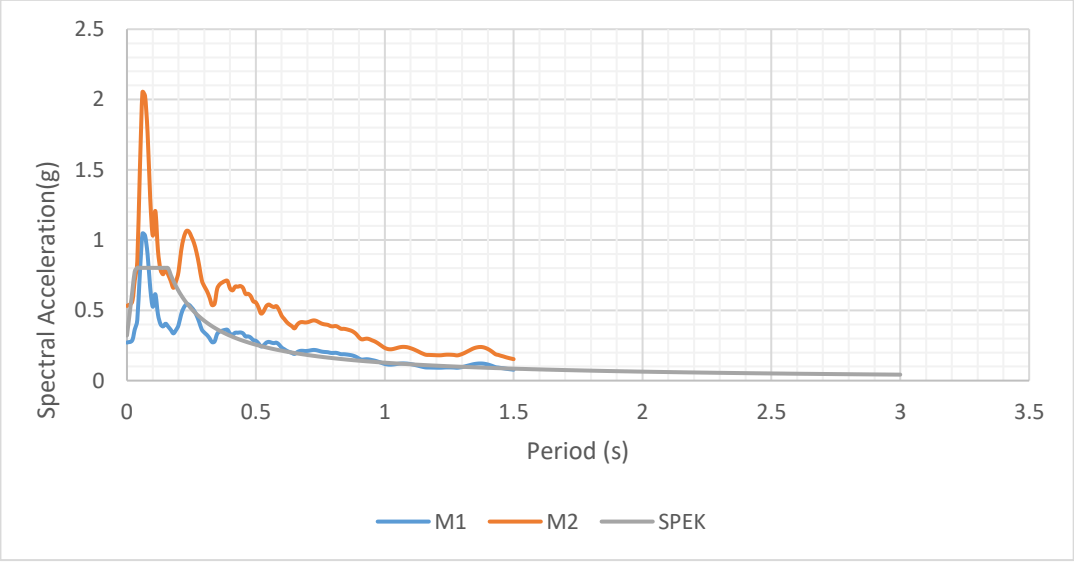

Figure A232. Scaled Vertical Response Spectra of Imperial Valley-06 (D1-167) Earthquake

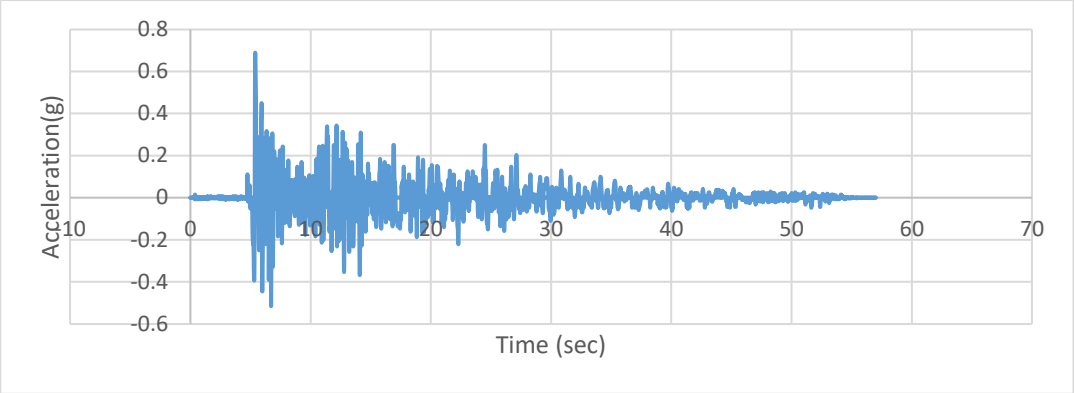

Figure A233. Scaled Acceleration Time Histories of Imperial Valley-06 (D1-167X) Earthquake

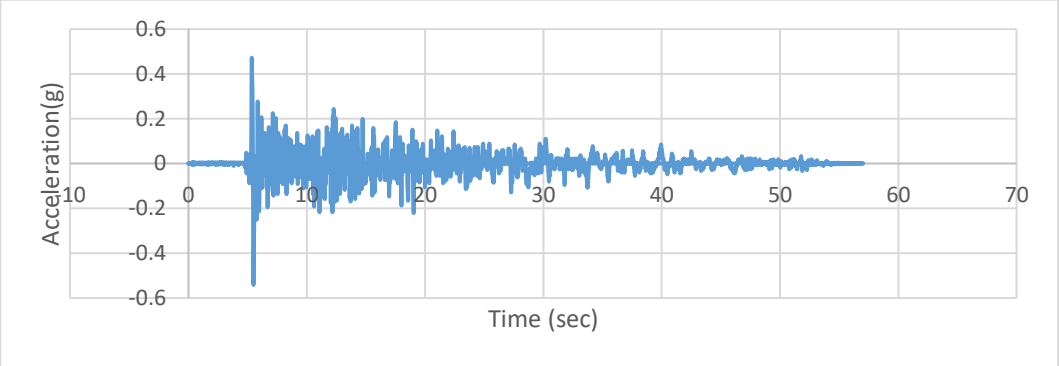

Figure A234. Scaled Acceleration Time Histories of Imperial Valley-06 (D1-167Y) Earthquake

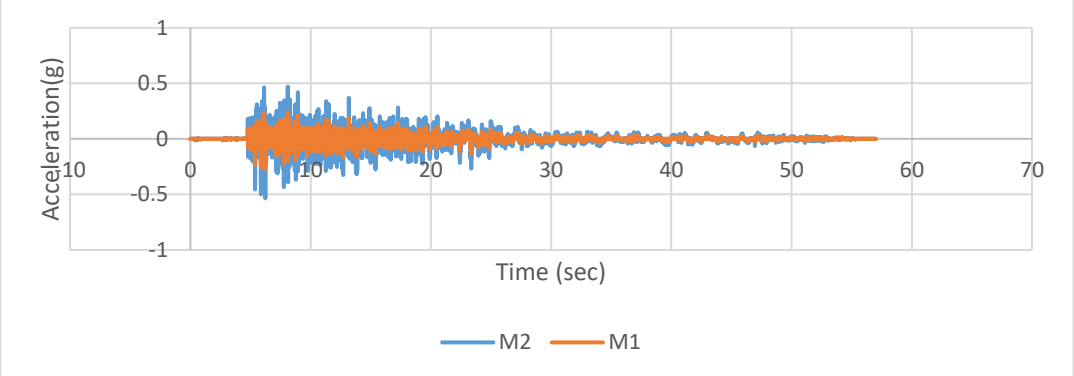

Figure A235. Scaled Acceleration Time Histories of Imperial Valley-06 (D1-167Z) Earthquake

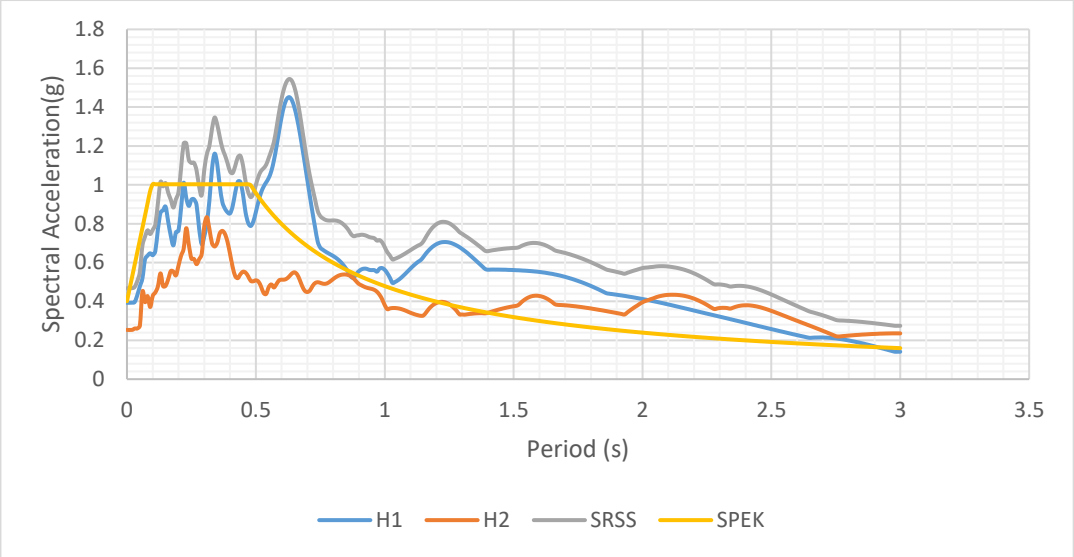

Figure A236. Scaled Horizontal Response Spectra of Victoria (D1-266) Earthquake

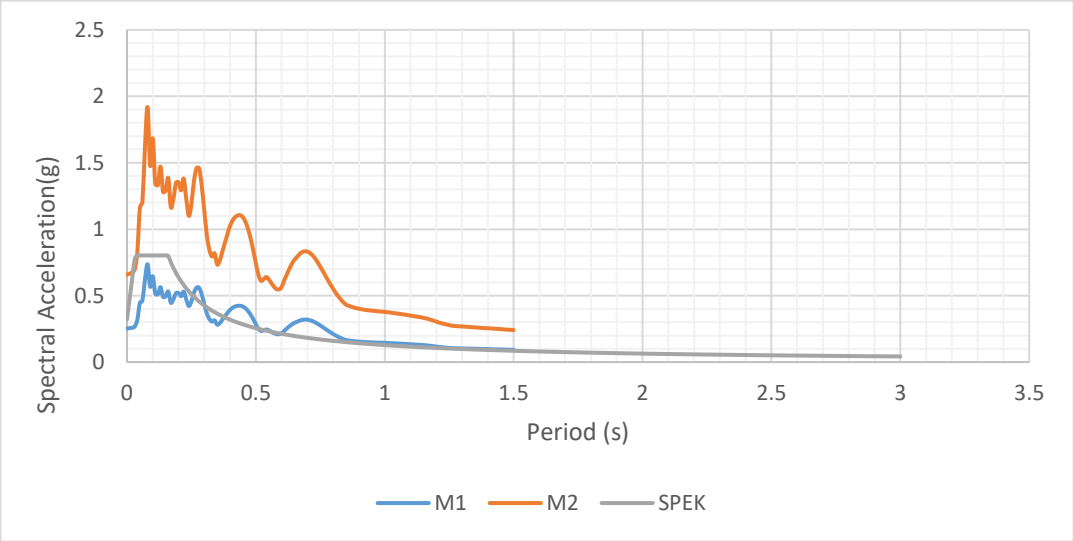

Figure A237.Scaled Vertical Response Spectra of Victoria (D1-266) Earthquake

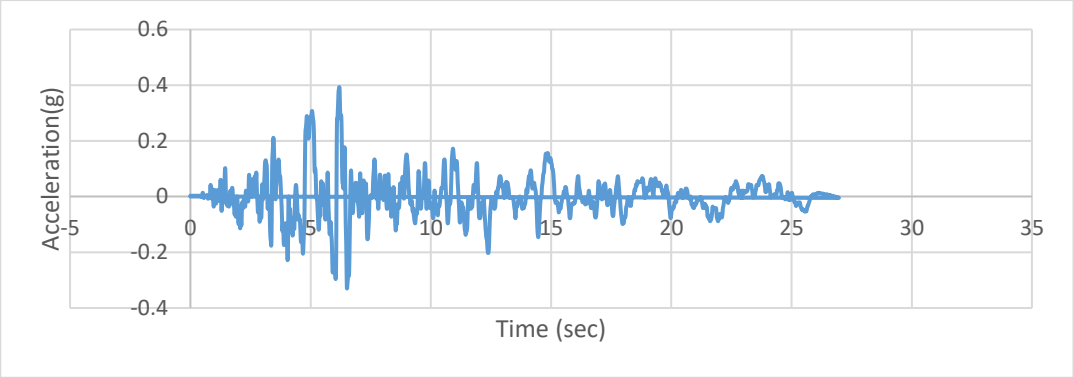

Figure A238. Scaled Acceleration Time Histories of Victoria (D1-266X) Earthquake

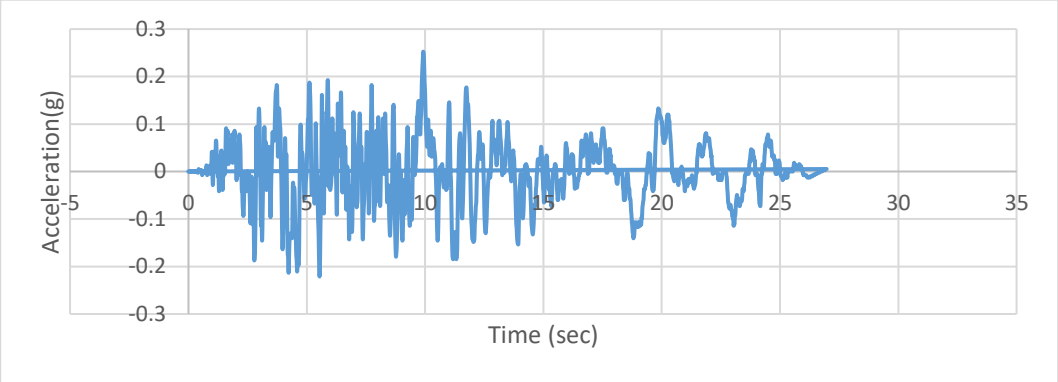

Figure A239. Scaled Acceleration Time Histories of Victoria (D1-266Y) Earthquake

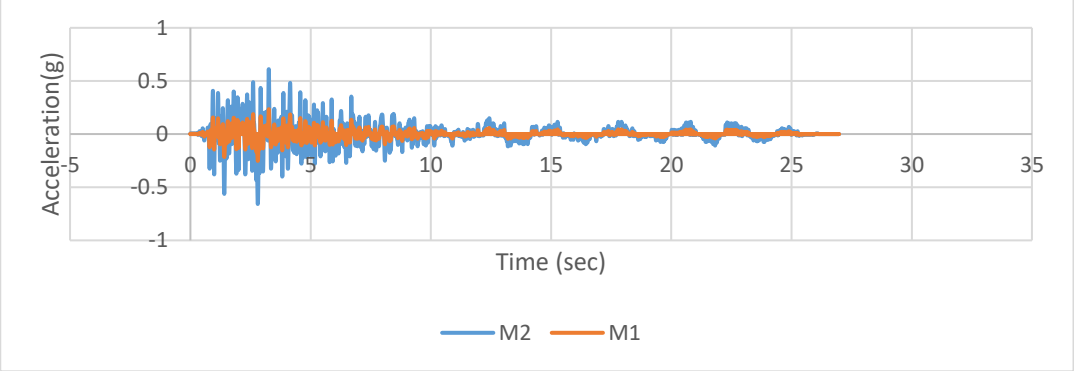

Figure A240. Scaled Acceleration Time Histories of Victoria (D1-266Z) Earthquake

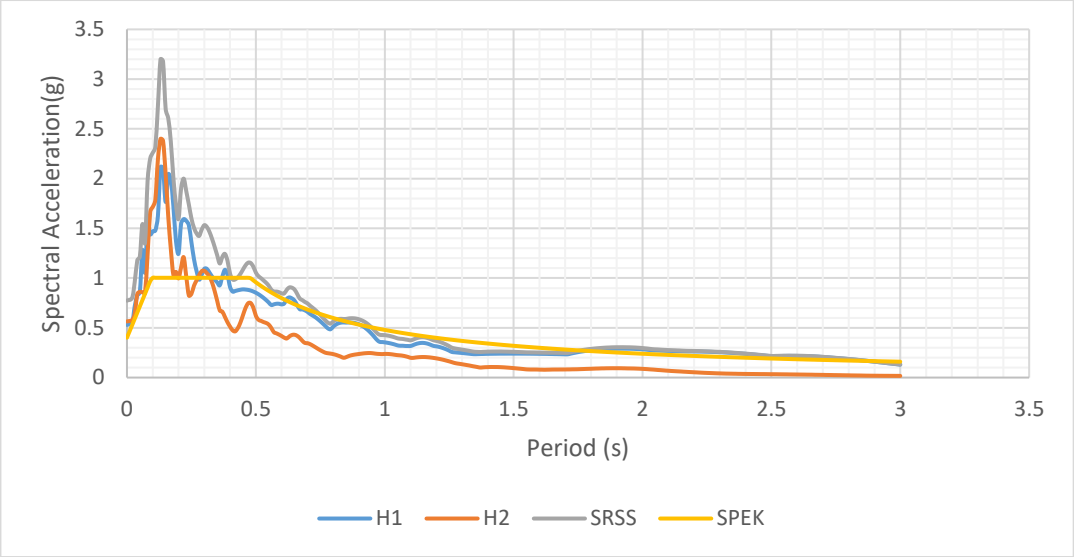

Figure A241.Scaled Horizontal Response Spectra of Westmorland (D1-314) Earthquake

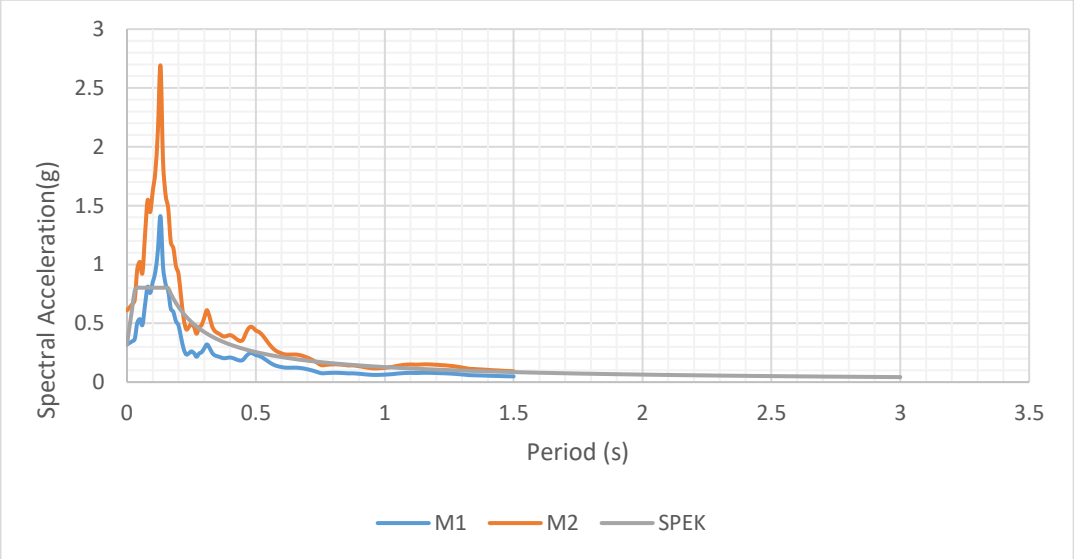

Figure A242.Scaled Vertical Response Spectra of Westmorland (D1-314) Earthquake

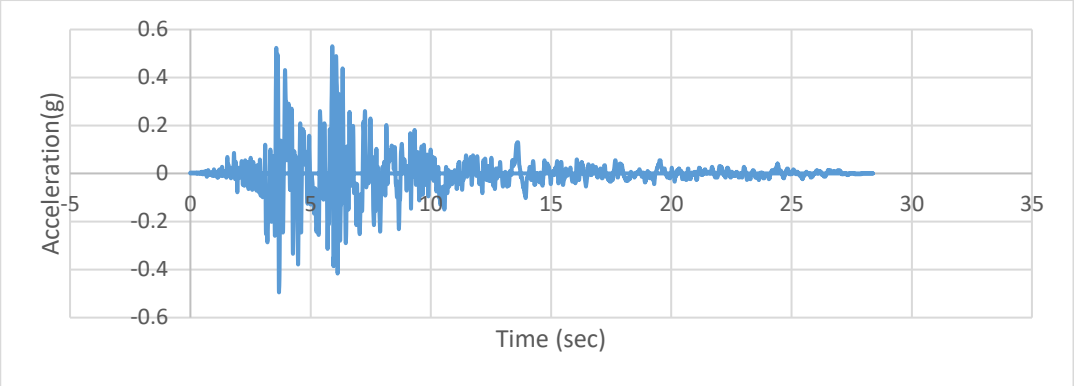

Figure A243. Scaled Acceleration Time Histories of Westmorland (D1-314X) Earthquake

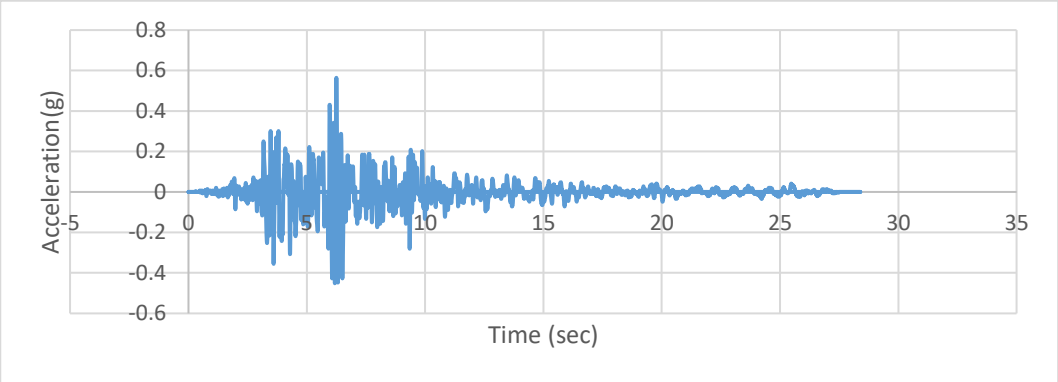

Figure A244.Scaled Acceleration Time Histories of Westmorland (D1-314Y) Earthquake

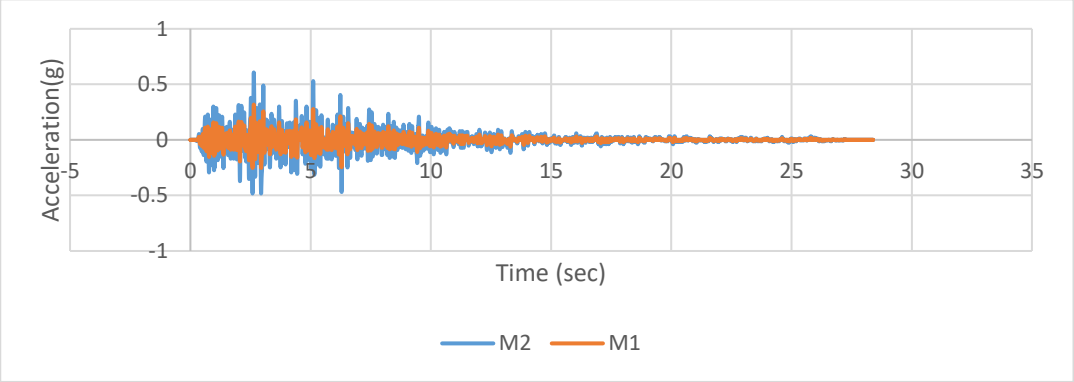

Figure A245. Scaled Acceleration Time Histories of Westmorland (D1-314Z) Earthquake

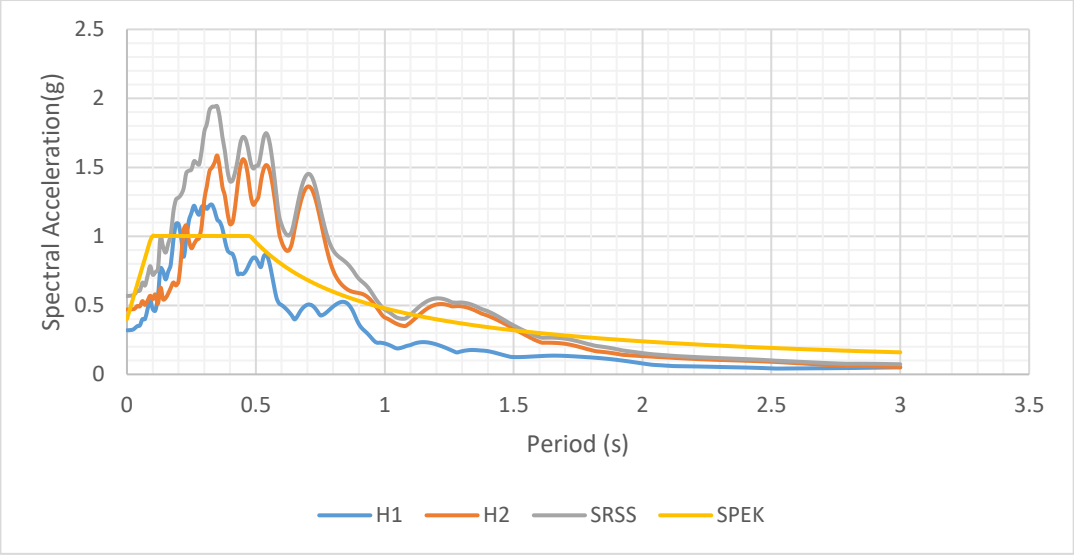

Figure A246. Scaled Horizontal Response Spectra of Landers (D1-848) Earthquake

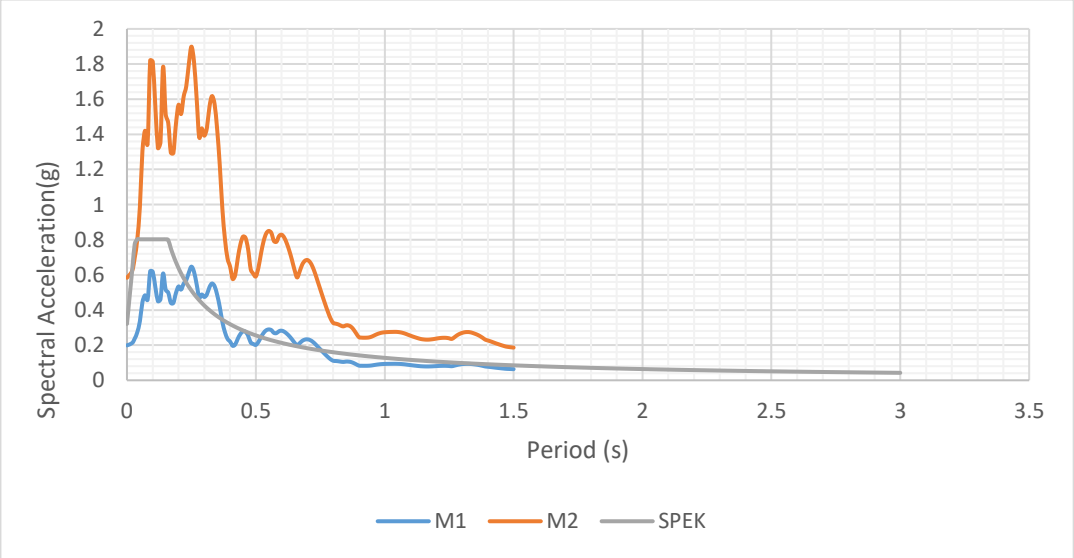

Figure A247. Scaled Vertical Response Spectra of Landers (D1-848) Earthquake

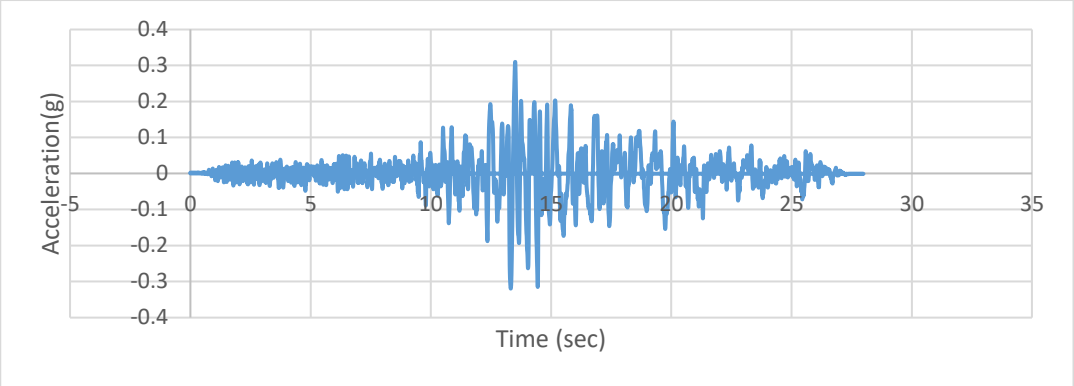

Figure A248. Scaled Acceleration Time Histories of Landers (D1-848X) Earthquake

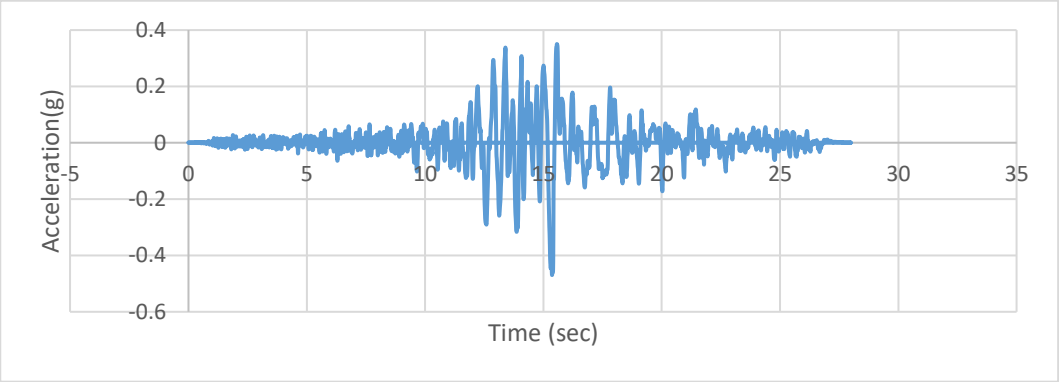

Figure A249. Scaled Acceleration Time Histories of Landers (D1-848Y) Earthquake

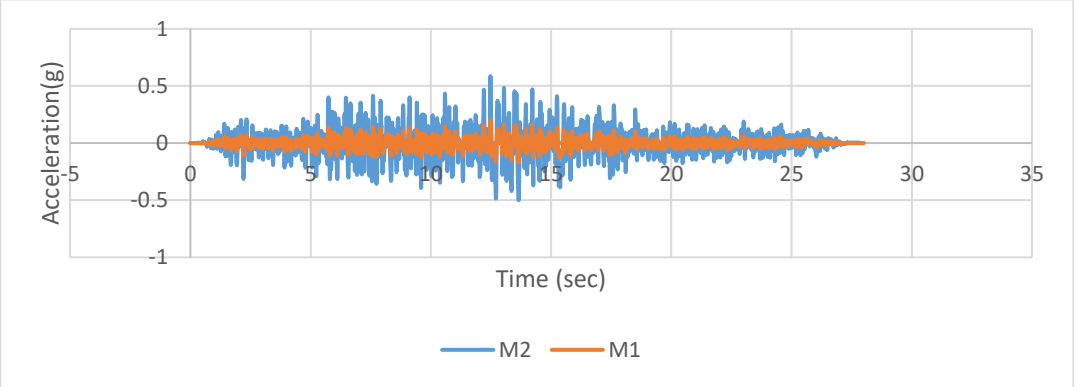

Figure A250. Scaled Acceleration Time Histories of Landers (D1-848Z) Earthquake

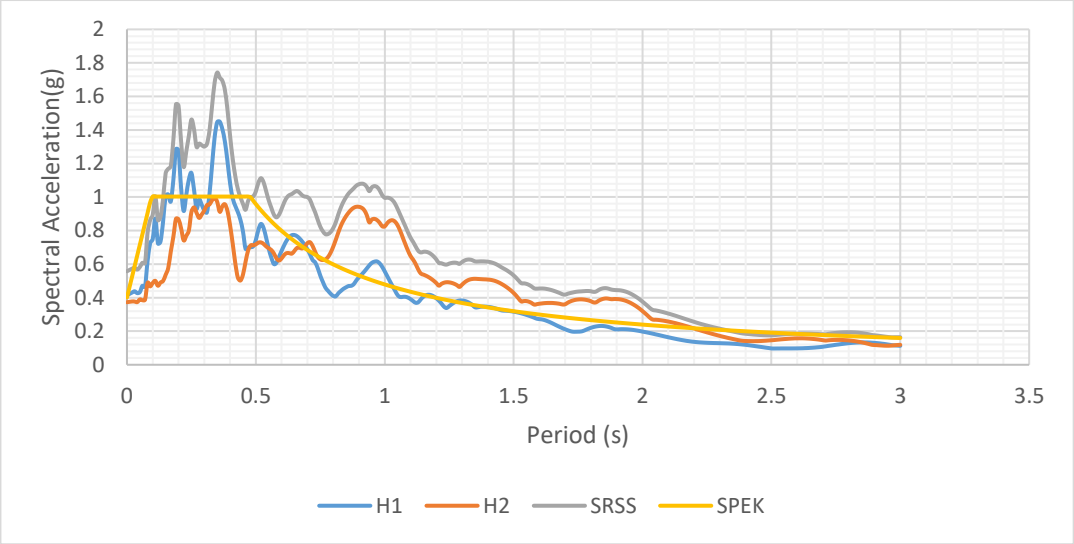

Figure A251.Scaled Horizontal Response Spectra of Landers (D1-850) Earthquake

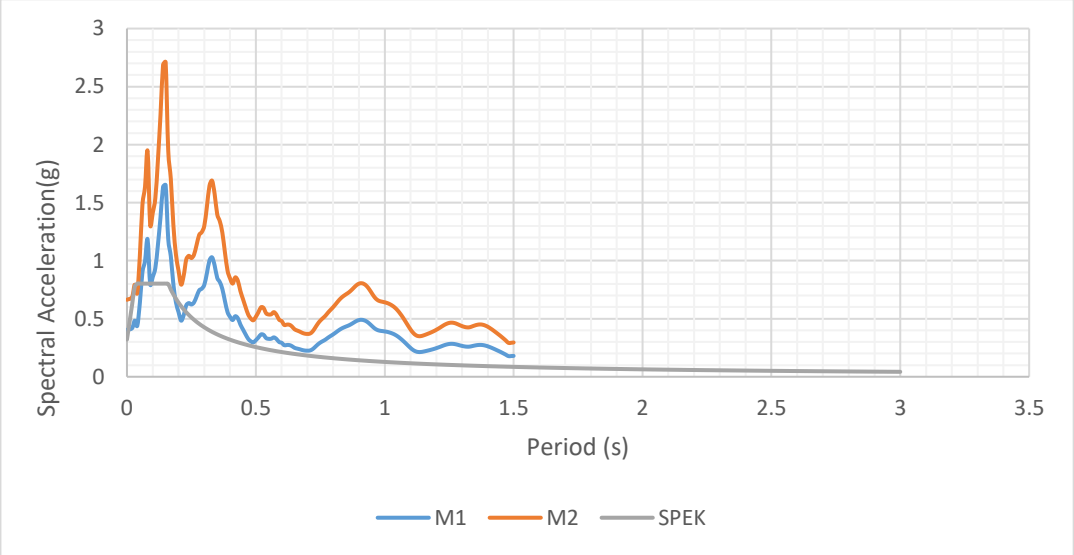

Figure A252.Scaled Vertical Response Spectra of Landers (D1-850) Earthquake

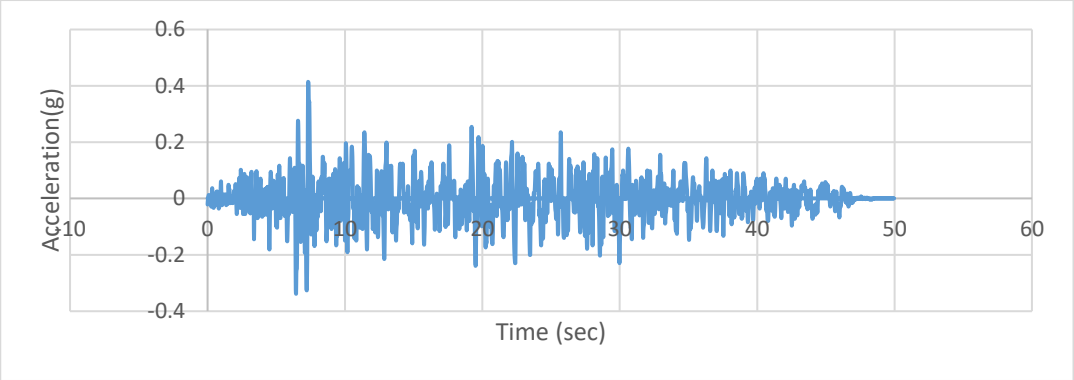

Figure A253. Scaled Acceleration Time Histories of Landers (D1-850X) Earthquake

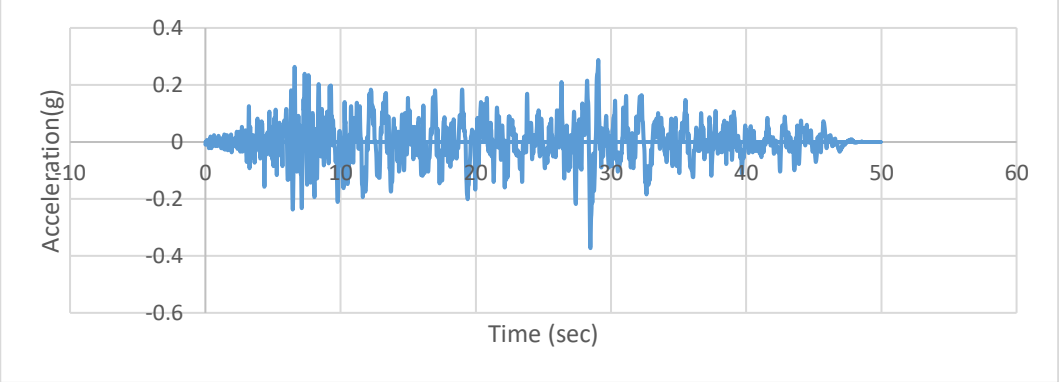

Figure A254. Scaled Acceleration Time Histories of Landers (D1-850Y) Earthquake

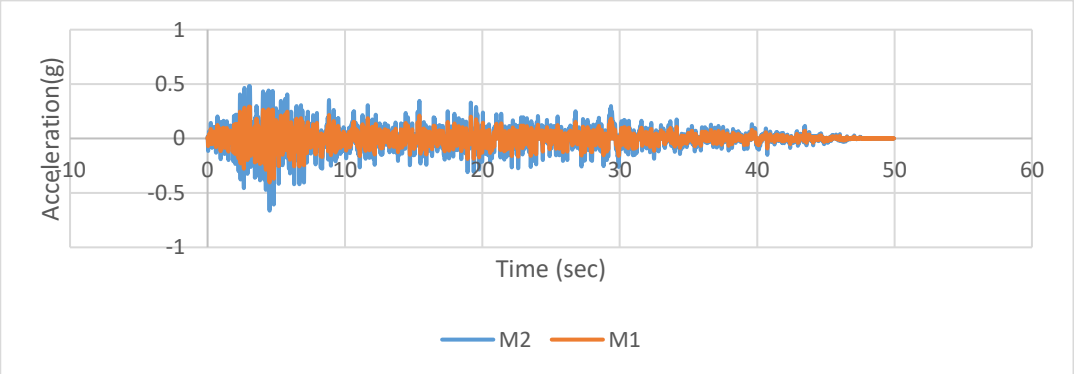

Figure A255. Scaled Acceleration Time Histories of Landers (D1-850Z) Earthquake

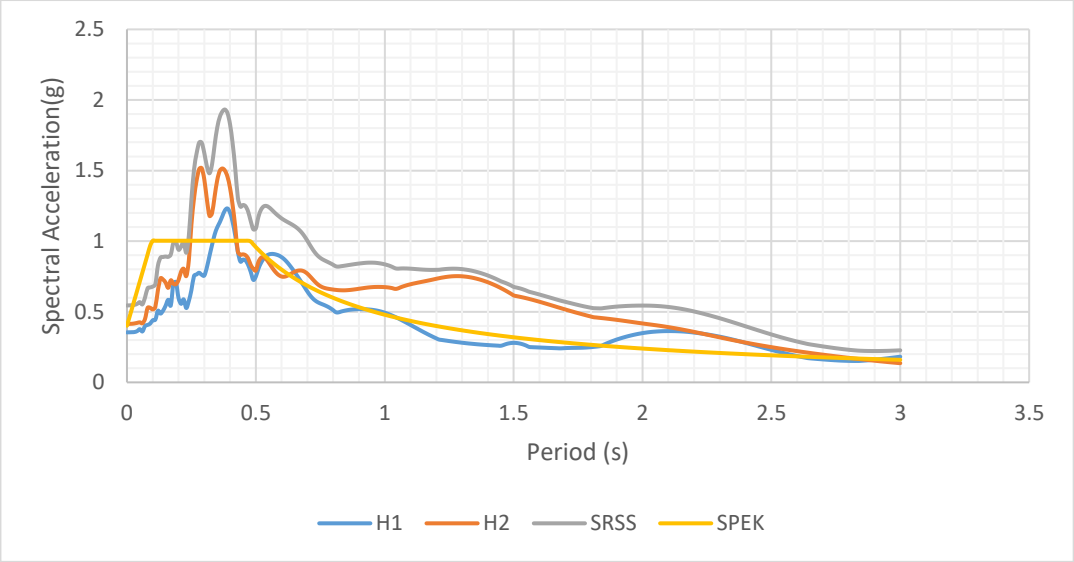

Figure A256. Scaled Horizontal Response Spectra of Kocaeli (D1-1158) Earthquake

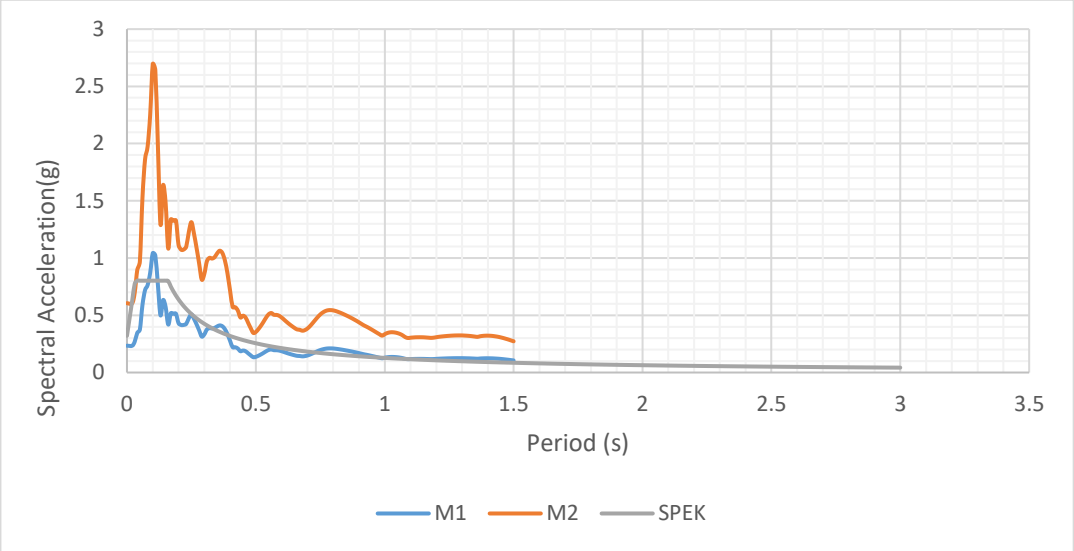

Figure A257. Scaled Vertical Response Spectra of Kocaeli (D1-1158) Earthquake

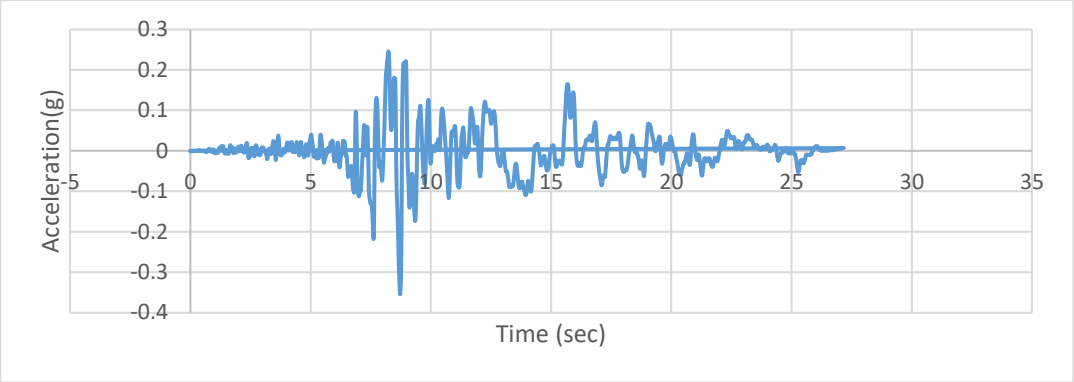

Figure A258. Scaled Acceleration Time Histories of Kocaeli (D1-1158X) Earthquake

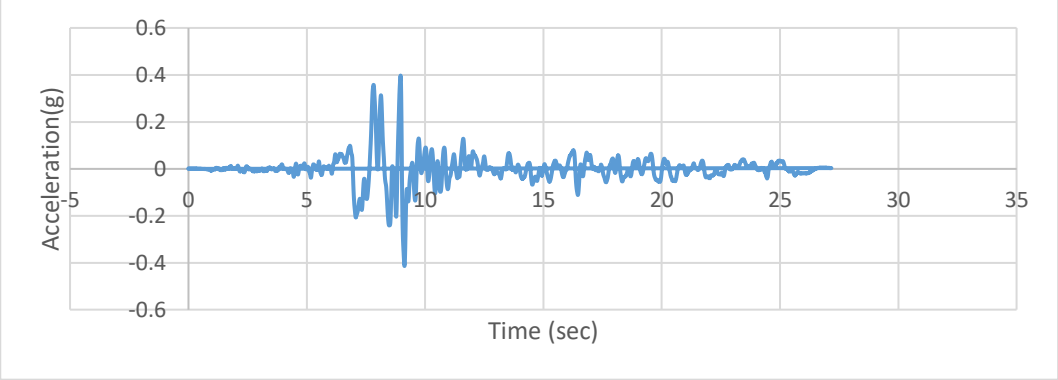

Figure A259. Scaled Acceleration Time Histories of Kocaeli (D1-1158Y) Earthquake

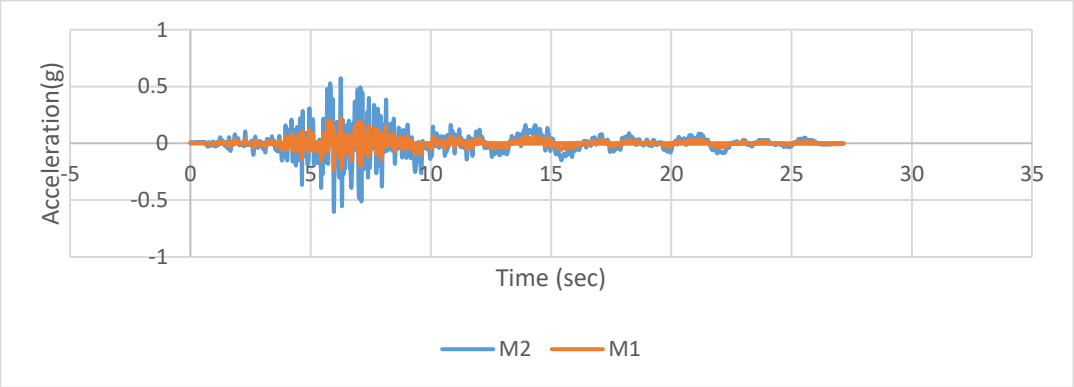

Figure A260. Scaled Acceleration Time Histories of Kocaeli (D1-1158Z) Earthquake

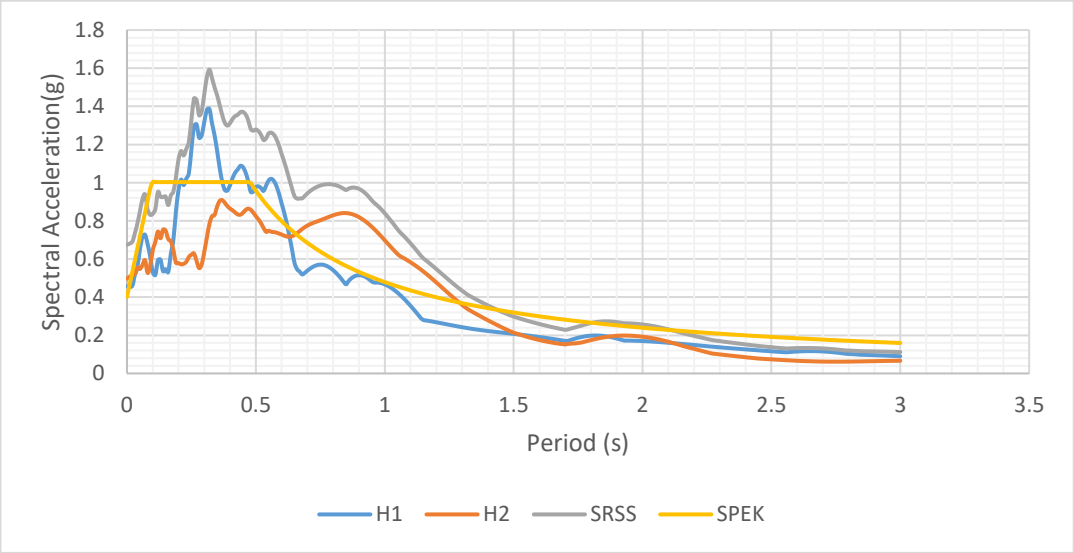

Figure A261.Scaled Horizontal Response Spectra of Duzce (D1-1602) Earthquake

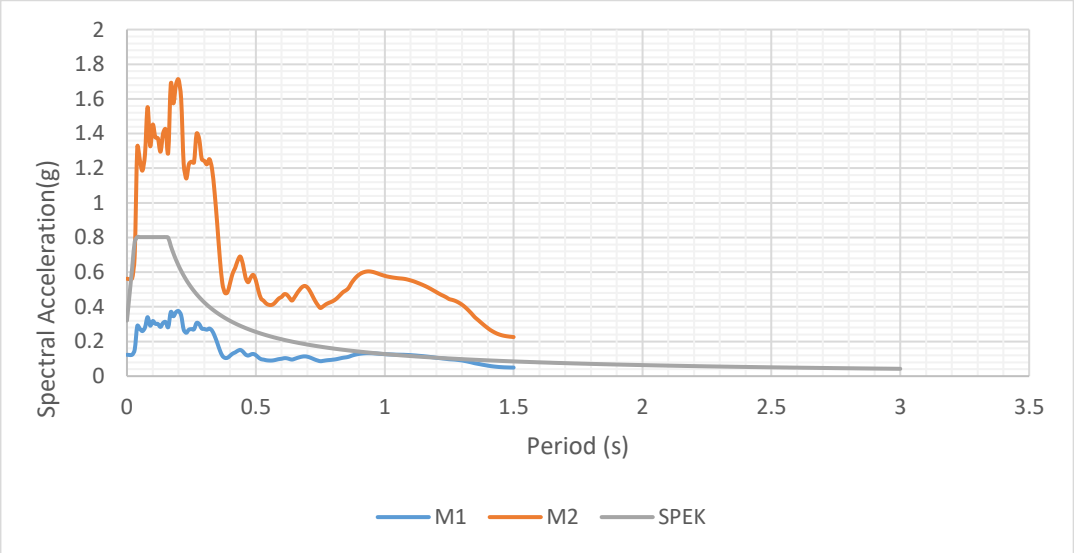

Figure A262. Scaled Vertical Response Spectra of Duzce (D1-1602) Earthquake

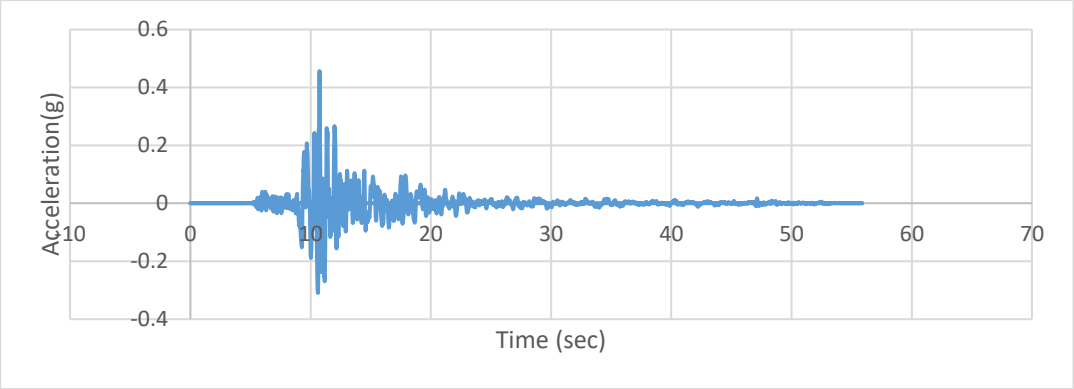

Figure A263. Scaled Acceleration Time Histories of Duzce (D1-1602X) Earthquake

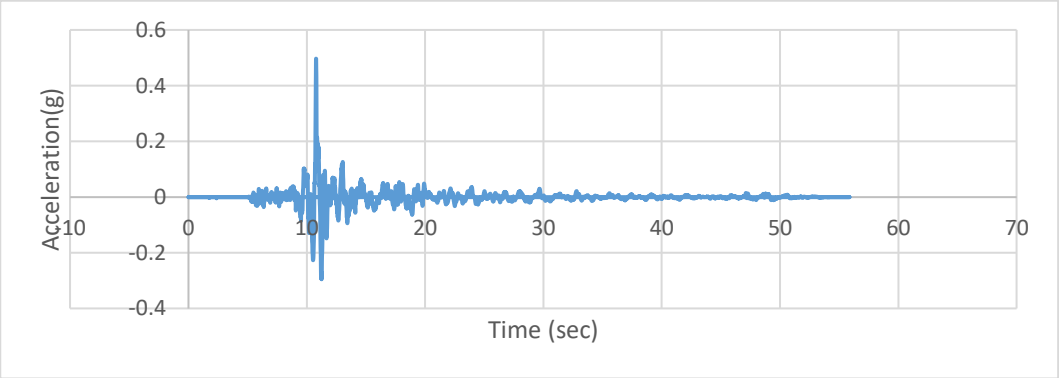

Figure A264.Scaled Acceleration Time Histories of Duzce (D1-1602Y) Earthquake

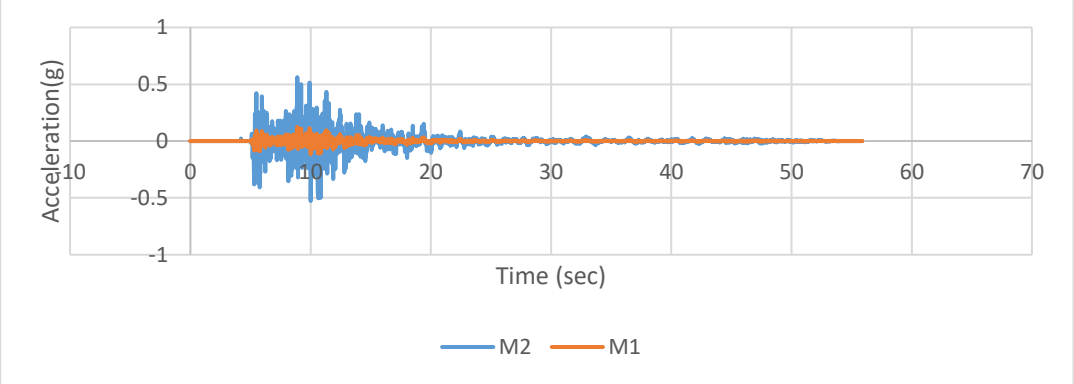

Figure A265.Scaled Acceleration Time Histories of Duzce (D1-1602Z) Earthquake

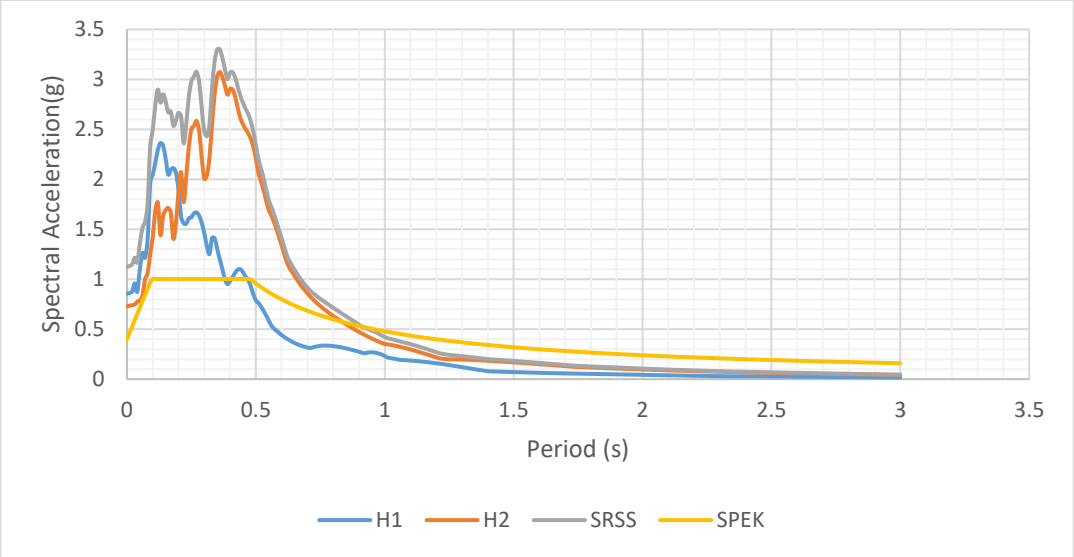

Figure A266. Scaled Horizontal Response Spectra of Northwest China-01 (D1-1748) Earthquake

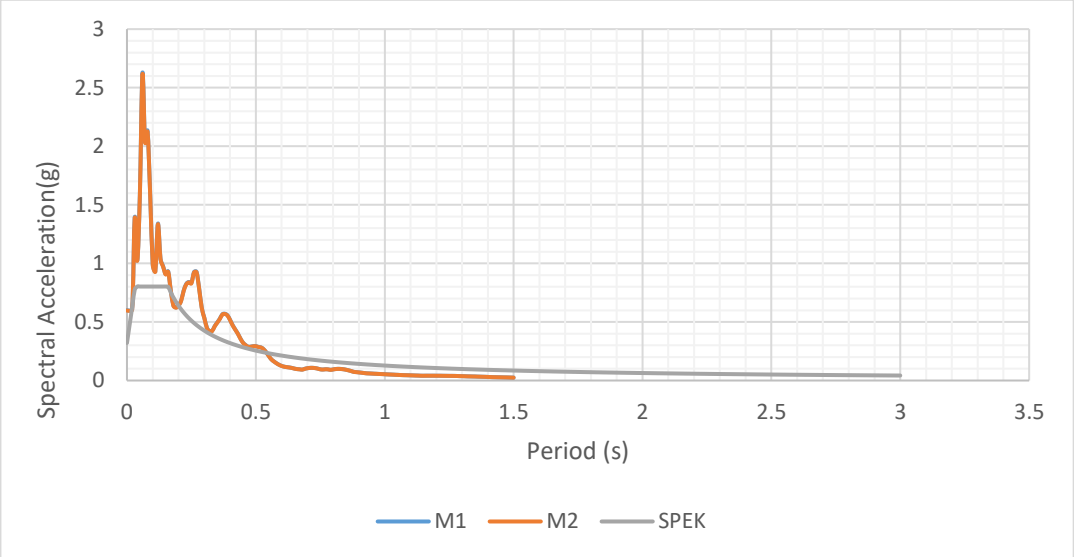

Figure A267. Scaled Vertical Response Spectra of Northwest China-01 (D1-1748) Earthquake

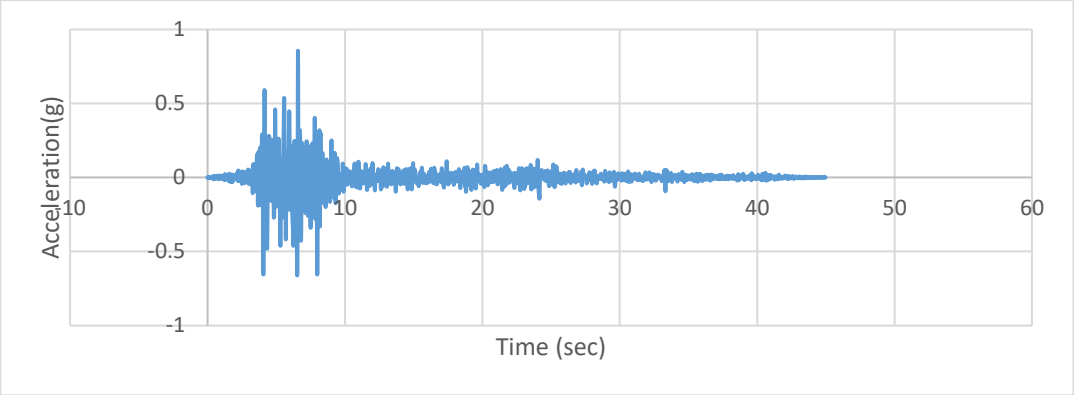

Figure A268. Scaled Acceleration Time Histories of Northwest China-01 (D1-1748X) Earthquake

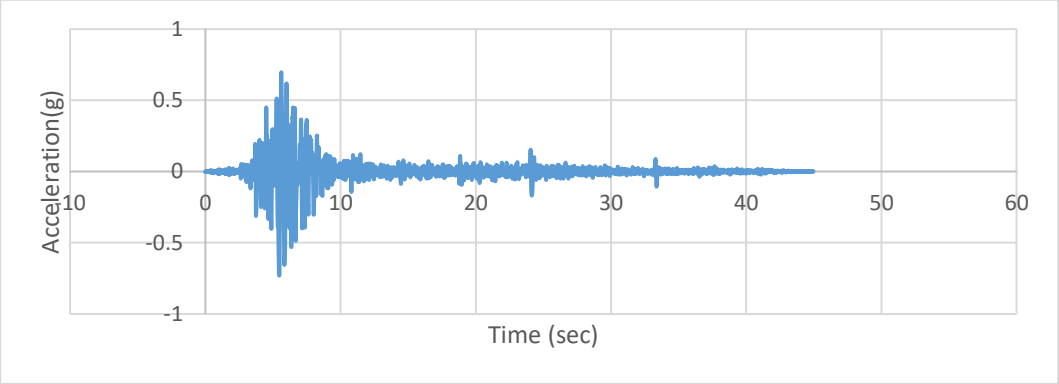

Figure A269. Scaled Acceleration Time Histories of Northwest China-01 (D1-1748Y) Earthquake

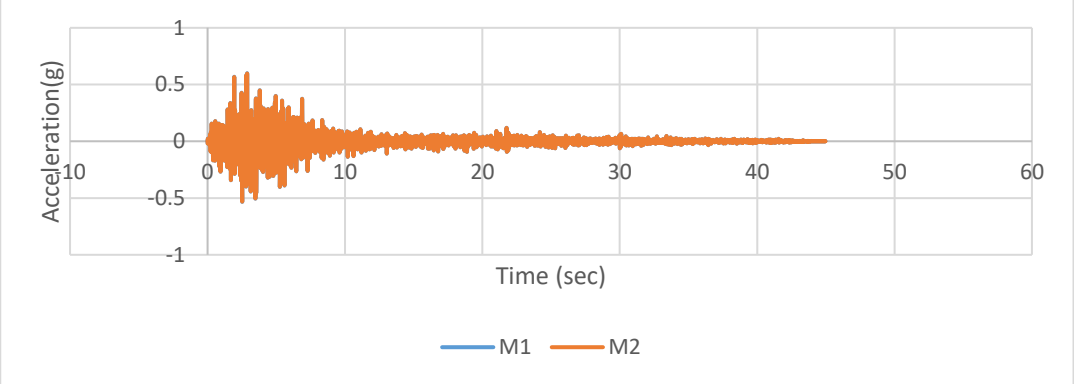

Figure A270. Scaled Acceleration Time Histories of Northwest China-01 (D1-1748Z) Earthquake

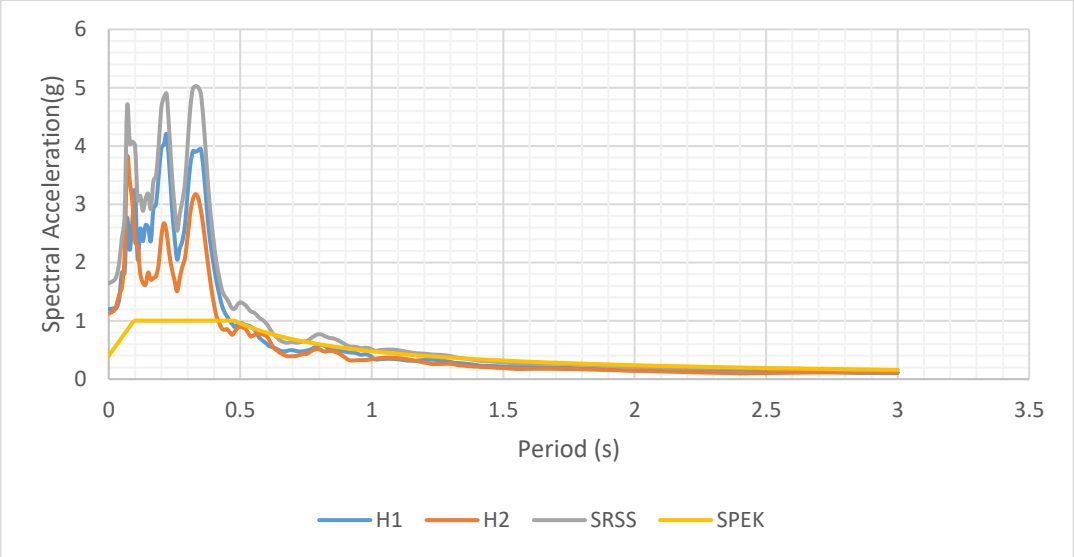

Figure A271. Scaled Horizontal Response Spectra of Parkfield-02 (D1-4125) Earthquake

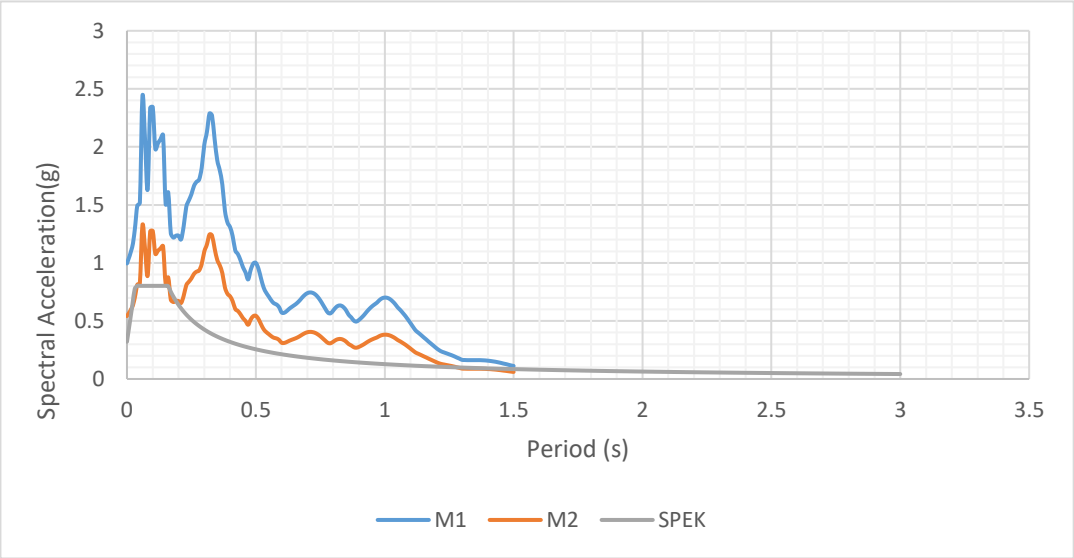

Figure A272. Scaled Vertical Response Spectra of Parkfield-02 (D1-4125) Earthquake

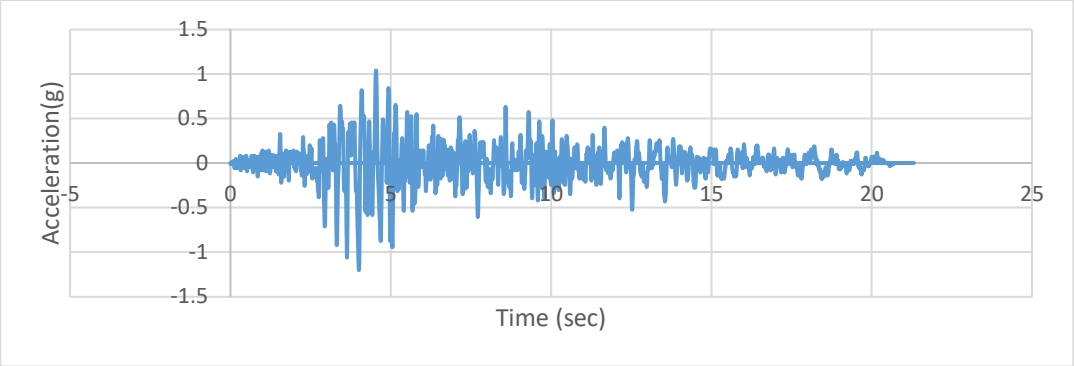

Figure A273. Scaled Acceleration Time Histories of Parkfield-02 (D1-4125X) Earthquake

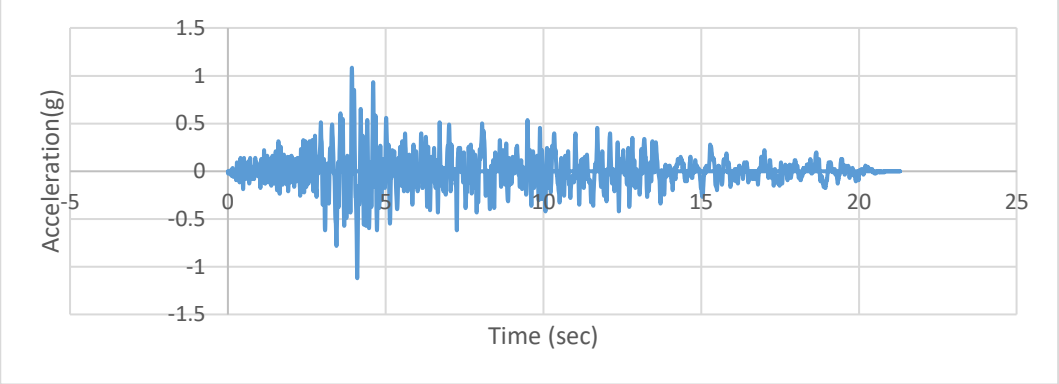

Figure A274.Scaled Acceleration Time Histories of Parkfield-02 (D1-4125Y) Earthquake

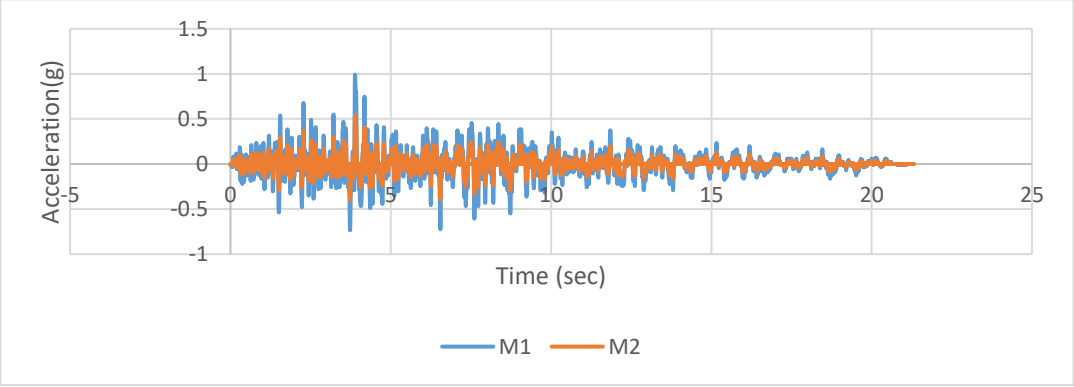

Figure A275.Scaled Acceleration Time Histories of Parkfield-02 (D1-4125Z) Earthquake

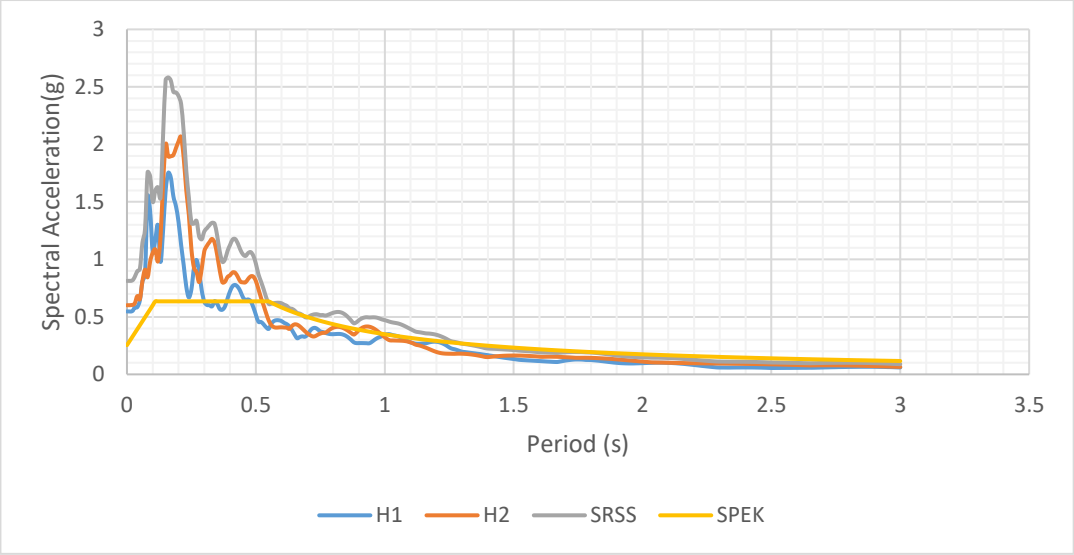

Figure A276. Scaled Horizontal Response Spectra of Parkfield (D2-31) Earthquake

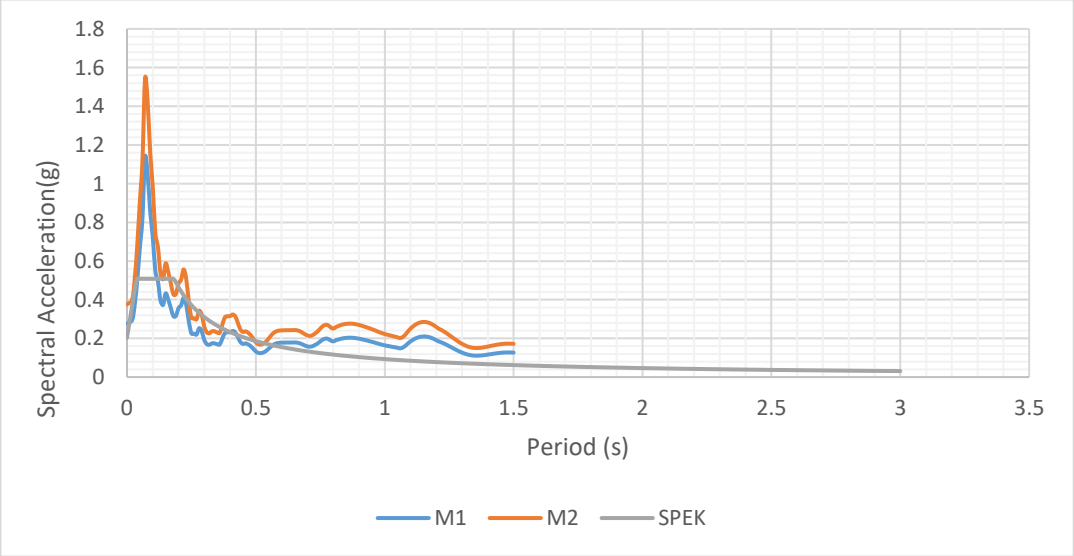

Figure A277. Scaled Vertical Response Spectra of Parkfield (D2-31) Earthquake

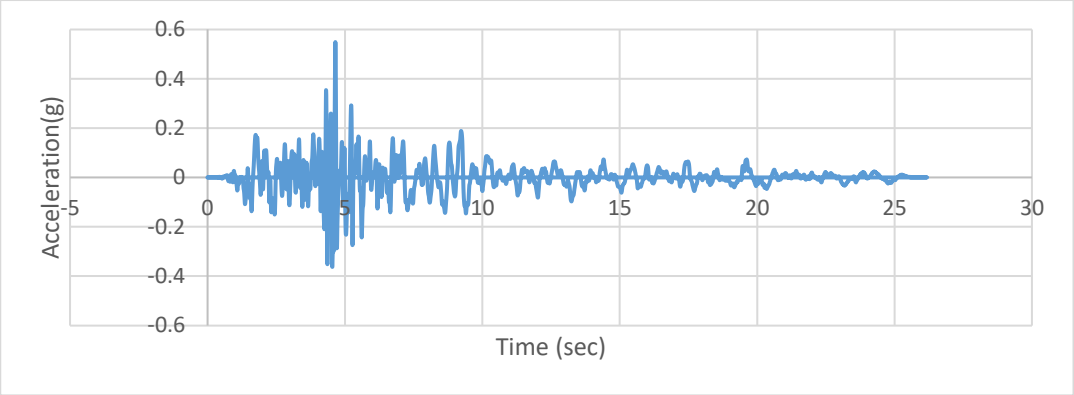

Figure A278.Scaled Acceleration Time Histories of Parkfield (D2-31X) Earthquake

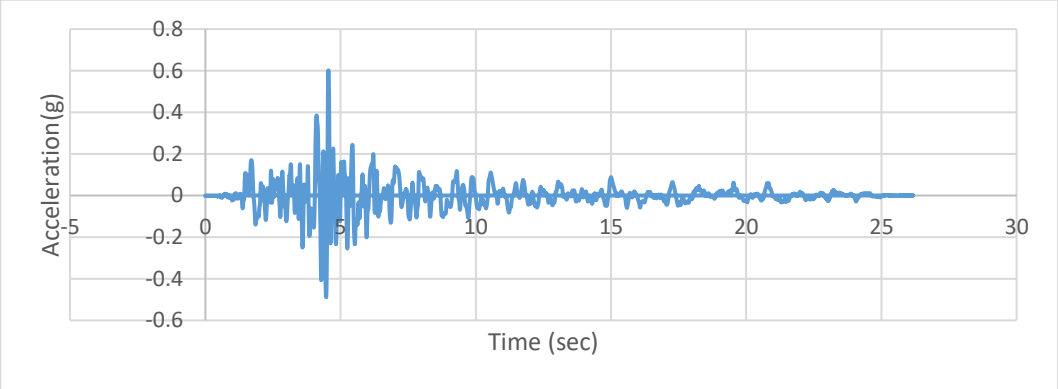

Figure A279. Scaled Acceleration Time Histories of Parkfield (D2-31Y) Earthquake

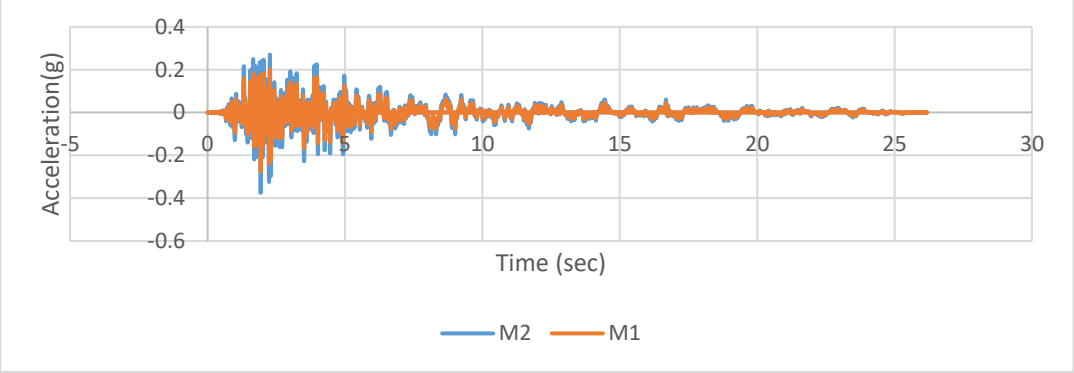

Figure A280. Scaled Acceleration Time Histories of Parkfield (D2-31Z) Earthquake

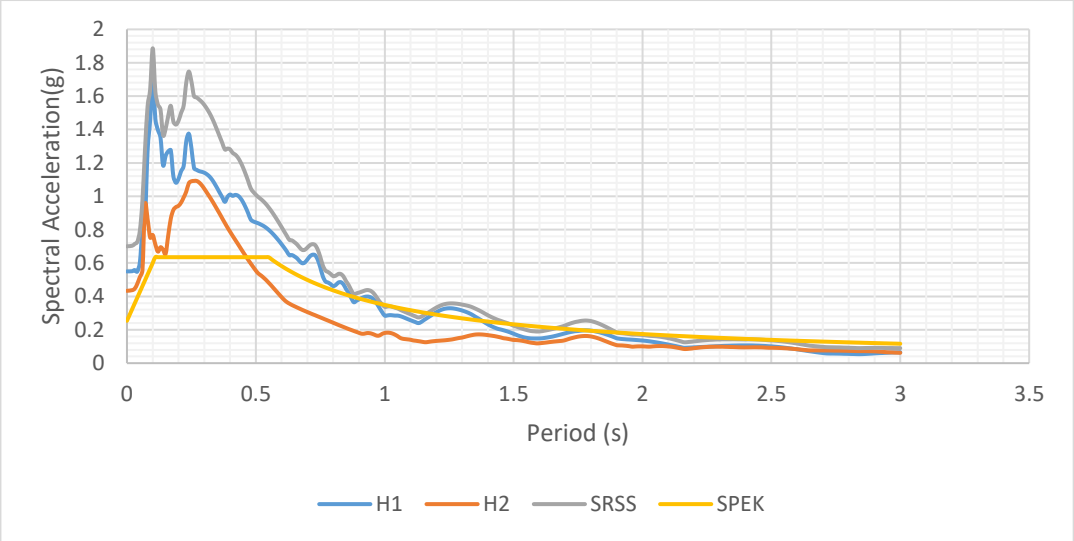

Figure A281. Scaled Horizontal Response Spectra of Imperial Valley-06 (D2-167) Earthquake

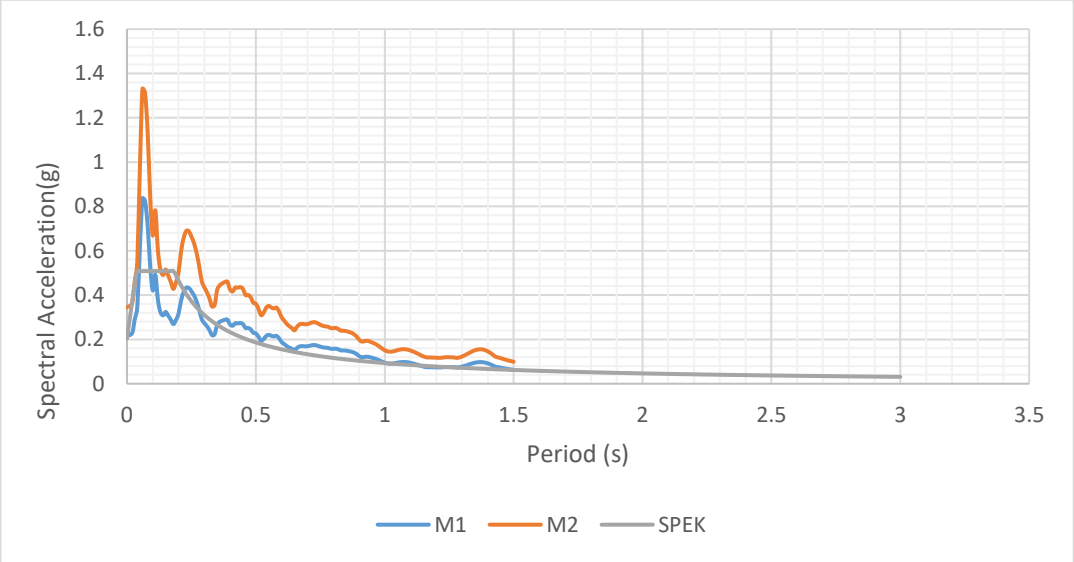

Figure A282. Scaled Vertical Response Spectra of Imperial Valley-06 (D2-167) Earthquake

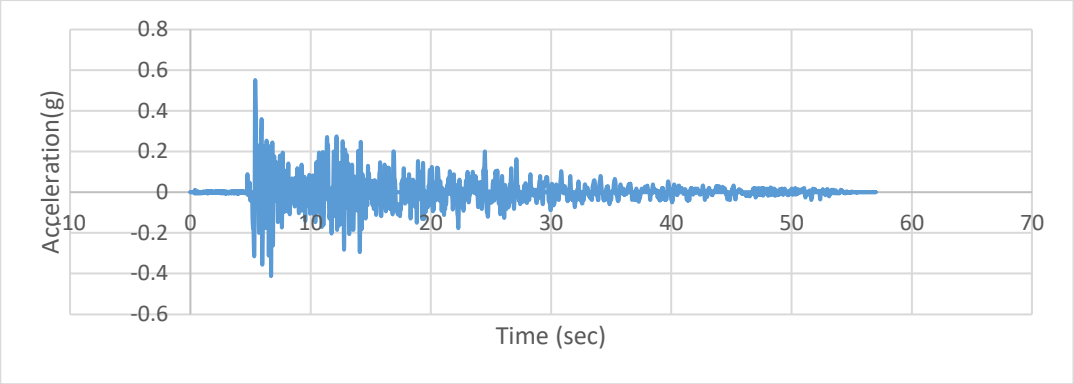

Figure A283. Scaled Acceleration Time Histories of Imperial Valley-06 (D2-167X) Earthquake

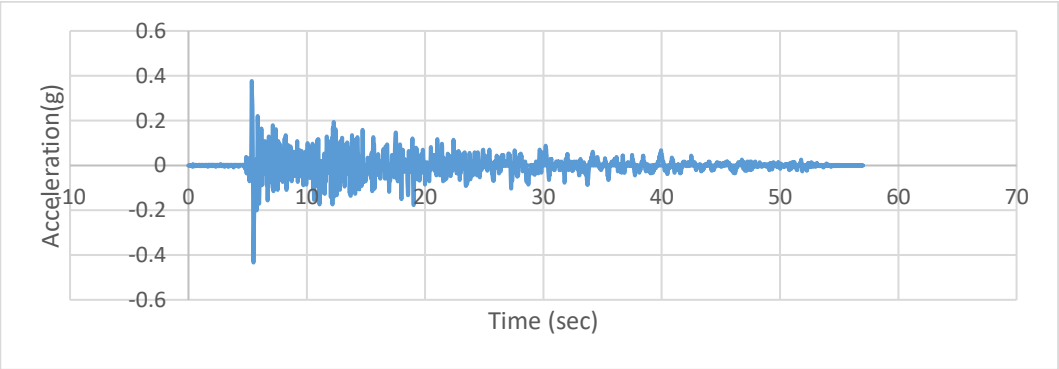

Figure A284. Scaled Acceleration Time Histories of Imperial Valley-06 (D2-167Y) Earthquake

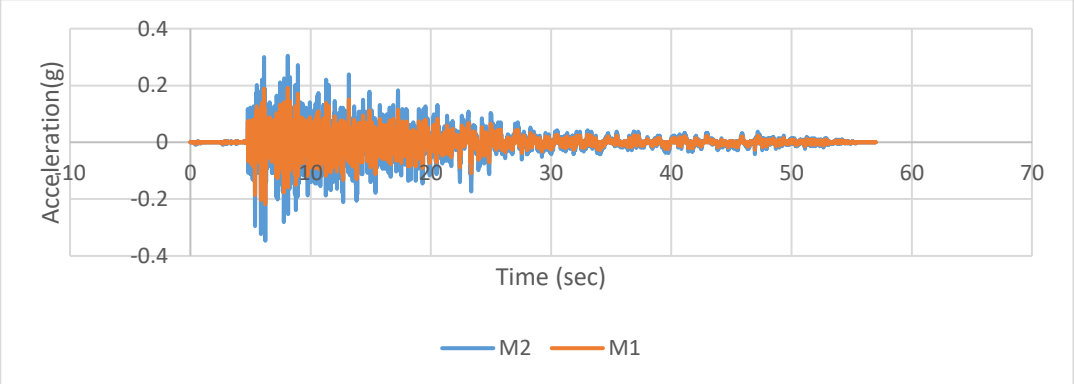

Figure A285. Scaled Acceleration Time Histories of Imperial Valley-06 (D2-167Z) Earthquake

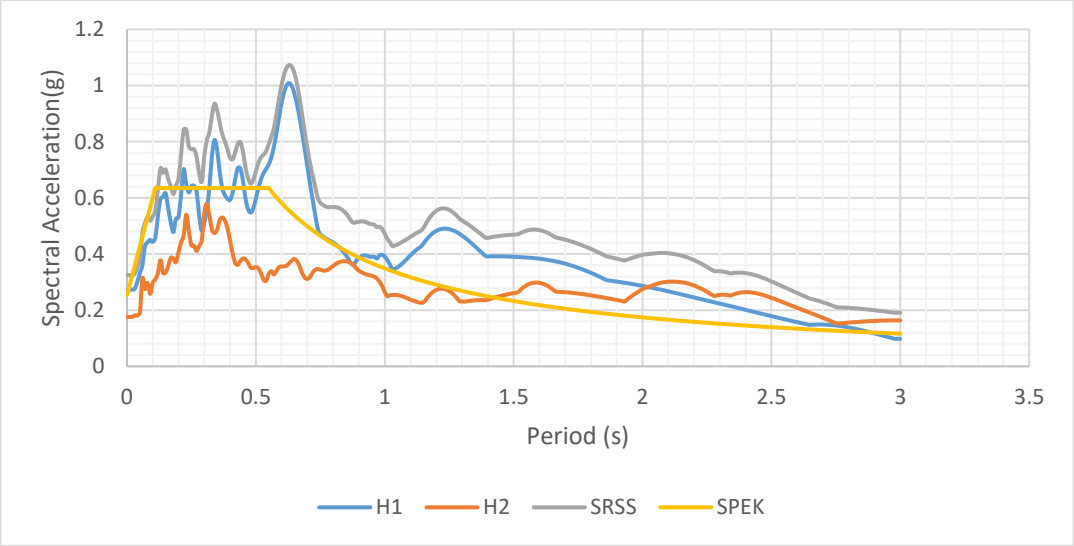

Figure A286. Scaled Horizontal Response Spectra of Victoria (D2-266) Earthquake

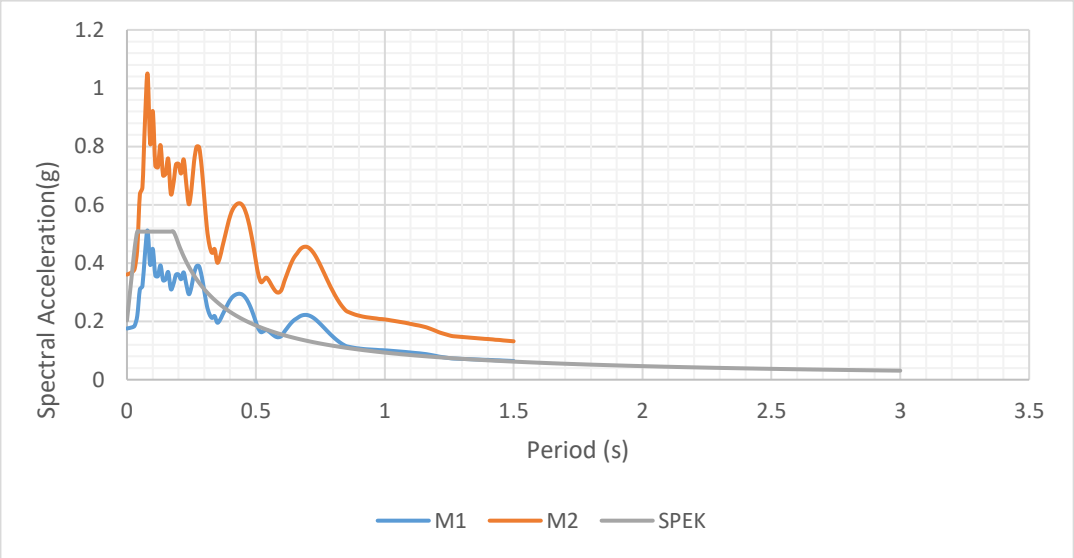

Figure A287. Scaled Vertical Response Spectra of Victoria (D2-266) Earthquake

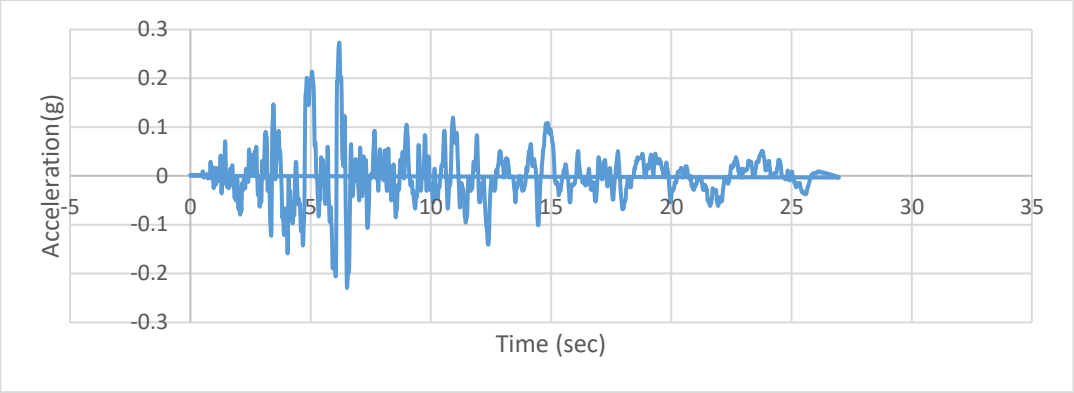

Figure A288. Scaled Acceleration Time Histories of Victoria (D2-266X) Earthquake

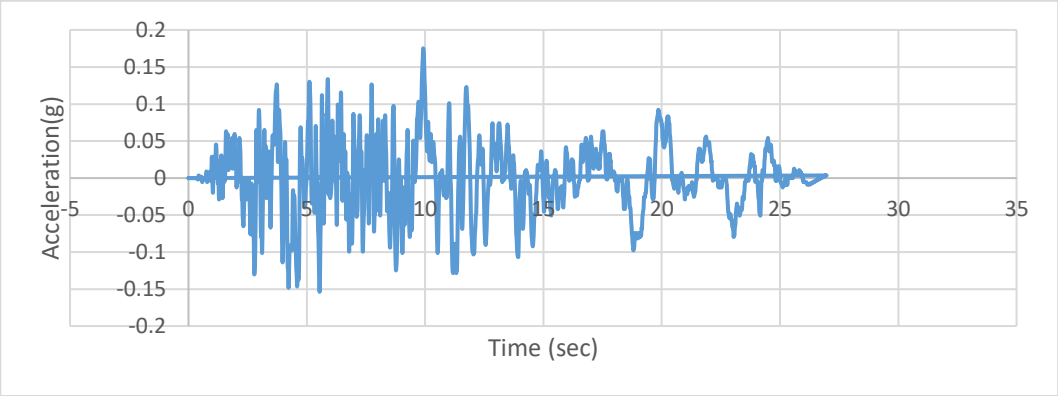

Figure A289. Scaled Acceleration Time Histories of Victoria (D2-266Y) Earthquake

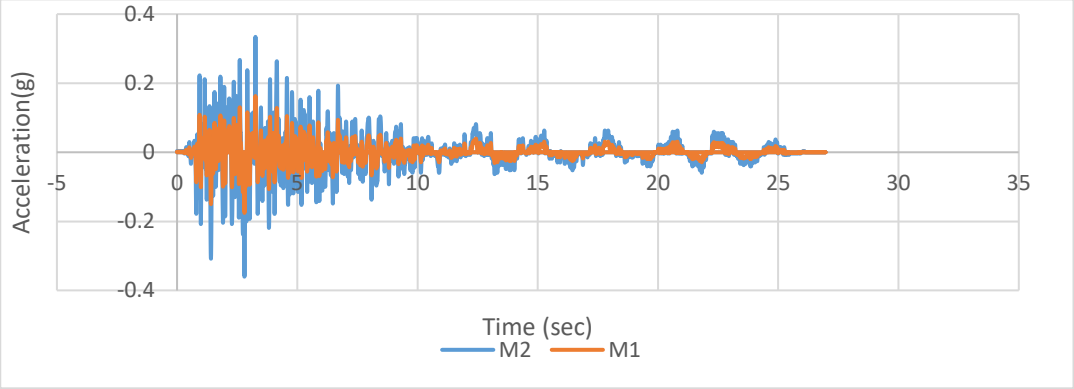

Figure A290. Scaled Acceleration Time Histories of Victoria (D2-266Z) Earthquake

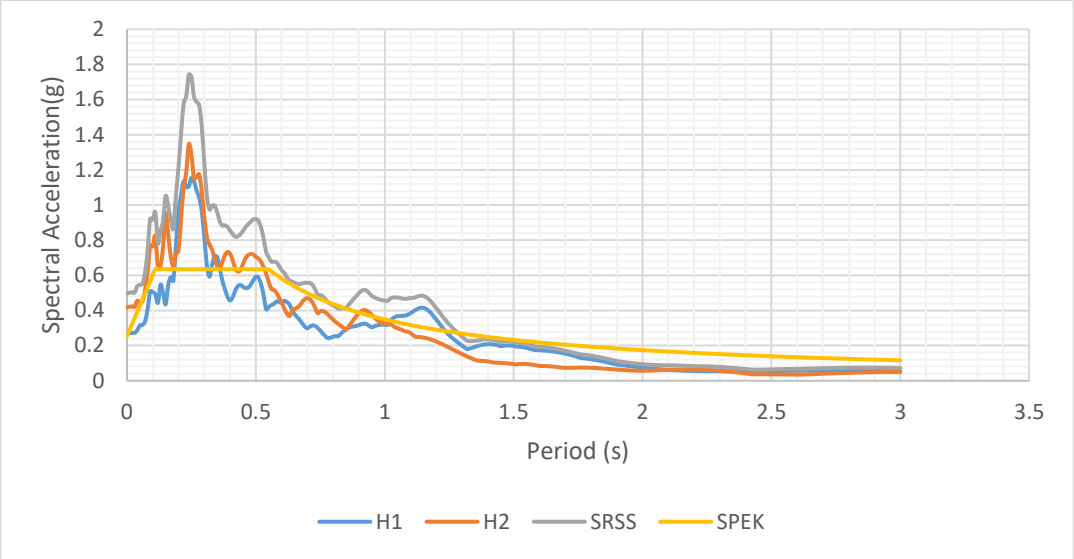

Figure A291. Scaled Horizontal Response Spectra of Morgan Hill (D2-458) Earthquake

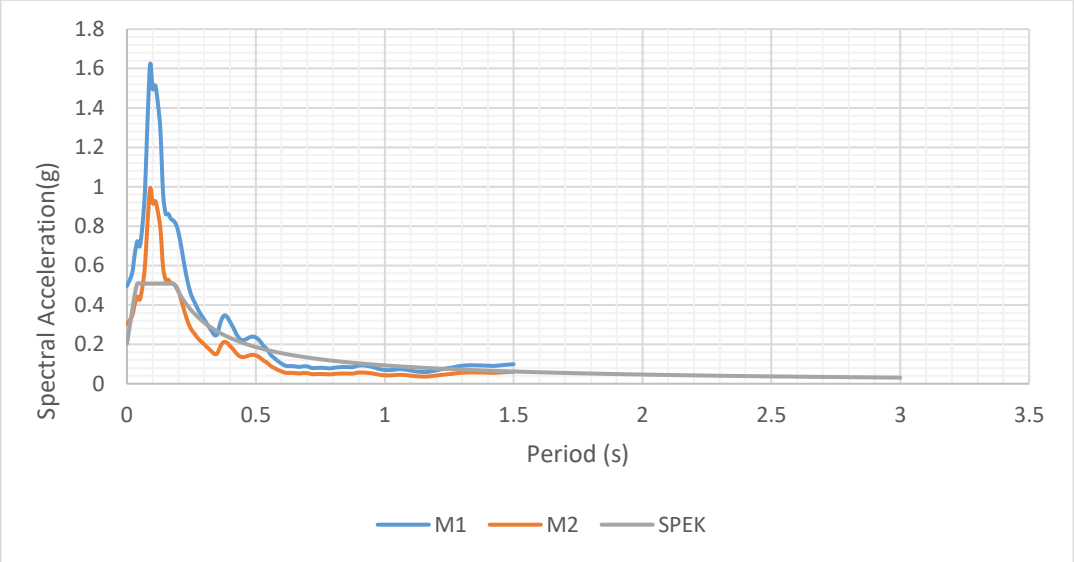

Figure A292. Scaled Vertical Response Spectra of Morgan Hill (D2-458) Earthquake

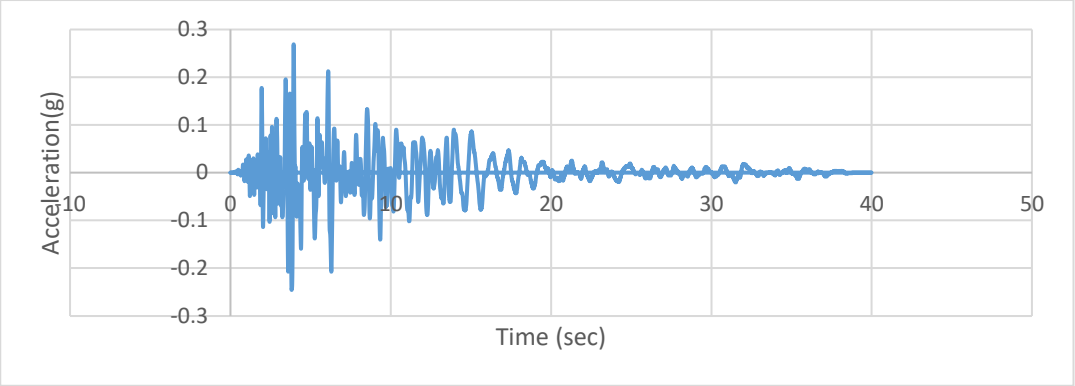

Figure A293. Scaled Acceleration Time Histories of Morgan Hill (D2-458X) Earthquake

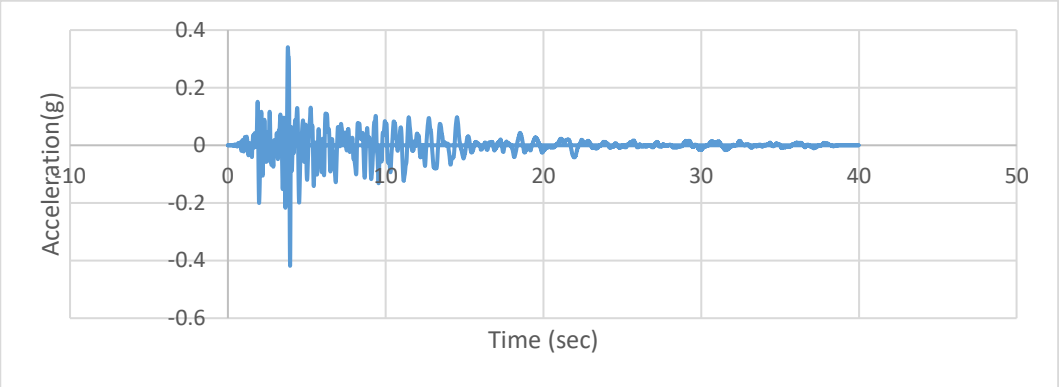

Figure A294. Scaled Acceleration Time Histories of Morgan Hill (D2-458Y) Earthquake

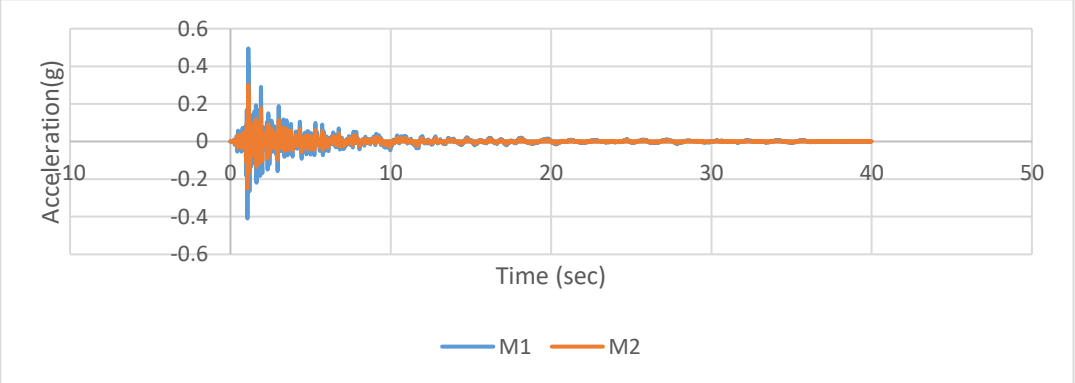

Figure A295. Scaled Acceleration Time Histories of Morgan Hill (D2-458Z) Earthquake

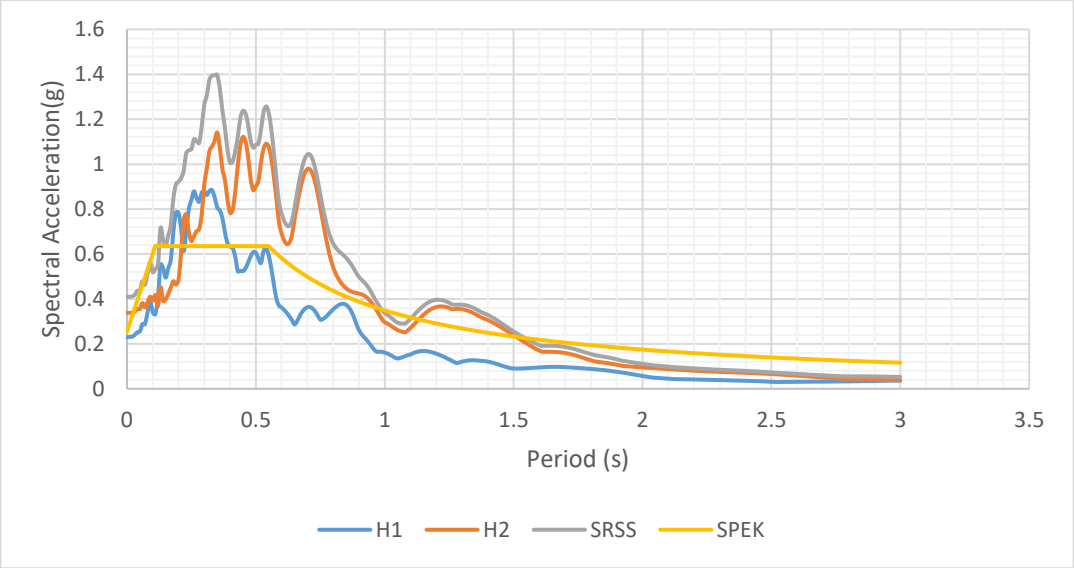

Figure A296. Scaled Horizontal Response Spectra of Landers (D2-848) Earthquake

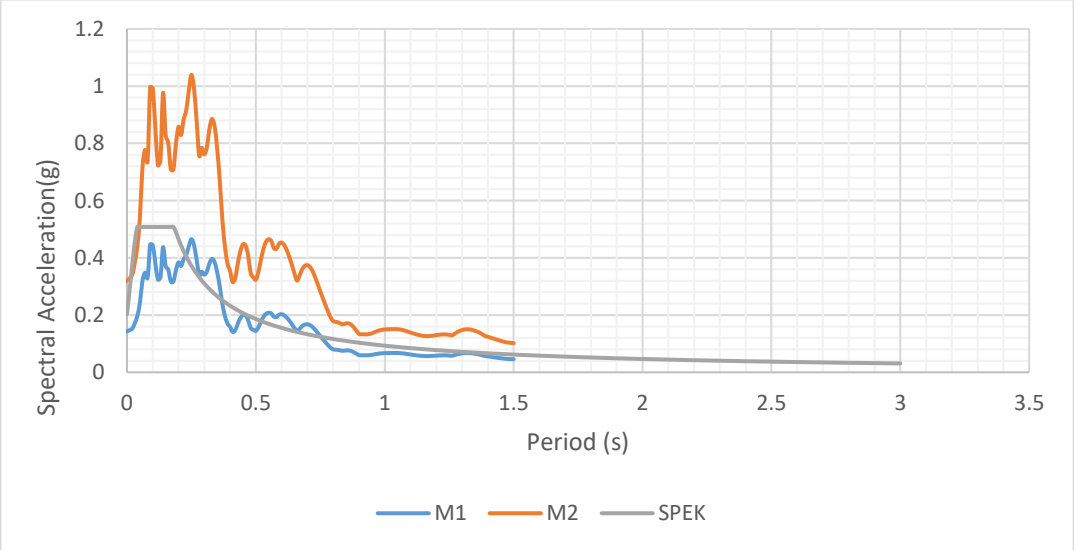

Figure A297. Scaled Vertical Response Spectra of Landers (D2-848) Earthquake

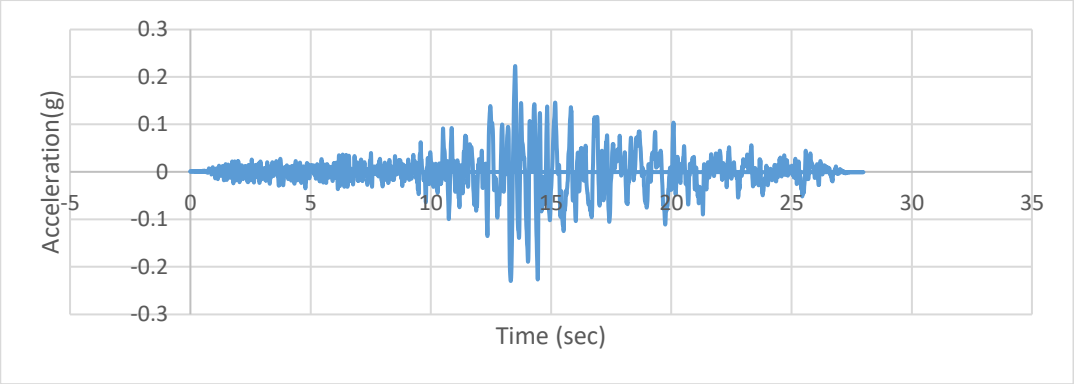

Figure A298. Scaled Acceleration Time Histories of Landers (D2-848X) Earthquake

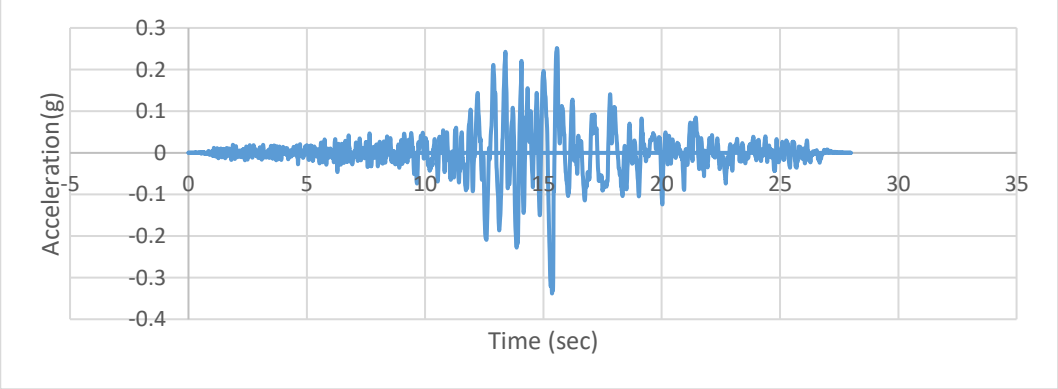

Figure A299. Scaled Acceleration Time Histories of Landers (D2-848Y) Earthquake

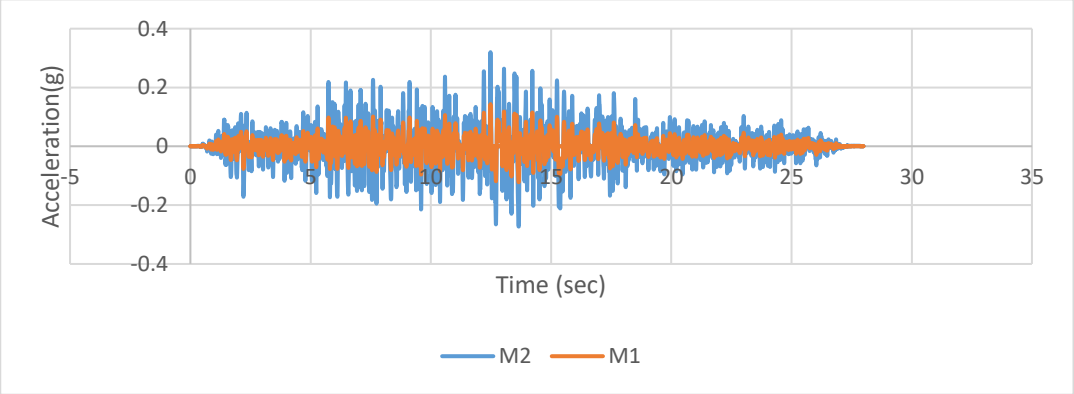

Figure A300. Scaled Acceleration Time Histories of Landers (D2-848Z) Earthquake

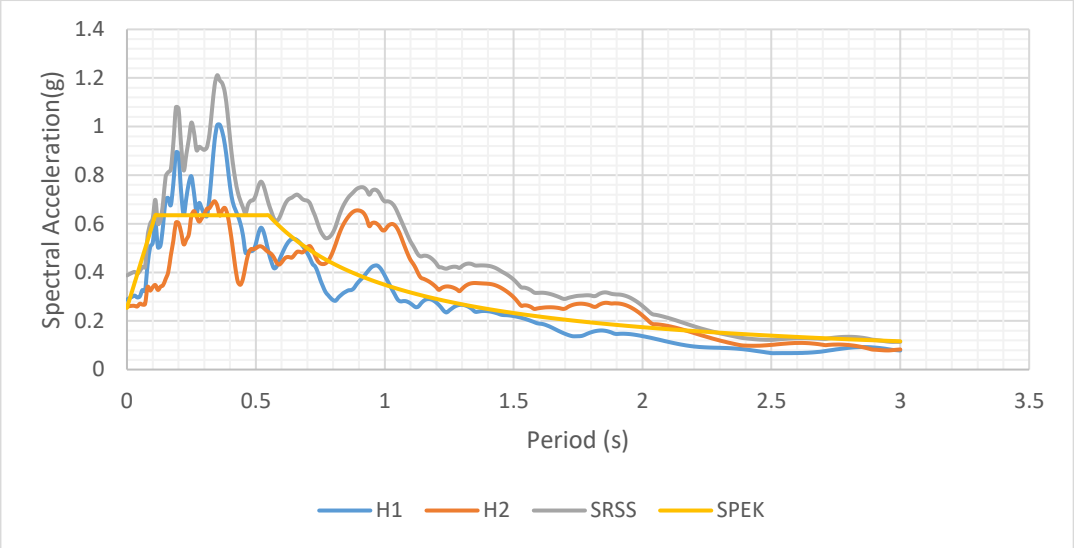

Figure A301. Scaled Horizontal Response Spectra of Landers (D2-850) Earthquake

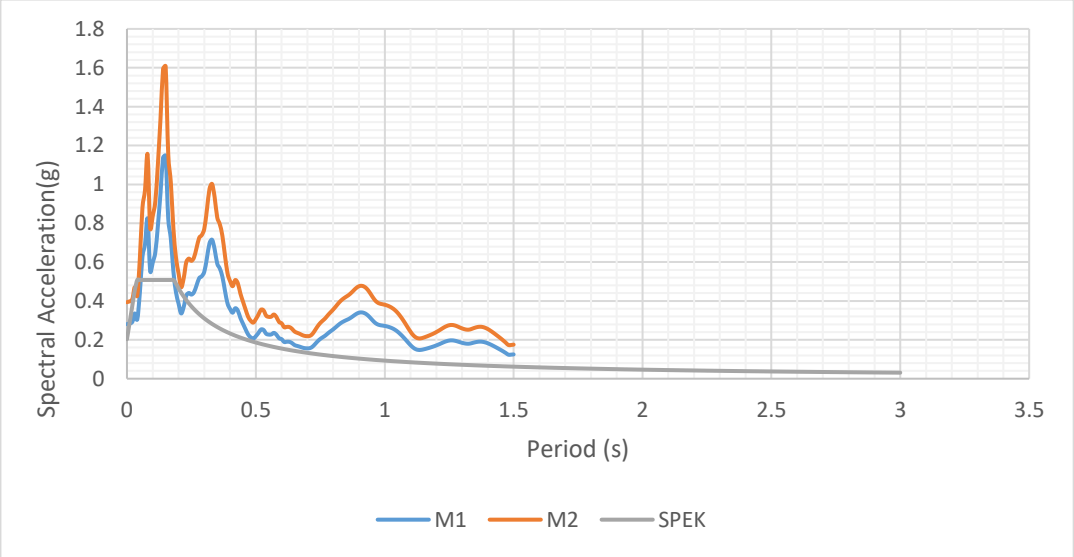

Figure A302.Scaled Vertical Response Spectra of Landers (D2-850) Earthquake

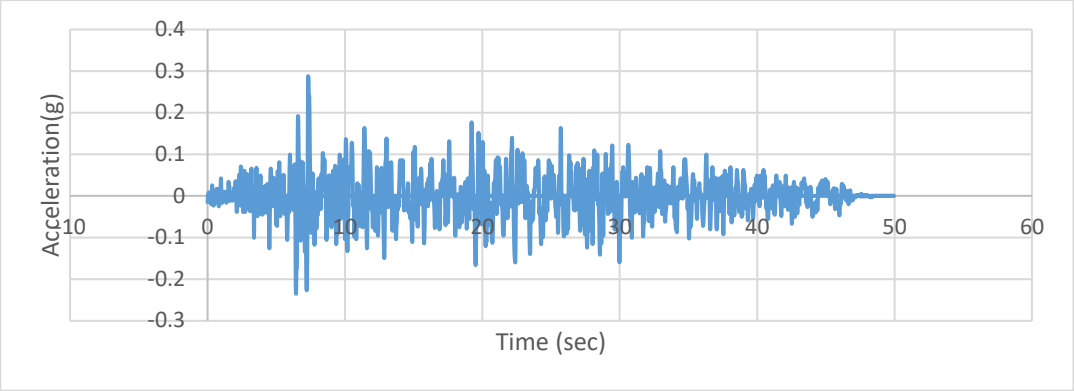

Figure A303. Scaled Acceleration Time Histories of Landers (D2-850X) Earthquake

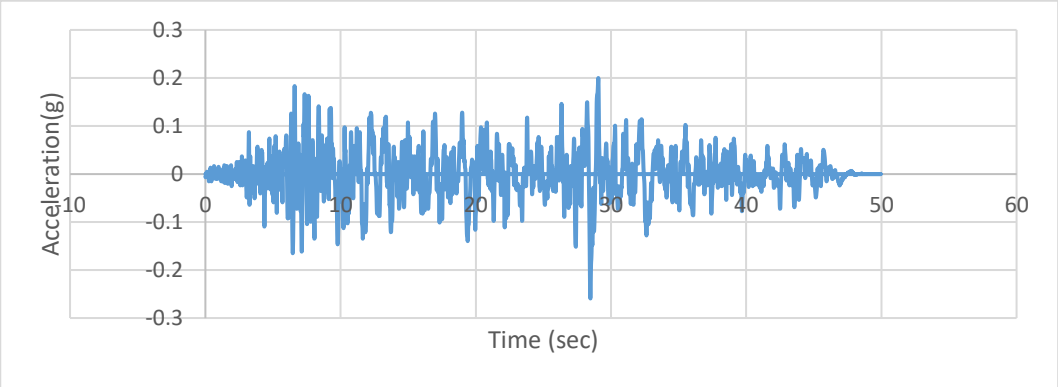

Figure A304. Scaled Acceleration Time Histories of Landers (D2-850Y) Earthquake

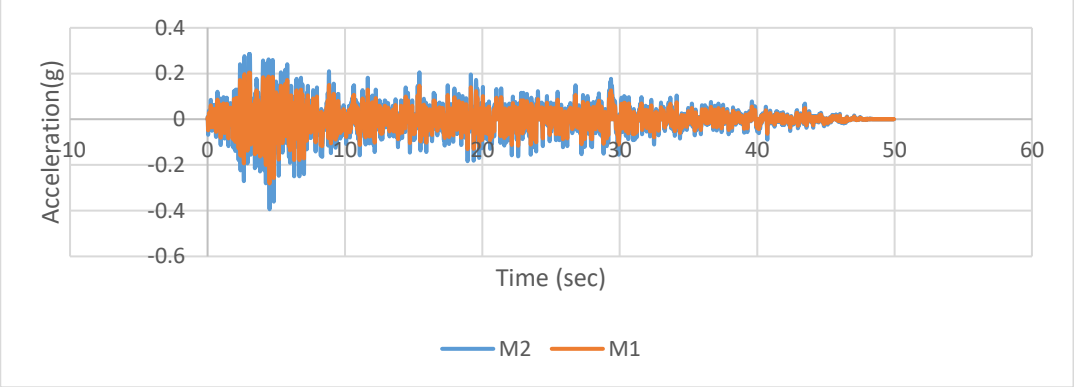

Figure A305. Scaled Acceleration Time Histories of Landers (D2-850Z) Earthquake

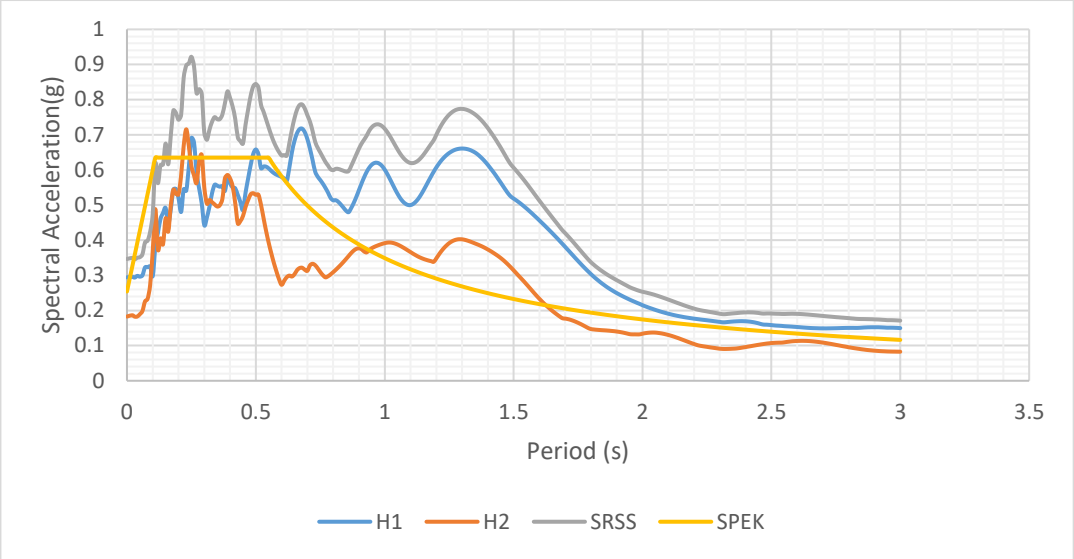

Figure A306.Scaled Horizontal Response Spectra of Landers (D2-900) Earthquake

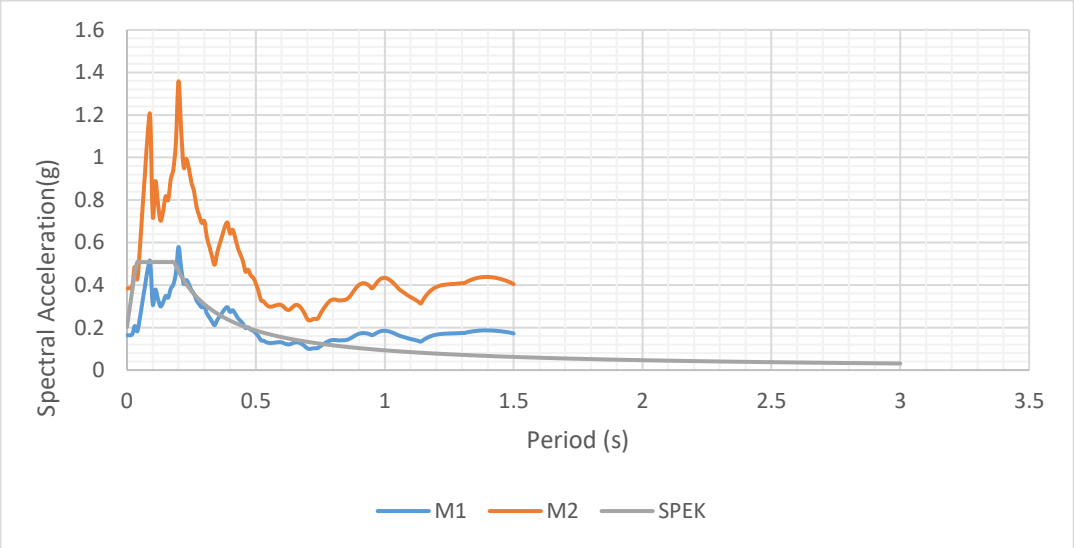

Figure A307. Scaled Vertical Response Spectra of Landers (D2-900) Earthquake

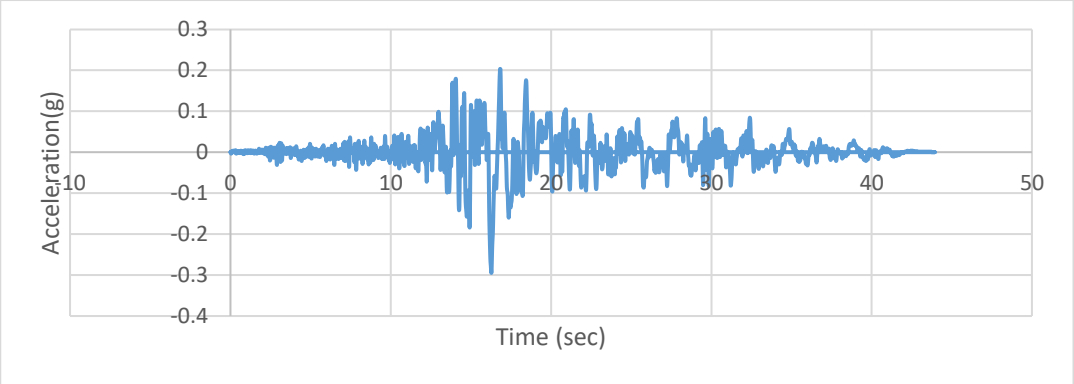

Figure A308. Scaled Acceleration Time Histories of Landers (D2-900X) Earthquake

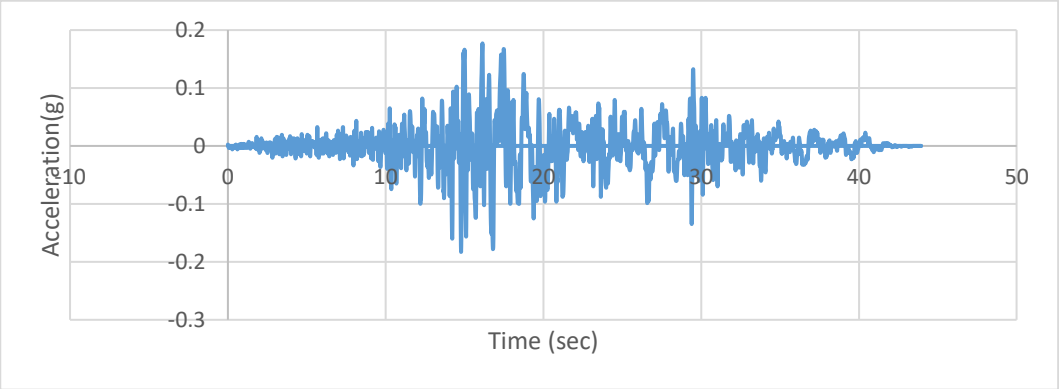

Figure A309. Scaled Acceleration Time Histories of Landers (D2-900Y) Earthquake

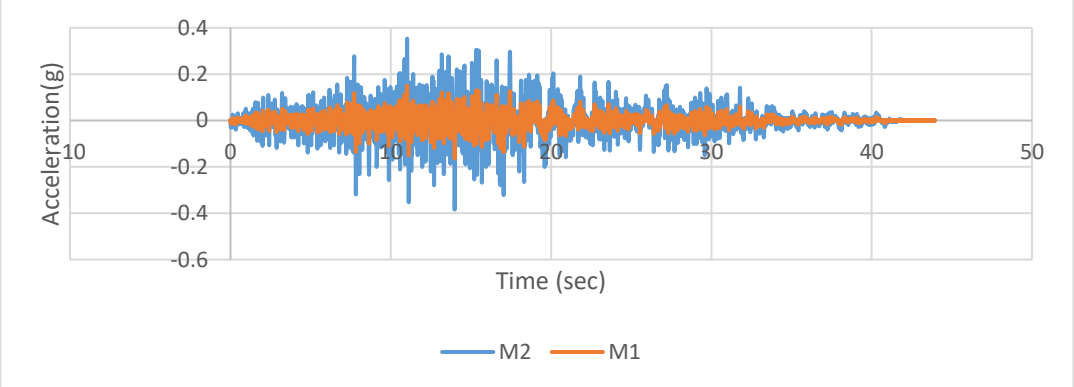

Figure A310. Scaled Acceleration Time Histories of Landers (D2-900Z) Earthquake

Figure A311. Scaled Horizontal Response Spectra of Kocaeli (D2-1158) Earthquake

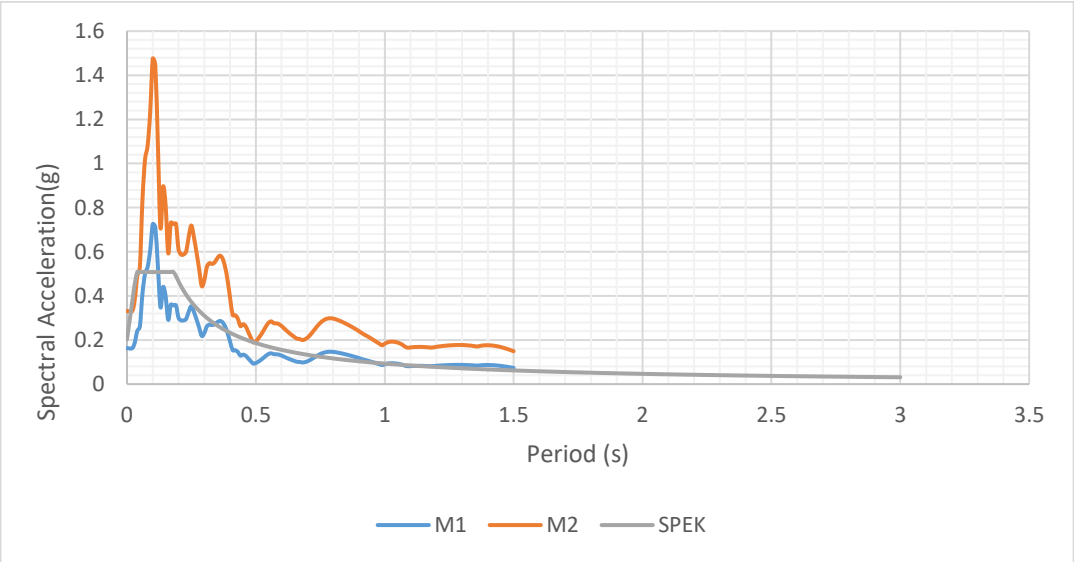

Figure A312. Scaled Vertical Response Spectra of Kocaeli (D2-1158) Earthquake

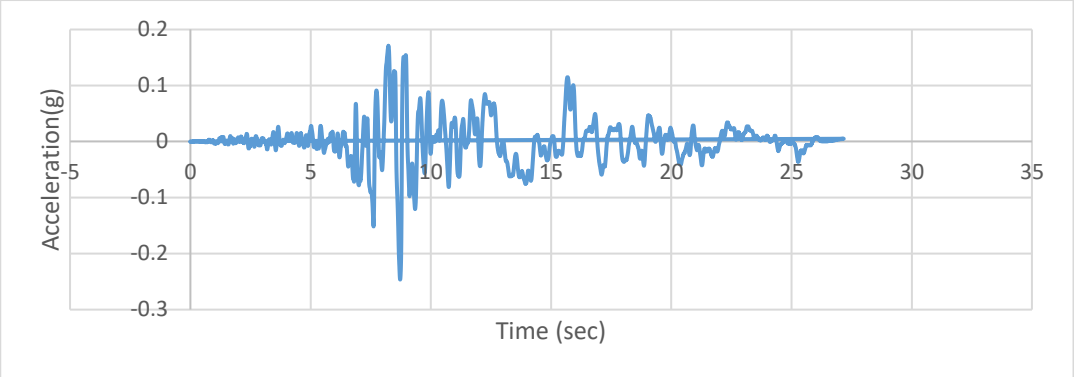

Figure A313. Scaled Acceleration Time Histories of Kocaeli (D2-1158X) Earthquake

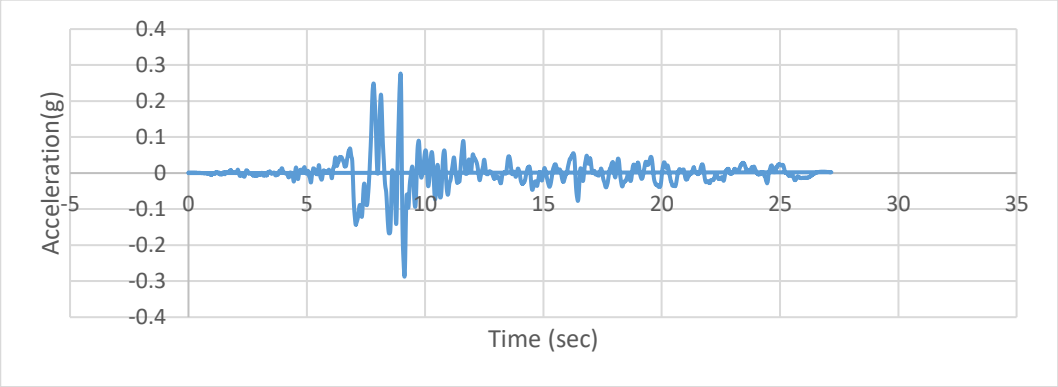

Figure A314. Scaled Acceleration Time Histories of Kocaeli (D2-1158Y) Earthquake

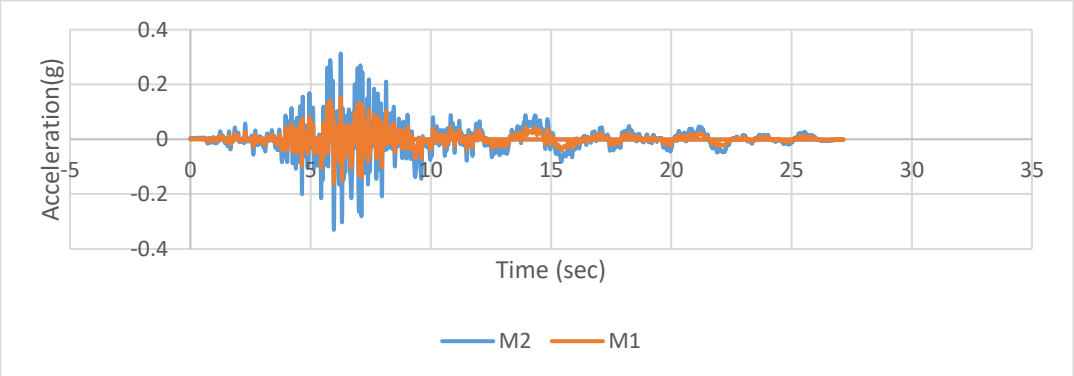

Figure A315. Scaled Acceleration Time Histories of Kocaeli (D2-1158Z) Earthquake

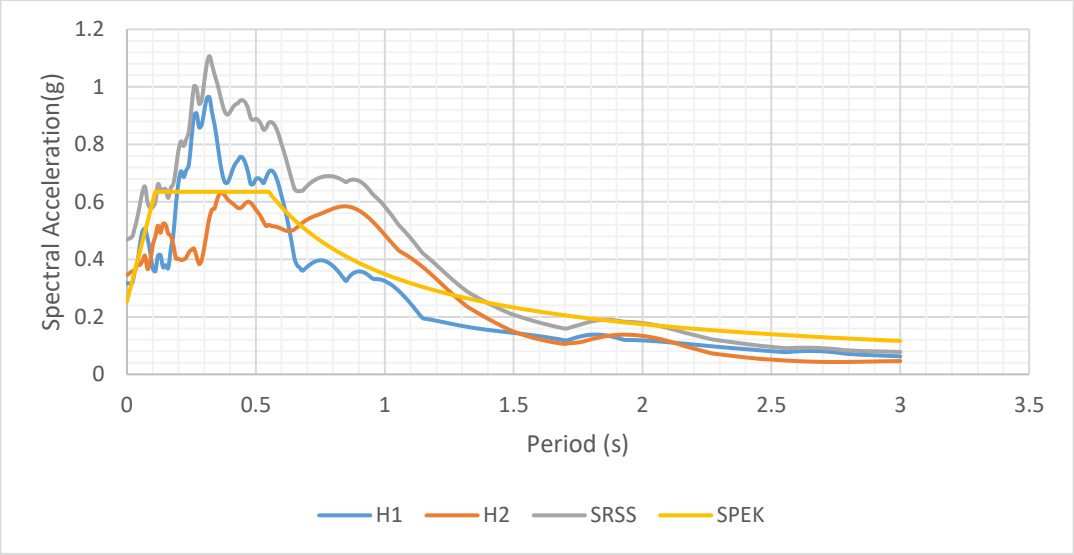

Figure A316.Scaled Horizontal Response Spectra of Duzce (D2-1602) Earthquake

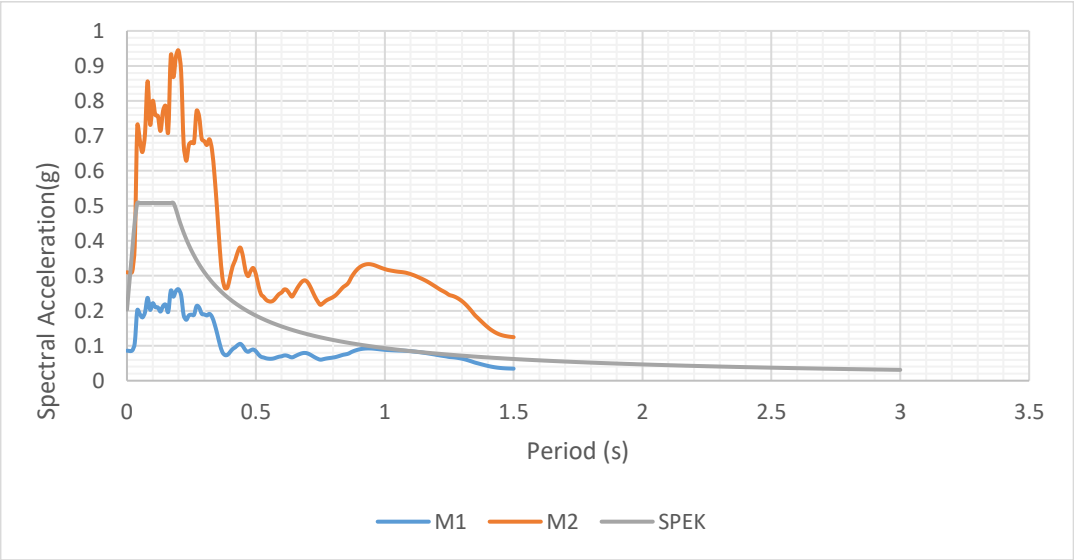

Figure A317. Scaled Vertical Response Spectra of Duzce (D2-1602) Earthquake

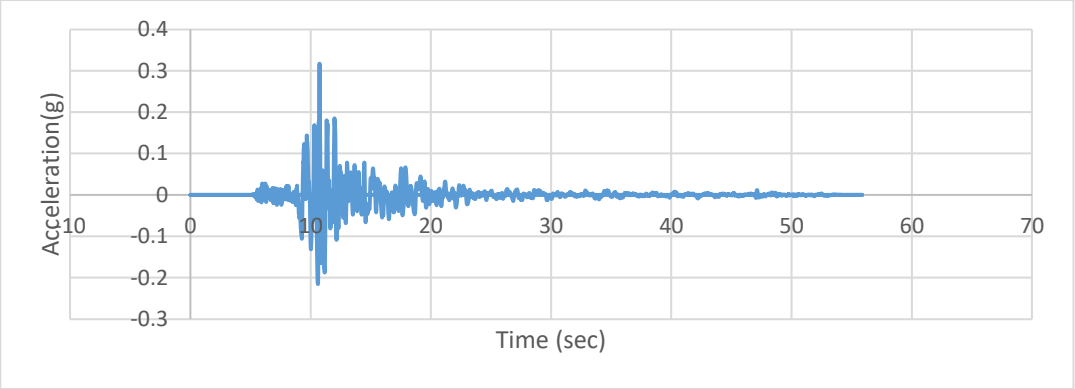

Figure A318. Scaled Acceleration Time Histories of Duzce (D2-1602X) Earthquake

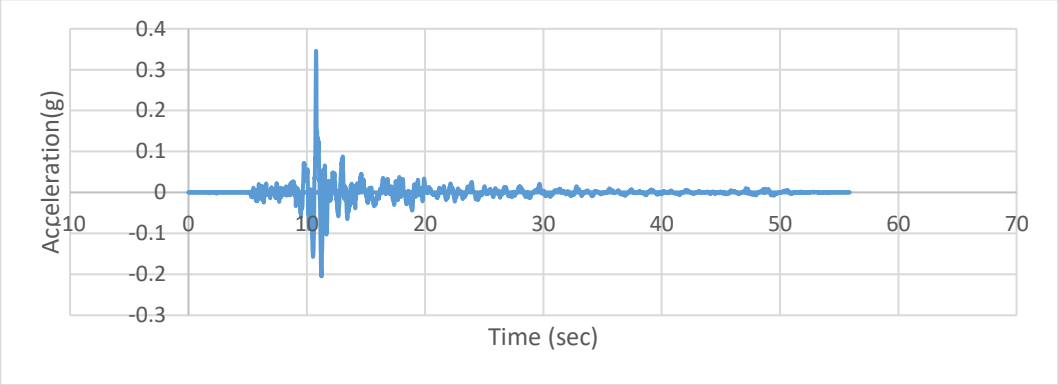

Figure A319. Scaled Acceleration Time Histories of Duzce (D2-1602Y) Earthquake

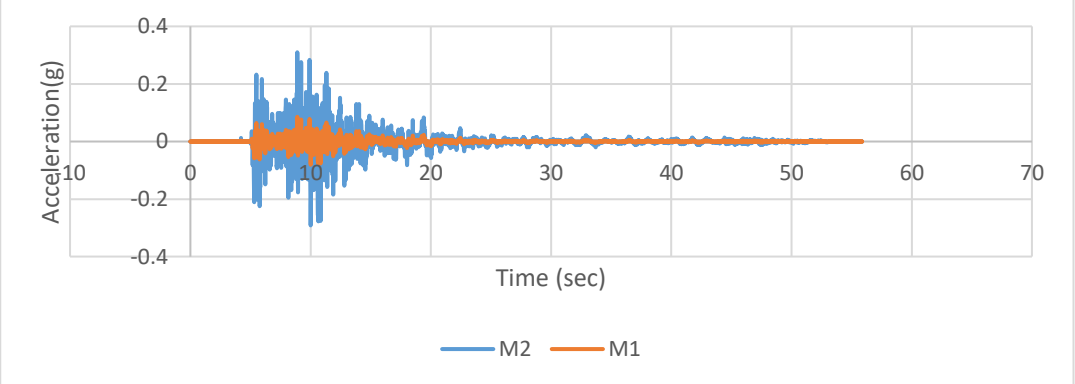

Figure A320. Scaled Acceleration Time Histories of Duzce (D2-1602Z) Earthquake

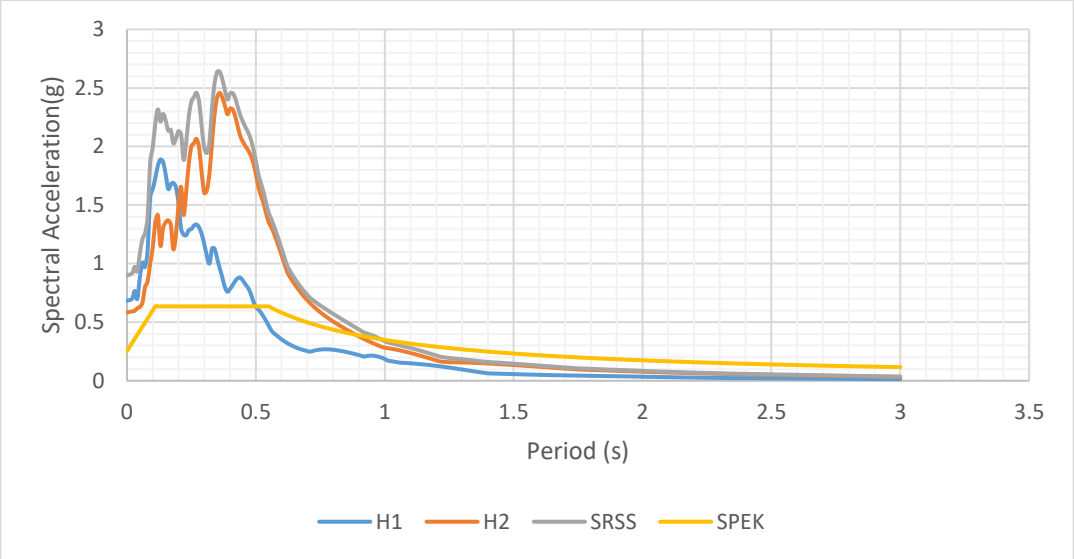

Figure A321. Scaled Horizontal Response Spectra of Northwest China-01 (D2-1748) Earthquake

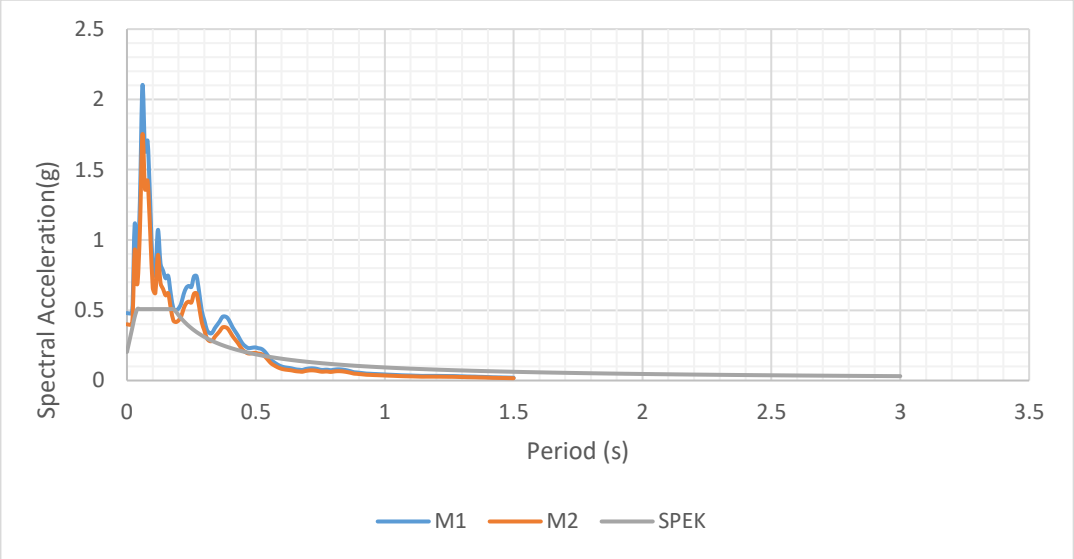

Figure A322. Scaled Vertical Response Spectra of Northwest China-01 (D2-1748) Earthquake

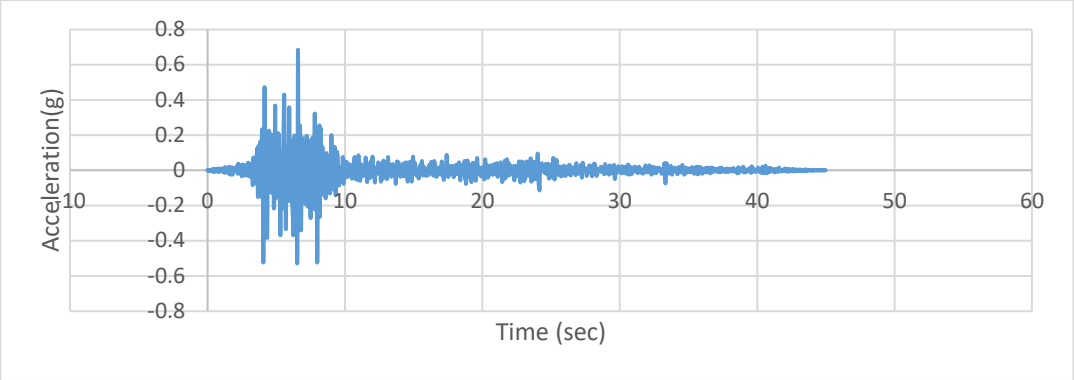

Figure A323. Scaled Acceleration Time Histories of Northwest China-01 (D2-1748X) Earthquake

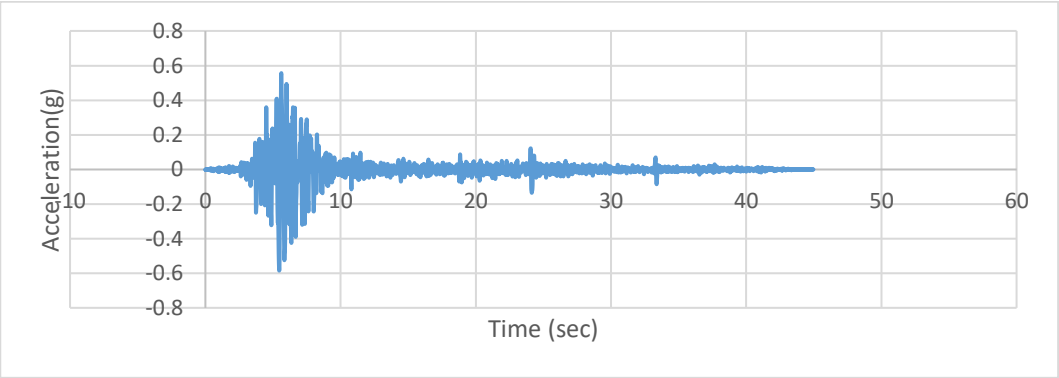

Figure A324. Scaled Acceleration Time Histories of Northwest China-01 (D2-1748Y) Earthquake

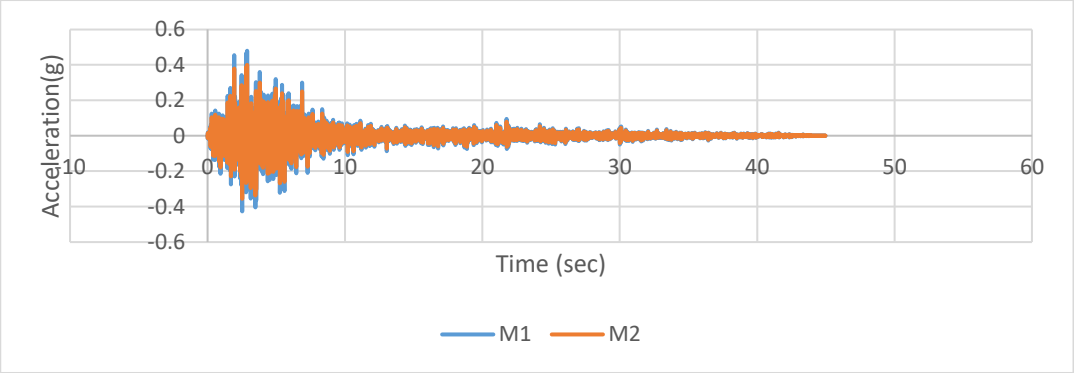

Figure A325. Scaled Acceleration Time Histories of Northwest China-01 (D2-1748Z) Earthquake

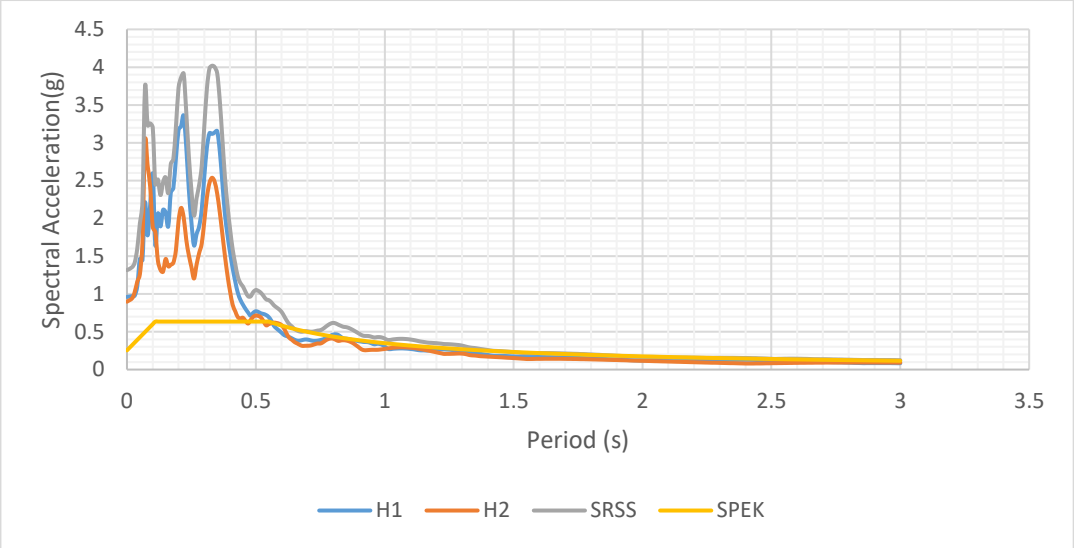

Figure A326. Scaled Horizontal Response Spectra of Parkfield-02 (D2-4125) Earthquake

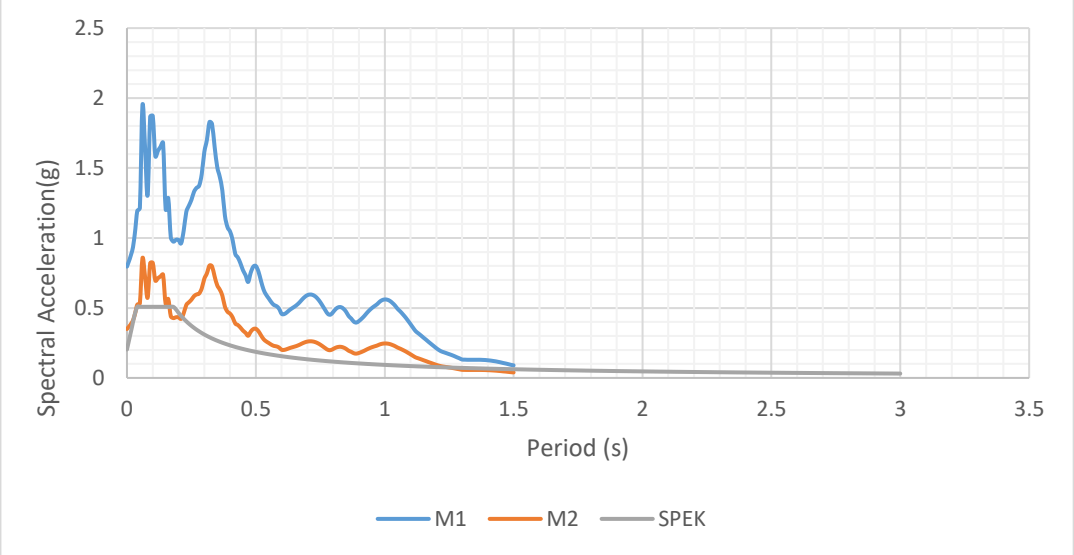

Figure A327. Scaled Vertical Response Spectra of Parkfield-02 (D2-4125) Earthquake

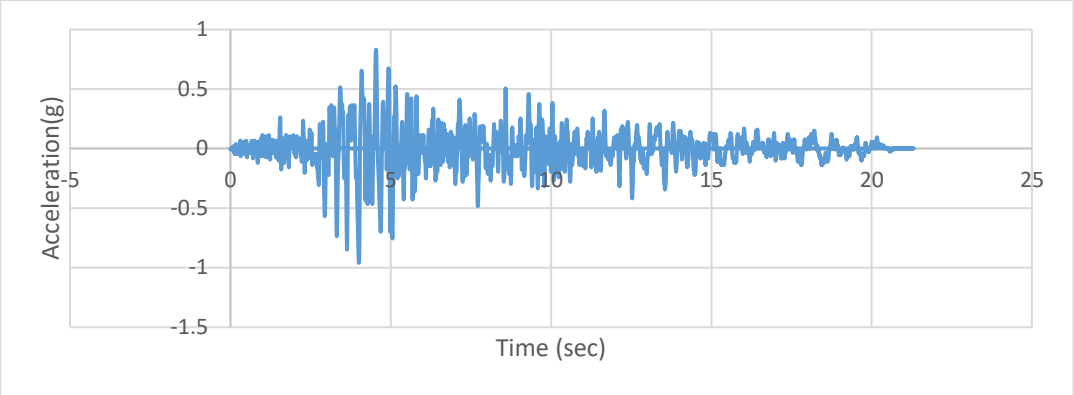

Figure A328. Scaled Acceleration Time Histories of Parkfield-02 (D2-4125X) Earthquake

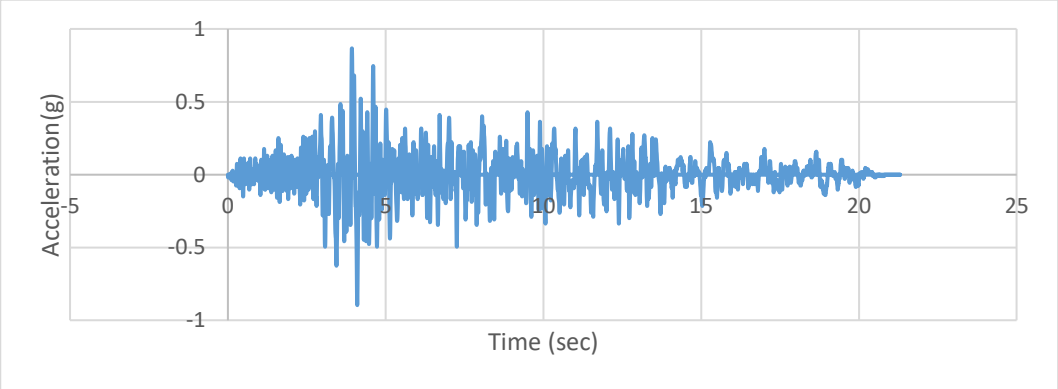

Figure A329. Scaled Acceleration Time Histories of Parkfield-02 (D2-4125Y) Earthquake

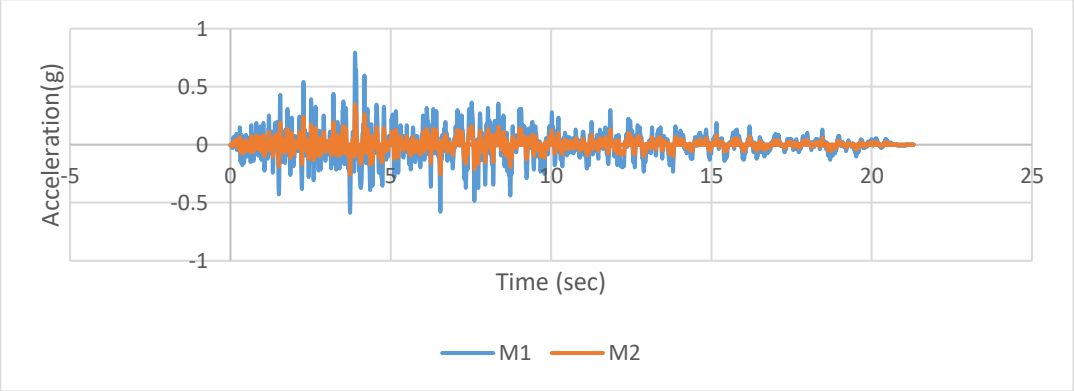

Figure A330. Scaled Acceleration Time Histories of Parkfield-02 (D2-4125Z) Earthquake

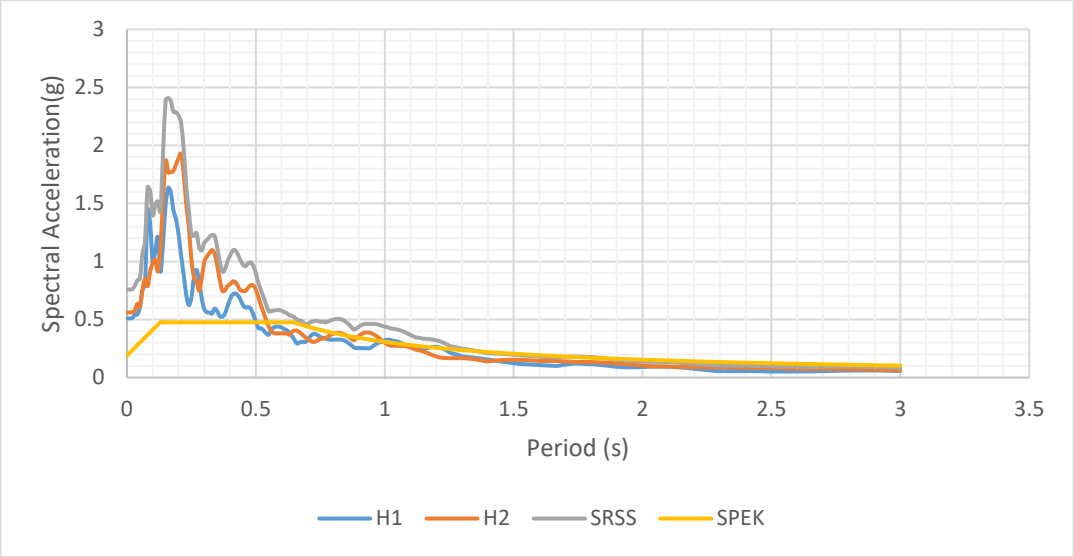

Figure A331. Scaled Horizontal Response Spectra of Parkfield (D3-31) Earthquake

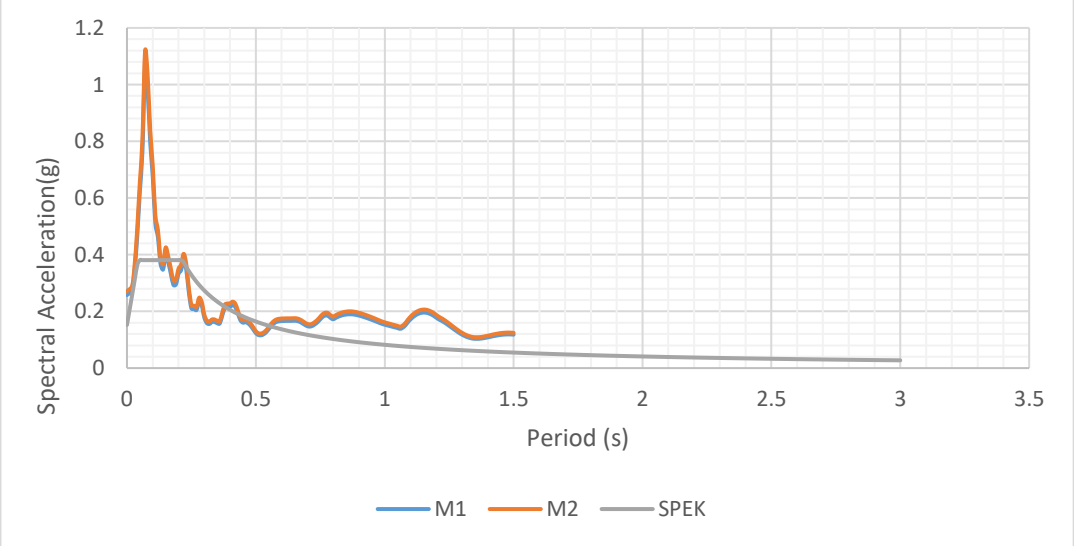

Figure A332.Scaled Vertical Response Spectra of Parkfield (D3-31) Earthquake

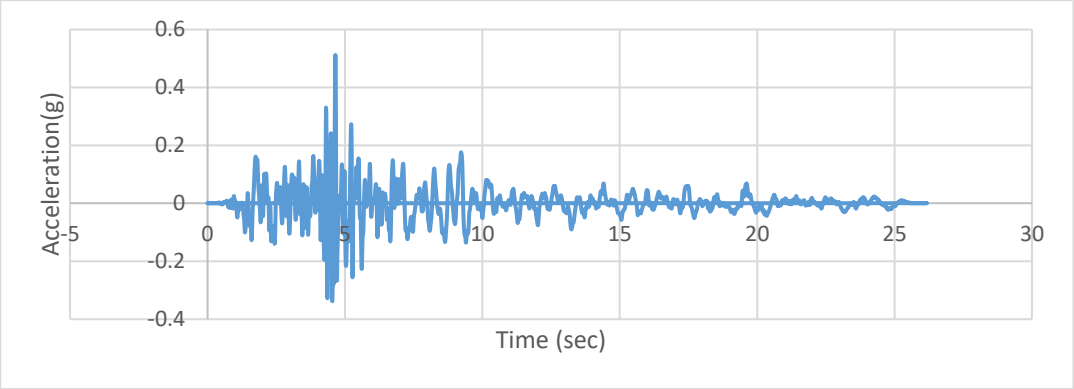

Figure A333. Scaled Acceleration Time Histories of Parkfield (D3-31X) Earthquake

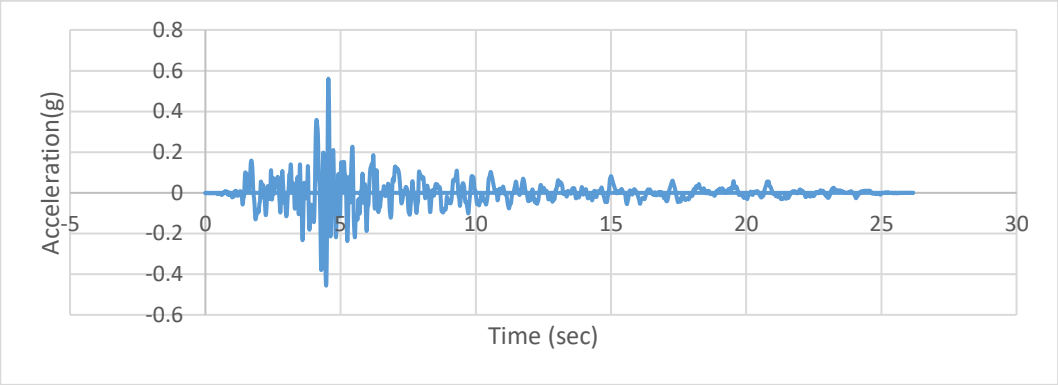

Figure A334. Scaled Acceleration Time Histories of Parkfield (D3-31Y) Earthquake

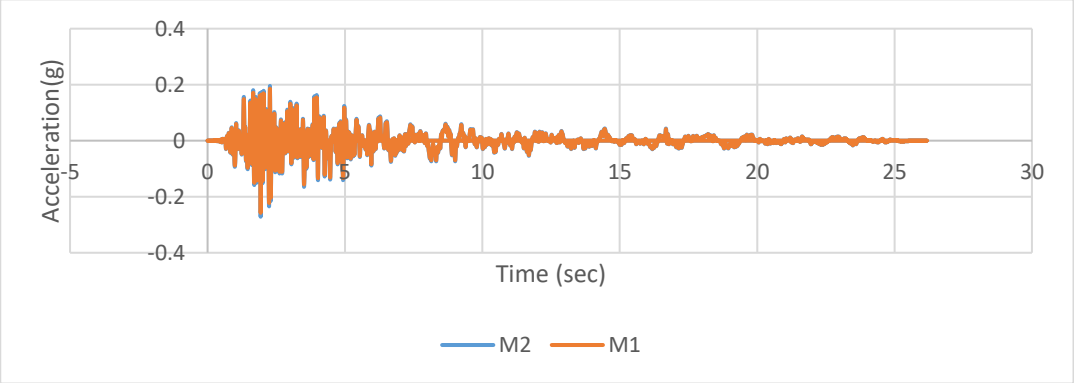

Figure A335. Scaled Acceleration Time Histories of Parkfield (D3-31Z) Earthquake

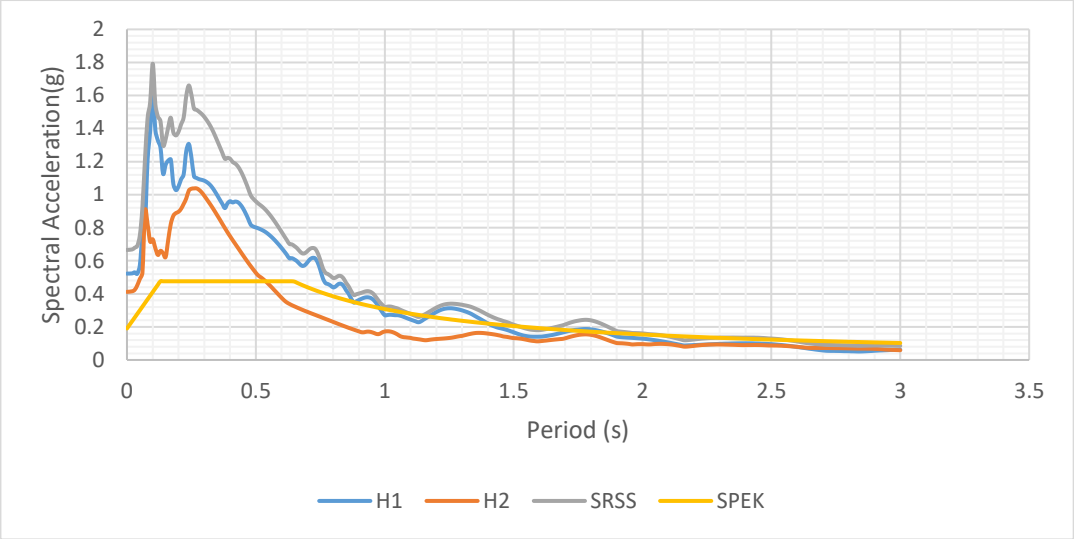

Figure A336. Scaled Horizontal Response Spectra of Imperial Valley-06 (D3-164) Earthquake

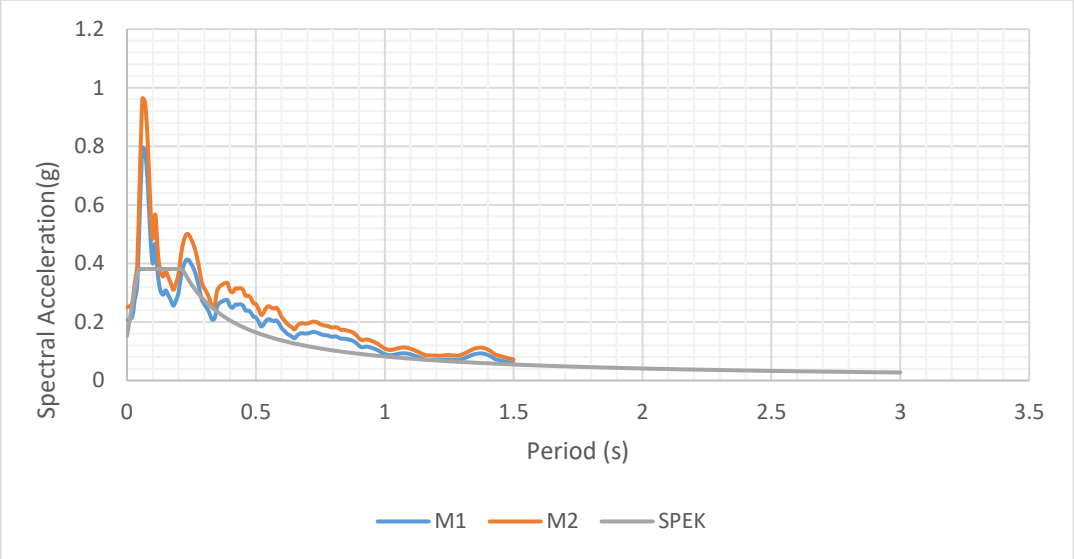

Figure A337. Scaled Vertical Response Spectra of Imperial Valley-06 (D3-164) Earthquake

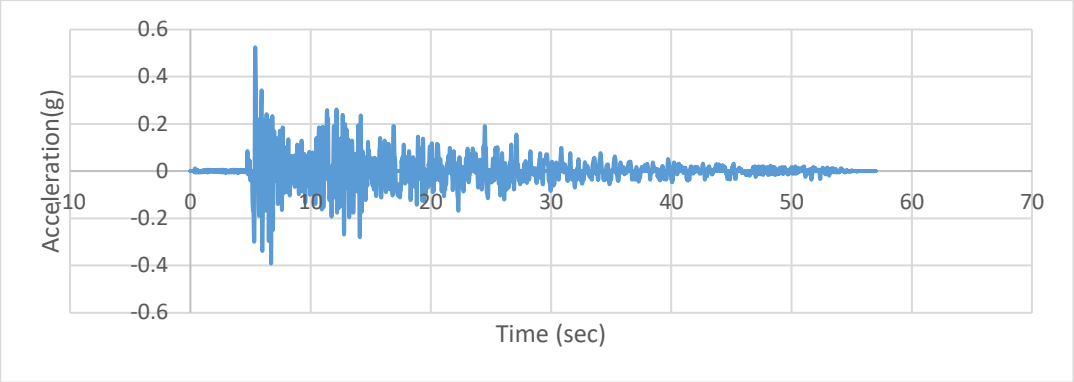

Figure A338. Scaled Acceleration Time Histories of Imperial Valley-06 (D3-164X) Earthquake

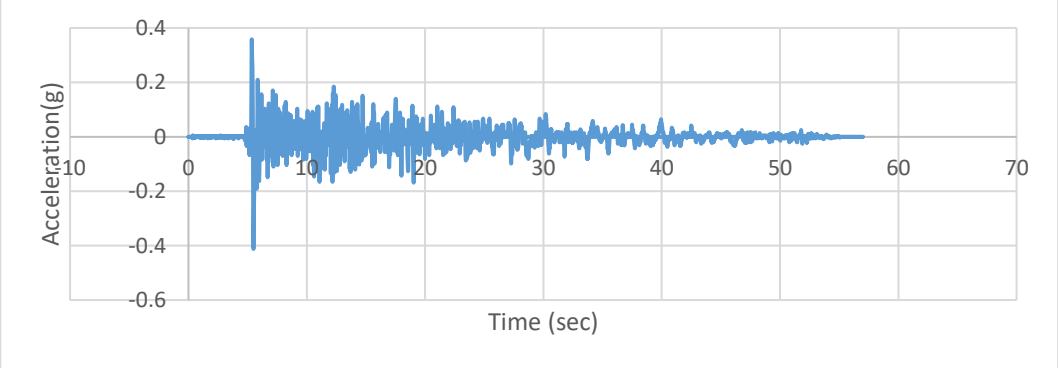

Figure A339. Scaled Acceleration Time Histories of Imperial Valley-06 (D3-164Y) Earthquake

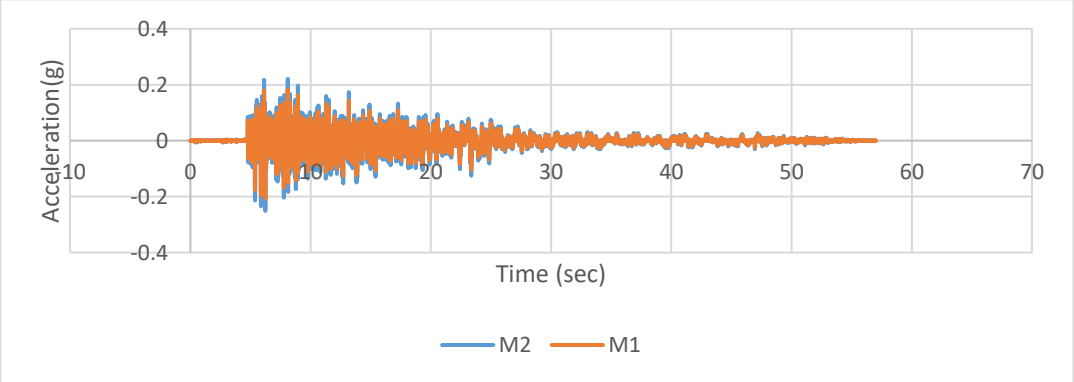

Figure A340. Scaled Acceleration Time Histories of Imperial Valley-06 (D3-164Z) Earthquake

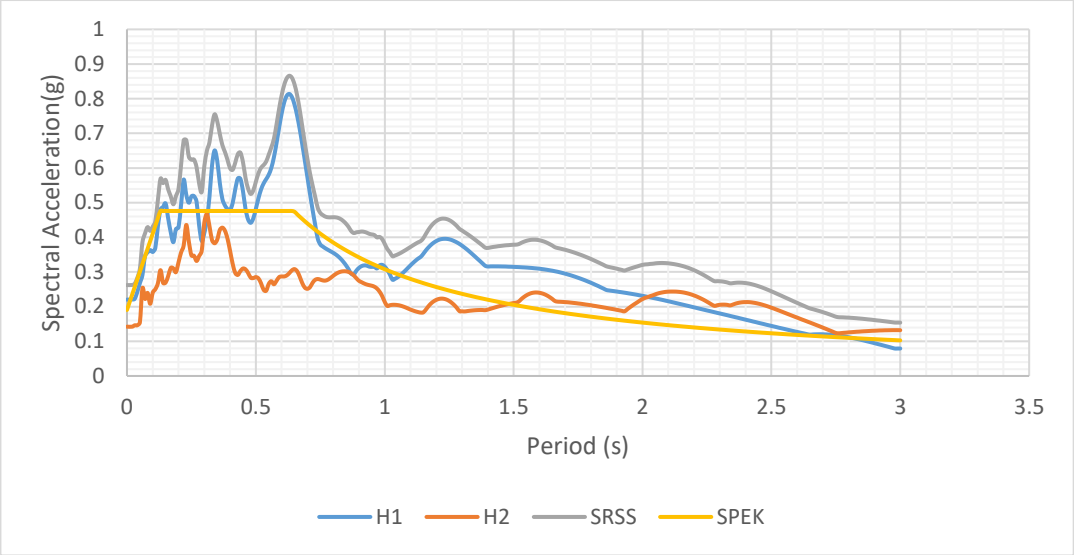

Figure A341. Scaled Horizontal Response Spectra of Victoria (D3-266) Earthquake

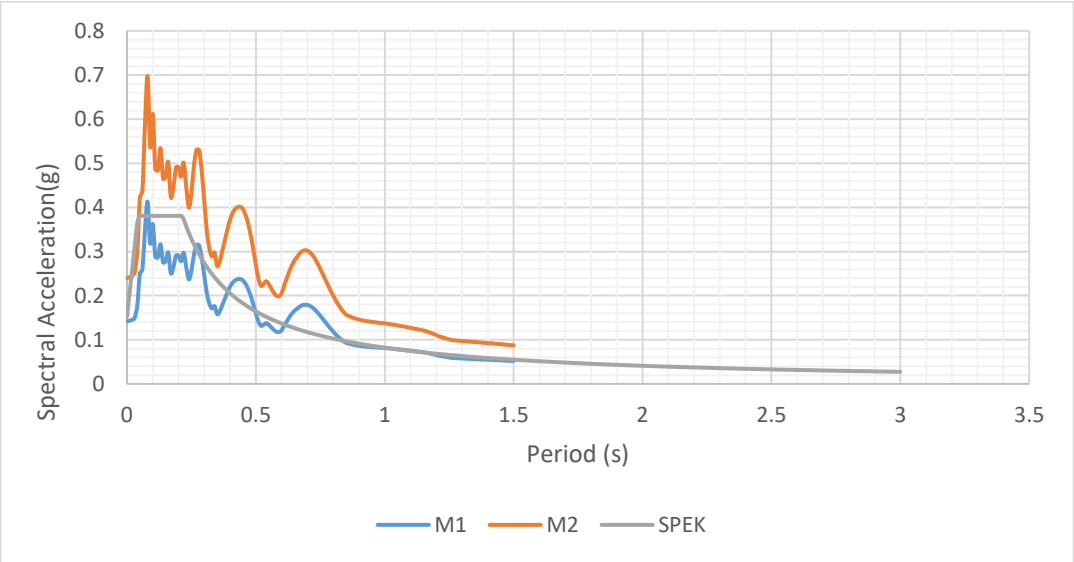

Figure A342. Scaled Vertical Response Spectra of Victoria (D3-266) Earthquake

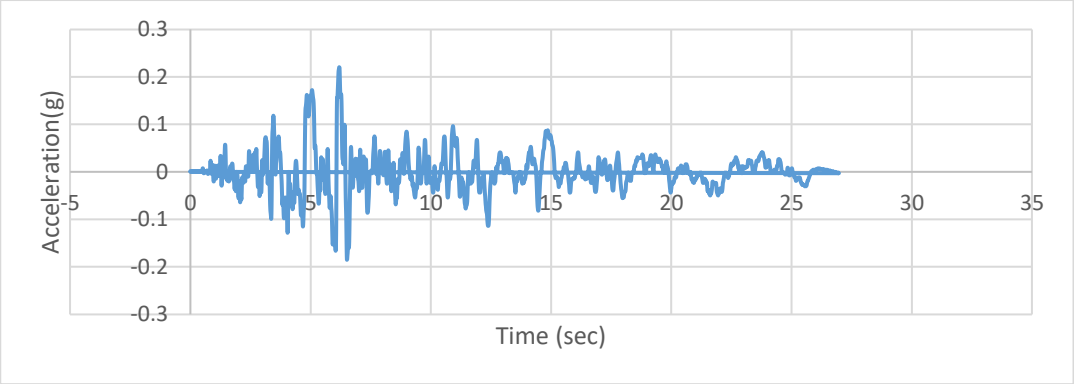

Figure A343. Scaled Acceleration Time Histories of Victoria (D3-266X) Earthquake

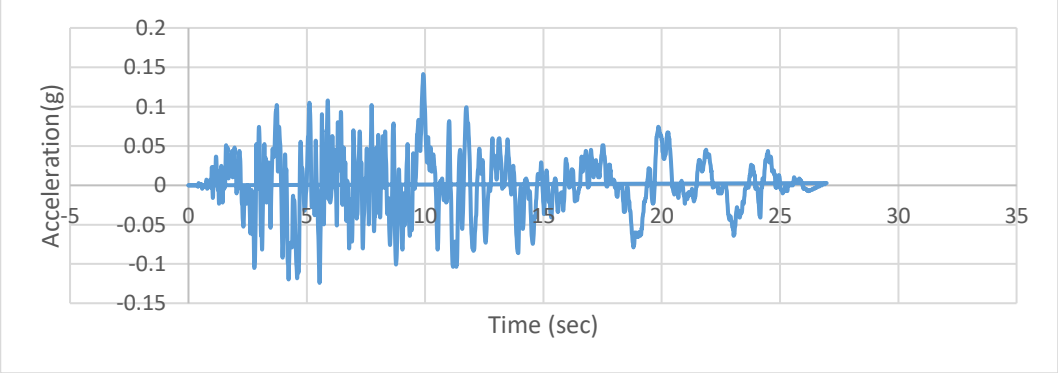

Figure A344. Scaled Acceleration Time Histories of Victoria (D3-266Y) Earthquake

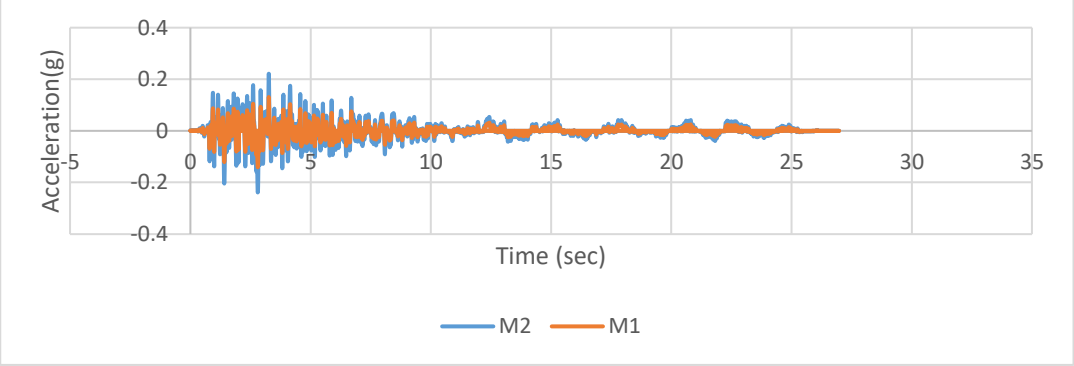

Figure A345. Scaled Acceleration Time Histories of Victoria (D3-266Z) Earthquake

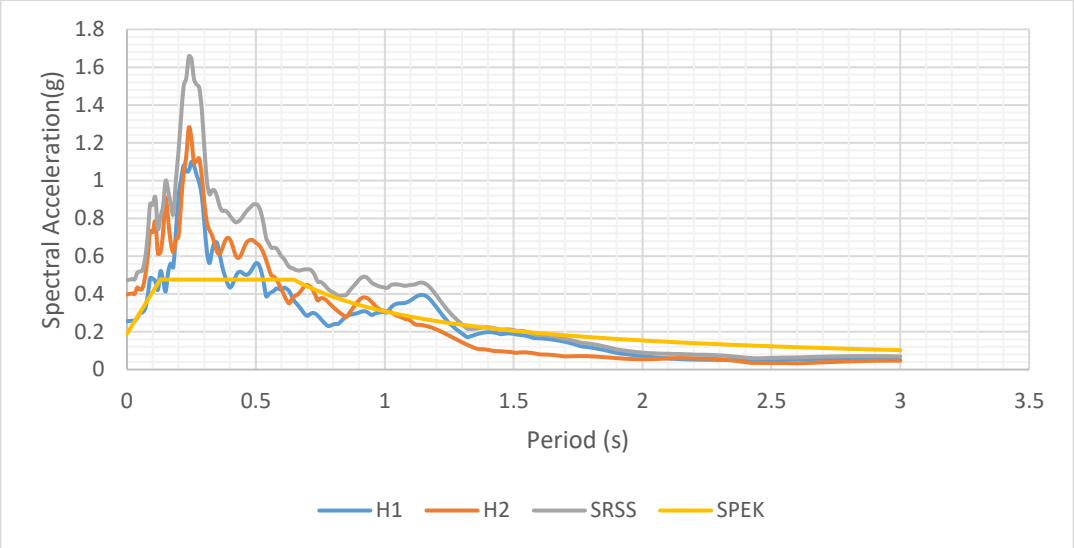

Figure A346. Scaled Horizontal Response Spectra of Morgan Hill (D3-458) Earthquake

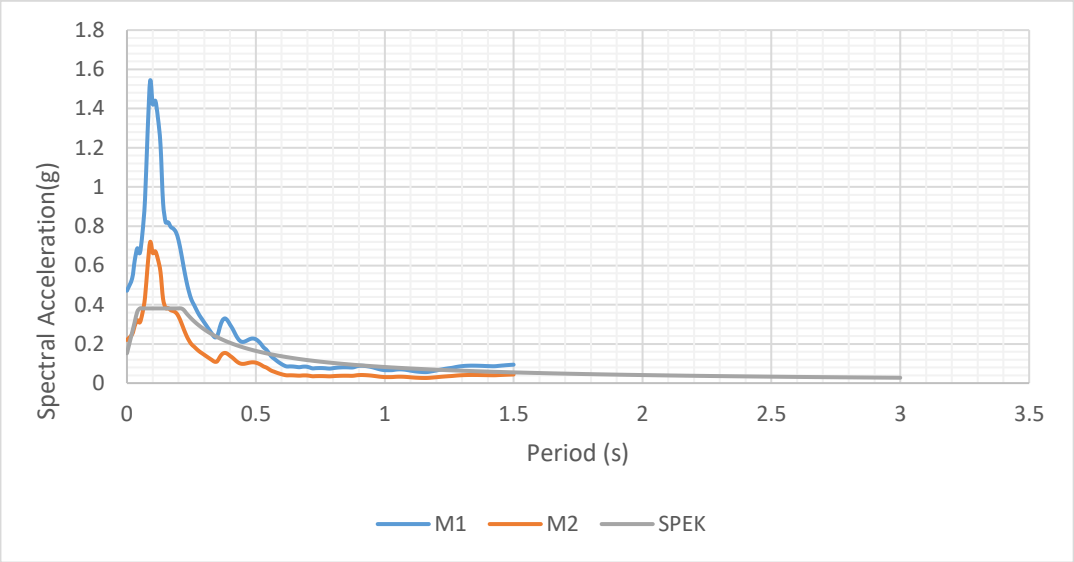

Figure A347. Scaled Horizontal Response Spectra of Morgan Hill (D3-458) Earthquake

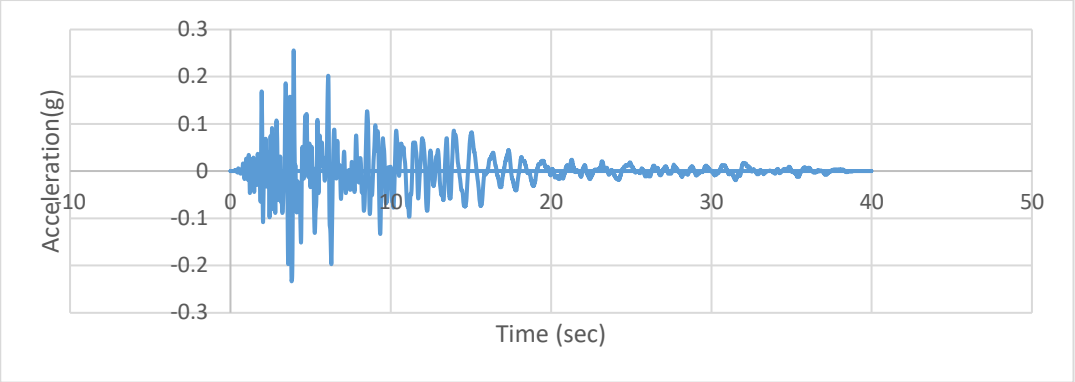

Figure A348. Scaled Acceleration Time Histories of Morgan Hill (D3-458X) Earthquake

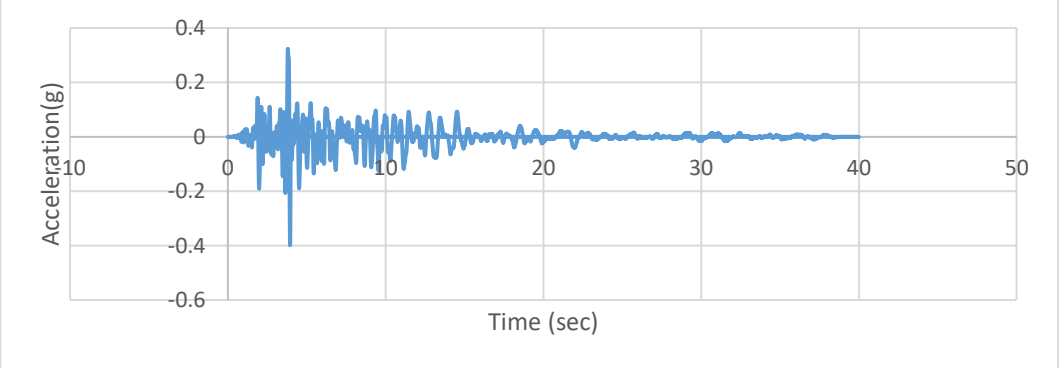

Figure A349. Scaled Acceleration Time Histories of Morgan Hill (D3-458Y) Earthquake

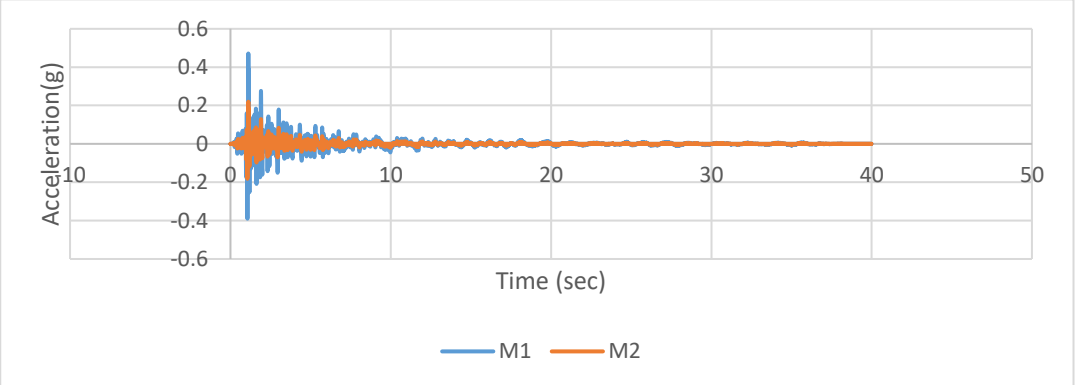

Figure A350. Scaled Acceleration Time Histories of Morgan Hill (D3-458Z) Earthquake

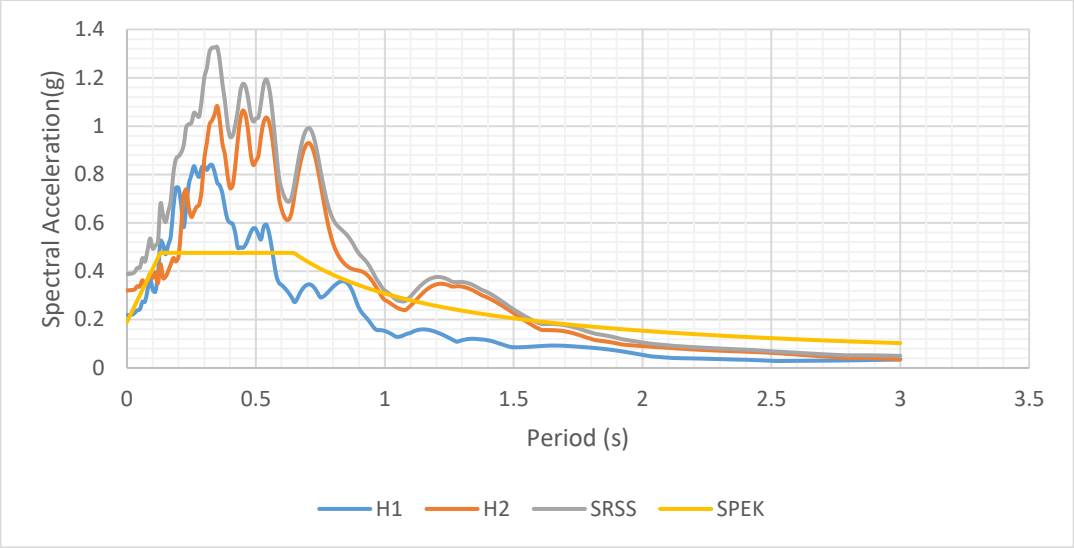

Figure A351. Scaled Horizontal Response Spectra of Landers (D3-848) Earthquake

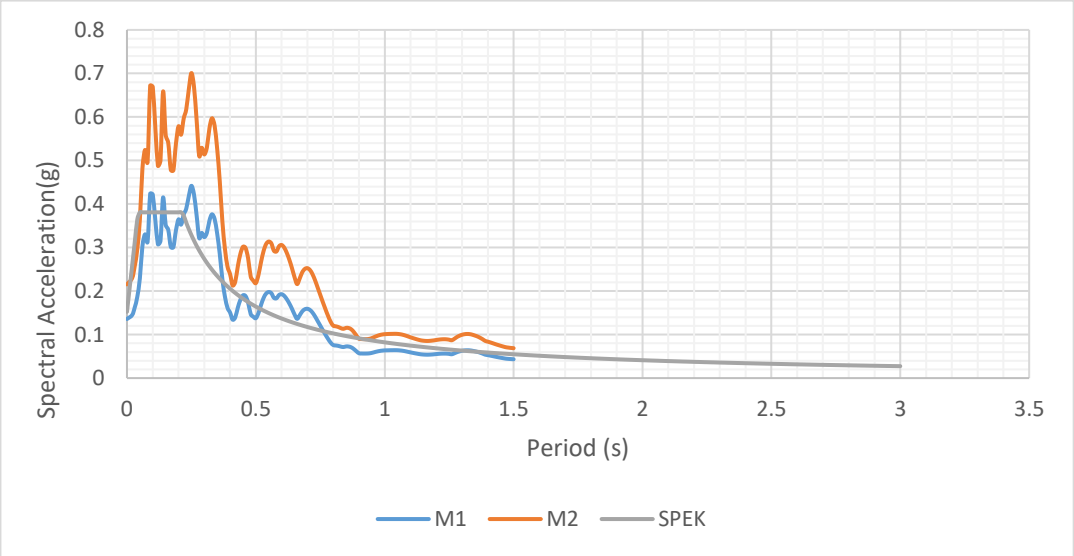

Figure A352. Scaled Vertical Response Spectra of Landers (D3-848) Earthquake

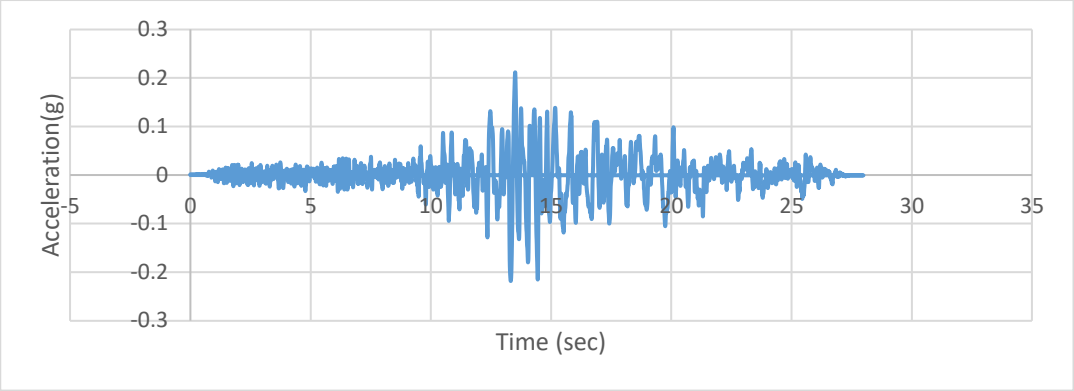

Figure A353. Scaled Acceleration Time Histories of Landers (D3-848X) Earthquake

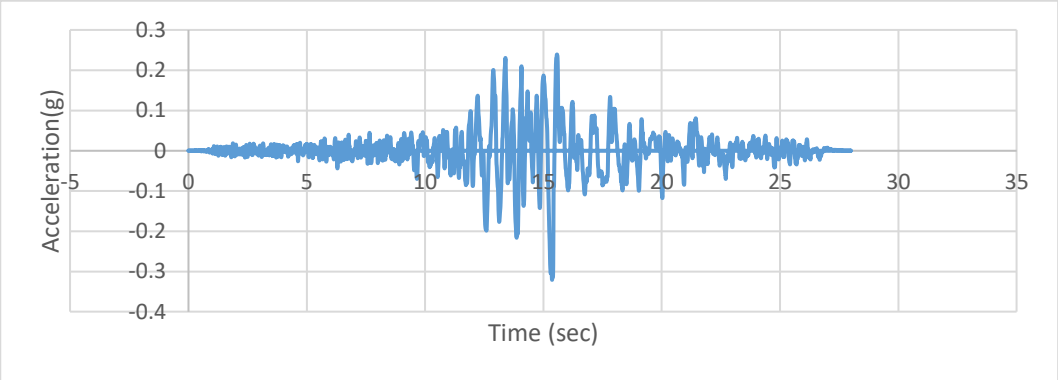

Figure A354. Scaled Acceleration Time Histories of Landers (D3-848Y) Earthquake

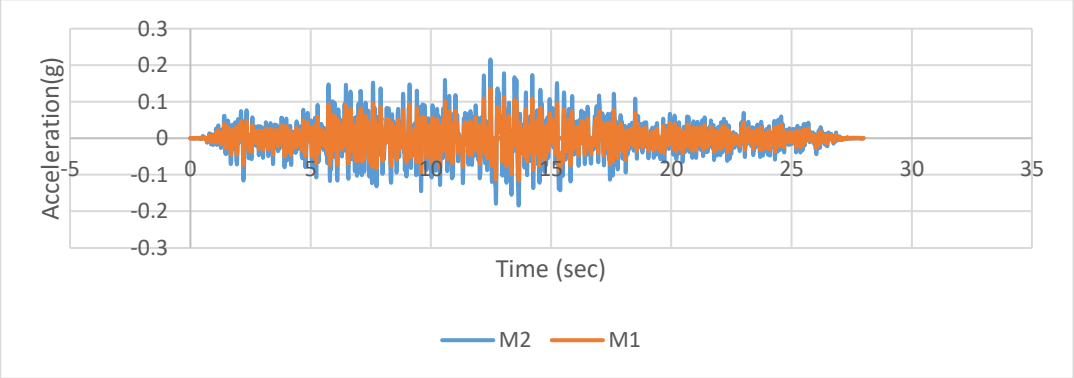

Figure A355. Scaled Acceleration Time Histories of Landers (D3-848Z) Earthquake

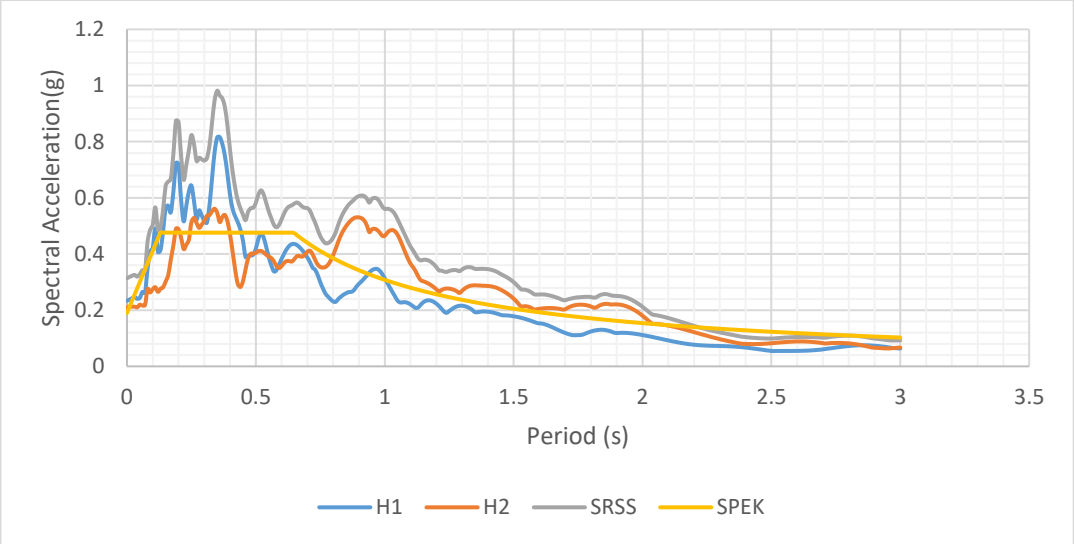

Figure A356. Scaled Horizontal Response Spectra of Landers (D3-850) Earthquake

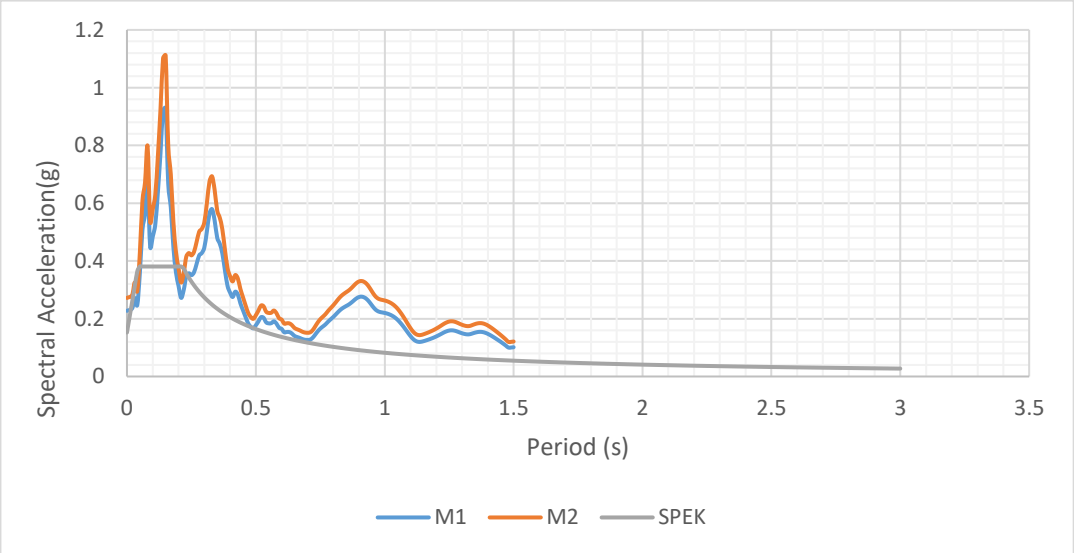

Figure A357. Scaled Vertical Response Spectra of Landers (D3-850) Earthquake

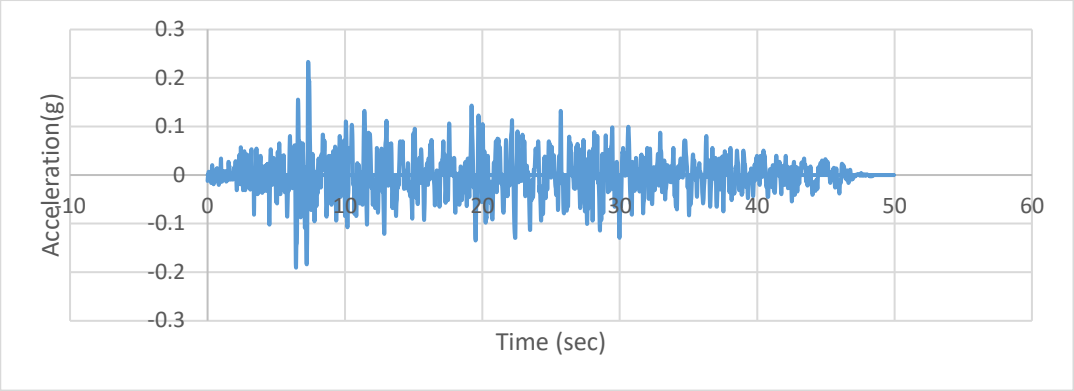

Figure A358. Scaled Acceleration Time Histories of Landers (D3-850X) Earthquake

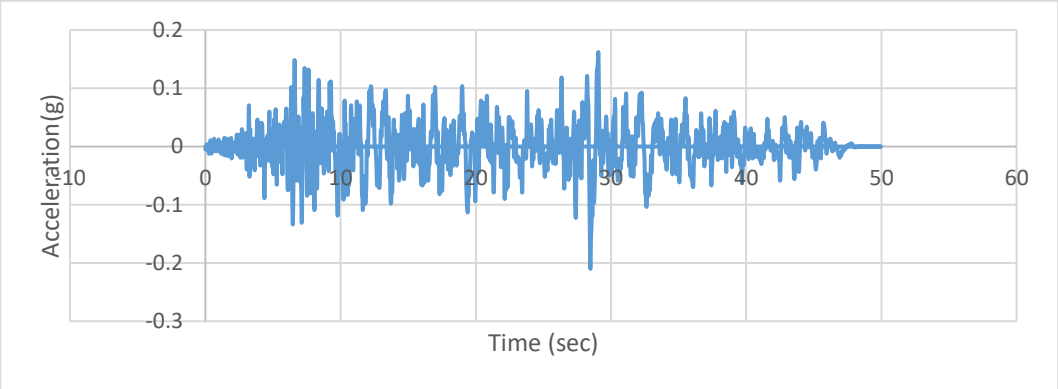

Figure A359. Scaled Acceleration Time Histories of Landers (D3-850Y) Earthquake

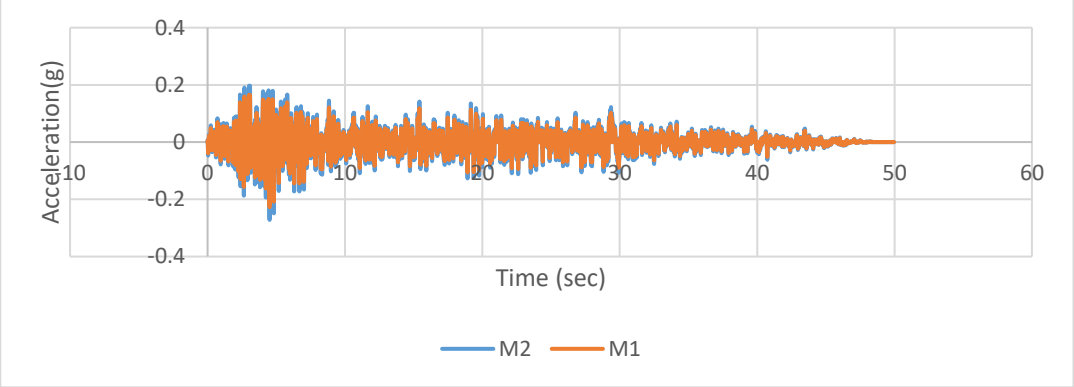

Figure A360. Scaled Acceleration Time Histories of Landers (D3-850Z) Earthquake

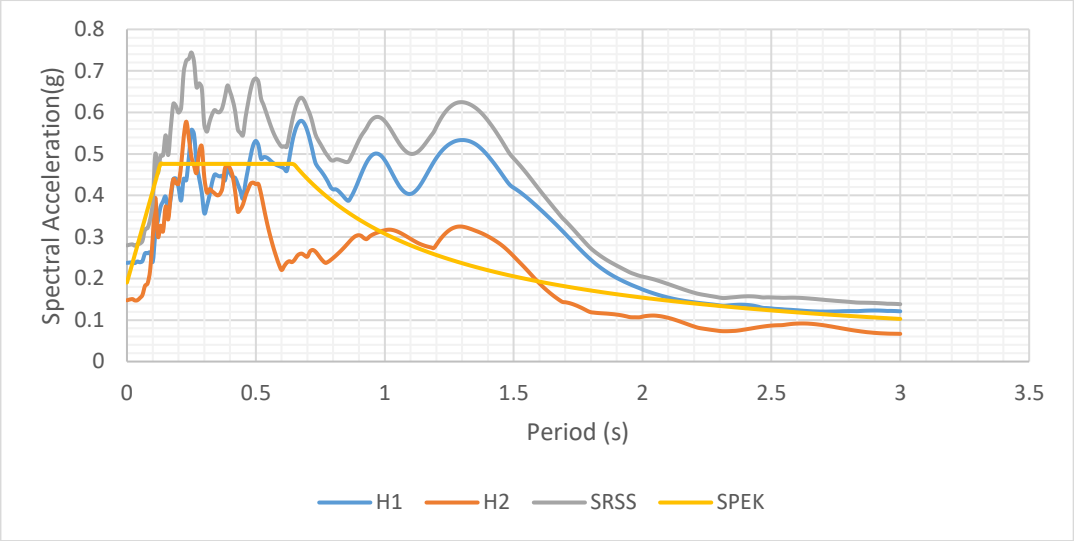

Figure A361. Scaled Horizontal Response Spectra of Landers (D3-900) Earthquake

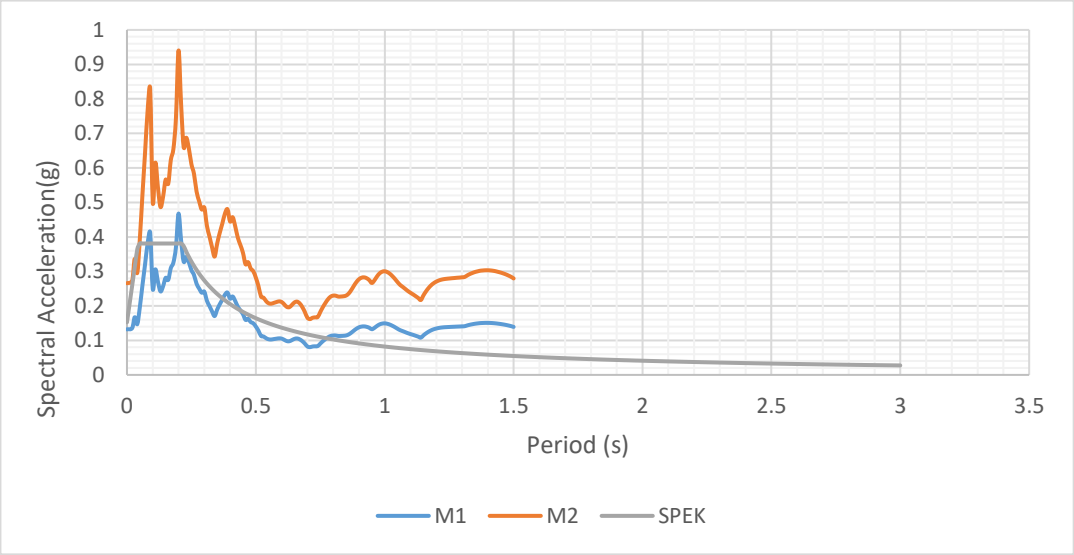

Figure A362. Scaled Vertical Response Spectra of Landers (D3-900) Earthquake

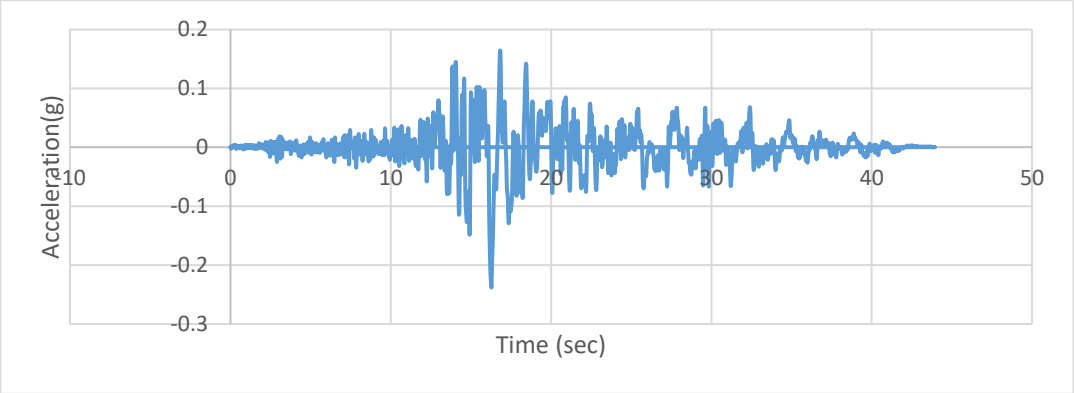

Figure A363. Scaled Acceleration Time Histories of Landers (D3-900X) Earthquake

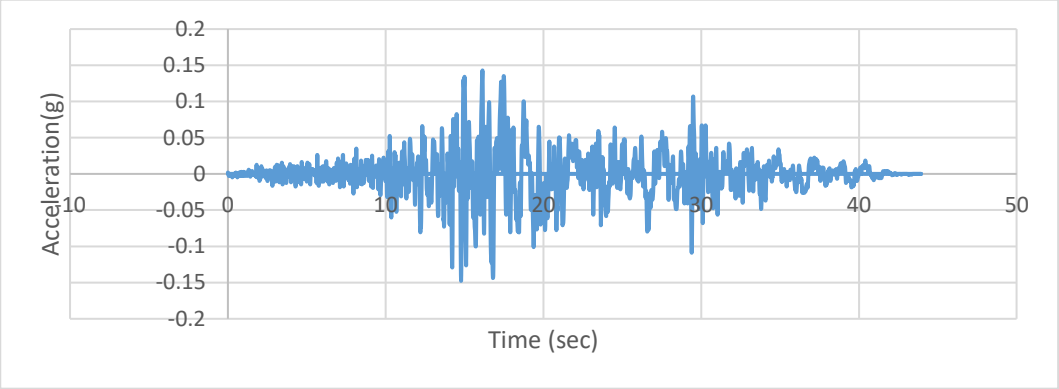

Figure A364. Scaled Acceleration Time Histories of Landers (D3-900Y) Earthquake

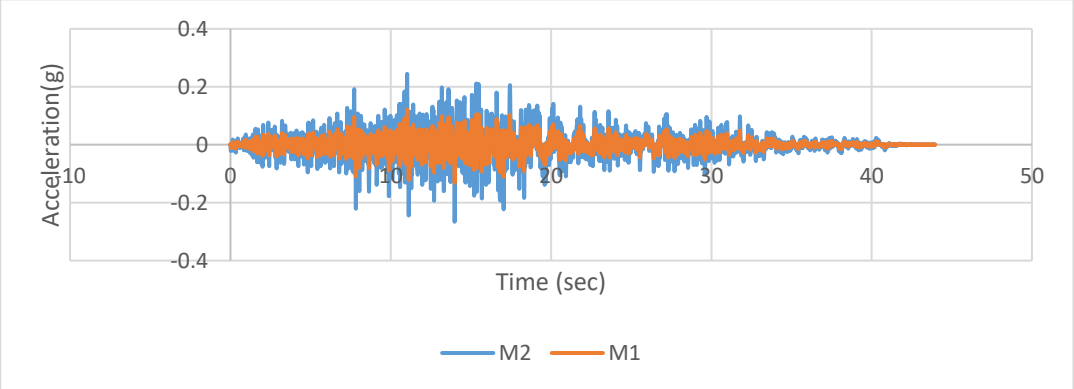

Figure A365. Scaled Acceleration Time Histories of Landers (D3-900Z) Earthquake

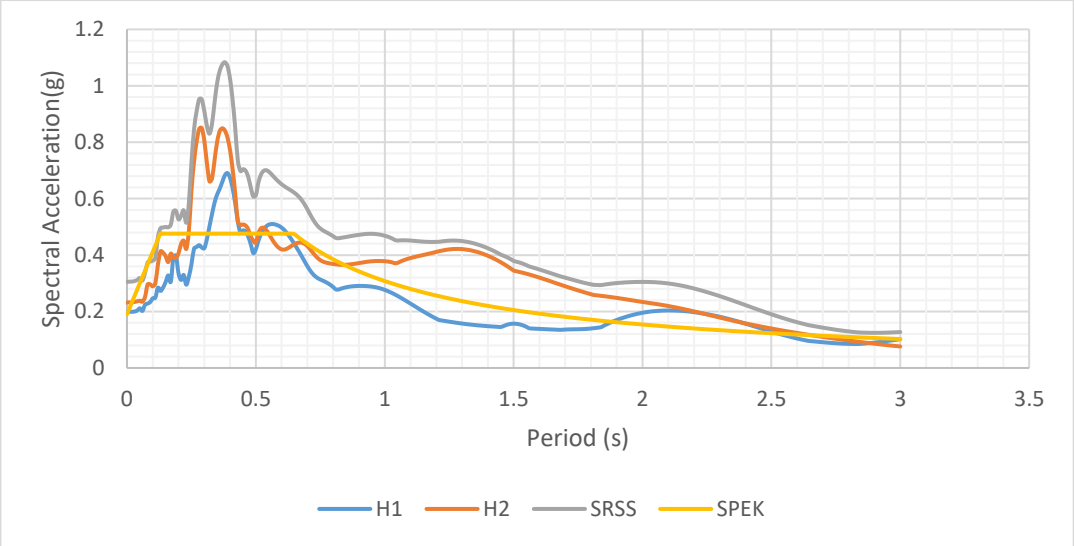

Figure A366. Scaled Horizontal Response Spectra of Kocaeli (D3-1158) Earthquake

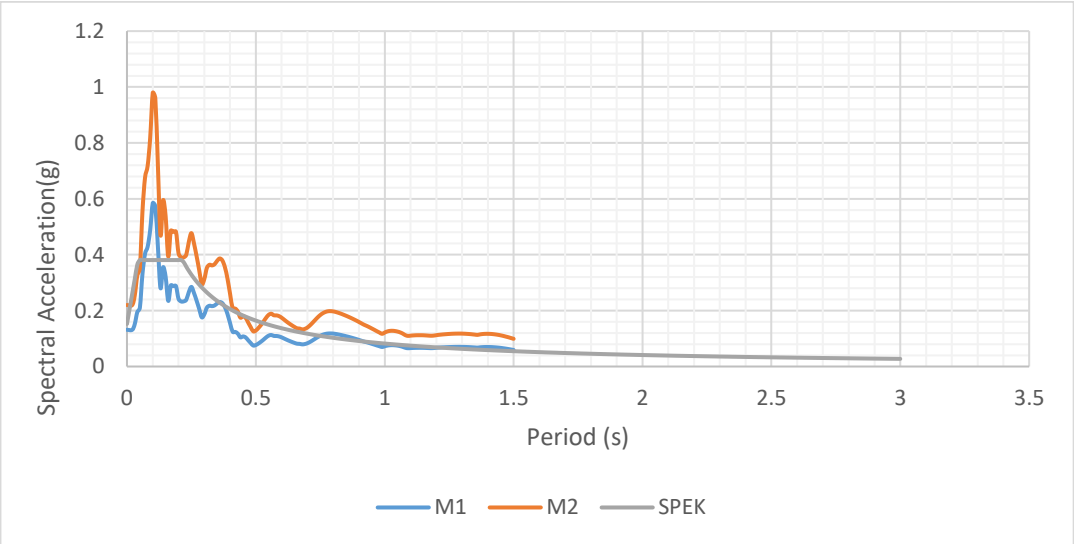

Figure A367. Scaled Vertical Response Spectra of Kocaeli (D3-1158) Earthquake

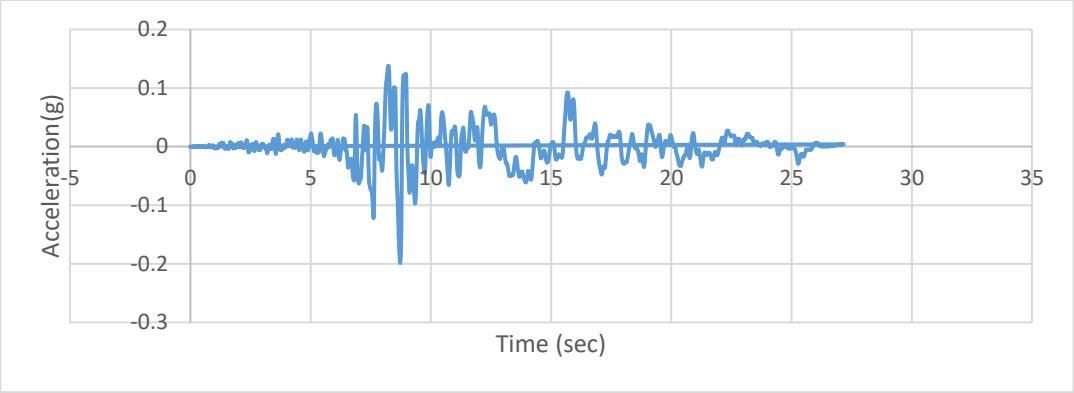

Figure A368. Scaled Acceleration Time Histories of Kocaeli (D3-1158X) Earthquake

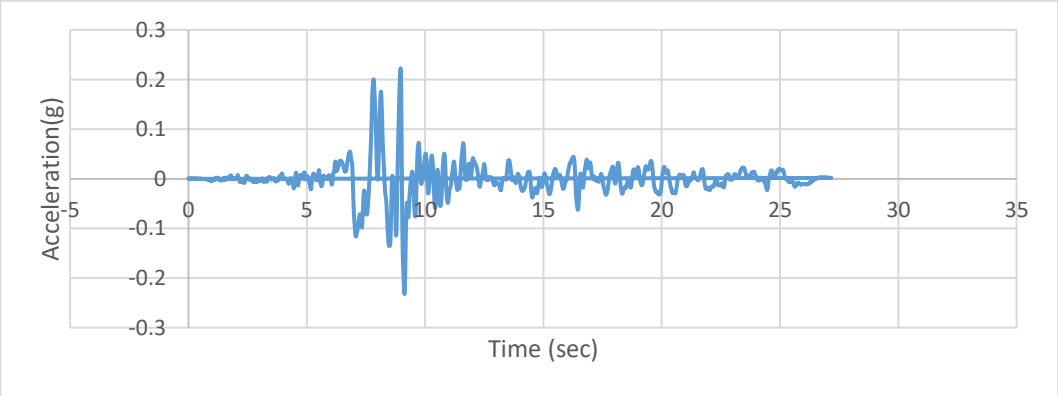

Figure A369. Scaled Acceleration Time Histories of Kocaeli (D3-1158Y) Earthquake

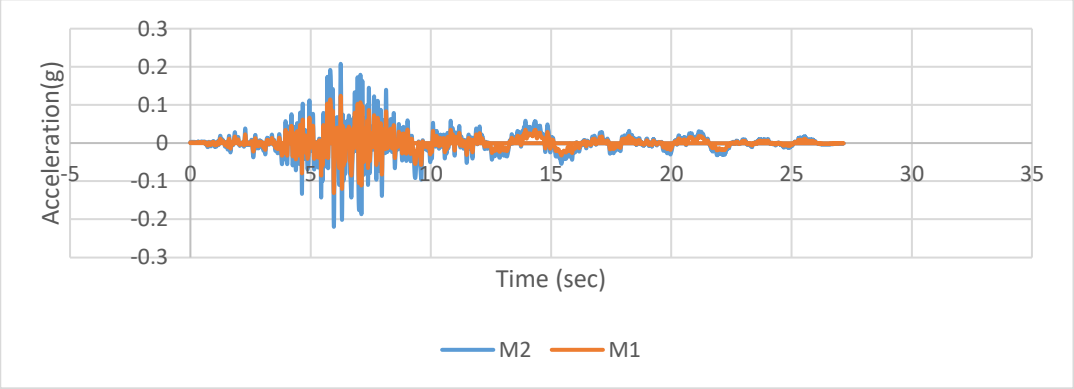

Figure A370. Scaled Acceleration Time Histories of Kocaeli (D3-1158Z) Earthquake

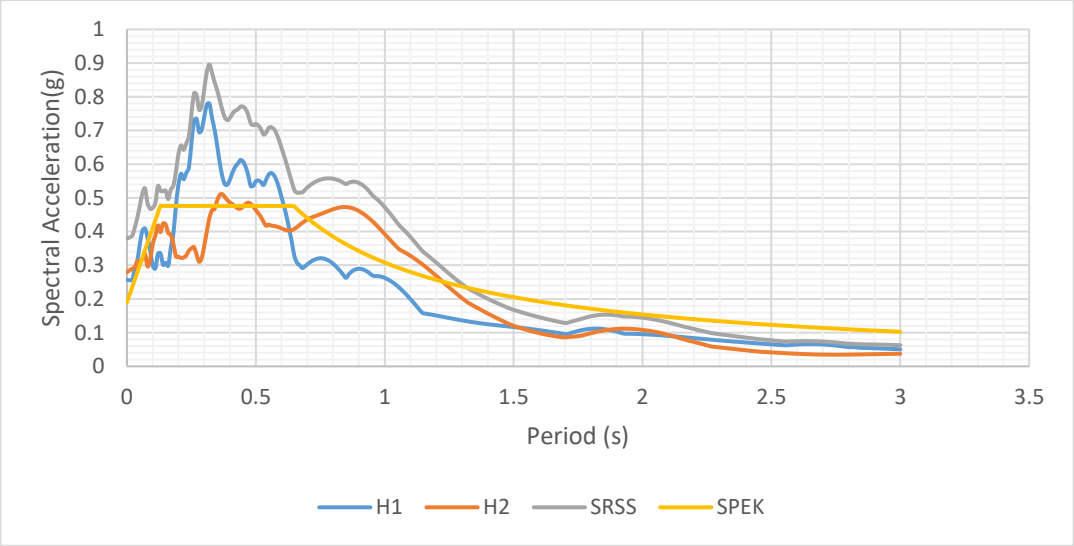

Figure A371. Scaled Horizontal Response Spectra of Duzce (D3-1602) Earthquake

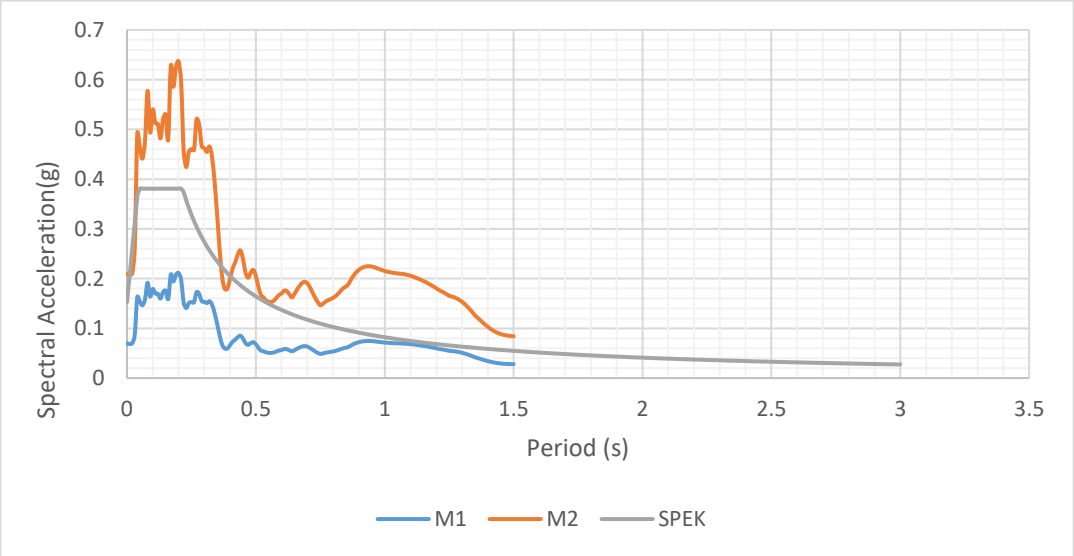

Figure A372. Scaled Vertical Response Spectra of Duzce (D3-1602) Earthquake

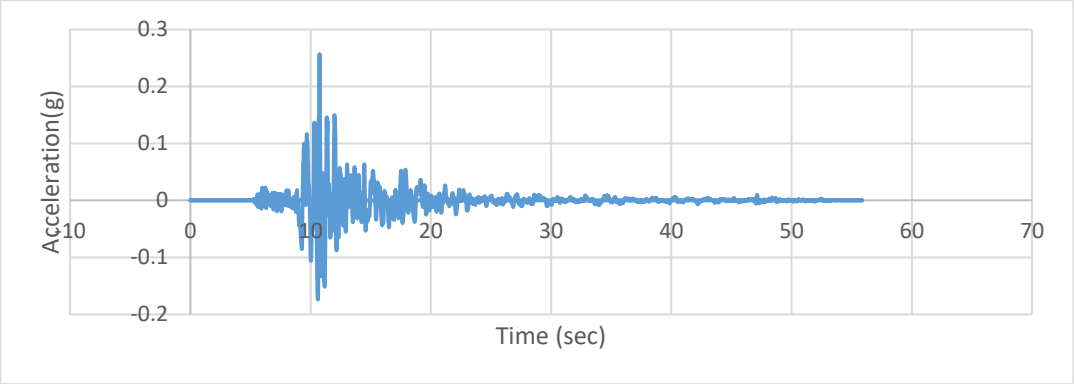

Figure A373.Scaled Acceleration Time Histories of Duzce (D3-1602X) Earthquake

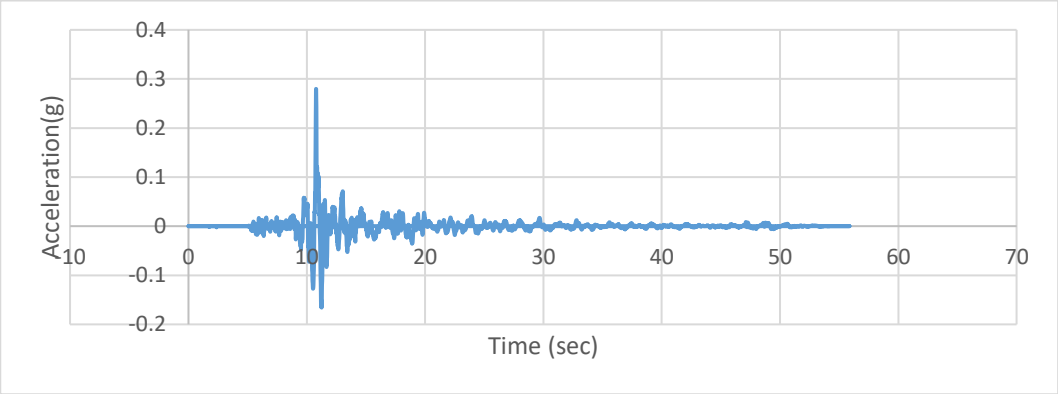

Figure A374.Scaled Acceleration Time Histories of Duzce (D3-1602Y) Earthquake

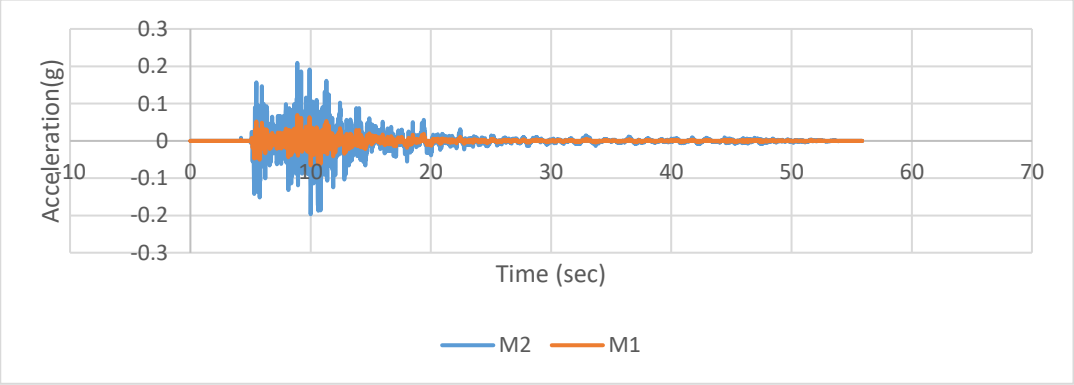

Figure A375.Scaled Acceleration Time Histories of Duzce (D3-1602Z) Earthquake

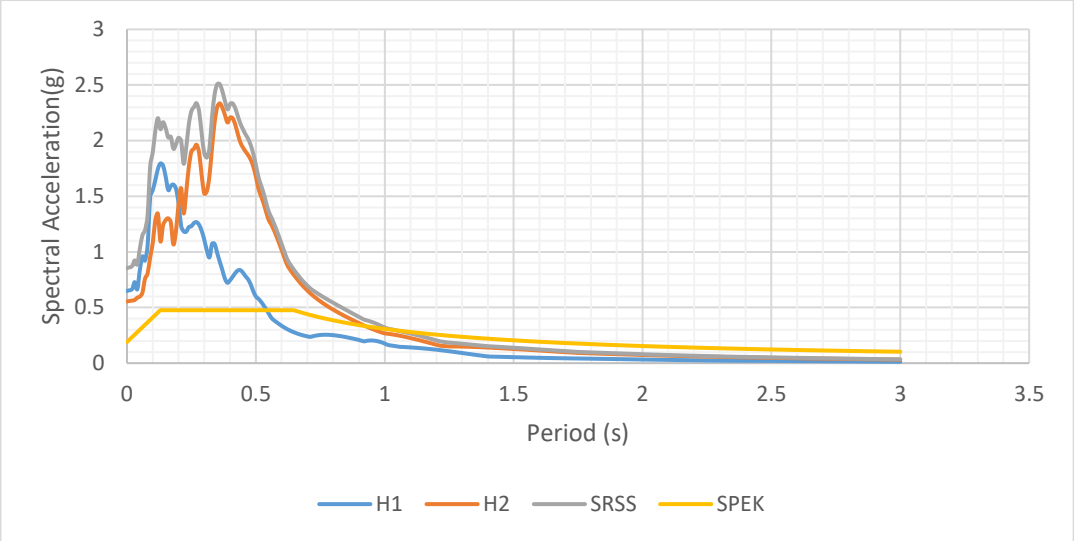

Figure A376.Scaled Horizontal Response Spectra of Northwest China-01(D3-1748) Earthquake

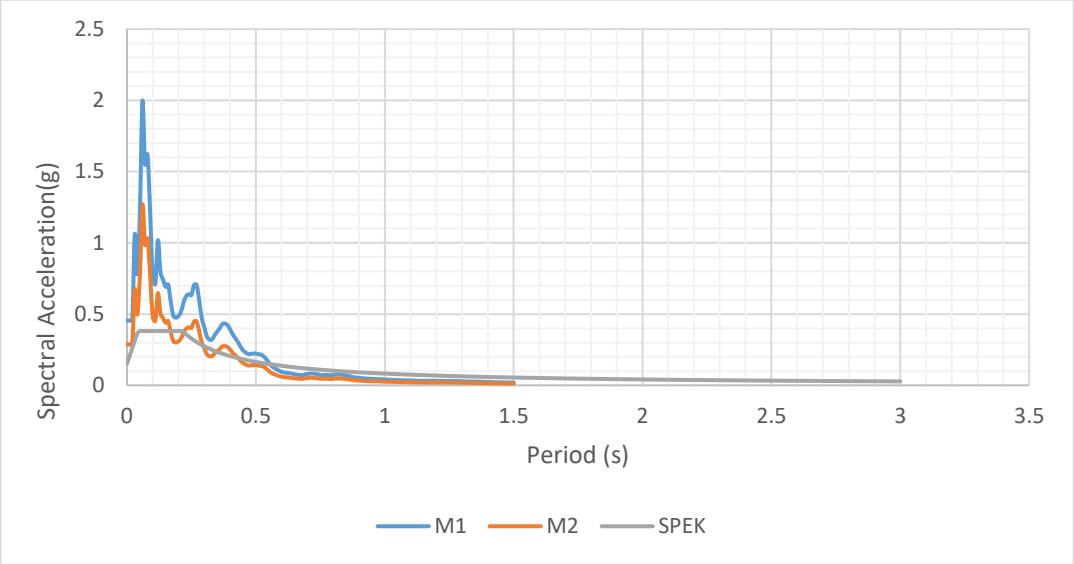

Figure A377. Scaled Vertical Response Spectra of Northwest China-01(D3-1748) Earthquake

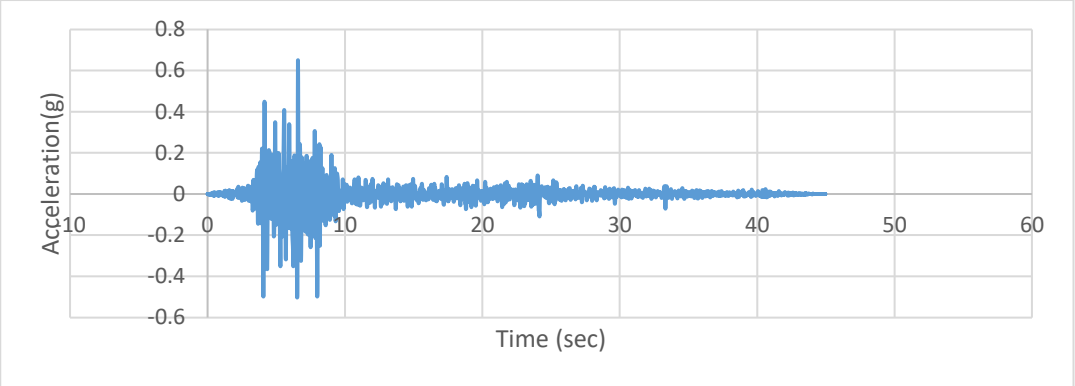

Figure A378.Scaled Acceleration Time Histories of Northwest China-01(D3-1748X) Earthquake

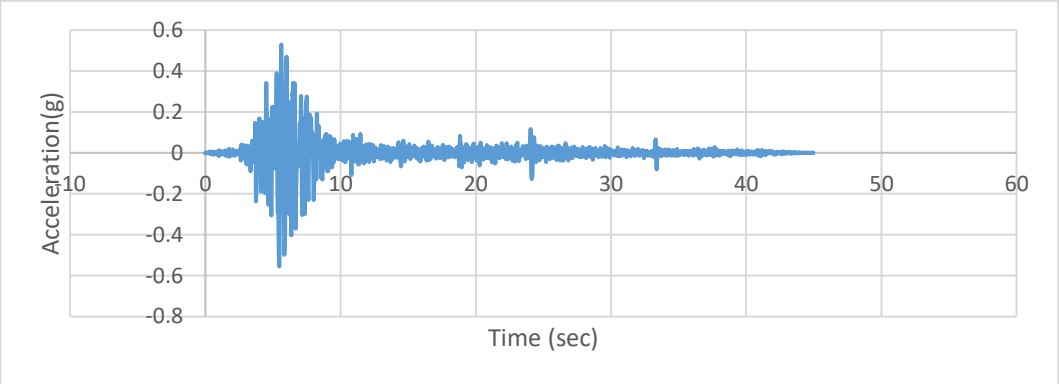

Figure A379. Scaled Acceleration Time Histories of Northwest China-01(D3-1748Y) Earthquake

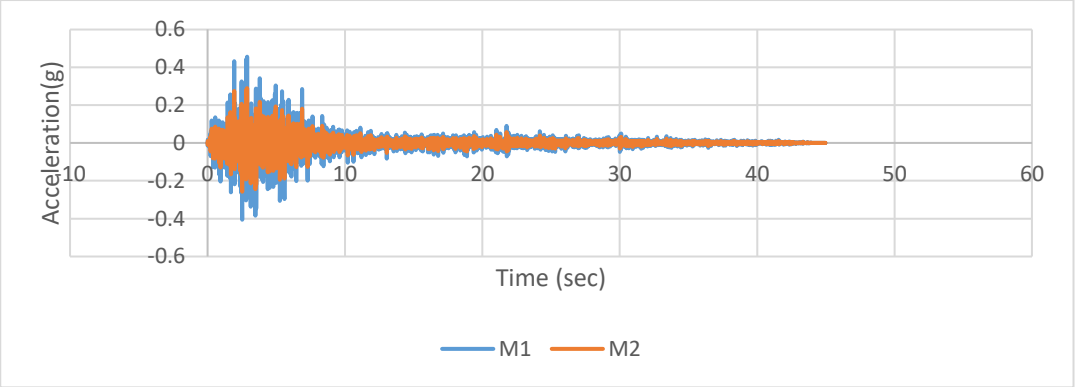

Figure A380. Scaled Acceleration Time Histories of Northwest China-01 (D3-1748Z) Earthquake

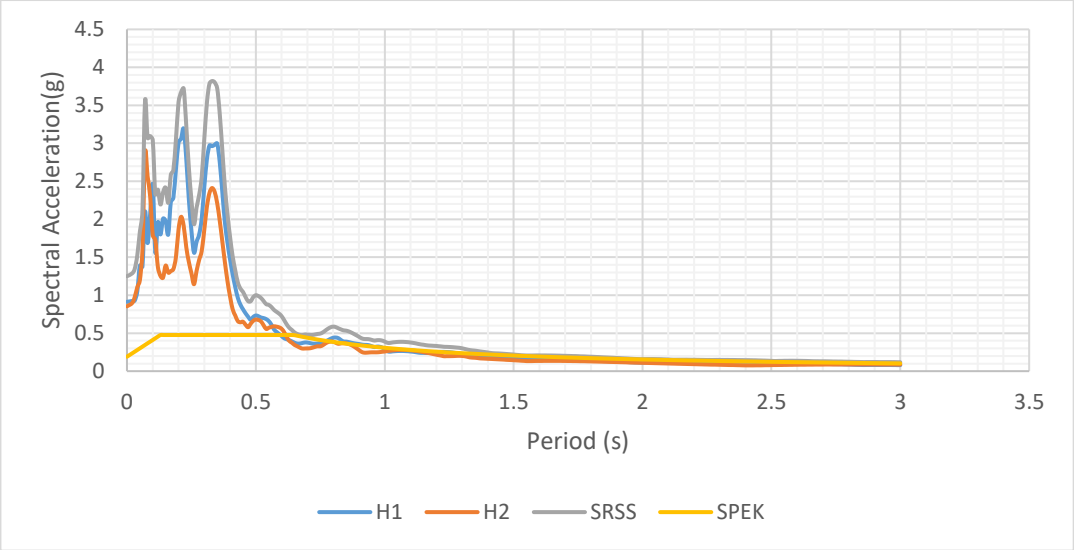

Figure A381.Scaled Horizontal Response Spectra of Parkfield-02 (D3-4125) Earthquake

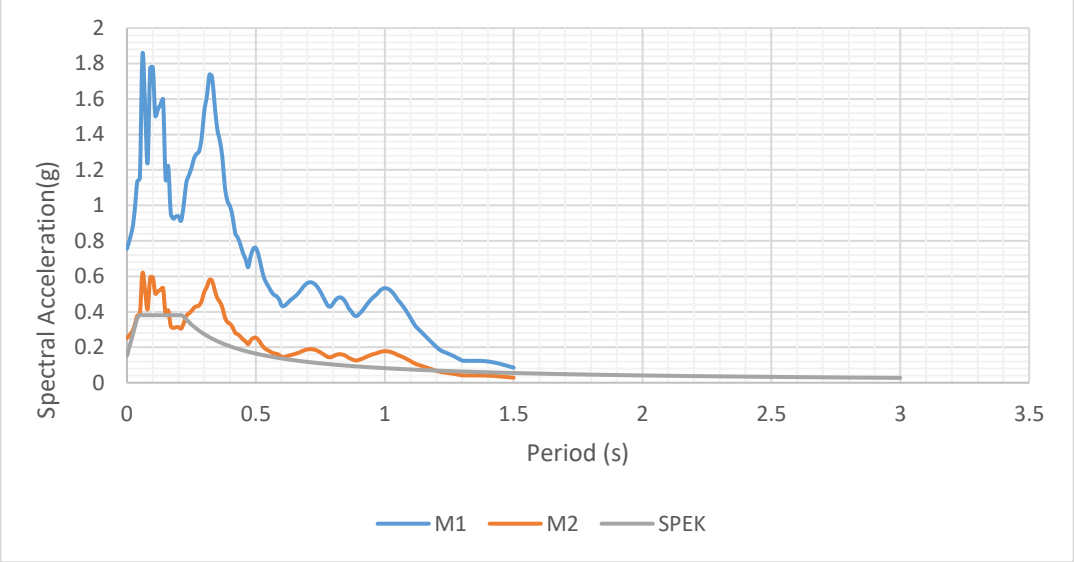

Figure A382. Scaled Vertical Response Spectra of Parkfield-02 (D3-4125) Earthquake

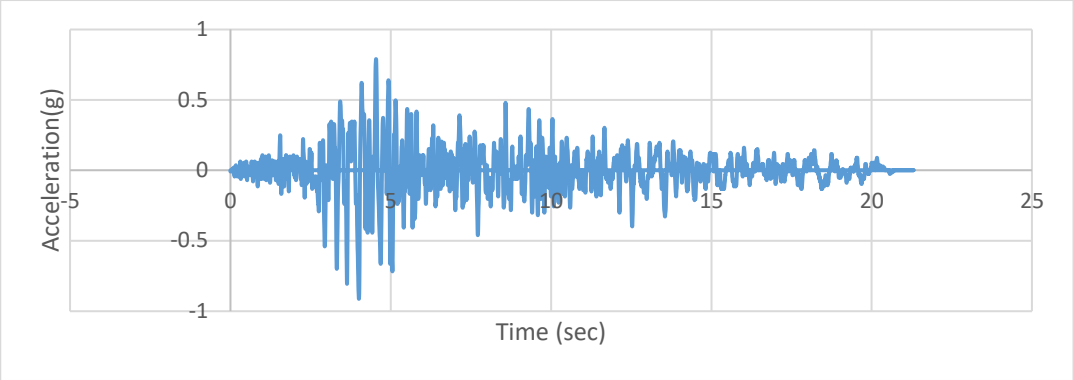

Figure A383. Scaled Acceleration Time Histories of Parkfield-02 (D3-4125X) Earthquake

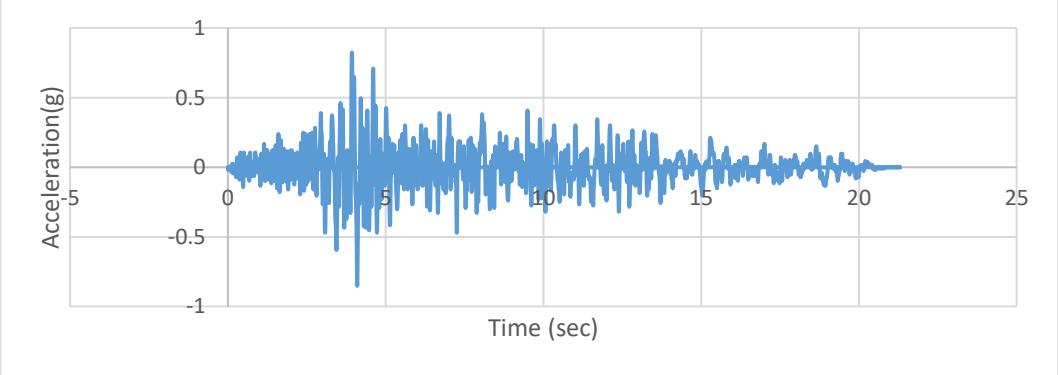

Figure A384. Scaled Acceleration Time Histories of Parkfield-02 (D3-4125Y) Earthquake

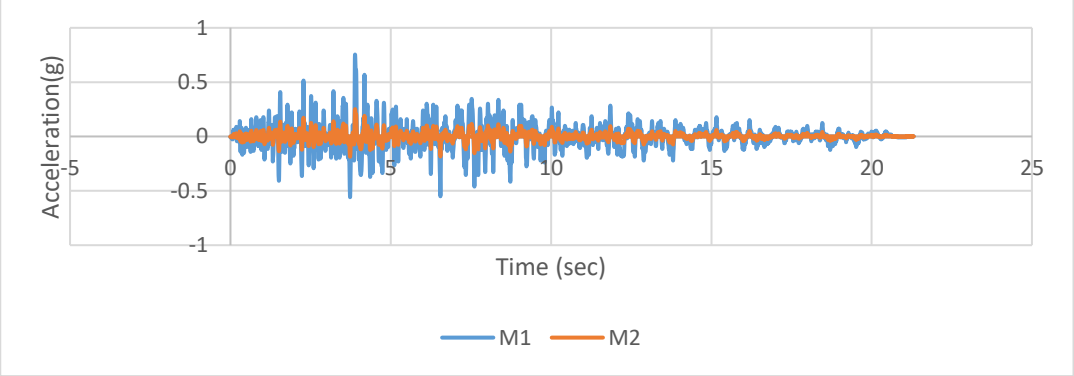

Figure A385. Scaled Acceleration Time Histories of Parkfield-02 (D3-4125Z) Earthquake

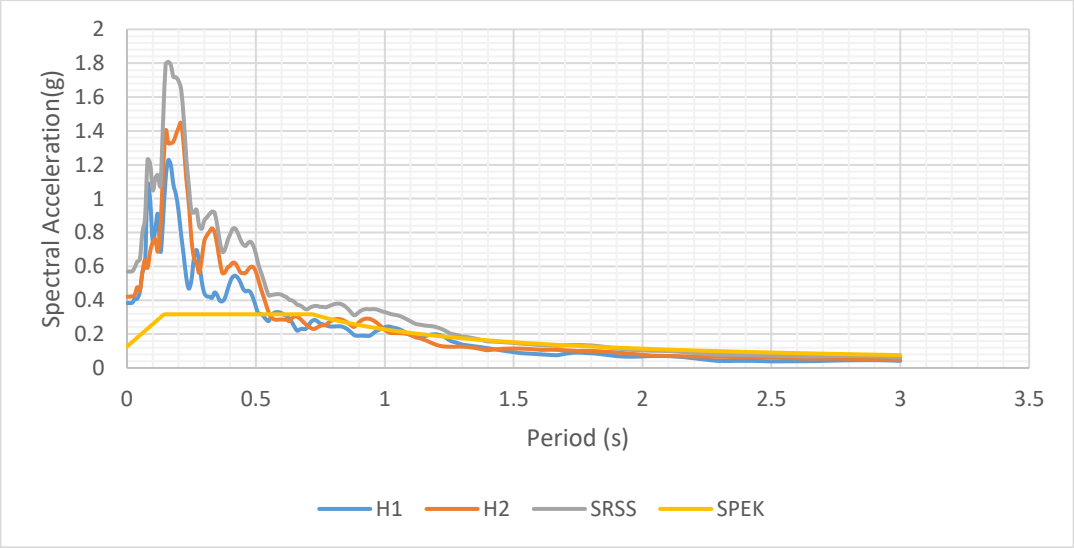

Figure A386. Scaled Horizontal Response Spectra of Parkfield (D4-31) Earthquake

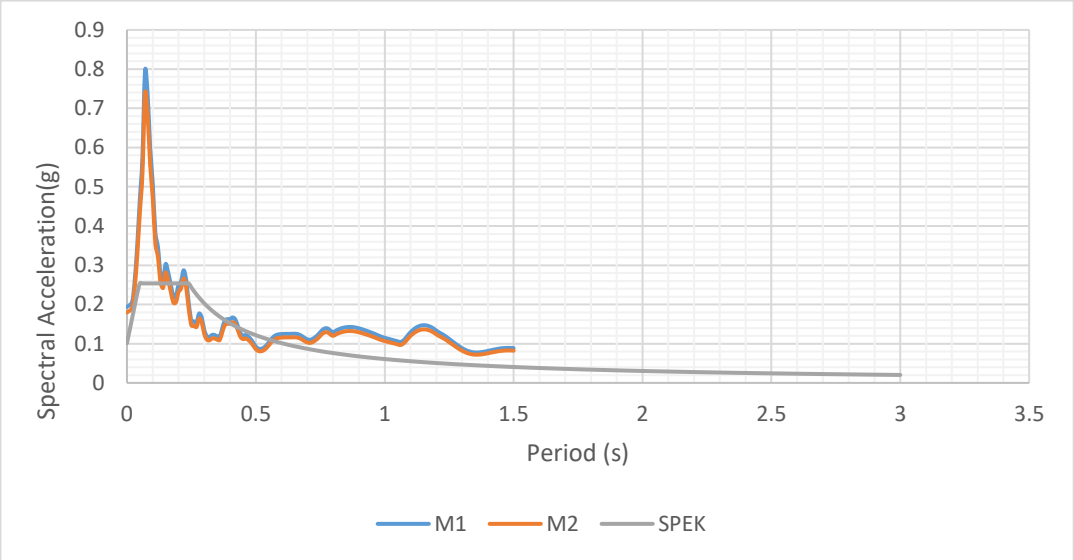

Figure A387. Scaled Vertical Response Spectra of Parkfield (D4-31) Earthquake

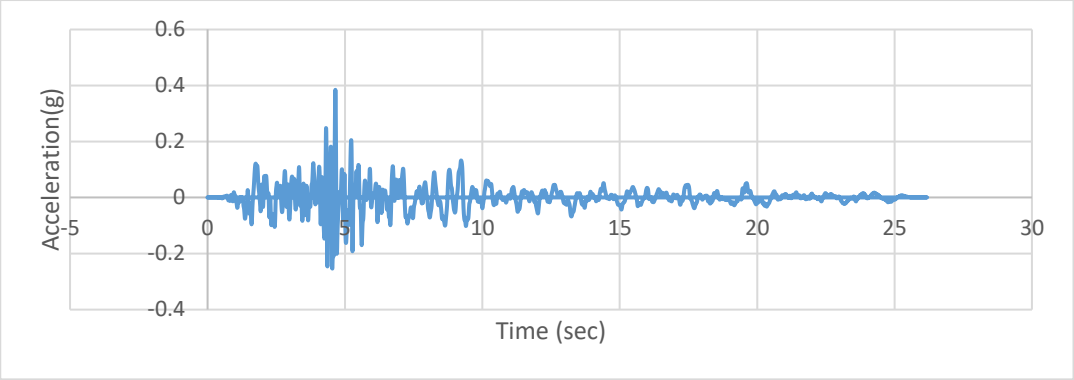

Figure A388.Scaled Acceleration Time Histories of Parkfield (D4-31X) Earthquake

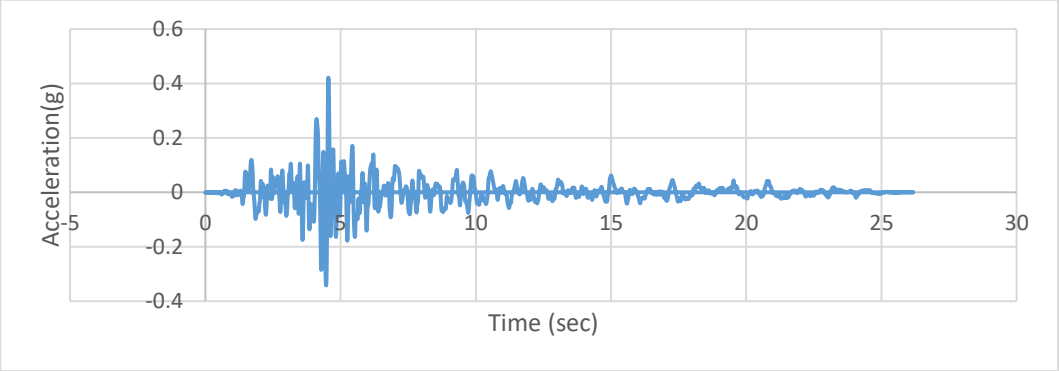

Figure A389. Scaled Acceleration Time Histories of Parkfield (D4-31Y) Earthquake

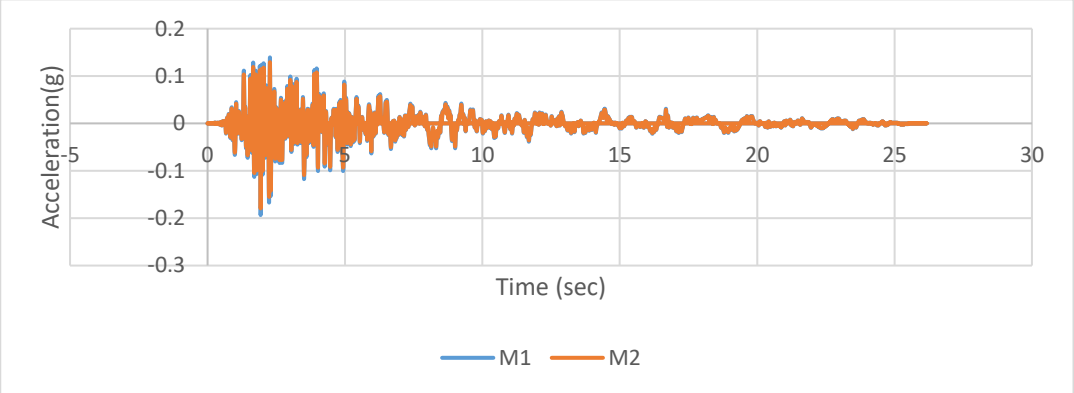

Figure A390. Scaled Acceleration Time Histories of Parkfield (D4-31Z) Earthquake

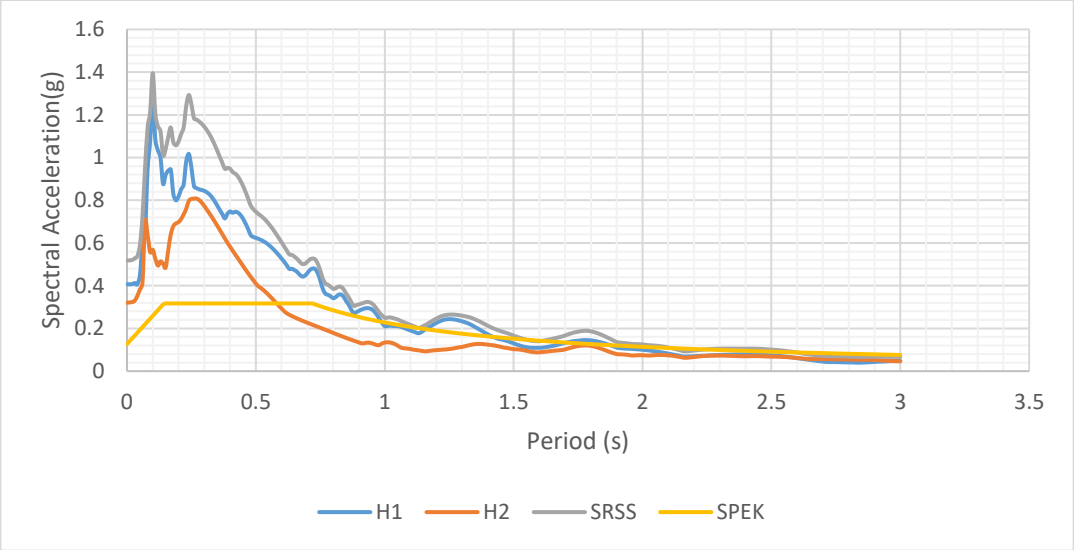

Figure A391.Scaled Horizontal Response Spectra of Imperial Valley-06 (D4-167) Earthquake

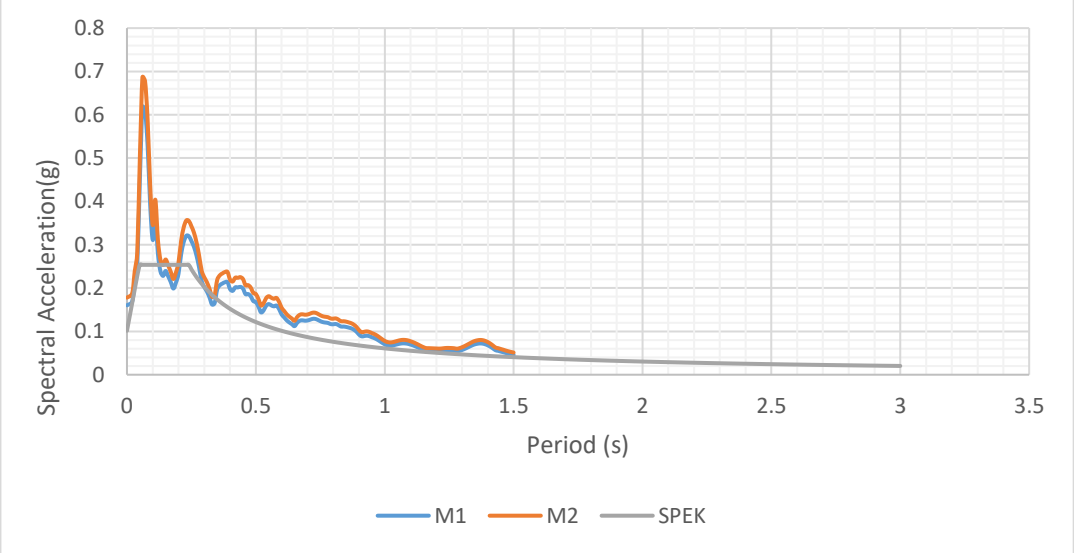

Figure A392. Scaled Vertical Response Spectra of Imperial Valley-06 (D4-167) Earthquake

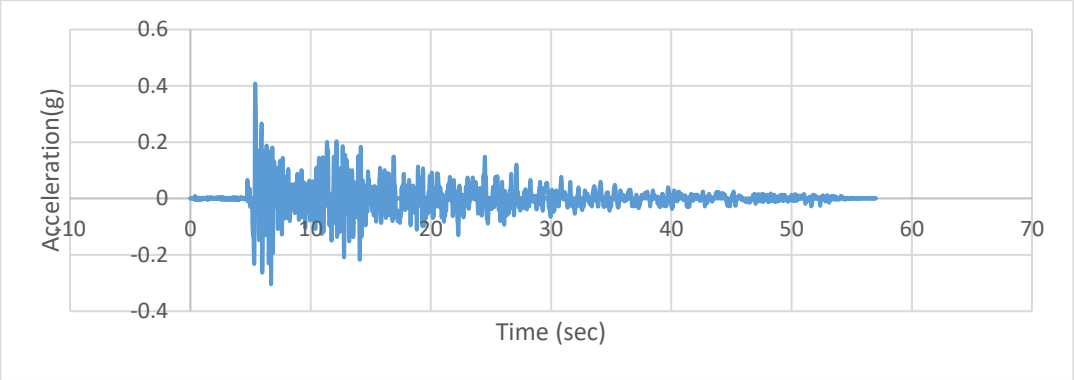

Figure A393. Scaled Acceleration Time Histories of Imperial Valley-06 (D4-167X) Earthquake

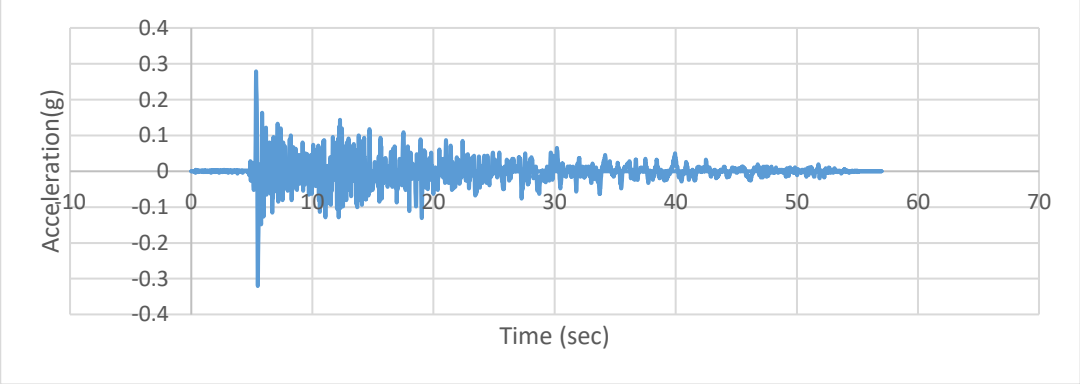

Figure A394. Scaled Acceleration Time Histories of Imperial Valley-06 (D4-167Y) Earthquake

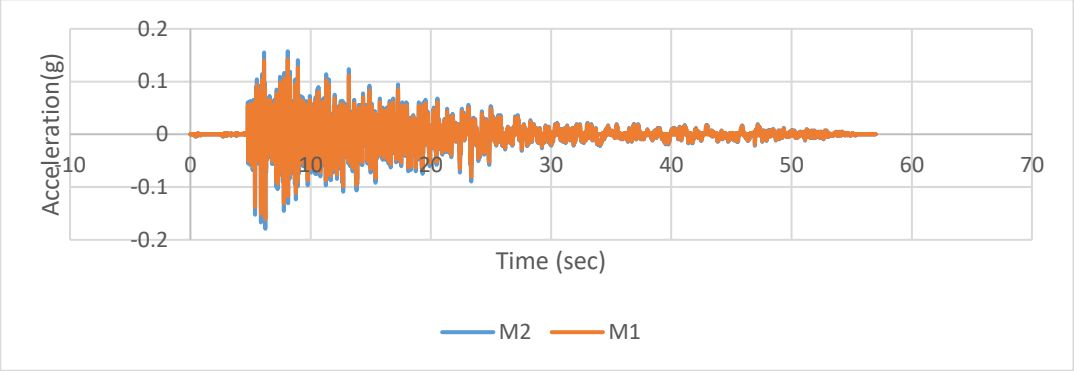

Figure A395 Scaled Acceleration Time Histories of Imperial Valley-06 (D4-167Z) Earthquake

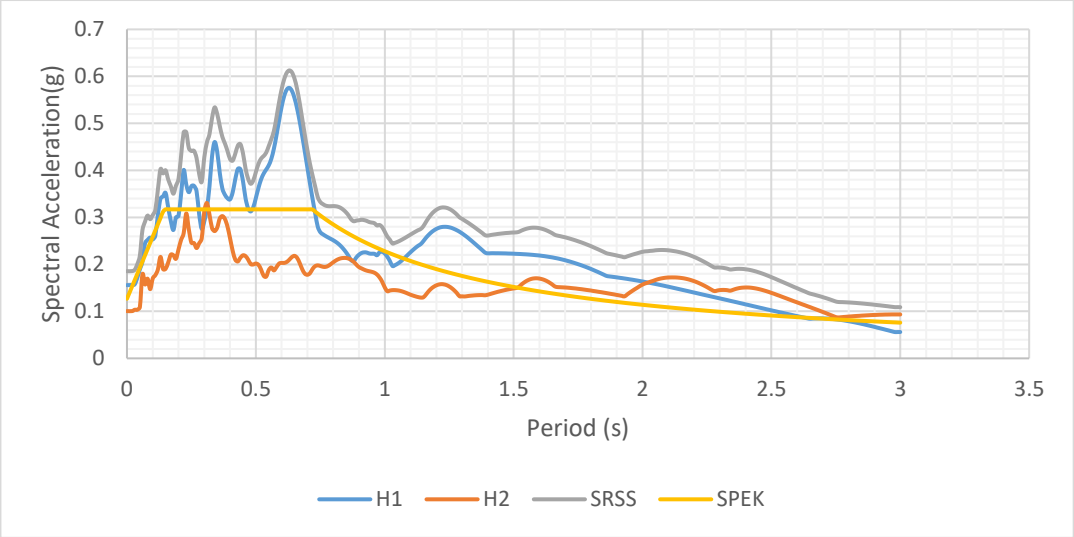

Figure A396. Scaled Horizontal Response Spectra of Victoria (D4-266) Earthquake

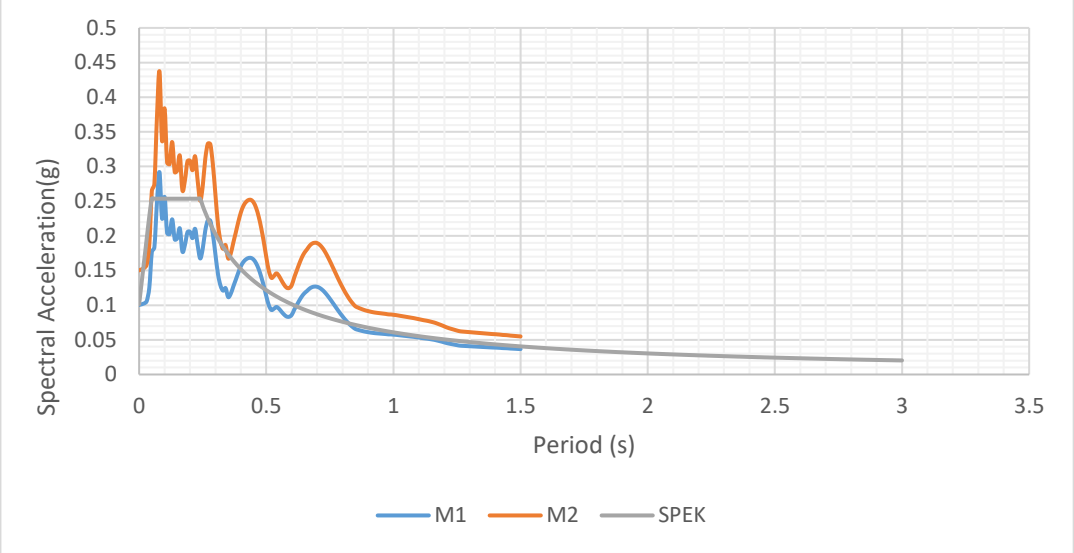

Figure A397. Scaled Vertical Response Spectra of Victoria (D4-266) Earthquake

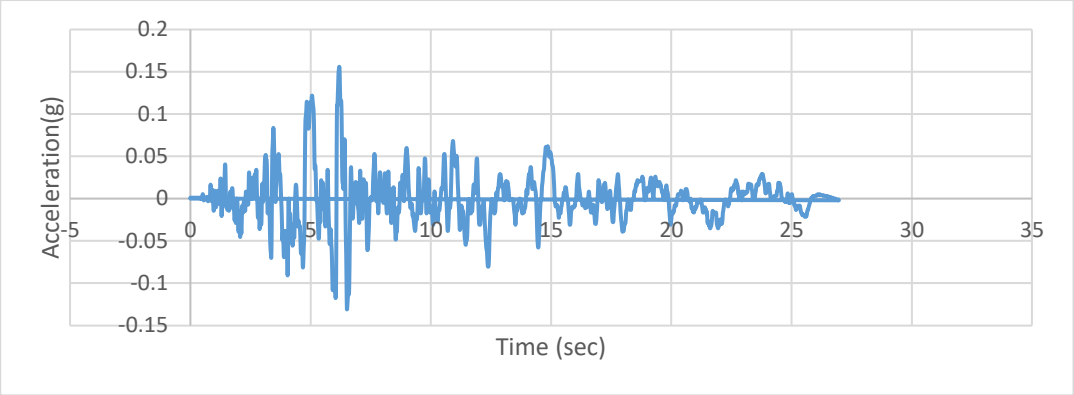

Figure A398. Scaled Acceleration Time Histories of Victoria (D4-266X) Earthquake

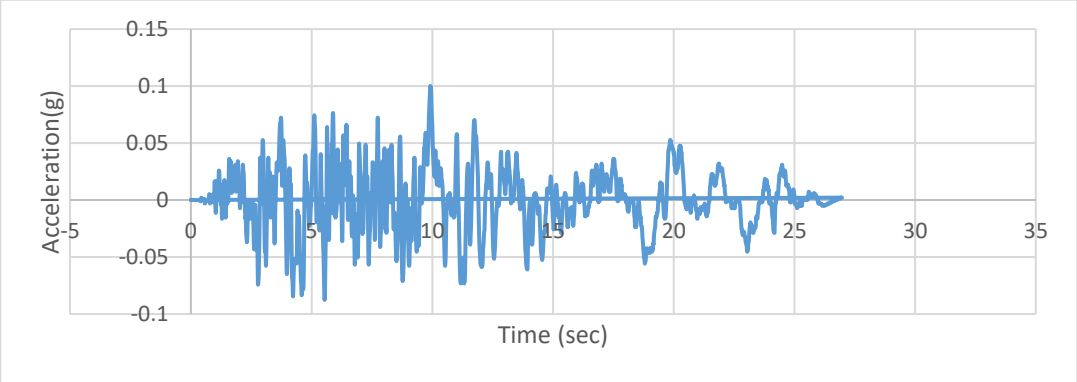

Figure A399. Scaled Acceleration Time Histories of Victoria (D4-266Y) Earthquake

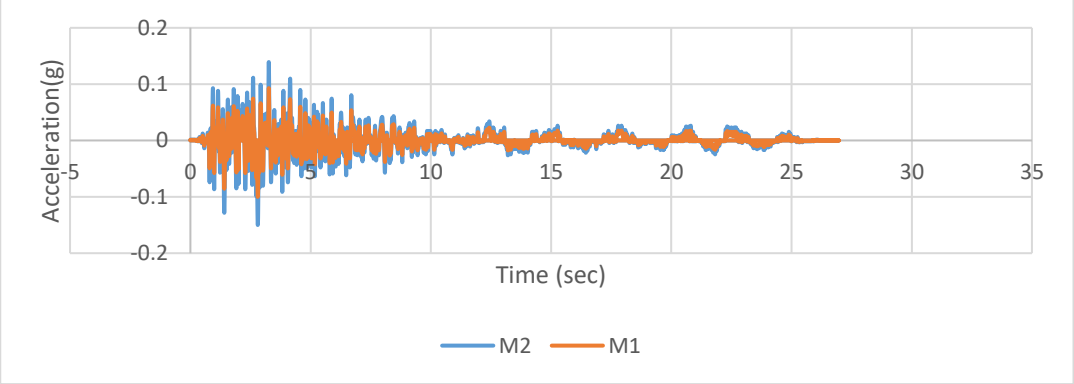

Figure A400. Scaled Acceleration Time Histories of Victoria (D4-266X) Earthquake

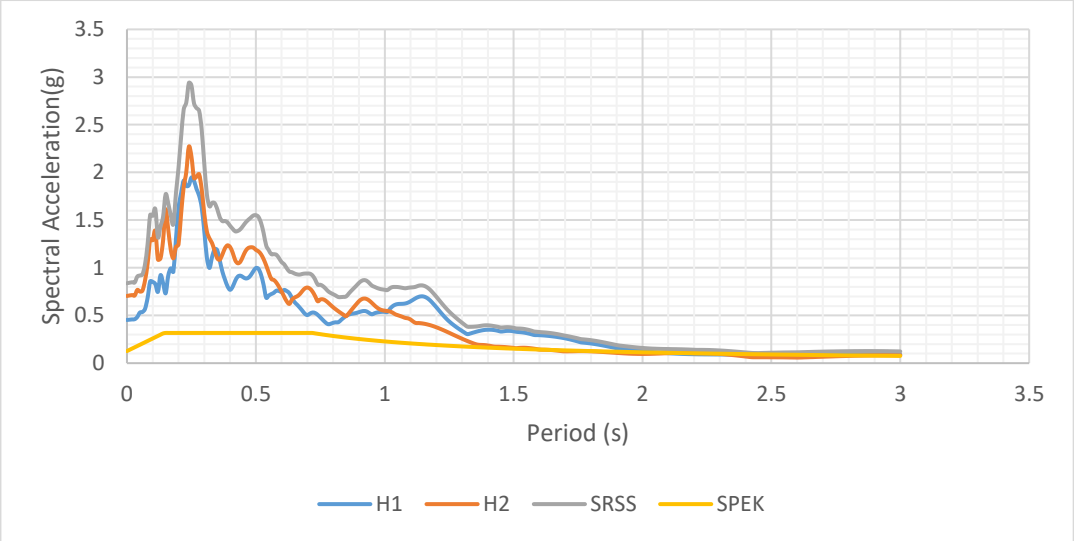

Figure A401. Scaled Horizontal Response Spectra of Morgan Hill (D4-458) Earthquake

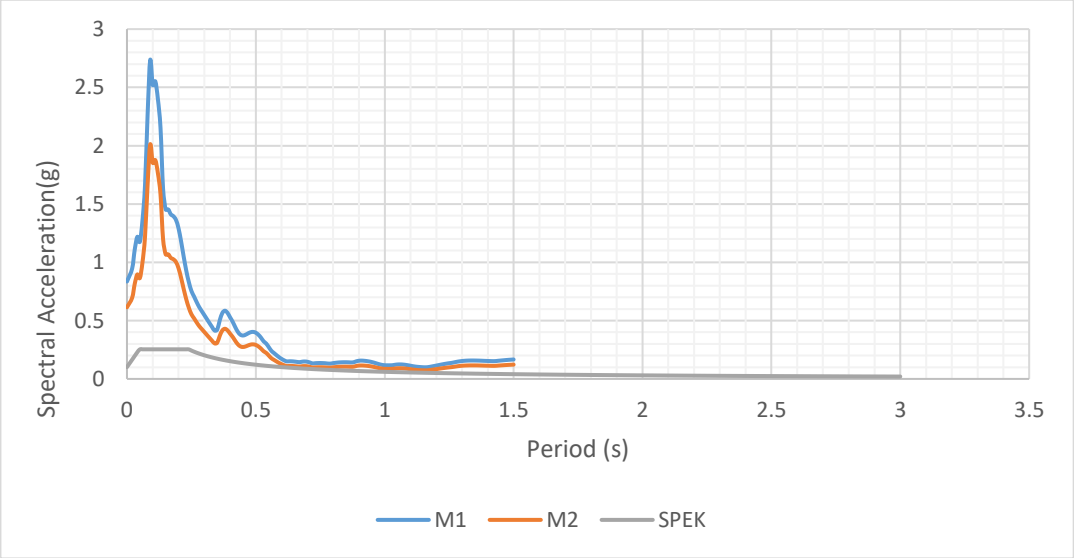

Figure A402.Scaled Vertical Response Spectra of Morgan Hill (D4-458) Earthquake

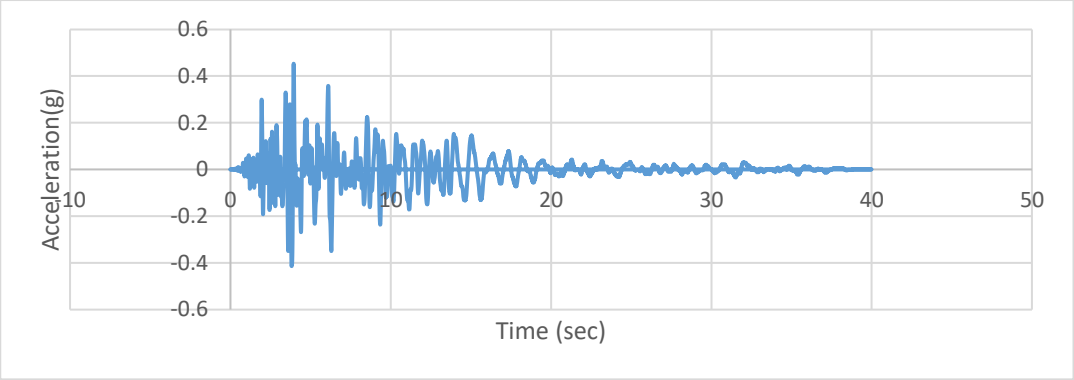

Figure A403. Scaled Acceleration Time Histories of Morgan Hill (D4-458X) Earthquake

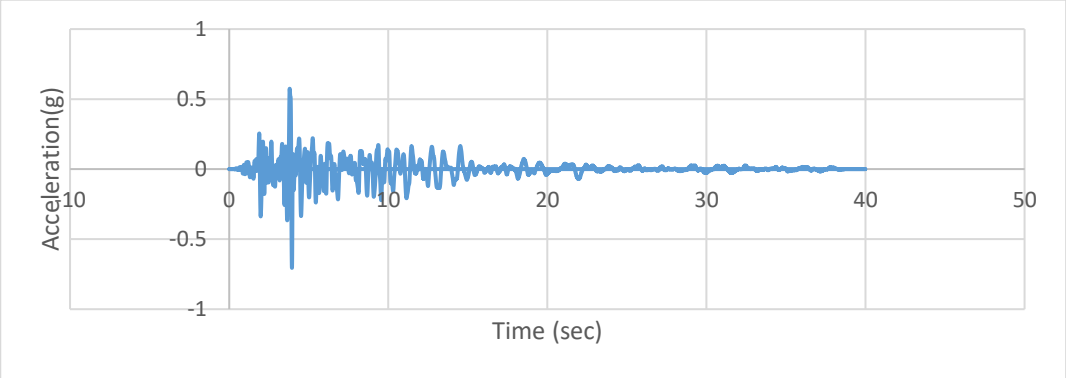

Figure A404. Scaled Acceleration Time Histories of Morgan Hill (D4-458Y) Earthquake

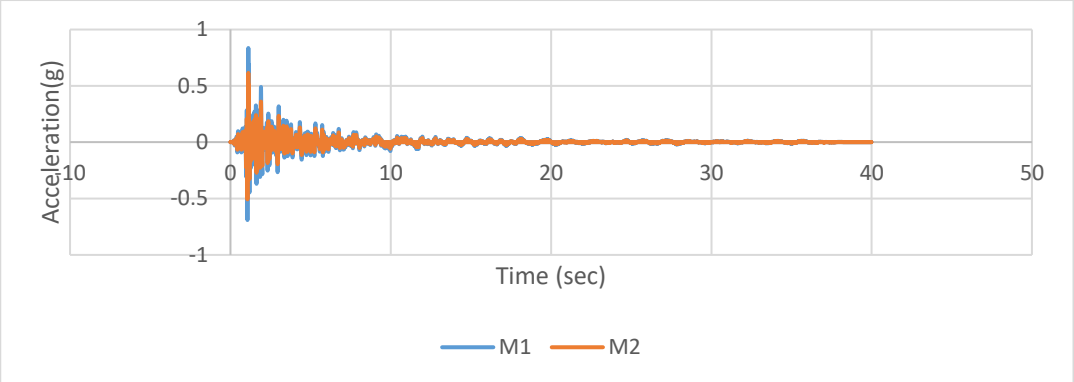

Figure A405. Scaled Acceleration Time Histories of Morgan Hill (D4-458Z) Earthquake

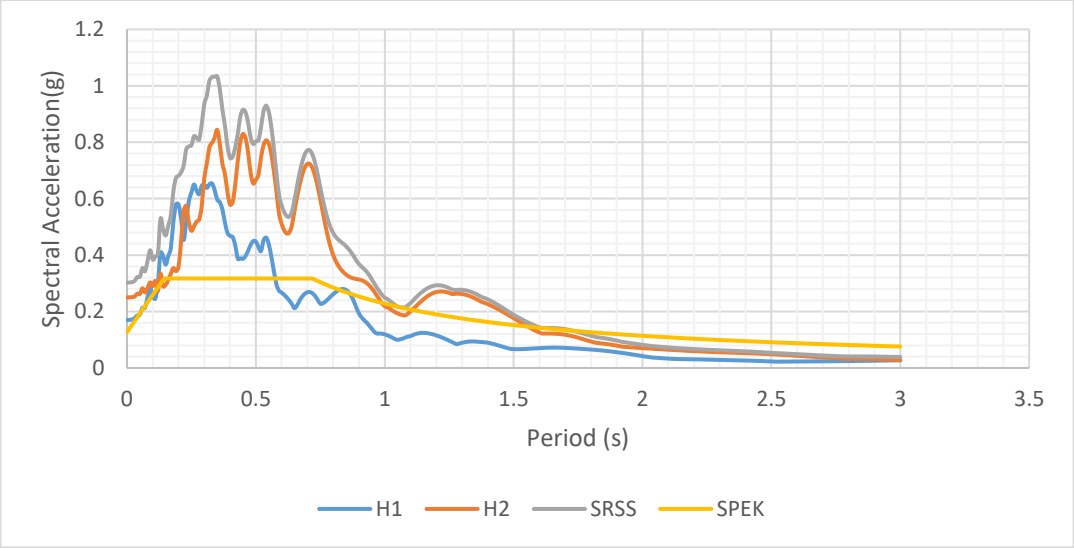

Figure A406. Scaled Horizontal Response Spectra of Landers (D4-848) Earthquake

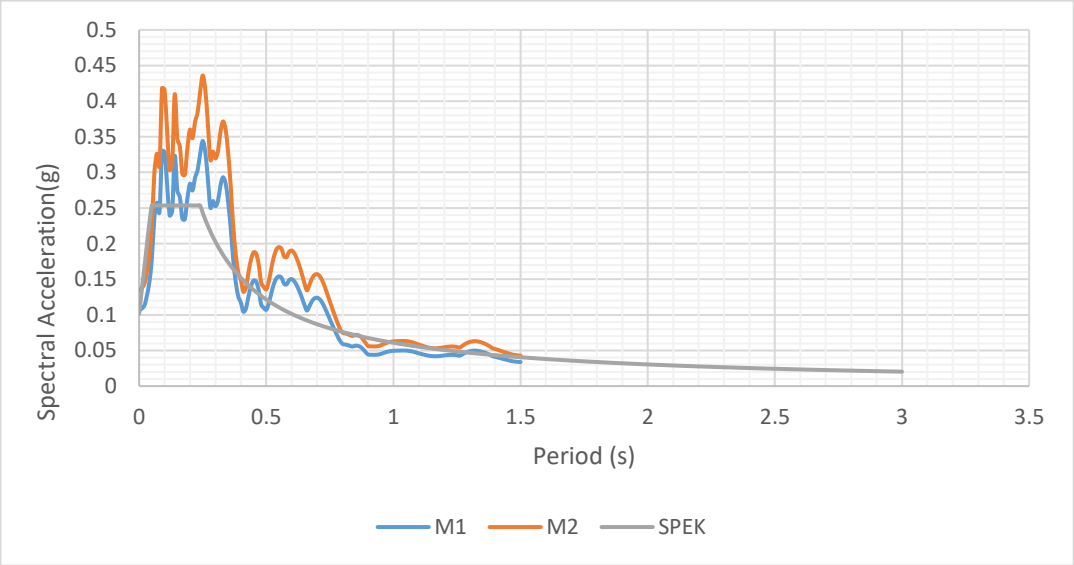

Figure A407. Scaled Vertical Response Spectra of Landers (D4-848) Earthquake

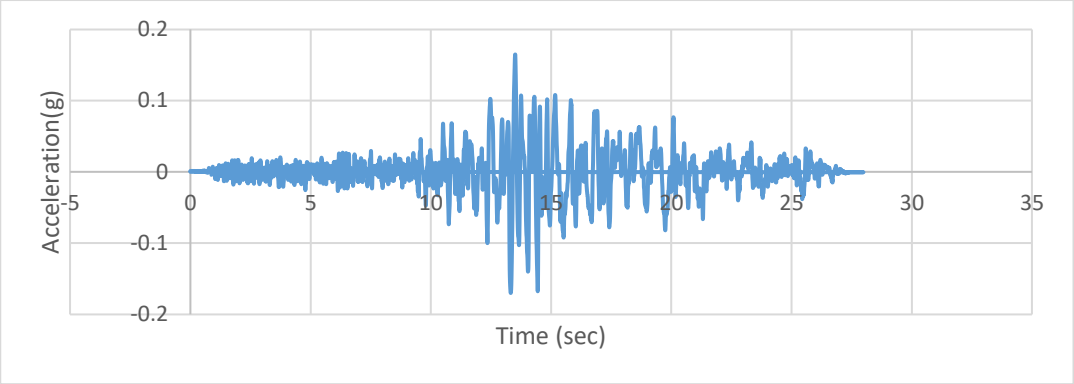

Figure A408. Scaled Acceleration Time Histories of Landers (D4-848) Earthquake

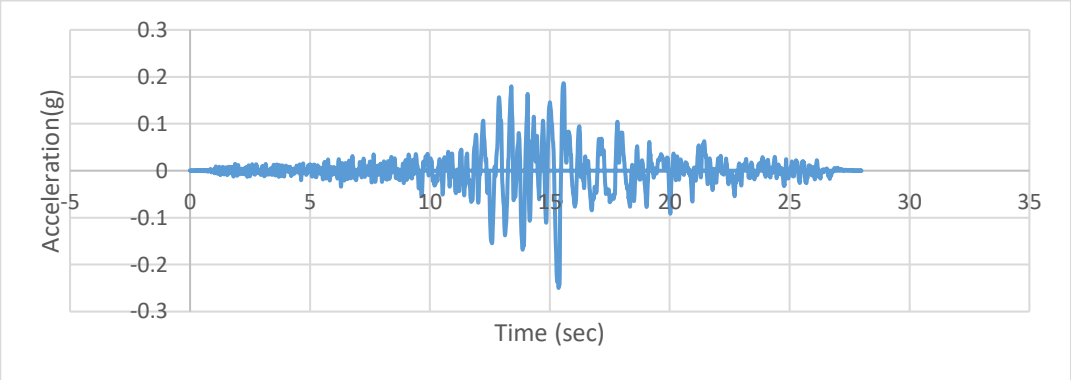

Figure A409. Scaled Acceleration Time Histories of Landers (D4-848) Earthquake

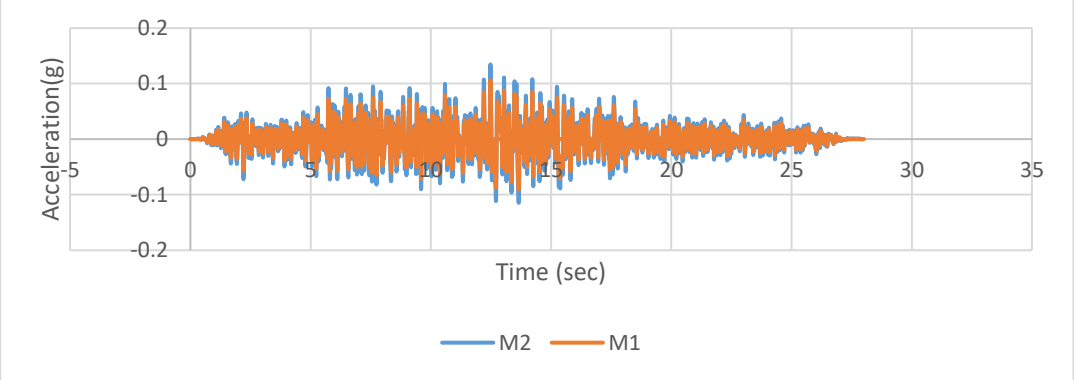

Figure A410. Scaled Acceleration Time Histories of Landers (D4-848) Earthquake

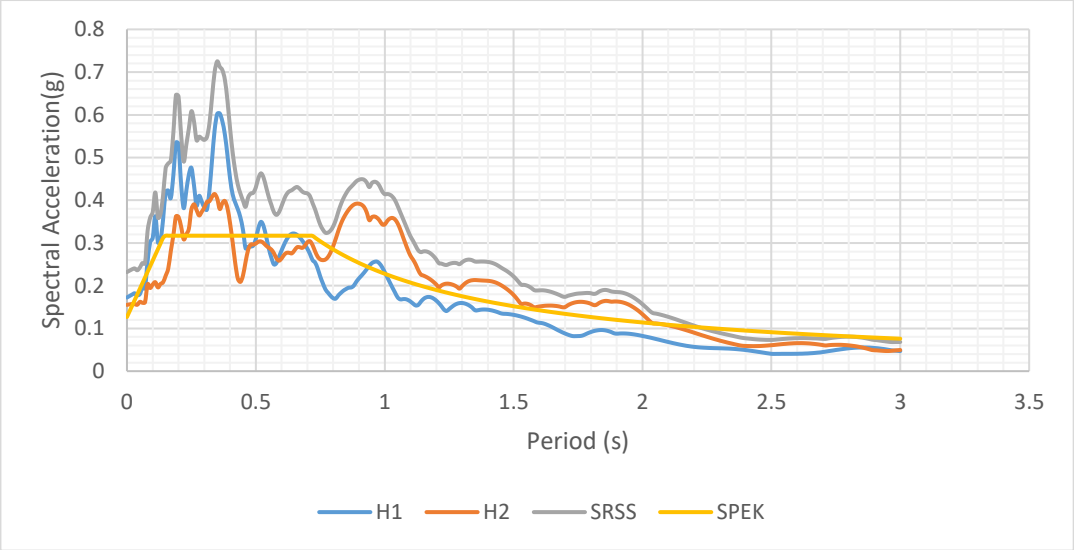

Figure A411. Scaled Horizontal Response Spectra of Landers (D4-850) Earthquake

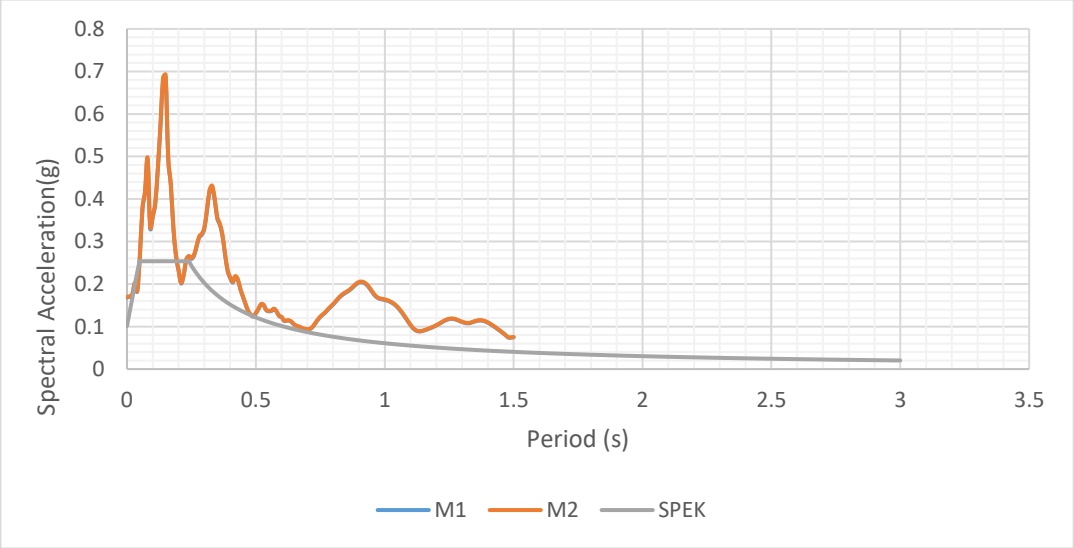

Figure A412. Scaled Vertical Response Spectra of Landers (D4-850) Earthquake

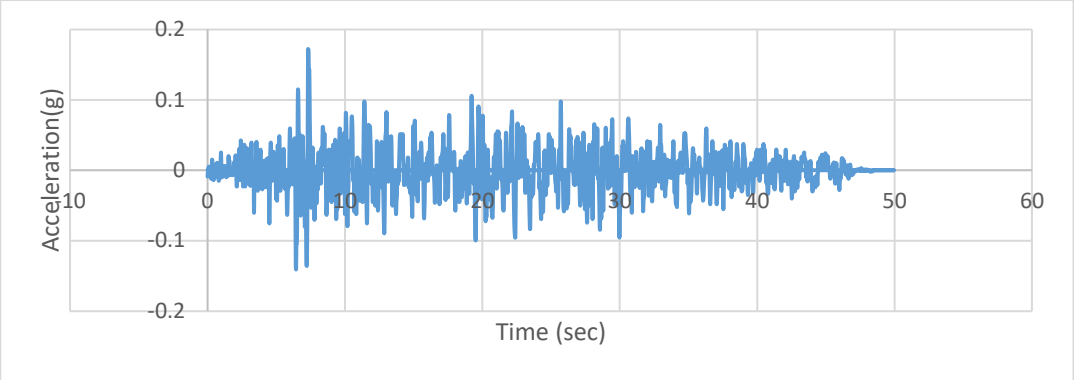

Figure A413. Scaled Acceleration Time Histories of Landers (D4-850X) Earthquake

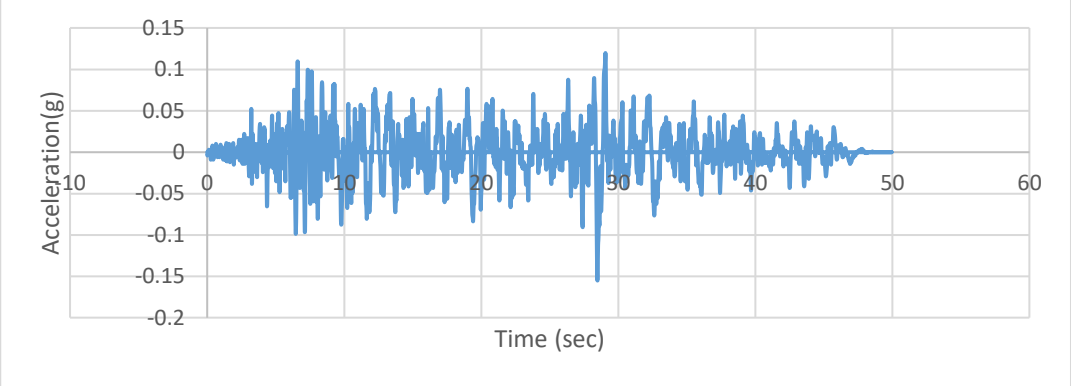

Figure A414. Scaled Acceleration Time Histories of Landers (D4-850Y) Earthquake

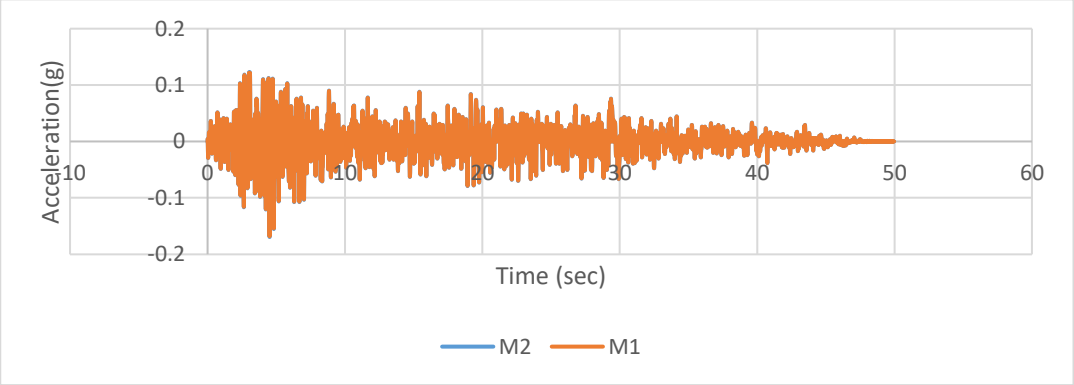

Figure A415. Scaled Acceleration Time Histories of Landers (D4-850Z) Earthquake

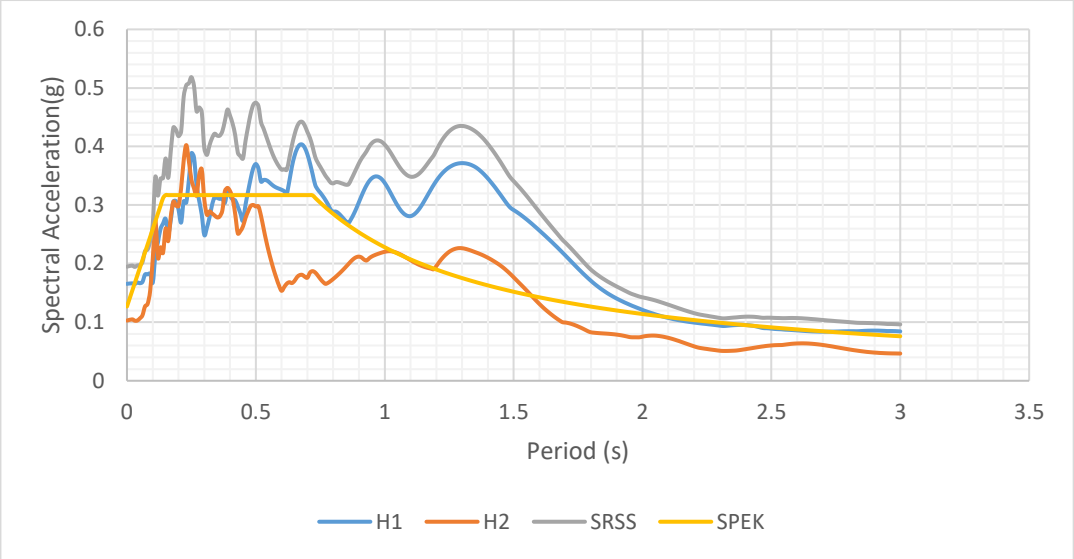

Figure A416. Scaled Horizontal Response Spectra of Landers (D4-900) Earthquake

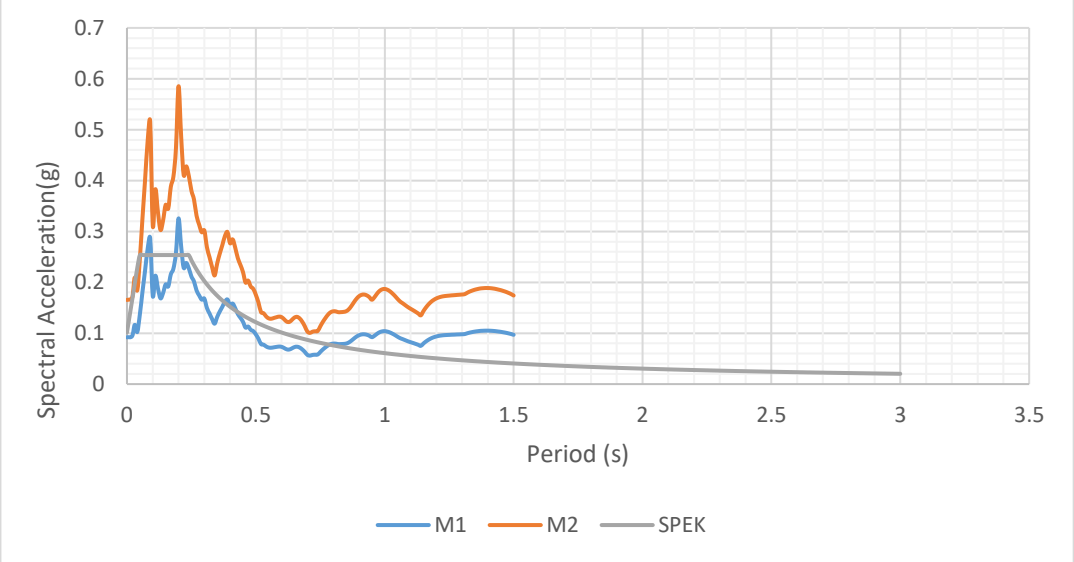

Figure A417. Scaled Vertical Response Spectra of Landers (D4-900) Earthquake

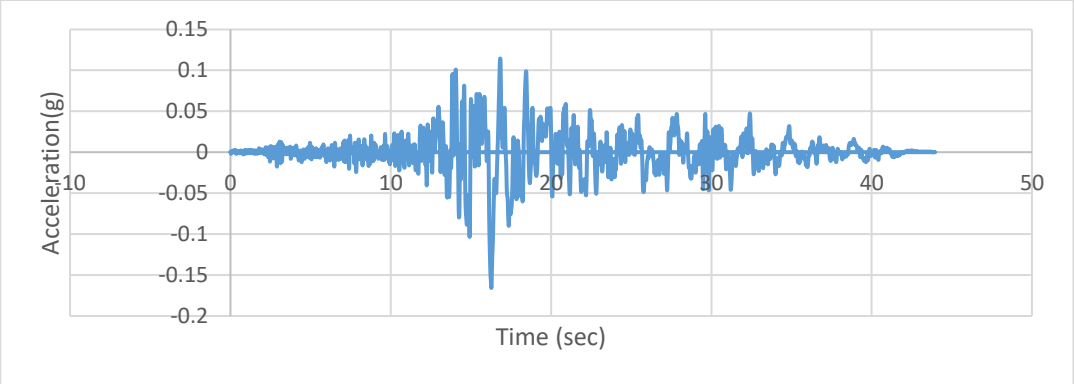

Figure A418. Scaled Acceleration Time Histories of Landers (D4-900X) Earthquake

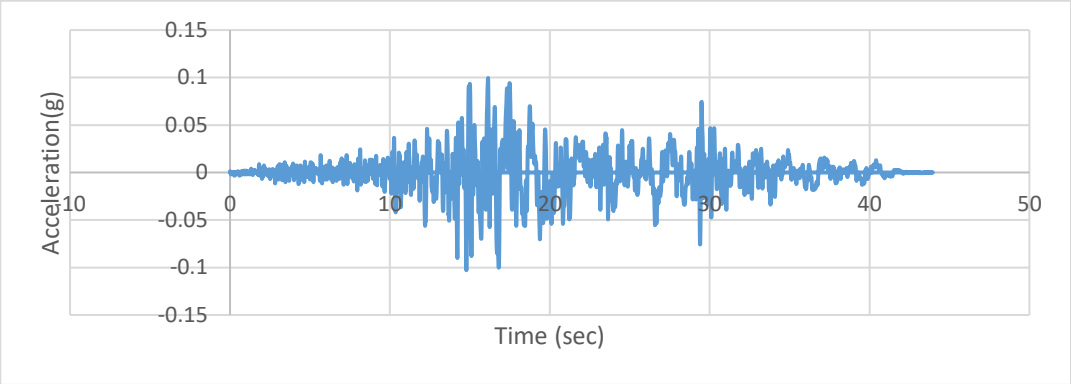

Figure A419. Scaled Acceleration Time Histories of Landers (D4-900Y) Earthquake

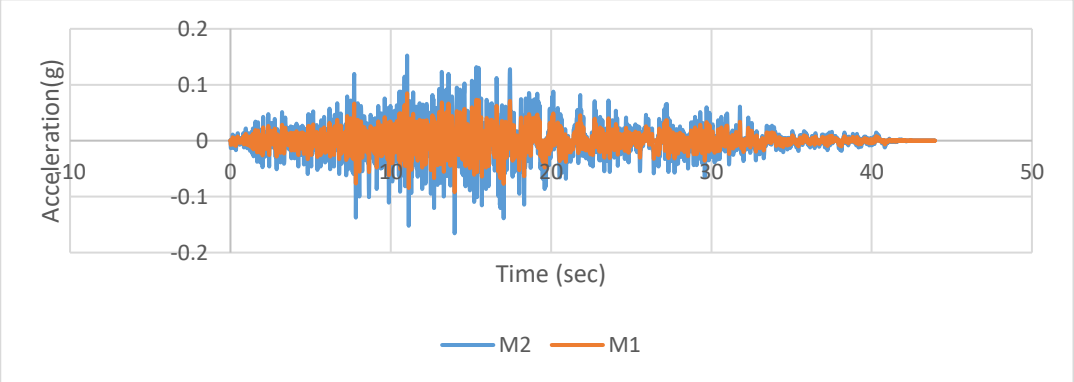

Figure A420. Scaled Acceleration Time Histories of Landers (D4-900Z) Earthquake

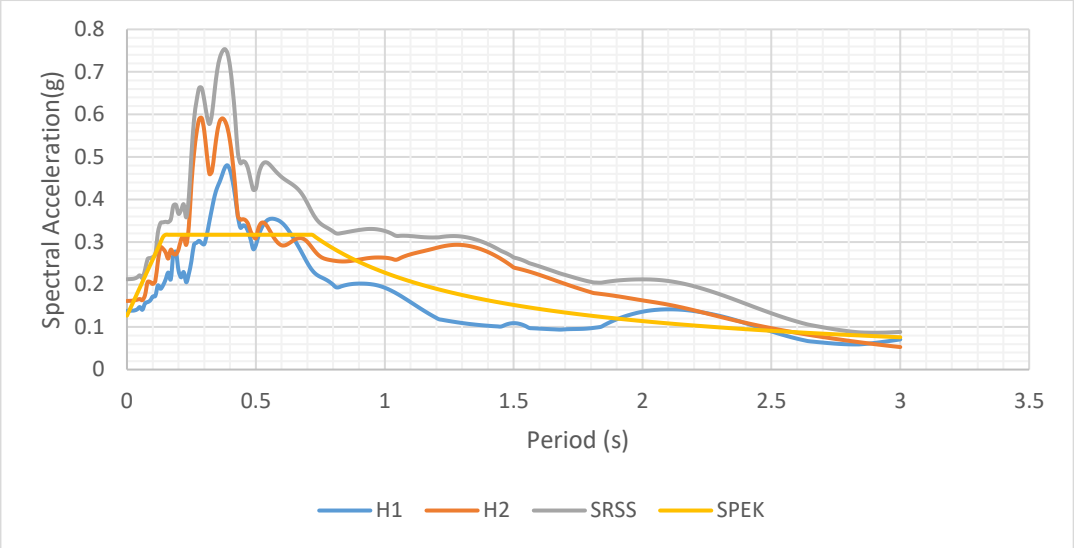

Figure A421. Scaled Horizontal Response Spectra of Kocaeli (D4-1158) Earthquake

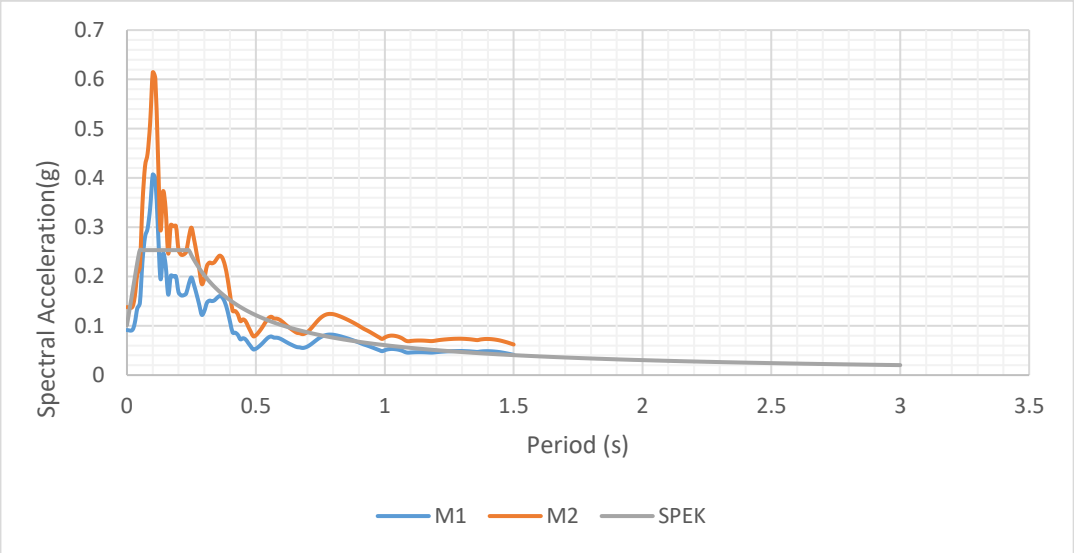

Figure A422. Scaled Vertical Response Spectra of Kocaeli (D4-1158) Earthquake

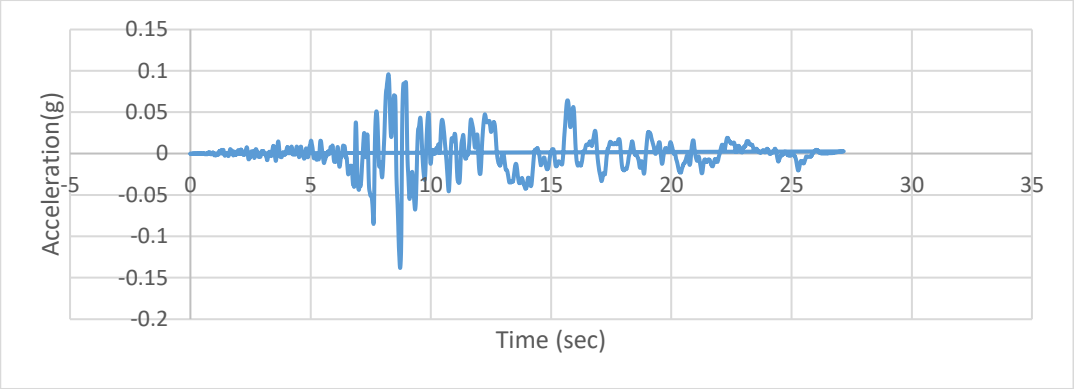

Figure A423. Scaled Acceleration Time Histories of Kocaeli (D4-1158X) Earthquake

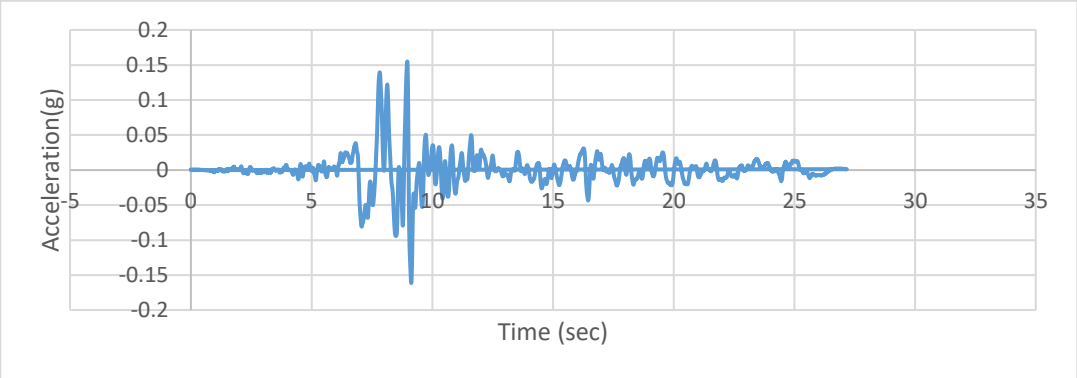

Figure A424. Scaled Acceleration Time Histories of Kocaeli (D4-1158Y) Earthquake

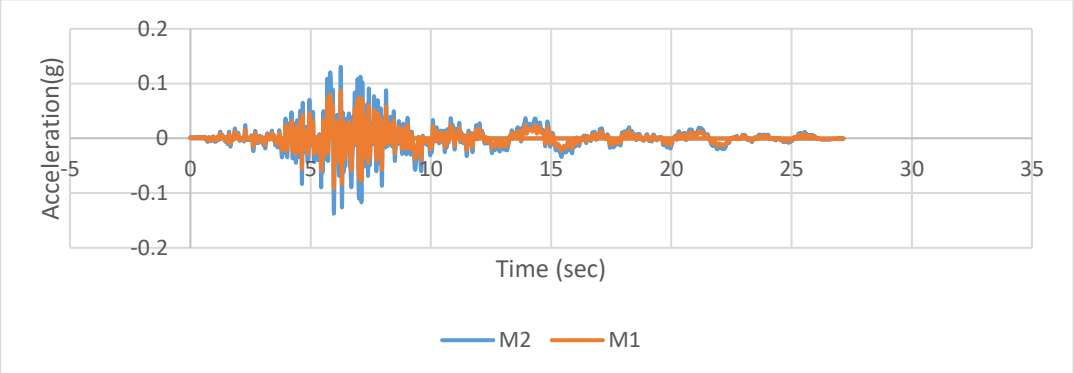

Figure A425 Scaled Acceleration Time Histories of Kocaeli (D4-1158Z) Earthquake

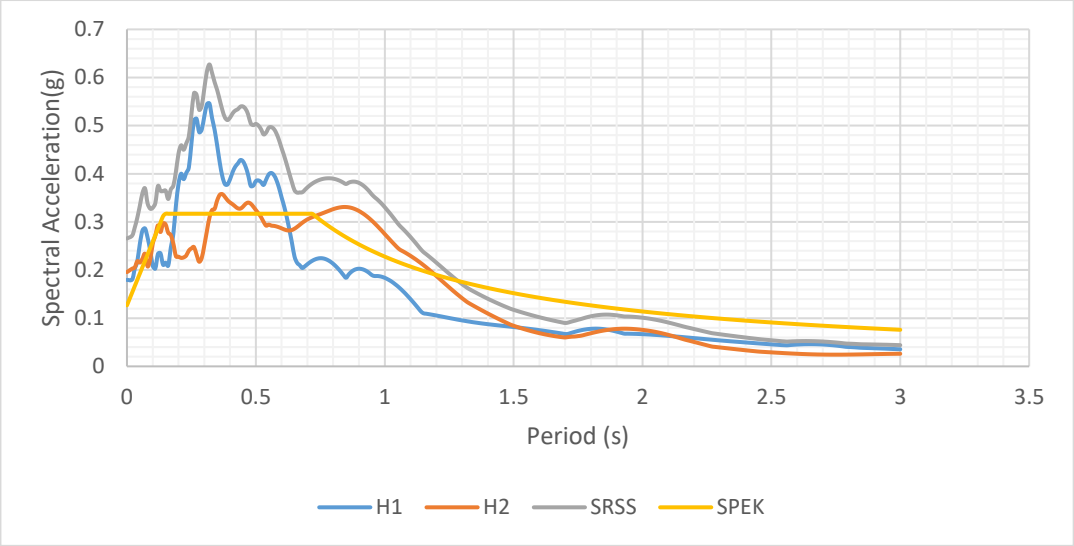

Figure A426. Scaled Horizontal Response Spectra of Duzce (D4-1602) Earthquake

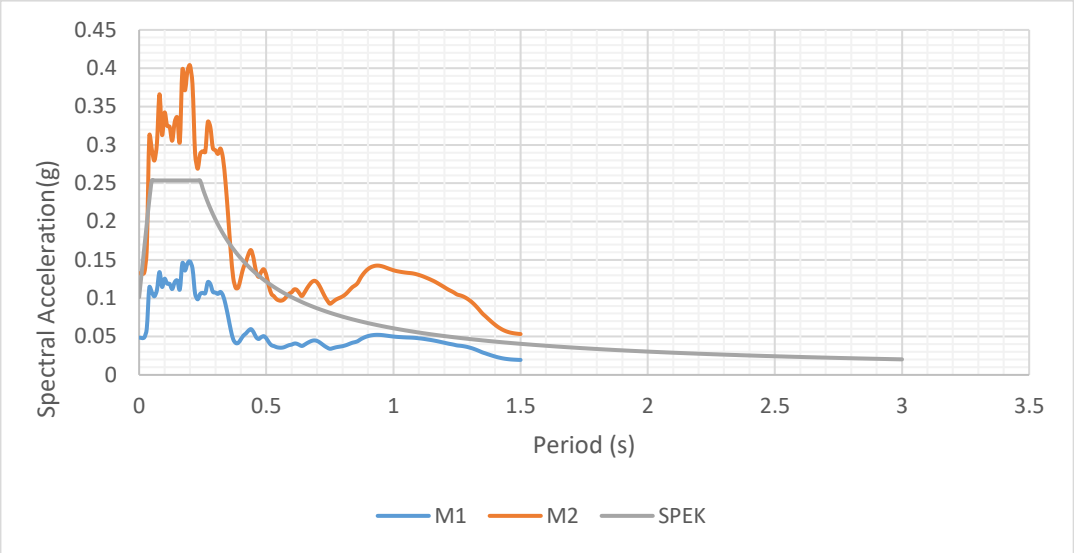

Figure A427. Scaled Vertical Response Spectra of Duzce (D4-1602) Earthquake

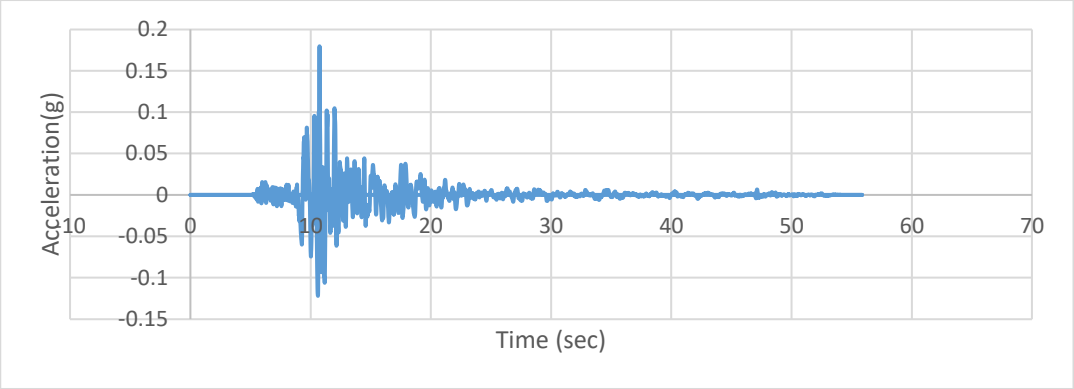

Figure A428. Scaled Acceleration Time Histories of Duzce (D4-1602X) Earthquake

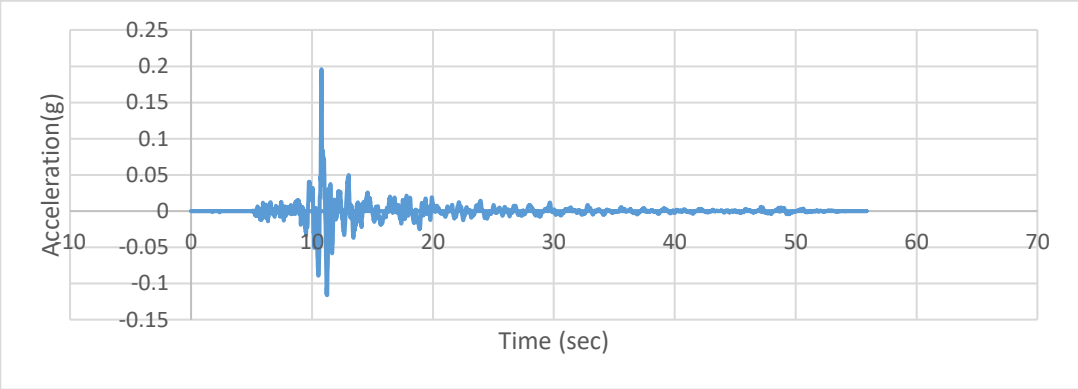

Figure A429. Scaled Acceleration Time Histories of Duzce (D4-1602Y) Earthquake

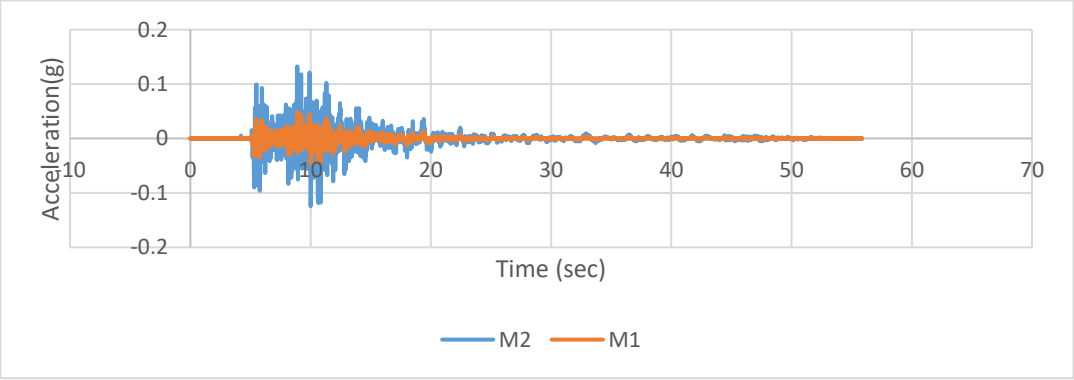

Figure A430. Scaled Acceleration Time Histories of Duzce (D4-1602Z) Earthquake

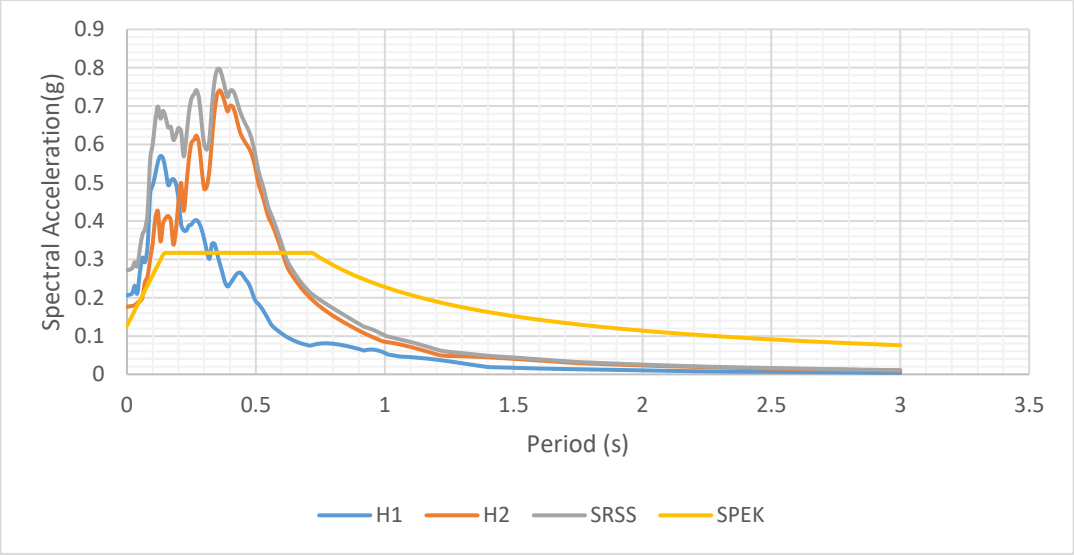

Figure A431. Scaled Horizontal Response Spectra of Northwest China-01 (D4-1748) Earthquake

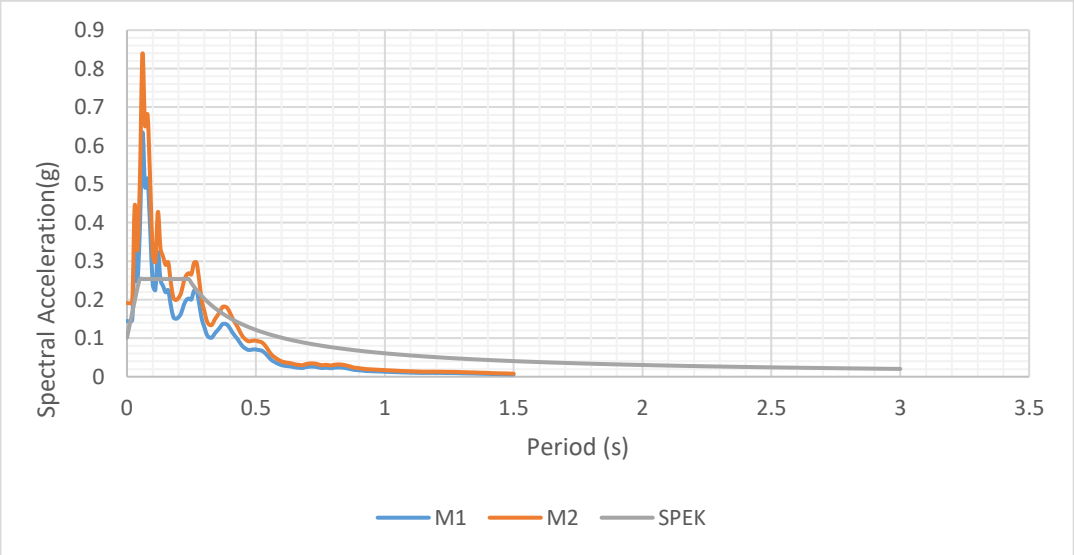

Figure A432. Scaled Vertical Response Spectra of Northwest China-01 (D4-1748) Earthquake

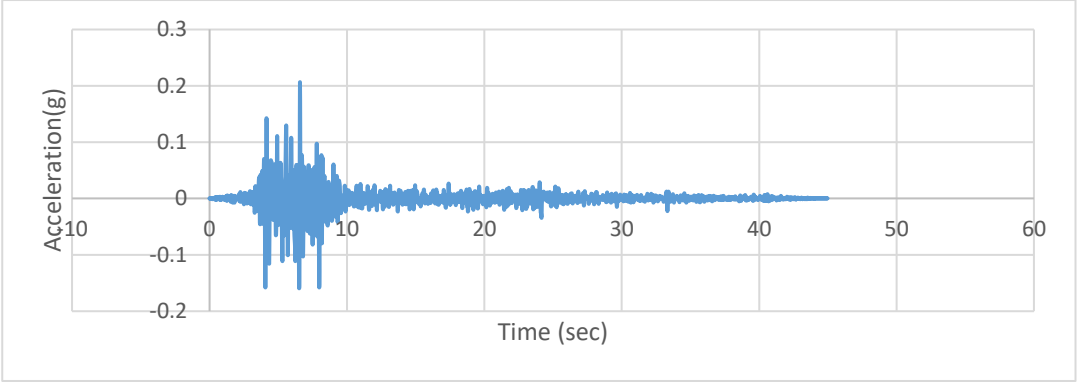

Figure A433. Scaled Acceleration Time Histories of Northwest China-01 (D4-1748X) Earthquake

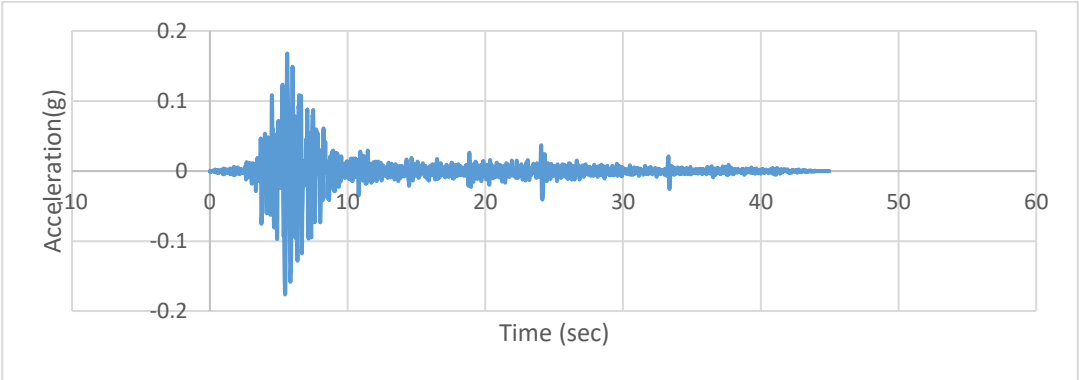

Figure A434. Scaled Acceleration Time Histories of Northwest China-01 (D4-1748Y) Earthquake

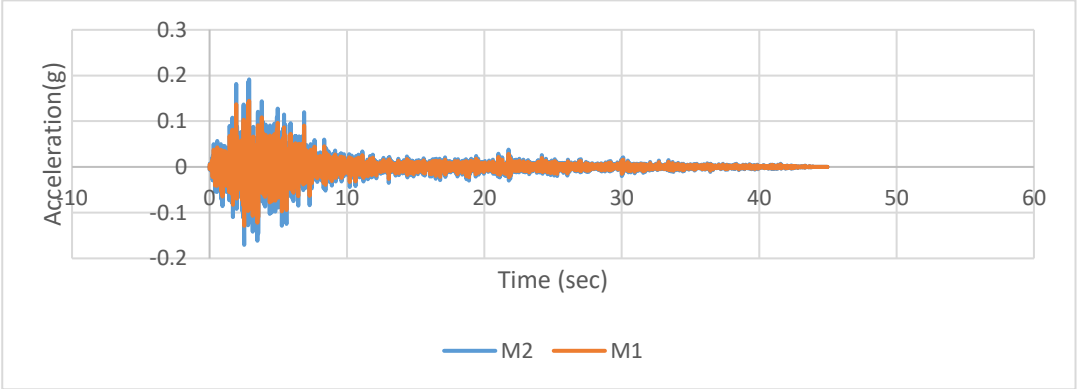

Figure A435. Scaled Acceleration Time Histories of Northwest China-01 (D4-1748Z) Earthquake

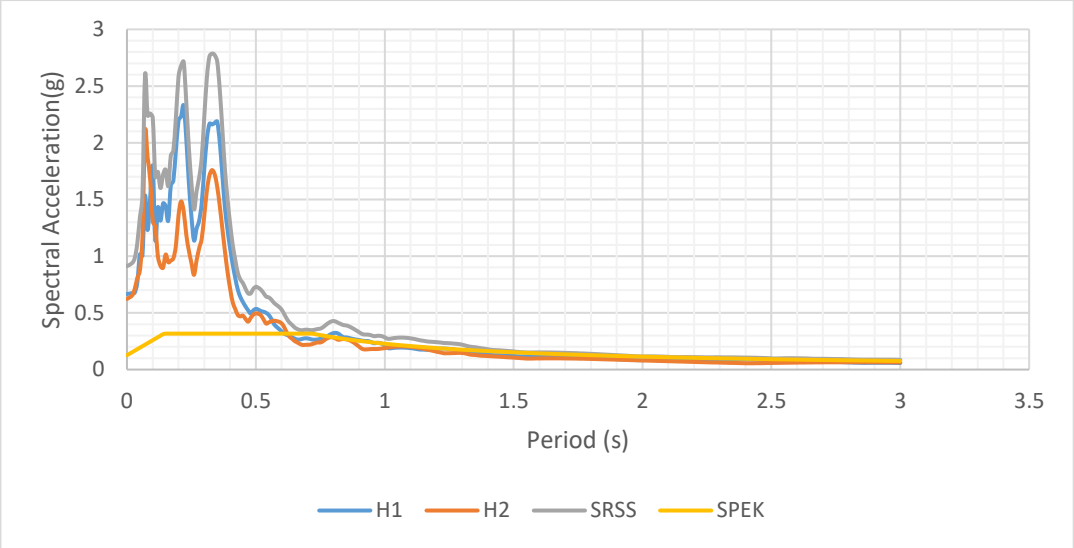

Figure A436. Scaled Horizontal Response Spectra of Parkfield-02 (D4-4125) Earthquake

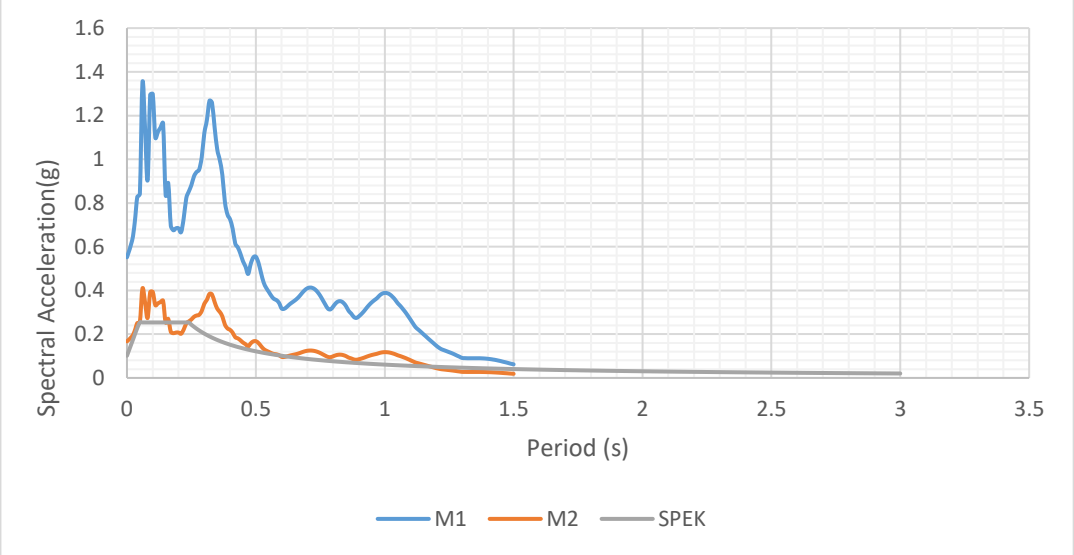

Figure A437. Scaled Vertical Response Spectra of Parkfield-02 (D4-4125) Earthquake

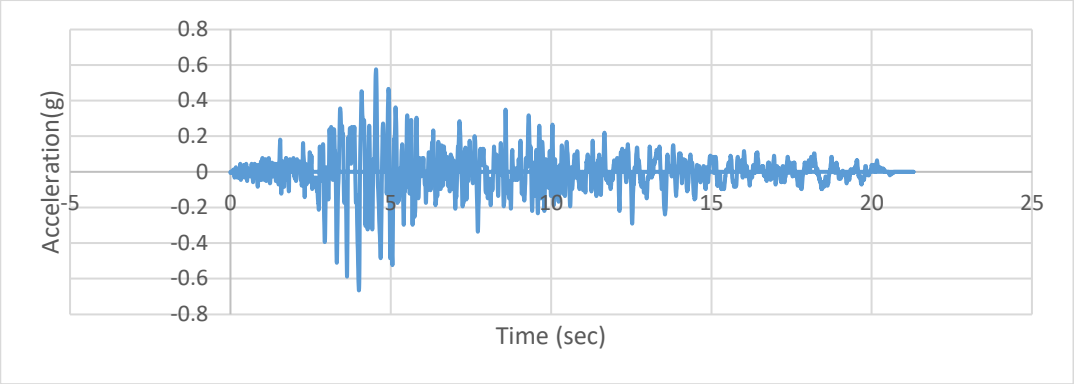

Figure A438. Scaled Acceleration Time Histories of Parkfield-02 (D4-4125X) Earthquake

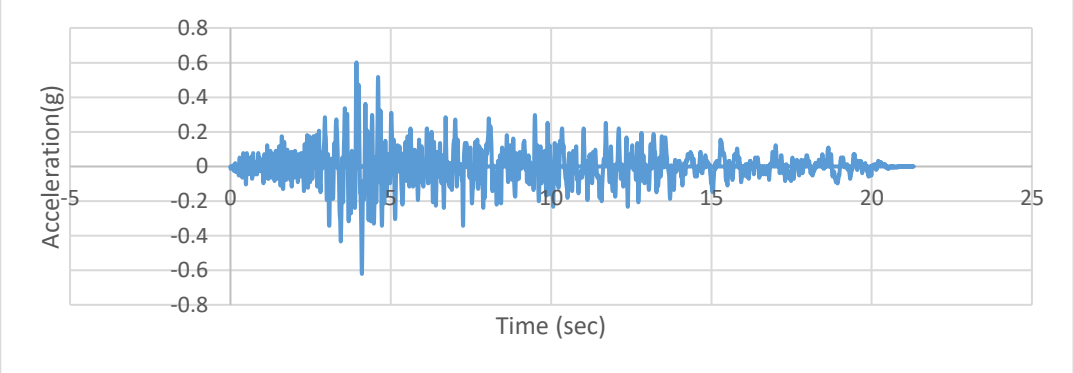

Figure A5. Scaled Acceleration Time Histories of Parkfield-02 (D4-4125Y) Earthquake

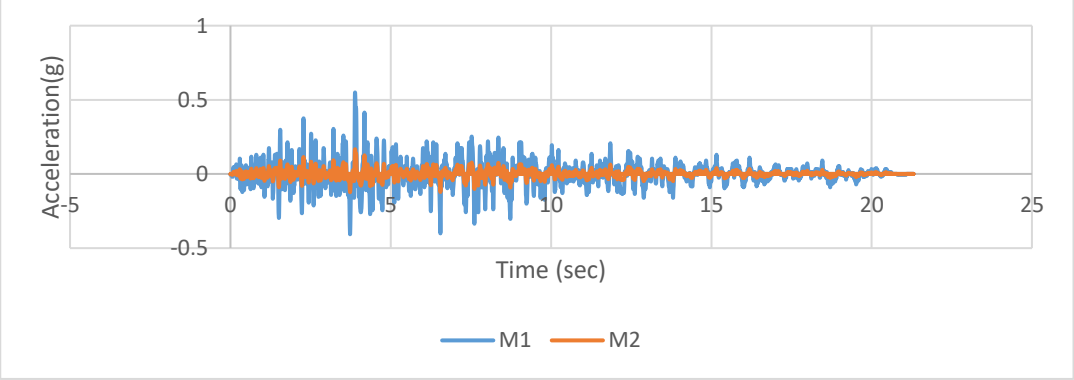

Figure A440. Scaled Acceleration Time Histories of Parkfield-02 (D4-4125Z) Earthquake